Investigation of the promoting roles of FABP5 and AR in malignant progression of prostate cancer cells and the relevant molecular mechanisms

PhD in Cancer Biology

Submitted to satisfy the requirements for the degree of Doctor of Philosophy

By:

Abdulghani Abdullah A Naeem

February 2023

**Department of Molecular and Clinical Cancer Medicine
University of Liverpool**

<p align="center">**بِسْمِ اللَّهِ الرَّحْمَنِ الرَّحِيمِ**</p>

<p align="center">***In the name of Allah***</p>

<p align="center">**وَمَا تَوْفِيقِي إِلَّا بِاللَّهِ عَلَيْهِ تَوَكَّلْتُ وَإِلَيْهِ أُنِيب**</p>

<p align="center">***My success comes only through Allah. In Him I trust and to Him I turn***</p>

It is with deep reverence that I dedicate this thesis to my late mother, who passed away in May 2022, after a courageous battle with cancer. Her unwavering love and support were a constant source of inspiration for me, and I am forever grateful for the sacrifices she made to ensure my success. I fervently hope that my research will contribute towards the development of a breakthrough in cancer treatment, and thus serve the scientific community. This would be a fitting tribute to my mother's memory and her struggles against the disease. I am also grateful for the unending support and encouragement of my wife, Alhasnaa Halikah, and our children, Abdulmalik and Ibrahim, who were my companions throughout the challenging journey of my PhD. Their love, understanding, and unwavering support were a constant source of strength for me. Finally, I would like to express my heartfelt gratitude to my brothers and sisters, Abdulrahman, Alla, Abeer, and Ola, who have always stood by me with their unwavering support and encouragement. Their presence in my life has been a source of immense strength and motivation, and I am truly blessed to have them as my siblings.

Abstract

FABP5 and the androgen receptor (AR) are two important promoting factors for the malignant progression of prostate cancer cells. To study the molecular mechanisms underlying their tumor-promoting function, we first knocked out *FABP5* or *AR* in the moderately malignant 22RV1 cells and in the highly malignant DU145 and PC3M cells, respectively. Then we investigated the effect of *FABP5-* or *AR-* knock out (KO) on the malignant characteristics of the cancer cells and detected the changes in expression status of the main factors involved the FABP5 or AR-PPARγ-VEGF signal pathway. To investigate the complexed signal network regulated by FABP5 and AR, we compared the expression profiles between the parental cells and the *FABP5-* or *AR-* KO cells. Our results showed that *FABP5-* or *AR-* KO significantly suppressed the cell proliferation rate, invasive ability, motility rate, and anchorage-independent growth through disrupting the FABP5 or AR-p-PPARγ-VEGF axis. It was found that FABP5 and AR interacted with each other in regulation of FABP5 or AR - p-PPARγ-VEGF axis, with FABP5 controlling the ARV7 splice variant and AR regulating the expression of FABP5. RNA profile comparison led to the identification of a large number of differentially expressed genes (DEG) between the parental and *FABP5-* or *AR-* KO cells. Six most pronouns DEGs were shown to be involved in the transition of the cells from androgen-responsive to androgen-unresponsive prostate cancer or CRPC cells. Gene ontology enrichment analysis revealed that the top enriched biological processes of DEGs included those response to fatty acids, cholesterol, and sterol biosynthesis, as well as lipid and fatty acid transport. These pathways regulated by FABP5 or AR were crucial in transducing signals for cancer cell progression. Our results suggested that the interactions between FABP5 and AR contributed to the transition of prostate cancer cells to the androgen-independent state.

These findings provided novel insights into the complicated molecular pathogenesis of CRPC cells.

ACKNOWLEDGMENTS

Prophet Muhammad, peace and blessings be upon him, said, "He who does not thank people, does not thank Allah"

I would like to express my sincere gratitude to Professor Youqiang Ke for his invaluable guidance and support throughout my doctoral research. Professor Ke's mentorship extended beyond academic matters, and he has been a constant source of inspiration for me, demonstrating the importance of interpersonal skills, wisdom and gratitude. Despite his retirement from the University of Liverpool in 2021, Professor Ke remained dedicated to my research project and demonstrated unwavering commitment to my success. His extensive knowledge and expertise were instrumental in helping me address challenging research questions, without which, the completion of my thesis would not have been possible. I would also like to extend my appreciation to my research group, Dr Asmaa Imad Al-Bayati, Dr Bandar Theyab A Alenezi, and Mr Saud Abdulsamad for their unwavering support and contribution to my research project. Their support and team spirit have been crucial to my success. I am also grateful to the University of Liverpool for fostering a conducive environment for scientific research, providing access to resources and facilities that facilitated my work. Finally, I would like to acknowledge the generous support of King Saud Bin Abdulaziz University for Health and Sciences (KSAU-HS) in providing and subsidizing my scholarship, which enabled me to pursue my doctoral studies.

Thank you all for your contribution to my academic and personal growth.

DECLARATION

The work presented in this thesis has not been previously submitted in support of an application for any other degree or qualification, either from this university or any other institute of learning.

DECLARATION OF ORIGINALITY

This thesis represents the culmination of my independent research conducted during my PhD studies in the Department of Molecular and Clinical Cancer Medicine (Cancer Biology) at the University of Liverpool between February 2019 and May 2023. The experiments presented in the results chapter were performed under the guidance and supervision of Professor Youqiang Ke, while all data analysis, interpretation, and conclusions drawn from the findings are solely my own.

Publications

Naeem AA, Abdulsamad SA, Rudland PS, Malki MI, Ke Y. Fatty acid-binding protein 5 (FABP5)-related signal transduction pathway in castration-resistant prostate cancer cells: a potential therapeutic target. Precision Clinical Medicine 2019;2:192-6

Naeem AA, Abdulsamad SA, Jin X, He G, Zhang J, Wei Q, et al. Epidemiology of Prostate Cancer in Saudi Arabia. New Frontiers in Medicine and Medical Research Vol 14 2021:18-36

Naeem AA, Abdulsamad SA, Al-Bayati A, Zhang J, Malki MI, Ma H, et al. Prostate Cell Lines. Journal of Oncology and Medicine 2022

Zhang J, He G, Jin X, Alenezi BT, **Naeem AA**, Abdulsamad SA, et al. Molecular mechanisms on how FABP5 inhibitors promote apoptosis-induction sensitivity of prostate cancer cells. Cell Biology International 2023

Table of Contents

12

List of Abbreviations

Abbreviation	Full name
ADT	Androgen deprivation therapy
AR	Androgen receptor
ARFL	Androgen full length
ARV7	Androgen splice variants 7
AR KO	Androgen knockout
Bax	Bcl-2-associated X protein
BCL-2	B-cell lymphoma 2
BPH	Benign Prostatic Hyperplasia
BMF	Bcl-2-modifying factor
CAV1	Caveolin-1
cDNA	Complementary DNA
CL	Cell lysate
CRIP2	Cysteine-rich intestinal protein 2
CRPC	Castration-resistant prostate cancer
CRISPR	Clustered regularly interspaced short palindromic repeats
CZ	Central zone
DBD	DNA-binding domain
DMSO	Dimethyl sulfoxide
EDTA	Ethylene diaminetetraacetic acid
EGR	Early growth response
FABPs	Fatty acid binding proteins
Abbreviation	Full name
FABP5	Fatty acid binding protein 5
FABP5-KO	FABP5 knockout
FBS	Fetal bovine serum

13

FOSB	FBJ Murine Osteosarcoma Viral Oncogene Homolog B
GRPR	Gastrin releasing peptide receptor
GS	Gleason scores
kDa	kilo Dalton
LBD	Ligand-binding domain
mRNA	Messenger RNA
MTT	3-(4, 5-dimethylthiazl-2yl)-2, 5-diphenylterazolium bromide
NR1H4,	Nuclear Receptor Subfamily 1 Group H Member 4
OD	Optical density
PBS	Phosphate buffered saline
PIN	Prostatic Intraepithelial Neoplasia
PPAR	Peroxisome proliferator-activated receptors
p-PPAR γ	Phosphorylated- PPAR γ
PSA	Prostate-Specific Antigen
PZ	Peripheral Zone
SDS-PAGE	Sodium dodecyla sulphate polyarcrylamide gel electrophoresis
TBE buffer	Tris-Borate-EDTA buffer
Sp1	Specificity protein 1
TBS-T	Tris Base Salt-Tween
Abbreviation	Full name
TZ	Transitional Zone
VEGF	Vascular endothelial growth factor

Chapter 1 : Introduction

1.1 Epidemiology of prostate cancer

1.1.1 Incidence

Prostate cancer (PCa) ranks as the second most prevalent form of cancer worldwide, with 1.1 million first-time diagnoses in 2012 (1). PCa has the highest prevalence of any cancer among the male population of the UK. From 2014 to 2016, an estimated 47,700 new cases of PCa were diagnosed annually. PCa accounted for 26% of all new instances of male cancer in the UK in 2016. Over the preceding 20 years, the case numbers have consistently risen. As indicated in **figure1**, among the 20 most prevalent cancer forms, PCa ranked second in terms of the number of new cases diagnosed annually in the UK (2).
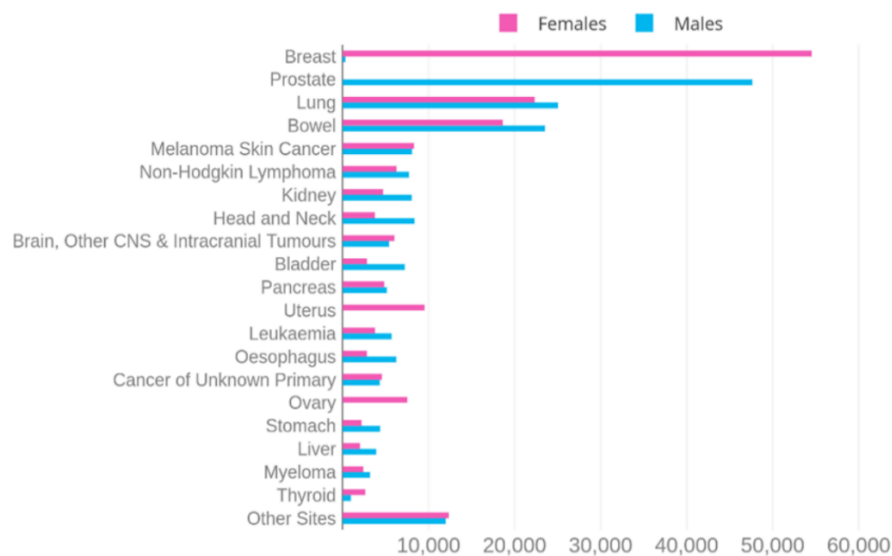
Figure1. Prevalence of prostate cancer (PCa) among the 20 most common cancer types in the UK. (2).

While in the past, it was widely considered that PCa was an illness affecting older males, of the mean age at diagnosis has decreased in recent years. According to an American study, the probability of developing PCa increases with age. Thus, males aged 39 had only a 0.005 percent chance of developing PCa, but the risk climbed to 2.2 percent and 13.7 percent, respectively, for men aged 40 to 59 and 60 to 79 (3).

As seen in **Figure 2**, the incidence of PCa was highest among males aged 75 to 79 years old. The incidence of PCa grows with the age of patients until they reach 79 years old, at which point it begins to decline until they reach 90 years of age (2).
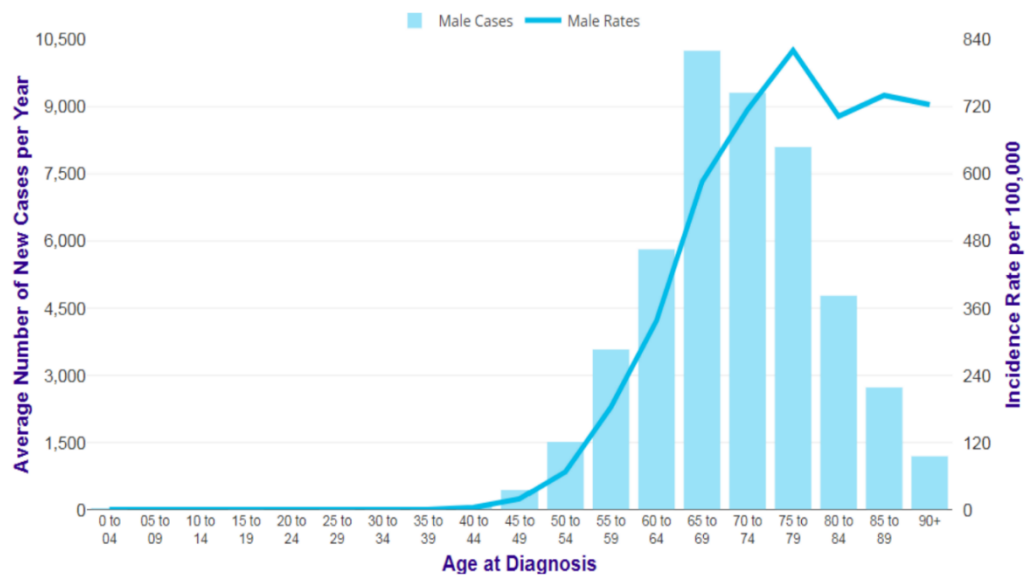
Figure 2. Age-specific incidence of prostate cancer (PCa) among males. This age-specific pattern demonstrates the age-dependent nature of PCa incidence, with a higher likelihood of diagnosis in older individuals followed by a gradual decrease in incidence in the later years(2).

The majority of PCa cases are diagnosed in industrialized nations, such as North American and Western European countries. As demonstrated in **figure 3**, North America, Oceania, West and North Europe had the greatest incidence of prostate cancer (4).
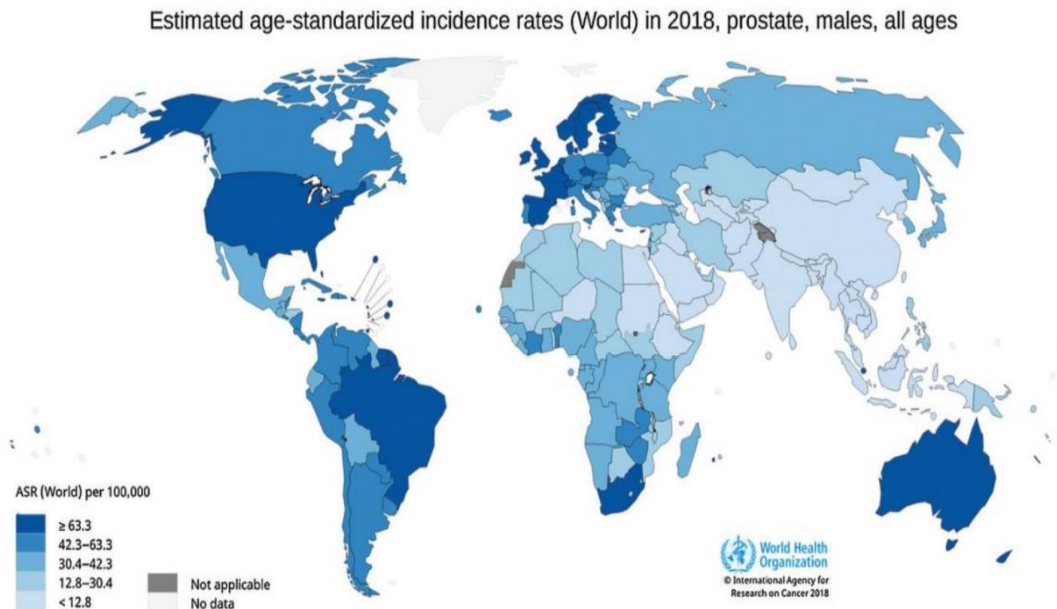
Figure 3. Incidence of PCa globally in 2018 (1). ASR: Age-standardized Rate/100,000**.**

1.1.2 Mortality

PCa leads to the second-highest mortality rate in British males of any cancer. There are around 11,700 fatalities annually, which equates to 32 deaths per day (2).Between 2014 and 2016, approximately 74% of prostate cancer deaths in the United Kingdom occurred in men aged 75 or older. The age-specific mortality rate began to rise as early as 55-59 and peaked among those aged 90 or older(**Figure 4)**.There is a clear correlation between age and PCa mortality, with deaths being greatest among the elderly(2,4).
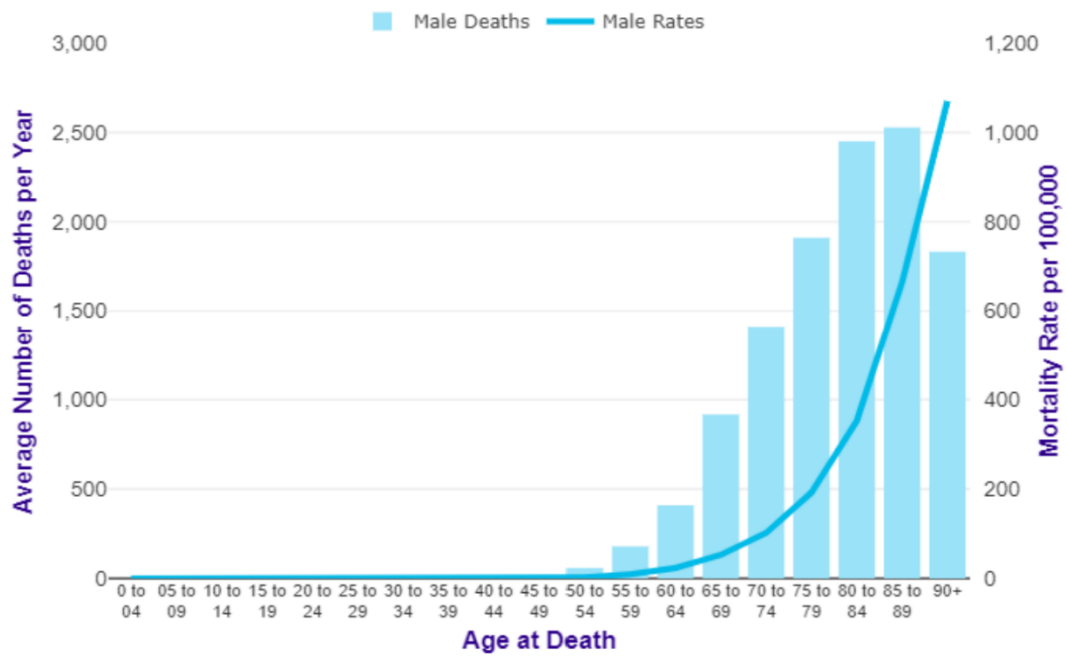
Figure 4. The average number of deaths related to prostate cancer and the mortality rates based on specific age groups in the United Kingdom between 2014 and 2016(2,4).

1.1.3 Survival

The anticipated ten-year survival rate for PCa in 2010 was 84 percent. As shown in **figure 5,** this rate has risen since 1970, increasing by 59% over a span of four decades, from 1971 to 2010. Currently, over eight out of ten men with an initial PCa diagnosis in England are anticipated to live for at least ten years. This may be a result of the public prostate-specific antigen (PSA) screen, as well as transurethral resection of the prostate (TURP) examinations (2,5).
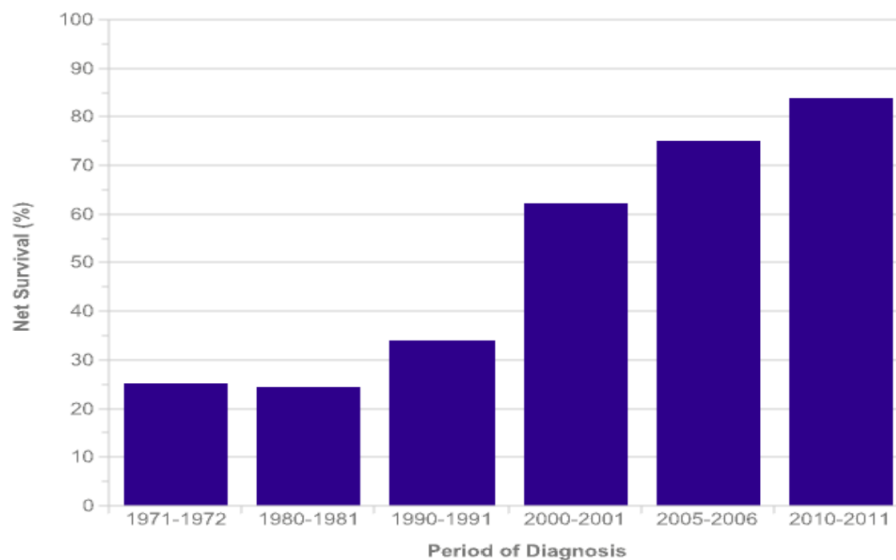
Figure 5. Trends in ten-year survival rate for prostate cancer (PCa) from 1971 to 2010. The graph demonstrates a significant increase in the survival rate since 1970, with a remarkable 59% improvement observed over this period. Presently, in England, over eight out of ten men diagnosed with PCa are expected to survive for at least ten years (2,5).

1.1.4 Risk factors

1.1.4.1 Age

Numerous studies have linked ageing to higher PCa risk. males between 75 and 79 have the highest PCa risk (2), while just 1 percent of people under the age of 50 were diagnosed with PCa, 20 percent of those of 50 and over were affected (6,7). Carter et al. found that the probability of malignant histological abnormalities in the prostate rose for older age groups, with 20% for the 50-to-60 category, and 50% for the 70-to-80 age group (8). It has been observed that men's chance of developing histologically undiagnosed PCa, clinical PCa, or fatal PCa is increased by percentages of 42, 9.5, and 2.9% respectively, when they reach age 50 (3).

1.1.4.2 Ethnicity

Different ethnic groups have varying PCa incidence rates. African-American males have been found to have the highest PCa risk, followed by white men. PCa risk is the lowest among Asian males. Numerous epidemiological studies examine the causes of risk variation amongst various ethnic groups, and it is currently unclear if socioeconomic, genetic, or environmental influences have a role in this phenomenon (9) (2). At least one study has suggested that PCa incidence levels among males migrating from Japan to North America more than 50 years ago was 43% greater than for those who had always resided in Japan. This study concluded that a westernized lifestyle, rather than hereditary factors, had greater impact on the risk of PCa (10). Dietary differences also contributed to the reduced PCa occurrence within the Asian population in comparison with the American one. It was hypothesized that Japanese men's use of isoflavonoid-containing foods such as soya beans may prevent them from acquiring PCa (3). Numerous studies suggest that African-American males have greater PCa prevalence and death rates than men of other ethnicities. Family history of PCa may contribute to the higher prevalence rate among this group, according to these studies. However, Makinen and colleagues

found no significant correlation between this factor and the greater incidence rate among African-American men (11,12). Genetic involvement was one of the explanations for the elevated incidence of PCa in particular ethnic groups. The genomic locus 8q24 was reported as a risk factor in PCa, being linked to a rise in risk of 8% in white Caucasian males, whereas African-American men had a 16% increased risk (13). More study is needed to assess ethnicity's role in PCa.

1.1.4.3 Family history

Compared with the baseline level, men for whom other family members have had cancer are at greater risk of developing PCa. If the PCa risk for a normal man is set as 1, the probability for individuals whose father, brother, or second-degree relatives have been diagnosed with PCa are 2.40, 3.30, and 1.80, respectively (2). Those who have PCa in their family histories have 6-7 years greater chance of getting the disease than males where this is not the case. However, research has postulated that, in addition to the possibility of genetic influence, there is a possibility that family members have been exposed to the same environmental unidentified conditions (14).

Smith et al. (1996) conducted research that revealed the presence of the HPC1 (hereditary prostate cancer 1) site, (located within chromosome 1, on its long arm) in Swedish and 22 American high-risk families characterized by the development of PCa at a younger age and the presence of five or more PCa-affected family members. However, a systematic meta-analysis comprising 772 hereditary PCa families indicated that HPC1 was only linked to 6% of families (10,14).

1.1.4.4 Diet

Numerous studies have sought to explain the relationship between fat consumption and PCa. High-fat foods were linked PCa occurrence, as was red meat consumption. An association has been found to link PCa to dietary fat levels in animals. According to a previous study, males who took linoleic acid were five times more likely to acquire PCa. An explanation put forward for increased PCa with high fat consumption was that fatty acids exert their influence on serum sex hormone levels, hence influencing the incidence of PCa (15,16). It was believed that using those men maintained a low PCa risk as control, Studies on Japanese immigrants to the US have been used to generate insights on influence from factors in the environment and in the diet. It was found that the men shifted to a high PCa risk group in line with the length of their stay in the USA. Another study examining the relationship between overall fat intake and PCa risk in African American and Asian American groups indicated a 15 percent greater prostate cancer incidence across African Americans (17-21). Although further research is necessary, there may be a link between red meat and PCa. Through activating insulin-like growth factor-1 (IGF-1), whose release from the liver is boosted when high levels of fats are consumed, fatty diets can also influence the development of PCa. IGF-1 can promote proliferation and inhibit apoptosis, as demonstrated by cohort studies in which males with greater IGF-1 levels showed 4.3 times the risk of PCa development (14,22).

1.2 Pathology in prostate cancer

1.2.1 Anatomical structure of the prostate

The prostate is part of the reproductive system in men, and forms a fibro-muscular gland surrounding the urethra and encapsulated by a thin covering forming a capsule. The gland is also covered from the front, back, and sides by three layers of a pseudo capsule. As illustrated in **Figure 6**, areas from above the gland extend around the neck of the
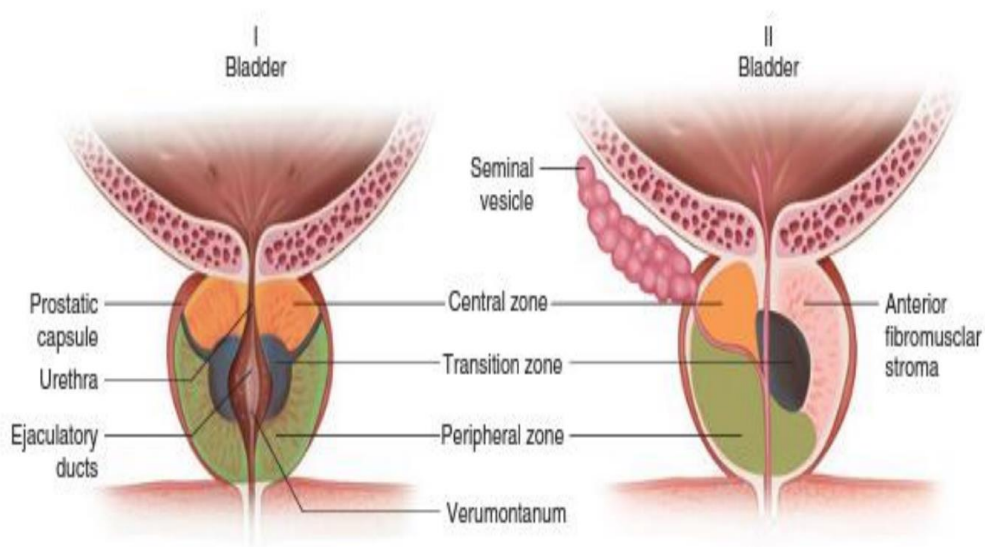
bladder. Within the gland are duct structures, stroma and basement membrane. The prostate has columnar channelling with secretory cells forming a lining. The prostate functions primarily to provide an electrolyte and protein supply to fuel prostatic fluid production. This fluid assists with the transport of sperm (23,24).

Figure 6. Anatomical representation of the three prostate gland regions in relation to the bladder (23).

There are three zones within the prostate: the transitional zone, central and peripheral zones. Seventy percent of this gland is composed of glandular tissue, while the remaining thirty percent consists of fibromuscular stroma tissue. Benign prostatic hyperplasia (BPH) predominantly occurs in the transitional zone (TZ) of the prostate, which constitutes 5%

of its overall volume. Ejaculatory ducts are in the central region, while 25% of this area consists of glandular tissues. Around 1-5% of PCa occurs in this zone. In contrast, the peripheral zone is seventy percent glandular tissue, and forms the prostate's sides and back, and a majority of prostate adenocarcinomas (70 percent) develop from this zone. This is the region that a digital rectal examination (DRE) test can detect. The central region of the prostate has a triangular form, the bottom of which is in continuity with the seminal vesicles, while the point of the triangle is the verumontanum (25-27)

1.2.2   Epithelial cells of the prostate

Three different cell types are found in the prostatic epithelium, each with a unique structure, function, and relationship to tumour progression. The most common form, as seen in **figure 7**, is the secretory luminal cell, which secretes prostatic proteins and is androgen dependent. As a result, secretory luminal cells express androgen receptor (AR) (28).
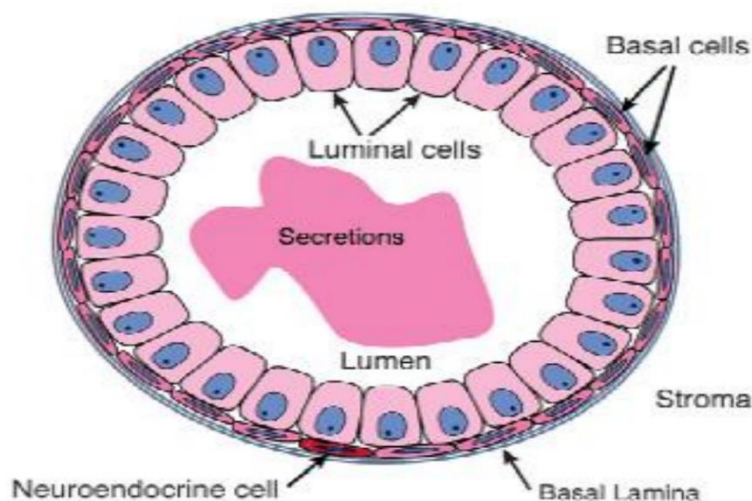
Figure 7. Prostate duct cell types (28).The basal cells are the second kind of cell, and they form a continual layer separating the luminal cells from the basement membrane. Neuroendocrine cells form a less common type. Neuroendocrine cells, due to their uncertain embryology origin, may aid in luminal cell proliferation via signaling. They are androgen-independent, frequently present in the basal layer, and express neuropeptides like serotonin. Regardless of their rarity, neuroendocrine cells are a distinguishing hallmark of aggressive PCa when they aggregate or acquire their traits (28).

1.2.3 Benign prostatic hyperplasia

Benign prostatic hyperplasia (BPH) is described as an enlargement of prostate cells which is not malignant. This condition occurs where prostatic epithelial cells located surrounding the urethra multiply, leading to excessive growth. In benign prostatic hyperplasia, enlargement of the prostate occurs, with growth of non-cancerous stroma and glandular tissues. Occurrence of BPH increases in older populations, and its source is not known, but the condition was originally thought to be stimulated through growth factor or hormones. Urine abnormalities such as high frequency, urgency, and so on are common in BPH patients. DRE or PSA is frequently used to diagnose BPH. BPH is thought to start within the submucosal layer of the transitional region. Compression of that area, which produces pain in the lower urinary tract due to surrounding the urethra (23,29,30).

1.2.4 Prostatic Intra-epithelial Neoplasia

The precancerous disease prostatic intra-epithelial neoplasia (PIN) is marked by the epithelial cell growth in the ducts without causing damage (23). These cells are different in their cytoplasm, architecture, nuclei, and nucleoli. These changes are only found in ducts and acini. PIN has both low grades and high grades, but the high grades are more common in males who have PCa. When it is found on a biopsy, the risk of discovering prostate cancer on a later biopsy goes up. However, occurrence of PCa in a later biopsy

does not go up with the low grade. High grade PIN might have patterns like tufting, micropapillary, cribriform, and flat forms (7).
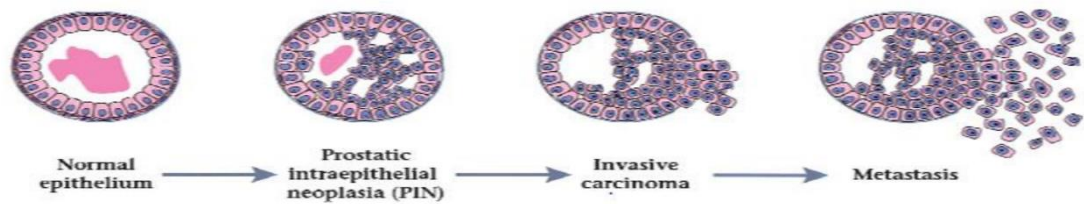
Figure 8. Showing how PIN and metastasis develop in prostate epithelium (28).

High-grade PIN has been identified as a pre-malignant lesion in studies for numerous reasons, including the fact that it is seen with deadly cancer in the peripheral zone, and that it predates carcinomas by a decade. HGPIN is structurally similar to cancer in that it damages the basal layer. In contrast, there are two distinguishing aspects that aid in the diagnosis of PIN, which are represented by the impossibility of PIN to pass through stroma due to its integrated membrane. Furthermore, because PIN has no effect on PSA, it is only found in tissue samples (28).

1.3 Gleason scale

For the last 50 years, the approach proposed by Gleason has been widely utilized across the globe for histological assessment of prostate cancer. This categorization was developed based on structural characteristics and increased mitosis. Carcinomas are classified from 1 to 5, indicating the degree of malignancy of the tumour. As seen in **figure 9**, Gleason grade 1 indicates the lowest level of malignant carcinoma, whereas Gleason grade 5 represents the greatest (31).
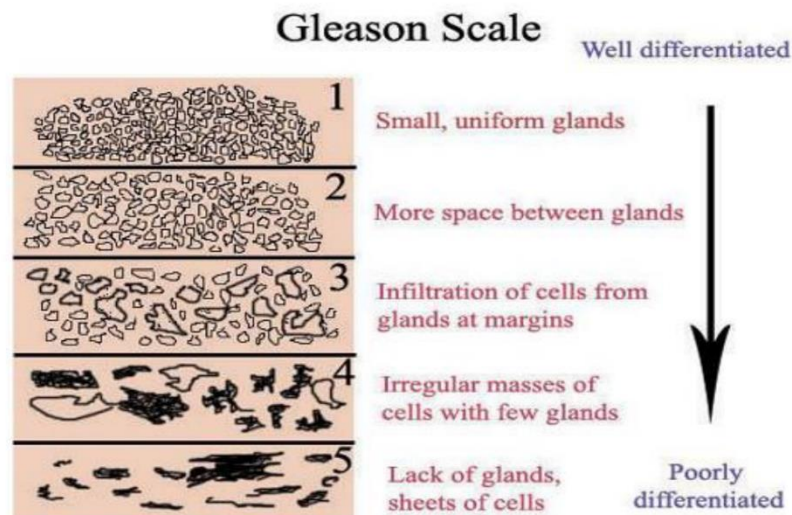
Figure 9. Gleason grading ranges from 1 to 5, with 1 being the least malignant and 5 being the most malignant alterations (32).

Multiple lesions are frequently identified in the same individual, owing to the variability of PCa. Also, because the Gleason grading method cannot fully capture the heterogenic character, the Gleason scale system was developed. A prostate carcinoma's combined Gleason scale comes from the Gleason grade for the major lesion in addition to the Gleason grade of the second biggest lesion in the same instance. As a result, the lowest combined Gleason scale is 2. Rising combined scores indicate a rise in disease malignancy, and the highest combined Gleason scale, at 10, reflect the most malignant cases, which often have a very poor prognosis (28). The most frequent lesion in a PCa case is the 'primary lesion,' while the next most frequently-occurring lesion is referred to as the 'secondary lesion.' PCa is classified or diagnosed based on the histological appearance of cancer cells as well as clinical behaviour (6).

1.4 Prostate cells line

In this research, six prostate epithelial cell lines were employed. PNT2 is a benign prostatic cell line, LNCaP is a line with weak malignancy, 22RV1 exhibits moderate malignancy, and DU145, PC3 and PC3M are extremely malignant lineages. A benign

line, PNT2, comes from normal prostatic tissue from a 33-year-old male with no history of prostatic disease. Transfection of simian virus 40 plasmid was used to create a stable cell line in order to immortalize the cells. These cells retain typical epithelial tissue characteristics, as evidenced by the expression of cytokeratins 8, 18, and 19, members of the Keratin family (33-35).The LNCaP weak-malignancy line was produced from a metastasis within the left supraclavicular lymph node occurring in a Caucasian male, fifty years old, who had primary PCa, in 1980. The cells were first extracted from the metastasis using a needle aspiration biopsy. Because AR and PSA expression is found in LNCaP: the cell line is classified as androgen-responsive (36). Because of this androgen responsiveness these cells can be used as a model for androgen research when cultured in culture media with testosterone-containing foetal bovine serum. However, it has been observed that in an androgen-free environment (for example, when charcoal-striped foetal bovine serum was used instead of serum albumin), these cells proliferate independently of androgen (37-39). A 1999 xenograft taken from a male who had bone cancer metastasized from the initial prostate cancer, and this was used to produce the moderately malignant PCa cell line 22RV1. PSA and AR were both expressed by these cells (35,39,40). DU145, a highly malignant prostate cancer cell line, came from a brain metastasis taken in 1975 from a 69-year-old Caucasian male with an extensively distributed PCa. There is no PSA or AR expression in this cell line. When nude mice were subcutaneously injected with cells from this line, the resulting tumour retained both genotypic and phenotypic characteristics of prostate (25,41,42), 196). The highly aggressive PC3 PCa cell line was created in 1979 from the rib metastases from a 62-year-old Caucasian man with PCa. These cells, like DU145, do not generate AR or PSA. Furthermore, several studies reveal that these cells resemble small cell carcinomas or neuroendocrine tumours (16,39,43,44). The most malignant subset of PC3 cells was used to create the highly malignant cell line PC3M. When PC3 xenografts of athymic mice

were created using PC3 cell injection, a portion of the xenografts were excised and cultured in primary tissue. This procedure was done several times, and PC3M cells were created from the mouse xenografts, implying that the PC3M cell line is more malignant than its mother cell line, PC3 (39,45).

1.5 PCa with and without androgen dependence

1.5.1 Androgen-dependent prostate cancer

Androgen exerts a major effect on how the prostate gland develops, grows, stays healthy, and works. The most common androgen in men is testosterone, which is made almost entirely in the testes. The last 5% of testosterone is provided by the adrenal glands (46), while androgen creation and release is controlled by the hypothalamus, sending out luteinising hormone-releasing hormone (LHRH) pulses when testosterone level in the blood drops. When the LHRH receptors of the pituitary gland are stimulated, more luteinising hormone (LH) is made and released into the blood. This leads Leydig cells to make more steroid hormones. In the prostate gland, 5-alpha-reductase enzymes change testosterone into an active form called dihydrotestosterone (DHT). This helps prostate cells grow and stay alive (46,47). Through binding to the AR, DHT moves it away from heat shock proteins. Next, the receptor makes two copies of itself and is phosphorylated (48). Within the nuclear region of the cell, activated receptor is bound to androgen response elements (AREs) within several target genes' promoter regions, including prostate-specific antigen (PSA), as well as regulating transcription (49,50).

For PCa, radical prostatectomy and radiation therapies have the highest rate of success when the tumour is in the localised stage (51). Standard therapies to treat locally advanced and metastasising PCa are androgen deprivation therapy (ADT), which can be accomplished through anti-androgen therapy, surgical/medical castration, or combined androgen blockade. This treatment can ultimately suppress androgen signalling (52).

While ADT is a successful therapy which is capable of inducing clinical response in 80–90 percent of patients, the cancer can nevertheless progress to androgen-independent PCa after two to three years as a median (53). In the vast majority of instances, AR expression is retained in androgen-independent tumour cells.

1.5.2 Androgen-independent PCa

Androgen-independent prostate cancer, commonly termed castration-resistant prostate cancer (CRPC), refers to a stage of illness which is not sensitive to castration, and with poorer prognoses as well as shorter survival duration from recurrence (54,55). Discovering molecular pathways important in the transformation in status from the androgen dependent to androgen-independent prostate cancer cell forms the foundation for development of novel therapies in CRPC. These pathways are as yet unknown. Nonetheless, various processes may lead to CRPC formation.

1.5.3 Molecular mechanisms in CRPC

CRPC results from the adaptation of PCa cells to surroundings deprived of testosterone. Most laboratories that have investigated the progression of CRPC from diverse perspectives have focused on the molecular pathways underlying its progression. Since the 1941 discovery of Huggins and Hodgkins that the disease is androgen-dependent, standard therapy for PCa in men has been ADT (55). Initially, a majority of males who have PCa respond positively to ADT. However, due to the development of CRPC cells, almost every patient will have a recurrence. Most of these cells go on expressing androgen-responsive genes, e.g. PSA, commonly expressing AR. The CRPC cell is aggressive and can survive and grow in a low-androgen environment or in the absence of any androgen. At this point, ADT has been rendered ineffective, metastases have spread, and curative treatment is no longer practicable. In recent years, multiple molecular mechanisms linked with ADT have been identified, and it has become apparent that different pathways which are AR-dependent or -independent are responsible for CRPC

cell migration. Progression of CRPC results from adaptation of prostate cancer cells to no-testosterone environments.

1.5.4 AR-dependent signalling pathways and CRPC

Androgen receptor is a ligand-dependent transcription factor within the steroid hormone receptor group. It comprises many functional domains, including ligand-binding and DNA-binding domains, a large N-terminal domain (NTD) and a hinge region (56). PSA expression is regulated by androgen response components in AR for the great proportion of CRPC patients (57). Furthermore, the continual androgen receptor activation in CRPC is found to be one of the more important cellular processes in CRPC proliferation (58). Irrespective of castration and the resulting decrease in blood androgen levels, CRPC patients' tissue testosterone or dihydrotestosterone levels are comparable with those of individuals prior to ADT (59). Multiple alterations at the cell and molecular level are associated with developing CRPC, such as amplification and mutation of AR, AR-ligand signalling, AR splice variants, and abnormal AR co-regulation factors (60).

1.5.5 Androgen receptor overexpression/amplification in CRPC

AR gene amplification forms a significant mechanism for sensitising CRPC cells to low levels androgen circulation, promoting CRPC development. The rate of AR gene amplification rose by between 20 and 30% for CRPC patients following ADT, although relatively low numbers of occurrences were identified for original PCa with no treatment (61). ADT might cause AR to be amplified within the CRPC cell cytoplasm, allowing tumour cells to respond to lower androgen levels, allowing these cells to maintain androgen-dependent growth despite castration (62). AR gene amplification has been found to be related to significant increases in proteins and mRNA level within CRPC tissue (63). Furthermore, amplified AR sensitivity is demonstrated to arise more frequently in cases where the patient originally reacted favourably to ADT, less frequently being observed for ADT-unresponsive individuals (61). Reduced retinoblastoma protein

(RB) and enhancement in E2F activity have also been linked to the overexpression of AR (64). AR amplification was observed in just a subset of people with CRPC, indicating that this does not form the sole mechanism involved in CRPC pathogenesis.

1.5.6 Mutation of AR in CRPC

The Androgen Receptor Gene Mutations Database reveals that AR contains the highest number of variants of any hormone receptor, having over 1110 distinct mutations, and 168 of those are linked to prostate cancer (65). Mutation in AR is extremely uncommon during early-stage PCa, yet was found in roughly 10-30% of individuals undergoing ADT treatment (66). Researchers have hypothesized a role for ADT in exerting selection pressure leading to a rise in AR mutations (67). The LBD (94 percent) or the NTD (40 percent) are most commonly affected by mutations, whereas the DBD (7 percent) and hinge area are affected less frequently (2 percent). AR gene mutation can boost the development and survival of CRPC cells at extremely low levels of androgens (68). The T877A mutation was identified in LBD and is present for approximately 33% of CRPC patients (69). LBD mutation lowered specificity in permitting prostate cells to grow independently of androgen, as well as letting binding of AR and its triggering by various usually-present ligands, such as oestrogens, corticosteroids, progesterone, and flutamide, which is an androgen antagonist (61,70). A number of additional LBD mutations, including L701H, H874Y, V730M, and W742C, made AR more sensitive to normal amounts of different hormones: e.g. glucocorticoids (71). Although the majority of mutations were detected within the LBD, NTD and DBD mutations occurred as well (8).

1.5.7 AR-associated co-regulators and collaborating factors in CRPC

AR-coregulator interactions form an additional essential mechanism for CRPC progression. Approximately fifty AR-associated coregulators have been discovered as being abnormally expressed in CRPC throughout the past decade. Deregulated expression

of co-regulator proteins can change AR's transcriptional activity via direct interactions with AR/AR transcriptional complex components. Co-regulators can be separated into 2 kinds: co-enhancers (like p160/steroid receptor coactivators (SRCs) and CBP/p300); and repressors (like NCoR and SMRT) (72). Different strategies are utilised by co-regulators to modulate AR transcriptional output. These processes include alterations in chromatin structure, facilitating RNA polymerase transcriptional machinery interactions, enzyme-mediated control of histone activity, and enzyme-mediated modulation of AR-bound chaperone function (73). The family of p160/SRCs is responsible for mediating transcriptional actions in transcription factors and nuclear receptor structures. SRC-1, SRC-2, and SRC-3 are SRC members, a group linked with PCa development (74). SRC1 has been identified as a crucial factor for induction of AR activation through IL-6 in CRPC (75).There is a direct relation between overexpressed SRC-3 and poor differentiation and advancement of PCa (76). In addition, CBP/p300 is demonstrated as essential to ligand-independent AR transactivation within the CRPC cell (77). In contrast, lower amounts of co-repressors have been identified in CRPC (78). Analysis of androgen-binding sites across the PCa cell's genome has led to evolution of components that contribute to AR transcriptional activity. Bioinformatics investigations of androgen-binding sites found enriched DNA sequencing with motifs for many cooperating components, such as FoxA1, GATA2, and OCT-1 (79). Cooperating factors' roles are linked with both their capacity to interact directly with AR, and also to their ability to operate as pioneering factors for androgen receptors at transcriptional regulatory locations (80). FOX proteins, particularly subgroup FOXA1 and GATA2, are demonstrated to have a significant function within CRPC by modulating AR expression (81,82).

1.5.8 CRPC AR splice variants

Multiple AR splice variants (AR-Vs) are found within cell, xenograft, and tissue samples in CRPC (83,84). AR-Vs with missing LBD, as targeted by androgen treatment, are

demonstrated to result in ligand-independent constitutive AR activation, causing CRPC to develop (85). The processes responsible for enhanced AR-V7 expression within the CRPC cell remain unclear. Genetic reorganisation at the AR gene locus, as well as/or intragenic deletion are potential causes for splicing (86). AR-V7 and ARV567ES are the most prevalent variations discovered, and when they are strongly expressed, this is linked to poor prognoses for the CRPC patient (87). AR-V7 is highly expressed within CRPC cell lines, as well as in patient tissue samples (87,88). ARV-7 levels cannot be decreased in mice, although ADT with abiraterone acetate and enzalutamide may improve them (89). AR-V7 has been identified for potential targeting in CRPC treatment (90).

1.5.9 Post-translational changes to AR in CRPC

Post-translational changes are typically responsible for ligand-independent AR activation, which is associated with prolonged AR activity. AR is known to undergo several post-translational changes, such as phosphorylation, acetylation, ubiquitination, simulation and methylation. Phosphorylation is more extensively researched among these processes. Most post-translational changes occur within AR's activation function-1 (AF1) region, containing transcriptional activation unit 1 (TAU1) and 5 (TAU5) (91). When no androgen is present, growth hormones, such as IGF-1, keratinocyte growth factor (KGF), epidermal growth factor (EGF), and IGF-I are responsible for direct activation and phosphorylation of AR in CRPC (92,93). Moreover, CRPC cells are found to exhibit an exceptionally large quantity of RTK HER-2/neu receptor tyrosine kinase, as potentially triggered by several growth factors. Overexpressed RTK HER-2/neu stimulated the androgen receptor pathway where androgen was missing or present at low concentrations (94). Additionally, protein kinase A (PKA) has been shown to be capable of phosphorylation and activation of the receptor for androgens (95). Numerous serine/threonine and tyrosine kinases have roles in phosphorylating androgen receptor,

but tyrosine kinase (Ack1) is remarkable in that it increased castration-resistant proliferation in the LNCaP cell line (96).

1.5.10 Androgen receptor transcriptional activity in CRPC

Androgen and other proteins are expressed under the control of many processes (transcriptional and translational processes, and post-translational modifications). Moreover, transcription is believed be crucially involved in expressing genes. During CRPC progression, the transcriptional activity of the AR is altered, and many genes promoting cell proliferation/survival are found to be abnormally regulated. Many of the targeted AR genes increased by ADT had been absent prior to therapy, suggesting that the androgen signalling pathway was reactivated in conditions of low or no androgen (97). In addition, it is postulated that various other carcinogenic pathways could have crucial functions in generating androgen receptor signalling, hence enhancing androgen receptor response in a low-androgen environment (98). Overexpressed E2F transcriptional factor and reduction in retinoblastoma protein (tumour suppressor) jointly enhanced LNCaP cell androgen receptor transcription, potentially resulting in androgen-independent activation for numerous genes stimulated by androgen receptor (64). Dependent upon the degree to which it is expressed, androgen may function to enhance or repress transcription in downstream regulatory target genes in AR signaling. Lysine-specific demethylase 1 (LSD1) recruitment in androgen-dependent cells suppressed expression of the AR gene when the androgen-binding ARBS2 enhancer inside the AR gene's intron 2 was elevated. On the other hand, lowered amounts of androgen within CRPC cells can result in increase in the androgen enhancer component stimulation as well as increases in transcriptional activity of the AR gene, while not stimulating suppressor components. Thus, decreased androgen levels could promote the androgen expression as well as androgen-repressed genes assisting with CRPC cell androgen production, proliferative activity and DNA synthesis (99).

1.6 Possible markers for prostate cancer prognosis and diagnosis

Digital rectal examination (DRE) and prostate-specific antigen (PSA), as well as additional histological staging biopsies are used for prostate cancer diagnosis and are important factors to be considered when generating treatment options (100). In practice, each of these approaches has limitations that can cause overtreatment of low-risk individuals (101), needless biopsy, and unnecessary radical prostatectomy (102,103). Major biomarkers can be utilized to aid in individually produced treatment plan design for earlier detection of advanced illness and prediction of metastasis and recurrence after prostatectomy. Biomarkers are described by the National Cancer Institute as "biological molecules detected in blood, other bodily fluids, or tissues that indicates a normal or aberrant process or illness" (104). Therefore, the optimal biomarkers are required for screening for the illness and its course, for identification of high-risk patients, forecasting relapse and assessing therapy responses. Moreover, biomarkers must be cost-effective, not require invasive procedures, reliable, readily available, and simply quantified (105).

1.6.1 Prostatic Acid Phosphatase and Prostatic Specific Antigen

The dimer glycoprotein known as prostatic acid phosphatase (PAP) is generated primarily through the prostate, and was formerly employed as a blood biomarker for diagnosing metastatic PCa (106): however, it has been substituted for prostatic specific antigen (PSA) because it has limited sensitivity in detecting localised illness (107).

Release of this 33 kDa serine protease (human kallikrein-3) occurs in prostate epithelial cells. The *PSA* gene, which is 6 kb in size and situated on chromosome 19, encodes for a single chain 33 kDa glycoprotein (108). This is released into secretory ducts by the prostatic epithelium as a component of seminal fluid, liquefying seminal coagulum through cleavage of semenogelin proteins to form tiny peptides, making sperm more motile (109). On the other hand, rupture of the basal-cell layer in PCa permits the escape of PSA into circulation, which leads to higher serum PSA. Non-cancerous BPH,

prostatitis, dietary changes, certain drugs, and some surrounding conditions can all raise PSA levels in the blood, although other human cancers seldom do (110,111). PSA levels cannot be used to discriminate malignancies from benign illnesses, and they cannot differentiate by disease stage. Hence, PSA testing does not give good sensitivity or specificity for making appropriate treatment decisions (112). Using the standard PSA cut-off value for screening trials (4 ng/mL) as a prostate biopsy indication, PSA was assessed as around 40-50 percent sensitive and 60-70 percent specific (113-115). Further research has found that employing a 10 ng/ml cut-off increased the sensitivity to 72% and specificity to 95% in detecting prostate cancer (115). While the PSA biomarker is now utilized in diagnosis and prediction of PCa across the world, certain major clinical trials threw doubt on the efficacy of population-wide for PSA in identifying cancer cases (116,117). The PSA was modified to improve diagnostic accuracy by assessing multiple molecular PSA types and the PSA rise rate as total PSA (tPSA). tPSA is total unbound PSA as well as bound PSA (mostly complexed to -1-antichymotrypsin) (118). Despite the fact that tPSA level is heavily impacted by unbound PSA levels, this nevertheless caused a significant number of false negatives or positives (119). Because PSA screening efficacy remains debated, there is critical need to identify biomarkers with greater specificity and sensitivity.

1.7 Biomarker candidates

Biomaterials which might be utilized to discover PCa biomarkers include blood, urine, sperm, and prostate tissue. Serum proteomics analysis provides a valuable tool in identifying biomarkers, limited by the vast quantity of proteins present. A further challenge with the technique is identifying proteins which are not abundant, owing to their being masked by more abundant protein types. There are also different issues with serum proteomics, such as interference caused through excessive quantities of salt or other substances, severe variability across people, and a lack of repeatability (120). Semen

forms a very non-invasive source for analysing prostate biomarkers, as prostate-derived proteins may be readily accessible; nonetheless, this differs between persons. Because of its non-invasive nature, urine is also a prominent source for finding proteome biomarkers. The issue with utilizing urine is that it often has low concentrations of biomolecules, however (105). Genomic analysis is commonly utilized to investigate biomarkers. A genome-wide study is able to identify patients at high risk of cancer. Germline genetic markers are often utilized since they are present in unchanging levels across time and may be tested irrespective of age (121). Identification of biomarkers and comprehension of fundamental pathways functioning in cancer are critical in developing novel, enhanced diagnostic and prognostic approaches. Various possible biomarkers for prostate cancer were found, and investigated for predictive power. As well as PSA, numerous additional biomarkers have been identified and explored for their diagnostic and prognostic value in prostate cancer (122). These identified biomarkers include Cell-free DNA (cfDNA) or circulating tumor DNA (ctDNA)(123) , breast cancer mutant gene BRCA1/BRCA2 (tumour suppressor) (124,125), prostate cancer antigen 3 or PCA3 (non-coding RNA) (126,127), TMPRSS2- ERG fusion gene Transcription factor (128,129), early prostate cancer antigen 2 or EPCA2 (nuclear matrix protein), the cytokine Interleukin-6 (IL-6) (130-132) transforming growth factor 1 (TGF 1) (133,134), proteins in the S100 (Calcium-binding protein family) (135,136), PSCA (glycoprotein) (137,138), PPARs (139), and the Fatty acid binding proteins (FABPs)(140).

1.7.1 Cell-free DNA (cfDNA) or circulating tumor DNA (ctDNA)

Circulating tumor DNA (ctDNA) in prostate cancer refers to fragments of tumor-derived DNA that are present in the bloodstream of individuals with prostate cancer. Prostate cancer cells release ctDNA into the blood as a result of tumor cell death, apoptosis, or active secretion. ctDNA in prostate cancer can serve as a valuable biomarker for various aspects of disease management. Its detection and analysis can

provide insights into the genetic alterations, genomic profile, and clonal evolution of prostate tumors. This information can be used for several purposes, including early detection, monitoring treatment response, assessing disease progression, detecting minimal residual disease, and identifying the emergence of resistance to therapy.

The use of ctDNA as a biomarker in prostate cancer holds promise for personalized treatment approaches, allowing for more precise monitoring and targeted therapies. However, further research is needed to optimize the sensitivity and specificity of ctDNA analysis in prostate cancer and to determine its clinical utility in routine practice(141,142).

1.7.2 BRCA1/2 gene mutations

The BRCA1 and BRCA2 genes inhibit tumour growth. Mutations in germ-line BRCA2/BRCA1 cause an inherited breast/ovarian cancer syndrome, and this is further linked to an 8.6 times and 3.4 times increased respective risk of prostate cancer for males younger than 65 (143,144). According to studies, a broad range of pathogenic BRCA2/1 mutations gave phenotypes of PCa with heightened aggressiveness, leading to an increased likelihood of local progression in metastasis. In addition, a BRCA2 mutation has been identified to form a prognostic marker related to a lower prognosis for survival (125). Among PCa patients, 1.2% and 0.4% were found to have mutations in germ-line BRCA2 and BRCA1, respectively (143,144).

1.7.3 Prostate cancer antigen 3

 Prostate cancer antigen 3 (PCA3) is in commercial production as a biomarker for diagnosis of prostate cancer. It is noncoding RNA which can be found solely within the prostate, being found within prostatic fluid and urine. PCA3 testing presents a more intrusive compared to blood testing since the prostate must be digitally stimulated before collecting the urine sample. PCA3 is overexpressed among 95% of the biopsy tissues of

individuals with prostate cancer against BPH or healthy cohorts (126). In comparison with serum PSA (47% specificity with 65% sensitivity), urinary PCA3 levels of more than 35 units is documented at 66% sensitivity and 76% specificity on average in diagnosing PCa (127). The test's reliability depends upon a complete DRE prostate massage immediately prior to obtaining a urine specimen, which is unpleasant and variable depending on the examining professional.

1.7.4 TMPRSS2-ERG gene fusion

TMPRSS2-ERG forms the most common PCa gene fusion, with a specificity of more than 90% and a positively predictive value of 94% (128). Sadly, there are no diagnostic tests available clinically for this marker, and existing research does not find predictive importance for TMPRSS2-ERG analysis, and results are unclear in terms of outcome (128). TMPRSS2-ERG gene fusion was discovered in individuals who had a favourable outlook , but there is no link with incidence of prostate cancer and Gleason scores in patients with a positive diagnosis (129,145).

1.7.5 Early prostate cancer antigen 2

early prostate cancer antigen 2 (EPCA2) is a nuclear structure protein and has an association with adenocarcinomas of the prostate. Detection of Serum EPCA2 is possible, and higher blood concentrations are connected to tumour growth and poorer prognoses (131). According to certain research, EPCA2 expression may arise early in the development of cancer, making it a possible biomarker for predicting the beginning of incidental prostate cancer: yet, in patients with PCa, EPCA2 tissue stain and plasma EPCA absorbance did not show association with stages of tumours or Gleason score (130).

1.7.6 Interleukin-6

In some cancers, Interleukin-6 (IL-6) shows involvement with the host immune defence system to mediate B cell differentiation and control differentiation and growth (146).

Through blocking cancer cells from apoptosis, activation of angiogenic activity, and development of treatment resistance, overexpression of IL-6 is demonstrated to contribute to tumour growth. Patients who have advanced-stage tumours in many malignancies: for example, multiple myeloma, Pca, non-small cell lung cancer, colorectal cancer, renal cell carcinoma, and breast and ovarian cancers, a shorter survival time is associated with elevated blood IL-6 concentrations. In individuals with high IL-6 levels, responsiveness to hormone therapies and chemotherapeutic approaches was less pronounced than in patients who had a lower level (147). Therefore, inhibiting IL-6 signaling may be explored as a viable treatment method (i.e. anti-IL-6 therapy) for individuals with pathologically elevated IL-6 levels. To establish the therapeutic effectiveness of anti-IL-6 treatment in human cancer, more studies in xenograft tumor models are required (132).

1.7.7 Transforming growth factor β1

Transforming growth factor β1 (TGF β1) regulates cell proliferation, chemotaxis, immunological responses, angiogenesis and differentiation. TGF β1 expression was identified as associated with high-grade tumours, invasive activity and the cancer metastasising to regional lymph nodes and bone, as well as biochemical recurrence in prostate cancer (133). More study is needed before a decision is made on whether TGF β1 is a suitable marker for Pca (148).

1.7.8 S100 Proteins

The multigene calcium-binding protein group, or S100 protein family, is essential in the cell for phosphorylating protein, enzymatic function, and calcium homeostasis. In addition, this group regulate transcriptional factors, macrophage activators, and cell proliferation modulators (149). Recent studies showed their implications in several intra- and extra-cellular processes, such as cell growth, cell-to-cell communications, energy consumption, and intracell signal transduction (150). In addition, differential expression

across malignant and normal tissue was evaluated, and their role in the metastatic process was identified (136). S100 genes have been identified so far on human chromosome 1q21, which is often altered in various cancers . Several members of the group, notably S100A2, S100A4, S100A8, S100A9, and S100A11, have been linked to Pca recurrence and the disease progressing to a more advanced stage (135,151,152). Despite the fact that overexpressed S100A4 has been discovered within tissue and cell-line prostate cancer material, it is not substantially linked to lowered survival (153).

1.7.9 Prostate Stem Cell Antigen

The glycosylphosphatidyl-inositol prostate stem cell antigen (PSCA), which is part of the Thy-1yLy-6 family, contributes to control of proliferation. Its expression has been identified as increased for prostate cancer xenografts irrespective of androgen dependence or independence, and it is linked to PCa Gleason score, advanced stages of disease and metastasis distribution (154,155). PSCA's precise biological role is unclear: however, it is positioned on the cellular surface, offering a potential diagnostic and treatment target (105). The way PSCA is expressed in prostate cancer gives support to the idea of malignancies as caused by basal cell transition (156). However, in order to use PSCA as a serum marker, improved detection and measurement procedures must be developed (155).

1.7.10 Peroxisome proliferator-activated receptors

Peroxisome proliferator-activated receptors (PPARs) are a type of nuclear receptor, ligand-activated transcription factor that was discovered in the Xenopus frog in the early 1990s as receptors that activate peroxisome proliferation in cells (139). PPARs have a role in control of catabolising fatty acids, storing lipids, and metabolising glucose. PPARs can be classified into 3 isoforms: PPARα, PPARβ, and PPARγ. PPARs arise in a variety of tissue types, and exhibit a variety of functions that are related to cancer progression (139).

1.7.11 Fatty acid binding protein family

Several studies revealed a relationship between strong prevalence of clinical prostate cancer and high dietary fat consumption in Western industrialized countries. Fatty acids, in addition to supplying energy, are cell signalling molecules, controlling the way genes are expressed, as well as proliferation and cell death (153). Fatty acids have high solubility after they are released from fat cells into aqueous cytoplasm. These free fatty acids may be passively diffused or transported, and flow across the plasma membrane. When they enter cytoplasm, the fatty acids can join metabolic pathways or become bound to intracellular FABPs, to be transported to other organelles. FABPs in the cytoplasm bind lipophilic components including long chain fatty acids, retinoids and eicosanoids, and have strong affinity (157). FABPs have 12 members, as shown in Table 1.

Table 1. Chromosomal location and distribution of human FABP genes.

Gene	Chromosomal location	No. of amino acids	Protein localization
FABP1	2p11	127	Liver, intestine, pancreas, kidney, lung and stomach.
FABP2	4q28–q31	132	Intestine and liver.
FABP3	1p33–p31	133	Cardiac and skeletal muscle, brain, kidney, lung, stomach, testis, adrenal gland, mammary gland, placenta, ovary, brown adipose tissue.
FABP4	8q21	132	Adipocytes, macrophages, dendritic cells, skeletal muscle fibres and prostate.
FABP5	8q21.13	135	Skin, tongue, adipocyte, dendritic cells, mammary gland, stomach, intestine, kidney, lung, heart, skeletal muscle, testis, retina, lens, spleen, placenta and prostate.
FABP6	5q23–q35	128	Ileum, ovary, adrenal gland, stomach
FABP7	6q22–q23	132	Brain, central nervous system (CNS), glial cell, retina, mammary gland
FABP8	8q21.3–q22.1	132	Peripheral nervous system, Schwann cells
FABP9	8q21.13	132	Testis, salivary gland, mammary gland.
FABP12	8q21.13	140	Retinoblastoma cell, a retina (ganglion and inner nuclear layer cells), testicular germ cells cerebral cortex.

FABPs are small proteins that are produced within cells. Their molecular weights are all around 15kDa. all FABP members are distinct in their pattern of expressed tissue. Despite the fact that FABPs were named after the tissue in which they were discovered, none of them are located in only one tissue or kind of cell. In fact, some tissues have several FABPs, implying that they serve diverse roles. Some FABPs are exclusively present in several tissues, whilst others are prevalent in a variety of cell types. Liver FABP (FABP1), for example, has extensive expression in the liver, as well as being detected in the gut, kidneys, pancreas, and lungs. E-FABP (FABP5), on the other hand, is one of the most abundant FABPs. Skin tissues, the tongue, adipocytes, macrophages, dendritic cells, mammary glands, brain, gut, kidneys, liver, lungs, heart, skeletal muscle, spleen, testes, retinas and lens are all home to it (158). FABPs are abundant in hepatocytes, adipocytes, and myocytes compared to other organs (159). This is due to the fact that fatty acids are essential substrates for lipid production, storage, and degradation in these cells. When the quantity of fatty acids increased, FABP was more strongly expressed for the majority of kinds of cell (160). The findings reveal FABP responsiveness to a higher level of fatty acids by initiating signalling pathways that affect how cells behave.

1.8 Structures of fatty acid binding proteins

Nuclear magnetic resonance, X-ray crystallography and other methods are employed to examine FABP structural features. The sequence diversity of FABP members varies widely, ranging from 17 to 67 percent (161). As shown in **figure 10**, despite the sequence changes amongst different FABPs, their three-dimensional architectures are quite similar.
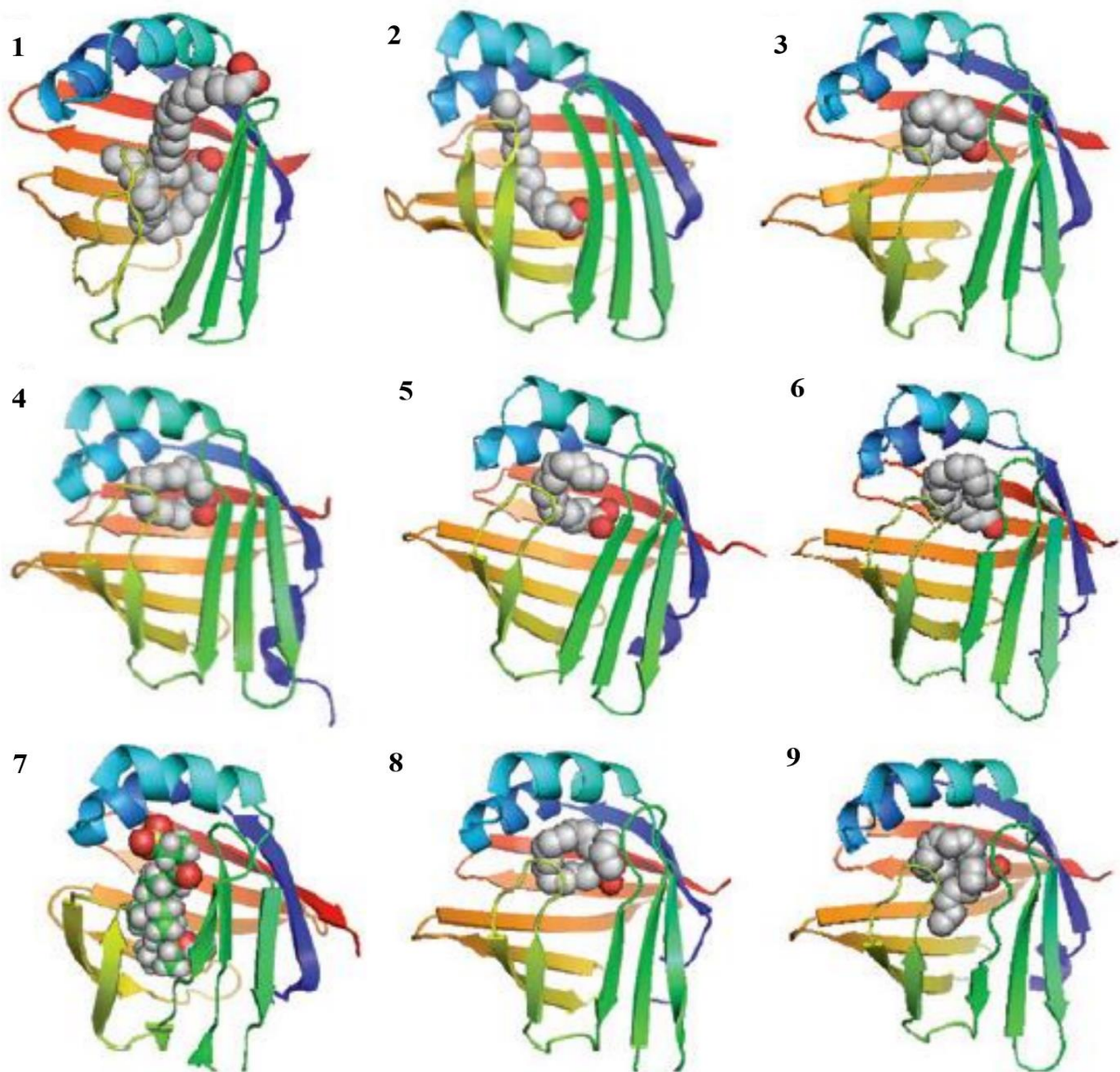
Figure 10. Three-dimensional structure of FABP 1-9 (158). The figures were created using PyMOL. This figure depicts the structural characteristics of FABPs, including their barrel-shaped structure with two orthogonal strands, each comprising five antiparallel sheets. A conserved fingerprint pattern has been identified across all FABPs, serving as a distinctive hallmark for this protein family. This conserved fingerprint provides a

characteristic feature that is shared among all FABPs and aids in their identification and classification

All FABPs exhibit a barrel shape with 2 orthogonal strands, each with 5 antiparallel sheets.This barrel formation contains the fatty acid binding site and has a helix-loop-helix motif cap that joins each strand (162,163). The barrel structure also houses a sizeable cavity which has a polar and hydrophobic amino acid lining (157). A majority of FABPs bind one, inwardly directed fatty acid, fixed within the cavity by tyrosine and two arginine residues (164). As demonstrated in **figure 11**, the conserved fingerprint discovered in each FABP serves as a hallmark for all FABPs in this family.
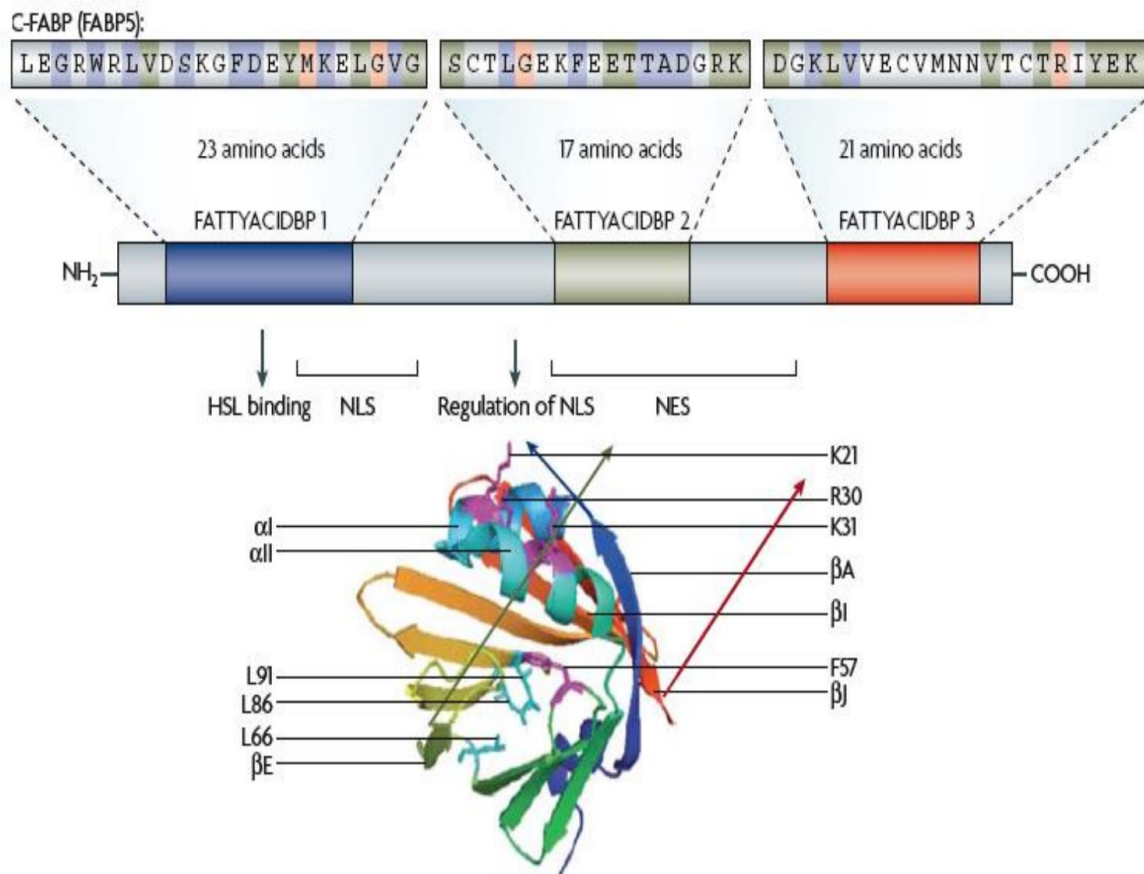
Figure 11. FABP fingerprint (158). Prints pattern FATTYACIDBP; PR00178.The ribbon diagram shows three motifs that are very stable. The blue ribbon, FATTYACIDBP1, is included in the first t β strands (βA). Additionally, it has a hormone-sensitive lipase

binding site and a nuclear localization signal (NLS). There is a nuclear export signal (NES) domain within FATTYACIDBP2 (green ribbon), and this has β sheets 4 and 5 (βE). B sheets 9 (βI) and 10 (βJ) are encoded by FATTYACIDBP3 (red ribbon). Blue, green, and red are also used to mark the important amino acids.

1.9 Functional roles of FABPs

Many functional roles are performed by FABPs, which are capable of active binding and transportation of lipids to particular cellular sites or organelles, as lipid chaperones. They comprise lipid droplets to store lipids, and an endoplasmic reticulum used in signal transduction, transportation, and membrane formation (165). Fatty acid delivery is possible to several cellular locations, including mitochondria and peroxisomes to allow oxidation, the cytosol or different enzymes involved in modulation of enzyme research, and the nuclear region for lipid-mediated transcription regulation (165). Fatty acids are able to deliver extracellular signalling by autocrine or paracrine mechanisms (166) (**Figure 12**). FABP may also reach the nucleus, transferring fatty acids to transcriptional regulators, to permit PPARs members to carry out their biological activities (167-169). Evidence shows FABP controlled movement of fatty acids between the cytoplasm and the nuclear receptor PPAR (165). Additionally, it has been shown FABP is expressed in a localised manner within cytoplasmic and nuclear regions of cancer tissue (168,170). Research has shown that FABPs are involved in nucleus-specific signalling networks that regulate gene expression. Figure 12 depicts the mechanism for fatty acid transit and metabolic pathway within the cell.
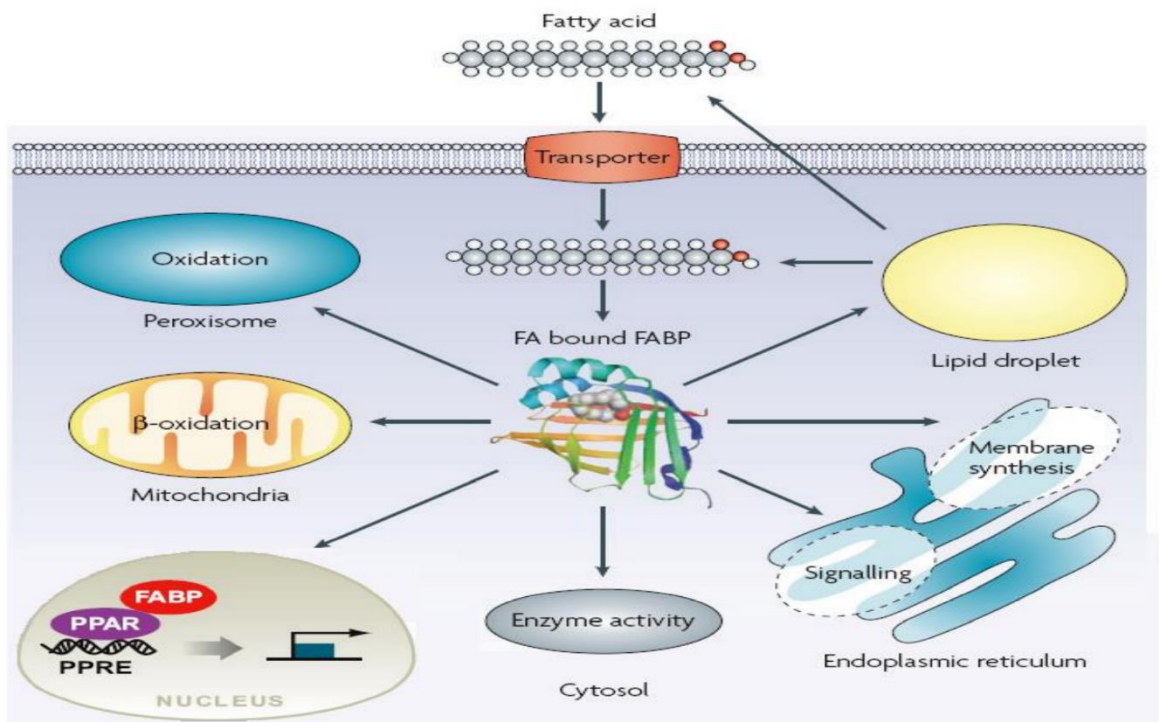
Figure 12. Functional roles and mechanisms of Fatty Acid Binding Proteins (FABPs) in lipid transportation and signaling. This figure illustrates the diverse functional roles of FABPs in lipid metabolism and signaling within cells. FABPs serve as active lipid chaperones, binding and transporting lipids to specific cellular sites or organelles. They are involved in various processes, including lipid storage within lipid droplets, signal transduction in the endoplasmic reticulum, lipid transportation, and membrane formation.FABPs facilitate fatty acid delivery to different cellular locations, such as mitochondria and peroxisomes for oxidation, the cytosol where they modulate enzyme activity, and the nucleus for lipid-mediated transcriptional regulation.Fatty acids can also act as extracellular signaling molecules through autocrine or paracrine mechanisms(165) (167-169).

1.10 Role of FABPs in cancer

1.10.1 FABP1 and cancer

FABP1 is expressed in the liver, gut, and kidney, as previously reported. Research investigated potential associations between FABP1 and cancer in various organ types. At least one investigation identified a link associating FABP1 with colon cancer; FABP1 was observed to be substantially downregulated within circulating colon cancer cells in circulation (171). Lowered FABP1 has been recognized to be a key contributor in microsatellite unstable colorectal cancers (140,172) in two investigations which suggest that FABP1 could be a tumour suppressant. In contrast, a different investigation investigating FABP1's effects in hepatocellular carcinomas (HCC) has indicated that FABP1 could promote tumour growth. FABP1 stimulated the production of vascular endothelial growth factor (VEGF) via interacting with VEGF receptors, resulting in angiogenesis. This study showed that FABP1 enhanced migratory capabilities in cancer cells via the VEGFR2 pathway, indicating that FABP1 promotes metastasis in HCC (173). FABP1 has been identified as significantly elevated in the HCC cell. This elevated status is associated with lymph node metastases and cancer progression (140,174).

1.10.2 FABP2 and cancer

Fatty acid binding protein 2, alternatively named intestinal fatty acid binding protein, is associated with development of certain disorders that may lead to cancer. Diabetes, myocardial infarction, stroke, and gallbladder disease are among these conditions (158). Little research has been conducted to determine FABP2 involvement in the development of cancer. Nonetheless, a study in 2021 investigated the connection between expression of FABP2, diet and intake of lipids in colorectal cancer. The research highlighted a negative relationship linking FABP2 with fat absorption. This means that FABP2 is not likely to reliably predict colorectal cancer risk (175).

1.10.3 FABP3 and cancer

It is debatable whether FABP3 promotes or inhibits cancer, as its involvement in cancer is still not fully investigated. FABP3 is overexpressed in four forms of cancer, according to previous research: non-small cell lung cancer (176), gastric cancer (177), leiomyosarcoma (178) and melanoma (179). On the other hand, it has been discovered to aid in suppressing breast cancer (180,181), lung adenocarcinoma (182), lymphoma (183), and embryonic malignancies (176).

1.10.4 FABP4 and Cancer

FABP4 was implicated with the aggressiveness of a variety of malignancies, including prostate (184) and breast cancers (185), cholangiocarcinoma (186), glioblastoma(187), and leukaemia(186). FABP4 is a unique molecular marker assisting in studying, predicting and monitoring cancer of the bladder, and could be targeted to develop new therapies, according to recent data (188). FABP4 has been implicated in cancer cell epithelial-mesenchymal transition (EMT). Overexpressed FABP4 is associated with EMT in cholangiocarcinoma (186) and cervical cancer (189).

1.10.5 FABP5 and cancer

Strong expression of FABP5 occurs in cancerous cells and contributes to aggressiveness in phenotypes of cancer through enhancing proliferative and invasive characteristics of the cell, metastasis and tumorigenicity. Highly expressed FABP5 has also been linked to therapy-resistant disease and lower prognoses across a number of cancers, such as gastric cancer (177,190), melanomas (191), cervical (192), breast (193), and prostate cancers (194-196), cholangiocarcinoma (197) and oral cancers (198). Compared to other cancer types, more studies have been conducted on FABP5's involvement in promotion in PCa. Various work *in vivo* and *in vitro* has demonstrated FABP5 enhanced tumour invasion (199).

1.10.6 FABP6 and cancer

Numerous attempts were made to investigate the involvement of FABP6 in colorectal cancer. FABP6 is strongly expressed in colorectal carcinomas in comparison to benign tissues. Although research found that it was broadly expressed in the ileum, metastatic tissue levels of FABP6 were low (140). Thus, further research is necessary to understand FABP6's precise function in colorectal cancer and different cancers.

1.10.7 FABP7 and cancer

FABP7 is essential to the Notch1 signalling pathway. Its role was studied in breast cancer when an FABP7-positive patient group was linked to triple-negative breast cancer. It was associated with a poor prognosis for patient survival, a high tumour grade, and an enhanced proliferation (200). Slipicevic et al.'s 2008 report on melanoma revealed that highly expressed FABP7 present in primary tissue and metastases was associated with an increased tumour dimensions as well as reduced survival time without relapse (140,201), but the function of FABP7 remains unclear.

1.10.8 FABP8 and cancer

Until recently, there was no proof of FABP8's participation in any form of carcinoma, and additional research is required to determine FABP8's function in cancer cells.

1.10.9 FABP9 and cancer

Overexpression of FABP9 occurs within PCa tissue and cells, , as observed, and is associated with more malignant disease and a poorer prognosis for survival. When cells with *FABP9* knockdown were assessed in comparison with parental PCa lines, reduction of FABP9 expression resulted in a substantial reduction in proliferative activity. However, invasive activity and anchorage-independent growth, which are indicators of metastasis, were not significantly altered (202). To determine if FABP9 could be involved with cancer, further studies are required.

1.11 Therapeutically targeting FABP5

FABP5 is a 15kDa cytosolic protein belonging to the FABP group and binding to long and medium chain fatty acids with high affinity (203). FABP5 show extensive expression by endothelial cells within the heart, the placenta, skeletal muscle, renal medulla, small intestine, renal medulla, and in the lung's goblet cells (204). Earlier research demonstrated highly elevated FABP5 levels in PCa cells (195,205). Additionally, strong FABP5 expression can promote the VEGF production to promote metastasis (206-208). FABP5 was demonstrated to be promising prognostic marker for predicting patient outcomes and a treatment target (205,209). Knocking down *FABP5* by siRNA can significantly limit growth and expansion of PCa in nude mice (206). It is proven that the tumour promotion action of FABP5 in PCa cells are due to its abilities to bind and transport fatty acids. These fatty acids function as signalling molecules for activation of the nuclear receptor PPAR in the CRPC cell (210). Furthermore, highly expressed FABP5 in the cytoplasm has been established to be substantially connected to rising nuclear PPAR, with elevated levels of PPAR and FABP5 associated with worse patient survival (170). Previous studies showed fatty acid activation of PPAR to induce the FABP5-PPAR-VEGF signal pathway, pointing to potential therapeutic targeting (211). The FABP5-PPAR-VEGF- signalling transduction axis and its operation in PCa cells are shown in **figure 13**.
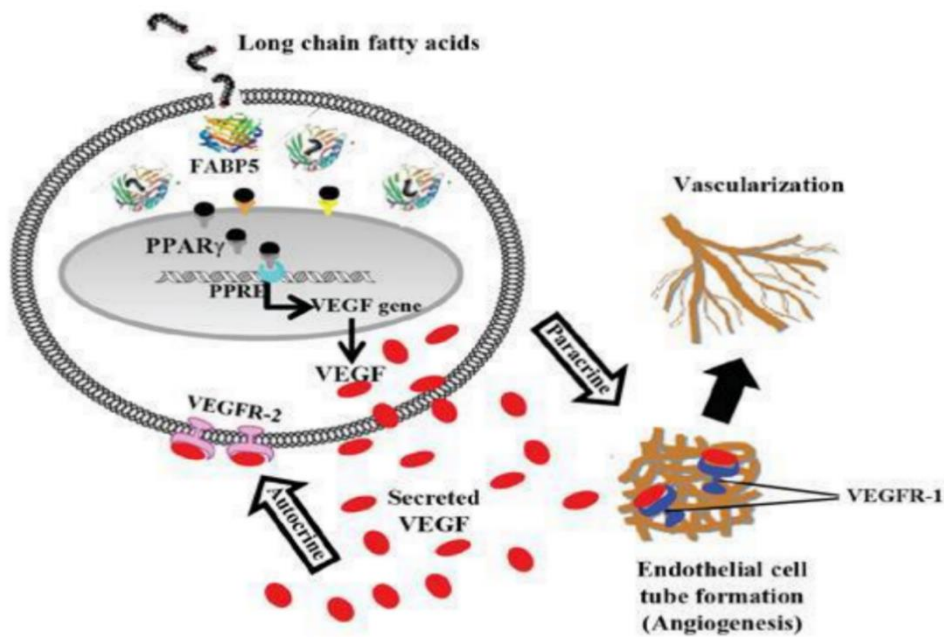
Figure 13. FABP5-PPAR-VEGF signaling axis and its role in prostate cancer (PCa) cells.(211).This figure explain the tumour-promoting action of FABP5 in PCa cells stems from its ability to bind and transport fatty acids, which function as signaling molecules activating the nuclear receptor PPAR in castration-resistant PCa cells. Moreover, highly expressed cytoplasmic FABP5 has been correlated with increased nuclear PPAR levels, and elevated levels of PPAR and FABP5 are associated with worse patient survival. Previous studies have demonstrated that fatty acid activation of PPAR induces the FABP5-PPAR-VEGF signaling pathway, highlighting potential therapeutic targets(206-208) (170).

To study the potential to target FABP5 therapeutically in PCa treatment, knockdown of the gene coding for FABP5 occurred in high-malignancy PC3M cells through RNA interference, resulting in drastically reduced FABP5 levels being produced in a subline

(Si-clone-2) (205). Si-clone-2 generated a 63 times lower average tumour size, seven times lower incidence of tumours, and reduced metastases by 100% when orthotopically transplanted into nude mice prostate glands and compared to the control (205). The findings show that short FABP5 siRNA created inside the cancer cell is particularly efficient in lowering malignant evolution of the cancer in a murine model. On the other hand, siRNA molecules are unstable and short-lived at body temperature, and therefore will degrade quickly after being administered as external reagents. This means that siRNA is unsuitable for direct utilisation as a therapy in PCa. On dissolving siRNA targeting FABP5 in stabilising agent (Atolecollagen, derived extract of bovine skin) for direct application to established tumours in a nude murine model, the siRNA molecules were capable of slowing and stabilising the growth of tumours, , but not of decreasing tumour size or reversing malignant progression (209). Thus, the identification of highly potent, selective, and reasonably stable and advanced technique like Crispr cas9 (Gene knockout) to cause a total loss of FABP5 function is critical in developing optimal prostate cancer treatment, screening and discovering other molecular pathways and genes from candidates that exhibit different expression levels when the expression profiles are compared with the control.

1.12 Clustered regularly interspaced short palindromic repeats (CRISPR)

Clustered regularly interspaced short palindromic repeats (CRISPR), in addition to the related Cas9 protein have formed an innovative approach to gene editing, which has been the core of modern studies in biology since the discovery of its fundamental components. This mechanism protects micro-organisms from invading viruses and plasmids as an adaptive immunological route (212). The invading viral DNA is broken into smaller segments (spacers) by the Cas complex, and these are then incorporated within the CRISPR site of the bacterial genome. When an invading virus is recognised and targeted

by Cas proteins, they are transcribed and converted to form short, distinct crRNA, complementary sequences (213,214). Because of its applicability, CRISPR/Cas9 is now considered the best technique to target DNA in a site-specific manner.

CRISPR/Cas systems are classified as: Class 1 (containing about 90% of Cas sites) and Class 2. Cas systems in Class 1 (types I, III, and IV) require numerous Cas proteins for the creation of effector complexes targeting RNA or DNA. Class 2 (which includes types II, V, and VI) needs just a single Cas protein, which means they are effective in gene editing (215,216). The Cas enzyme discovered in Streptococcus pyogenes (SpCas9) is categorised as Class 2, type II, is the most extensively utilized in genome editing. Cas9 endonuclease has 2 nuclease domains, RuvC and HNH, which respectively cleave non-complimentary and complementary strands (217). CRISPR RNA (crRNA) and trans-activating crRNA (tracrRNA), the other two components necessary for this system, enable DNA recognition (218). crRNA is sometimes called the protospacer, has guide sequence of between 18 and 20 nucleotides, recognising targeted genomic locations, and tracrRNAcan hybridise with crRNA to provide scaffolding to bind Cas9 (219). The Cas9-tracRNA (trans-activating crRNAs) complex is directed toward the complementary crRNA sequence in the DNA. A brief synthetic linker can join the tracrRNA and crRNA to form single guide RNA (sgRNA), as extensively employed in systems which deliver ribonucleoprotein (RNP) (220).

Cas9 DNA binding requires a protospacer adjacent motif (PAM), and SpCas9 requires a target upstream from a 5'-NGG-3' site. Cas9 binding partially unwinds before cleaving DNA 3 base pairs downstream from the PAM location, assuming the crRNA sequence is complementary to the DNA sequence before the PAM site (218, 219). As previously stated, once a DSB occurs, cells repair the damage via one of two repair pathways, NHEJ or HDR (220). One gRNA is usually used in knockout of genes leading to non-homologous end joining (NHEJ) double-strand break (DSB) repairs. NHEJ involves the

nucleotides being randomly inserted or deleted, frequently leading to frameshift mutations that might render the gene being studied inactive. Such alterations, however, may stay in frame, contributing to their inefficiency (221). An overview of CRISPR-Cas9 gene editing is shown in **figure 14**.

Figure 14. Diagram showing CRISPR-Cas9 gene editing - A) Cas9 binds to DNA upstream from an NGG PAM site that is complementary with sgRNA (blue). Triangles show the site of a broken double strand. B) Cas9-induced double strand breaks may be repaired by the NHEJ pathway, leading to randomly-generated minor deletions or insertions or through HDR where an appropriate repair template is present, enabling

precision mutations. Permission granted to adapt from Springer Nature: Nature Protocols (221).

1.13 Therapeutic Applications of CRISPR-Cas9 gene editing

Although the CRISPR/Cas system is yet to be deployed *in vivo*, a great advancement toward understanding the system has offered new discoveries in cancer gene research within human cellular and mice models during the last decade. Recently, the CRISPR-Cas9 technology was used to achieve disruption of as many as 8 alleles of murine embryonic stem cells (ESCs) through one, resulting in animals with numerous gene mutations (222). A hepatic cancer model was successfully developed through delivering a CRISPR/Cas9 plasmid in vivo, in which single guide RNAs targeted p53 and PTEN tumour suppressor genes (223). The CRISPR-Cas9 system has almost no limit in its uses as a strong genome-editing tool, and it may be applied for blocking, repression, activation, translocation, flipping or duplication of whatever gene is targeted. The development opens up a plethora of interesting possibilities for better understanding of cancers biology through models of disease and perhaps allowing treatment with the most effective tailored therapy (224).

1.14 Hypothesis

A key issue in prostate cancer molecular pathology is how the cancer cells were progressed from androgen-dependent to androgen-independent state to become a castration-resistant prostate cancer (CRPC). Past evidence suggested that the formation of CRPC was related to the interactions between FABP5 and the androgen receptor (AR). Based on the past observation, we hypothesized that the interaction between FABP5 and AR may play a crucial role in the process of the malignant transformation of androgen-dependent prostate cancer cells to CRPC cells. To test this hypothesis and to investigate the complicated molecular pathogenesis of CRPC cells, we proposed and planned to test the following working hypothesis:

- *FABP5-* or *AR-* knocked out in prostate cancer cells (22RV1, DU145, and PC3M) can disrupt the FABP5 or AR-p-PPARγ-VEGF signalling axis.

- *FABP5-* or *AR-* knocked can suppress cell proliferation, invasive ability, motility rate, and anchorage-independent growth of the cancer cells as consequence of disruption of the FABP5 or AR-p-PPARγ-VEGF signalling axis.

- FABP5 and AR or its splicing variant AR-V7, which involved to drug resistance, may interactively coordinate the FABP5 or AR-p-PPARγ-VEGF axis.

- Identification of differentially expressed genes (DEGs) between *FABP5-* or *AR-* knock out cells and their parent prostate cancer cells can provide clues to understand the transition from androgen-dependent to CRPC cells.

- The DEGs is very likely to relate to pathways responsible to fatty acids, cholesterol and sterol biosynthesis, lipid and fatty acid transport, which are critical for transducing signals involved in cancer cell progression.

Overall aim

- To measure the expression levels of key factors of the FABP5-related pathway, to compare the expression status of these factors between benign, weakly, moderately and highly malignant prostate cells to prove the existence of this high active signal transduction axis in prostate cancer cells, and to study the relationship between its strength and the degree of malignancy.

- To knock out *FABP5* in AR-positive 22RV1 cells and in AR-negative DU145 and PC3M CRPC cells and to establish FABP5-KO sublines.

- Knockout of *AR* in 22RV1 cells to establish a AR-KO subline.

- To assess the effect of *FABP5-* knock out on the malignant properties of the cancer cells by conducting 4 bio-assays.

- To assess the effect of *AR* knock out on the malignant properties of the cancer cells by conducting 4 bioassays.

- To assess the effects of *FABP5* knockout on the expression levels of the key factors of the FABP5-related signal transduction axis.

- To assess the effect of *AR* knockout on the expression levels of the key factors of the FABP5-related signal transduction axis.

- To identify the DEGs between *FABP5-* or *AR-* knockout sublines and their parent lines to assess the genes altered by FABP5 or AR and to identify their relevant signalling pathways to investigate further molecular mechanisms underlying FABP5's tumour promoting function.

Chapter 2 : Materials and Methods

2.1 . Material and methods

2.1.1 Cells and Culture

This work used the benign prostatic epithelial cell line PNT2 and 3 malignant prostate cell lineages: 22RV1,DU145 and PC3M, derived from prostate carcinomas, for the laboratory-based investigation as mentioned in Section 1.2.4.The cells were purchased from (ATTC UK).

2.1.2 Cell culture

Cells were cultured in a tissue culture hood (LabGard, USA) within the departmental tissue culture laboratory, in accordance with the safety criteria established by the institution. The medium used for all cell cultures comprised RPMI 1640, to which was added 10% (vol/vol) foetal calf serum, penicillin (100 U/ml) (Bioser, East Sussex, UK), streptomycin (100ug/ml), and L glutamine (20mM) (Invitrogen). In addition to the supplements listed above, LNCaP cells were given sodium pyruvate at a concentration of 100 ug/ml (provided by Sigma, Grillingham, UK). The cells were grown and kept in monolayer cultures at a temperature of 37^0C and with 5% CO_2 in a humidifier incubator (Boro, Labs UK).

2.1.3 Cell thawing

Following the removal of the cell vials from various racks inside a tank of liquid nitrogen where they had been housed, they were put into a water bath maintained at 37^0C so that the vials could gradually thaw. After that, the impact of the DMSO was neutralized by diluting the cells with 20 ml of new media. This was followed by centrifuging them at 91 g for three minutes before removing and discarding the supernatant, and resuspending the cell pellets in a flask with new media. A haemocytometer was used to determine the cell numbers, and the culture medium in the flask was adjusted to 25 cm^3. The cells were checked and the medium changed at 3-day intervals to replenish the nutrients.

2.1.4 Cell Subculture

Cells held in culture flasks were checked and monitored using microscopy. After they were 70–80% confluent, cell sub-culture was performed under a tissue culture hood under sterile conditions. After aspirating the flask medium cells were washed using phosphate buffer saline (PBS), before being subjected to a treatment of trypsin in versine (2.5%: 97.5%, v/v) for three minutes inside a 37^0C incubator. Then, the microscopy was used to examine cells to ensure that rounding up and separation had occurred properly. After adding new medium with 10% FBS at 2-fold the previous volume, the mixture was placed in the centrifuge at 91g for 90 seconds. Supernatant containing inactivated trypsin was aspirated and the pellet in each flask resuspended in fresh medium, dividing this between 3 new flasks. The fresh flasks were placed into the culture incubator to continue culturing.

2.1.5 Cryopreserving cells

Cryopreservation was used to preserve cells in a cold environment while they were stored. To store the growing and dividing cells, after discarding the medium and washing cells in PBS, they were trypsinized and resuspended in new medium. The cells were moved into Universal tubes, and a haemocytometer was used to count the cell number. After centrifuging the cells for three minutes at 91 g, they were resuspended in freezing media consisting of 7.5% DMSO in RPMI. After adding one millilitre of cells to each cryovial (specifically made for storage in liquid nitrogen), the vials were stored in a Mr. Frosty^{TM} freezer for one night at a temperature of -80^{0}C , then transferred to liquid nitrogen.

2.2 Assessing cell line protein expression levels through western blot

2.2.1 Cell pellet collection

Cells were harvested when the culture was at about 80% confluence, and the pellets of the grown cells were collected. The previous medium was discarded, and the pellets rinsed in PBS, trypsinizing and then centrifuging them as set out in the section on cell subculture. Each collected pellet was lysed in a universal tube using a CelLytic reagent combined with a protease inhibitor. This reaction mixture was placed in the tube and put on a roller mixture shaker, shaking for 15 min. Tubes were centrifuged at 11,200 x g for 10 min. before the supernatant was collected and analysed using Western blotting.

2.2.2 Bradford assay

To ensure the loading of identical amounts of total protein across the samples for Western blot analysis, protein weight was measured via Bradford assay. If proteins attach to Coomassie Blue G-250 dye, it can alter the colour of the dye from brown to blue in a manner proportionally related to their weight. Thus, the amount of proteins can be detected with a spectrometer (Biotech, UK) to measure light absorbance, which changes along with the changing colour. Bovine serum albumin (BSA) is a widely available protein which may be used to generate standard curves which can quantify protein concentrations in loading samples. Thus, the protein concentration of an unknown sample can be obtained by comparing its light absorbance to the standard albumin curve (225). After filtering the Bradford dye through a Whatman paper filter, a 1 ml addition was made for every albumin protein tube for the serial dilutions. Serial dilutions were divided in triplicates, and then absorbance at 595 nm was read using a microplate reader (Biotech, UK). A typical linear curve of protein concentration vs matching absorbance values was produced, and this standard curve can be used to calculate the protein concentrations of an unknown sample.

2.2.3 Western blot

2.2.3.1 Sodium dodecyl sulphate-polyacrylamide protein gel electrophoresis (SDSPAGE)

In an electrical field, the moving speed of proteins depends on their molecular weights: the smaller protein molecules move faster than larger protein molecules. Thus, proteins can be separated based on molecular weight using a method called sodium dodecyl sulphate-polyacrylamide protein gel electrophoresis (SDS-PAGE): a widely-applied procedure used in different laboratories. This approach is based on the fact that various proteins migrate through a gel at different speeds when subjected to the influence of an external electrical field. PAGE is used as a medium, and SDS is used to denaturing the proteins and coating them with SDS, a detergent that imparts a negative charge to the proteins. This ensures that the protein samples are uniformly charged and migrate towards the anode during electrophoresis. After performing plate sandwiching using BioRad ready gel, each protein sample was placed in 2x SDS-PAGE sample loading buffer before boiling for ten minutes at 95°C. Samples were then placed for 120 seconds on ice. Finally, after loading each sample, the gel containing them was run at 150V for between 40 minutes and 1 hour.

2.2.3.2 Transferring protein to the nitrocellulose membrane

Following SDS-PAGE, protein separation occurred based on molecular weight. BioRad small trans-blot technology was used to transfer proteins from SDS gel onto nitrocellulose membrane. For 5 minutes, this was immersed along with 2 Bio-Rad thick filter paper sheets in cold in transfer buffer. Then, a cassette was built as follows, starting at the black surface and working downwards:: one pre-wetted fibre pad, one leaf thick filter paper, equilibrated SDS gel, one nitrocellulose membrane, and a second thick filter paper, followed by a pre-wetted fibre pad, with the black side down. There must be no air

bubbles. The transfer was carried out in 1x transfer buffer run for 60 minutes at 100V in conditions of 4°C.

2.2.3.3 Target protein visualization and identification via immunoblotting

After protein transfer to a nitrocellulose membrane, incubation occurred in 5% blocking solution (20ml, made from 5g skimmed milk to 100ml TBST) for 60 minutes at ambient temperature. This was followed by further incubation in the correct concentration of antibodies in a milk-TBS-T combination (Table 2) with moderate shaking at 4°C overnight. To eliminate unbound primary antibody, Three 10-minute membrane washes were conducted, each using 1 T-TBS, before incubating the cleaned membrane in ambient conditions for 60 minutes with a secondary antibody at the appropriate concentration (Table 2). Another three washes were then performed, as before. Then, after 5 minutes at room temperature, visualisation of bound antibodies was achieved using the ECL reagents kit (combined with 1ml each of Reagent A and solution B). Using image analysis equipment, intensity was then quantified for the visible protein banding (ChemiDoc MP Imaging System, (Bio-Rad, UK).

2.2.3.4 Correcting potential loading discrepancy

To standardize the potential sample loading discrepancies, blot hybridisation was performed with anti-β-actin antibody. The primary antibody is stripped from the membrane in a Western blot by washing the membrane with an antibody stripping buffer(Restore™ Western Blot Stripping Buffe Thermofisher UK)incubating it in the buffer to dissociate the antibody-antigen complex, and thoroughly washing it.Then, the blot was rinsed in 1x TBS for 24 h with gentle shaking. The blot was then immersed in 5 percent blocking solution (20 ml) for 30 minutes, before incubation with anti- β-actin antibody at a dilution of 1:20,000 in ambient temperature for 0.5 h. The blot was washed 3 times in 1x TBS, for five min. per wash. After washing, an addition of secondary

antibody in a dilution of 1:20,000 was made and the blot was then incubated at ambient temperature for 0.5 h. while being gently shaken. After washing the blots for 5 minutes with 1x -TBS, which was done 3 times, the β-actin band was visualized with an ECL detection and image analysis system (Bio-Rad, UK). The antibodies for the experimental work in the project are listed in Table 2.

Table 2. Antibodies used in Western blot analysis

Target Protein	Primary Antibody	Secondary Antibody
FABP5	Monoclonal Rabbit Anti-human FABP5 (1:500) (HycultR Biotech)	Swine polyclonal anti-rabbit Immunoglobulin/HRP (Dako) (1:20,000)
PPARγ	Rabbit polyclonal anti-human PPARγ (Santa Cruz sc-7196) (1:200)	Swine polyclonal anti-rabbit Immunoglobulin/HRP (Dako) (1:20,000)
p-PPARγ	Phospho-PPARγ (Ser112) Polyclonal Rabbit antibody (1:250) (Thermo Fisher)	Polyclonal Swine Anti-rabbit Immunoglobulins-HRP (1:10,000) (Abcam)
VEGF	Mouse monoclonal Anti-VEGF ((Santa Cruz sc-7196) (1:200)	Rabbit polyclonal anti-mouse Immunoglobulin/HRP (Dako) (1:10,000)
AR	Mouse monoclonal Anti-AR Antibody ((Santa Cruz sc-	Rabbit polyclonal anti-mouse Immunoglobulin/HRP (Dako) (1:20,000)
NR1H4	Rabbit polyclonal Anti-Bile acid Receptor NR1H4(Abcam ab-85606) (1:500)	Swine polyclonal anti-rabbit Immunoglobulin/HRP (Dako) (1:10,000)
EGR3	Rabbit polyclonal Anti-EGR3 (Abcam ab-272903) (1:750)	Swine polyclonal anti-rabbit Immunoglobulin/HRP (Dako) (1:10,000)
CRIP2	Rabbit polyclonal Anti-CRIP2 (Abcam ab-229110) (1:1000)	Swine polyclonal anti-rabbitImmunoglobulin/HRP (Dako) (1:10,000)
FOSB	Mouse monoclonal Anti-FOSB(Abcam ab-11959) (1:1000)	Swine polyclonal anti-rabbit Immunoglobulin/HRP (Dako) (1:10,000)
β-Actin	Mouse monoclonal anti β-actin (Sigma) (1:50,000)	Rabbit polyclonal anti-mouse Immunoglobulin/HRP (Dako) (1:20,000)

2.3 Gene editing

2.3.1 CRISPR ribonucleoprotein

Ribonucleoprotein (RNP), which consists of Cas9 nuclease associated with crRNA, tracrRNA duplex or sgRNA, was used for the editing of the genome of the cells. The RNP materials were commercially provided by Integrated DNA Technologies (Coralville, IA, USA).

2.3.2 Ribonucleoprotein Transfection

FABP5 Knockout was generated in cell lines PC3M, DU145, and 22RV1 using CRISPR/Cas9 mediated technique for gene editing. The crRN sequences (shown in Table 3) targeting FABP5 or AR genes were designed with the AltR® CRISPR/Cas9 guide RNA designing tools. The ATTO-550-labeled tracrRNA was supplied by Integrated DNA Technologies (Coralville, IA, USA). Cell seeding was done into six-well plates, using 400,000 cells per well, 24 hours before transfection. Equimolar (1 µM) crRNA and tracrRNA-ATTO-550 concentrations were mixed to form a duplex, which was then heated at 95^0C for 5 minutes before cooling gradually to reach ambient temperature. An RNP complex was produced by assembling Cas9 protein (1 µM) and crRNA:tracrRNA-ATTO-550 duplex with Opti-MEM buffer (Thermo Fisher Scientific, UK) and leaving in ambient conditions for 10 min. Incubation of the RNP complex was done at ambient temperature using 9µL Lipofectamine CRISPRMAX (Thermo Fisher Scientific, UK) for between 10 and 15 minutes. Finally, the reverse transfection approach was used to obtain a high transfection percentage by adding the cell medium over the RNP (226), as shown in **figure 15**.

Table 3. Guide oligonucleotide sequences targeted FABP5 and AR

Guide RNA and PAM seq	Cell Line	KO Gene	Exons	Locus	REGION
AAGTATCAACTTCAT CATAG CAA	22RV1	FABP5	1	NG_028154	5079..5138
GATGAATACATGAA GGAGCT AGG	DU145	FABP5	1	HQ384161	5130..5189
AAGTATCAACTTCAT CATAG CAA	PC3M	FABP5	3	NM_000044	8156..8209
CAACGCCAAGGAGT TGTGTA AGG	22RV1	AR	1	NM_001348 06	1828..1847
GGTTACACCAAAGG GCTAGA AGG	22RV1	AR	1	NM_001348 06	1467..1486
GCAGAAATGATTGC ACTATT CAA	22RV1	AR	2	NM_001348 06	2234..2253
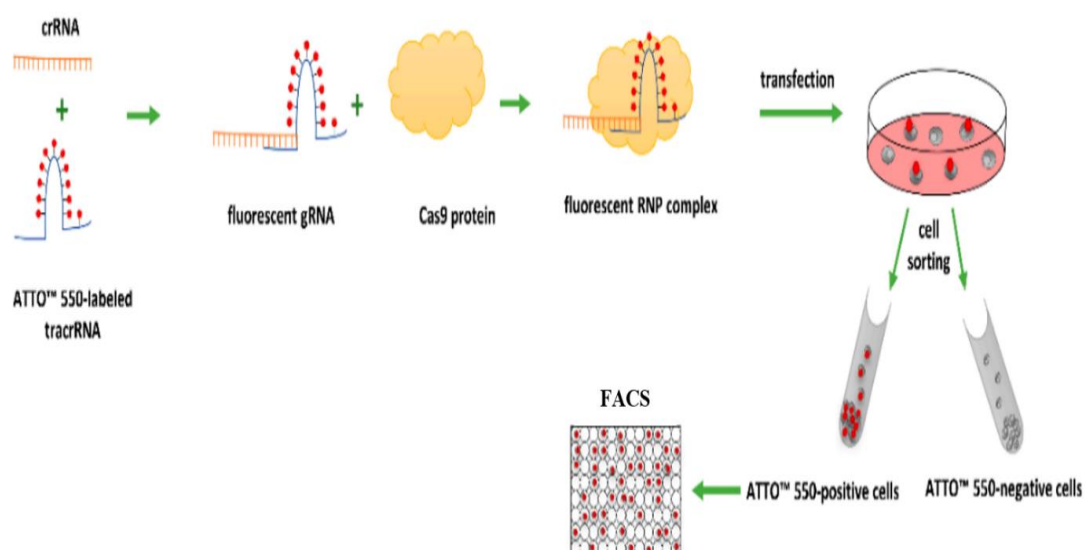
Figure 15. the production and transfection of CrRNA and ATTO-550-labeled tracrRNA (RNP) complex into cells are illustrated. The process begins with the synthesis of crRNA and ATTO550-labeled transactivating RNA (ATTO-tracerRNA), which subsequently combine to form fluorescent gRNA. The fluorescent gRNA then associates with the cas9 enzyme, resulting in the formation of the RNP complex. Following RNP complex formation, the complex is transfected into the target cells. To separate the ATTO550-positive cells from the population, fluorescence-activated cell sorting (FACS) is employed. This technique allows for the identification and isolation of cells that have successfully incorporated the RNP complex, as indicated by the presence of ATTO550 fluorescence. (226).

2.3.3 Flow cytometry / Cell-sorting

In order to verify that the transfection was successful and to isolate the single colony harbouring a fluorescent ATTO550 Ribonucleoprotein Crispr cas9 (RNP) complex, the transfected cells were separated at 24 hours post-transfection with fluorescence activated cell sorting (FACS), and then split in two parts: one part was subjected to cell sorting to isolate the fluorescent cells, and the second part was subjected to protein analysis to verify that the expected alterations in targeted gene expression were achieved. Flow cytometry analyses were conducted at the Faculty of Health and Life Sciences at Liverpool University, UK, using a FACSAria machine (BD Biosciences, Liverpool, UK), with the assistance of Cell Quest software (BD Biosciences, Liverpool, UK).

2.3.4 PCR amplification of DNA and Sanger sequencing

After the single cells were sorted using the fluorescence-activated cell sorting (FACS) technique and transferred into separate wells of a multi-well plate, FABP5 knockout single cell clones were cultured individually. Genomic DNA was then isolated from each clone for further analysis.To confirm the successful knockout, Sanger sequencing analysis was performed on the isolated genomic DNA. Primers were designed to target a specific segment of approximately 500 base pairs (bp) surrounding the guide RNA targets of interest. The forward primer sequence was5'GGCAAGAGGAGCTGGTTAG-

3' , and the reverse primer sequence was 5'-GAGGGTCACGGTAGTTATTTCA-3'. These primers were used to amplify the DNA sequence and analyze the region downstream of each guide RNA.

The Sanger sequencing analysis of the amplified DNA fragments allowed for the identification of any insertions, deletions, or other mutations within the targeted gene, confirming the knockout of FABP5 in the selected single cell clones.. Thus, the sequence of the DNA segment revealed ranged from 100 bp upstream to 400 bp downstream of each gRNA. (the Sanger sequencing service was provided by Azenta Inc. (South Plainfield, NJ). PCR was performed and refined in accordance with the standard operating procedures (SOP) of our laboratory. An enzymatic clean-up procedure was used to make the PCR amplicons more presentable with a 3730xl DNA Analyzer (Applied Biosystems, USA) and a reagent kit BigDye (version 3.1, Applied Biosystems, USA), used in line with the manufacturers' instructions.

2.4 RNA Extraction, RNA Library Preparation and NovaSeq Sequencing

Extraction of total RNA from frozen cell pellets was done using a Qiagen RNeasy Mini kit, following the guidelines of the manufacturer (Qiagen, Hilden, Germany). The QIAGEN FastSelect rRNA HMR Kit was used in the process of preparing the rRNA depletion sequencing library, as shown in **figure 16** (227) (Qiagen, Hilden, Germany). A NEBNext Ultra II RNA Library Production Kit for Illumina was used for preparation of the RNA sequencing library, used as specified by the manufacturer (NEB, Ipswich, Massachusetts, United States). In short, 15 minutes' fragmentation of enriched RNAs was conducted at a temperature of 94ºC. After that, both strands of cDNA were produced. End repairs and adenylations were performed on cDNA fragments at the 3' ends, before ligating them to universal adapters. The next step was inclusion of an index, and library

enrichment is performed using limited cycle PCR. Verification of the sequencing libraries used an Agilent Tapestation 4200 kit (Agilent Technologies, Palo Alto, California, USA), before they were quantified with a Qubit 2.0 Fluorometer (ThermoFisher Scientific, Waltham, Massachusetts, USA), and validated with quantitative PCR (quantitative PCR, ThermoFisher Scientific, Waltham, Massachusetts, USA) (KAPA Biosystems, Wilmington, MA, USA). Based on manufacturer recommendations, sequencing libraries were multiplexed before being placed onto the flow cell of the Illumina NovaSeq 6000 equipment. A 2x150 Pair-End Configuration version 1.5 was used to sequence the samples. Images were analysed and base calling performed on the NovaSeq instrument using NovaSeq Control Software version 1.7. Using the Illumina bcl2fastq application version 2.20, the raw sequence data that was produced by the Illumina NovaSeq and saved as .bcl files underwent conversion to fastq files, before being de-multiplexed. Index sequence identification permitted one mismatch.

2.4.1 RNA Sequencing Data Analysis

Following an analysis of raw data quality, trimming of sequence reads was performed by Trimmomatic version 0.36 in order to get rid of any potential adapter sequences and nucleotides that had low quality. STAR aligner version 2.5.2b was used to map trimmed reads onto the human reference genome, which is accessible on the ENSEMBL database. This splice alignment software recognizes splice junctions, integrating them into the alignment process so that the complete read sequence can be properly aligned. This resulted in the production of BAM files. Using the feature counts that came with the subread package version 1.5.2, designers were able to compute the number of unique gene hits. Only one-of-a-kind readings that occurred inside exon regions were included for the analysis. Following the gene hit count extraction, a table containing those counts allowed subsequent analyses of differential gene expression. gene expression levels of the

different sample groups were compared using DESeq2. Both the p-values and the Log2 fold changes were calculated via the Wald test. When comparing groups, genes with differential expression were determined to be those genes whose adjusted p-values were below 0.05, with absolute log2 fold changes of over 1. The programme GeneSCF was used to conduct a gene ontology study, which was then applied to the collection of genes whose significance was determined statistically. Clustering the collection of genes according to the biological process that they participate in and determining the statistical significance of those clusters was accomplished with the help of the goa human GO list. A scatter plot comparing the average expression of DEG, a hierarchical clustering heatmap, enriched tree of DEG, enriched network analysis of DEG, the KEGG pathway and protein-protein interactions were generated by the IDEP.96 Web Application for RNA-Seq Data Analysis (228). **Figure17** shows the Bioinformatics Analysis Workflow as developed by GENEWIZ (227).
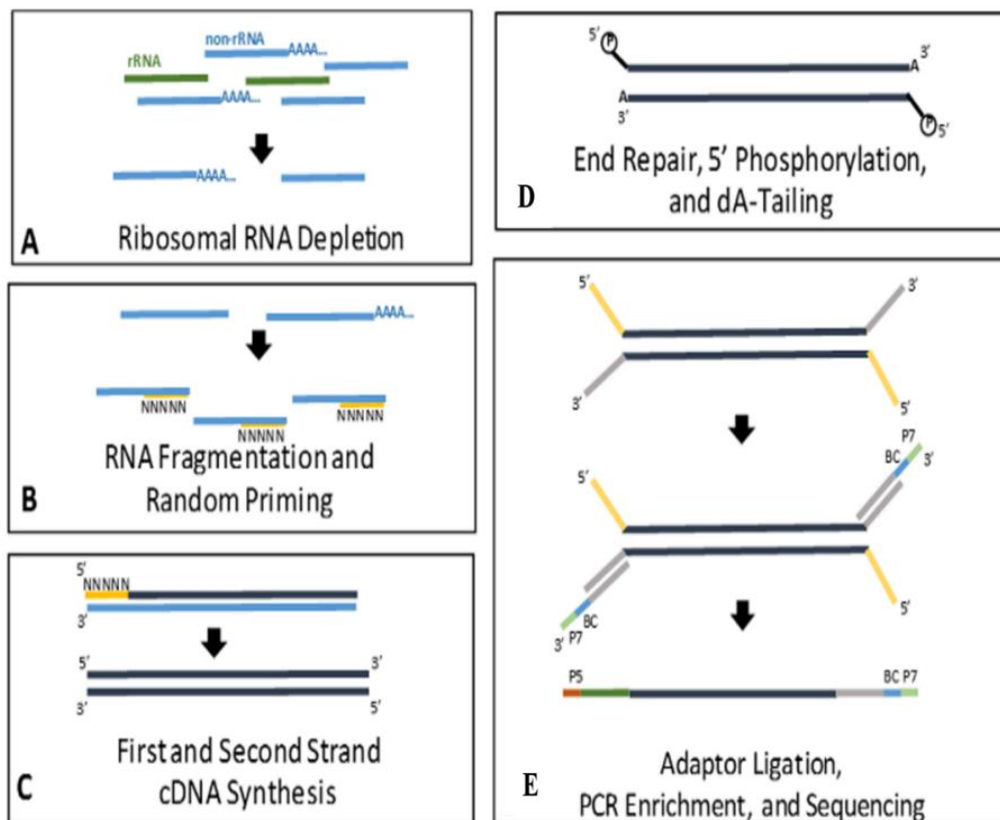
Figure 16. Whole transcriptome sequencing via the rRNA depletion method. Adapted with permission from GENEWIZ (227).   The figure illustrates the RNA depletion method used for transcriptome analysis. The workflow involves several key steps:

1. RNA Extraction: Total RNA is extracted from the biological sample using a
    suitable extraction method, such as TRIzol or a commercial RNA extraction kit.

2. rRNA Removal: The extracted RNA undergoes a selective depletion process
    targeting ribosomal RNA (rRNA), which constitutes a significant portion of the
    total RNA. This step is crucial to enhance the detection of rare or low-abundance
    transcripts of interest.

3. Depletion Method: Different methods can be employed for rRNA removal, such as enzymatic digestion, oligonucleotide-based capture, or hybridization-based approaches. These methods specifically target and remove the rRNA molecules from the RNA sample, leaving behind a diverse population of non-rRNA transcripts.

4. RNA Quality Assessment: The quality and integrity of the depleted RNA are assessed using techniques like agarose gel electrophoresis, capillary electrophoresis, or automated RNA analysis systems. This ensures that the depleted RNA is suitable for downstream applications.

5. Library Preparation: The depleted RNA is then subjected to library preparation, which involves the conversion of RNA into cDNA followed by the addition of sequencing adapters. This step prepares the RNA fragments for next-generation sequencing.

6. Transcriptome Analysis: The prepared libraries are sequenced using high-throughput sequencing platforms, generating millions of short reads that represent the transcriptome of the sample. These reads can be aligned to a reference genome or transcriptome to quantify gene expression levels or identify novel transcripts.

The RNA depletion method depicted in the figure enables the enrichment of non-rRNA transcripts, providing a more comprehensive view of the transcriptome. By removing highly abundant rRNA molecules, this method enhances the sensitivity and accuracy of transcriptome analysis, facilitating the identification and quantification of rare or specific transcripts of interest.

Figure 17. Bioinformatics analysis workflow: Differential Gene Expression and Gene Ontology Analysis (227). The figure illustrates a bioinformatics analysis workflow for studying differential gene expression and conducting gene ontology analysis. The workflow involves data preprocessing, differential gene expression analysis, data visualization, gene ontology analysis, pathway analysis, interpretation, and validation.

2.5 *In vitro* investigation of malignant features

2.5.1 Proliferation assay

In order to ensure the reliability and reproducibility of the results, this experiment was performed in triplicate at different times. Both the control cells and the FABP5 or AR knockout cells were seeded at a density of 5000 cells per well in a 96-well plate. The aim was to investigate the impact of gene knockout on the growth of prostate cancer (PCa) cells.To assess cell proliferation, a Resazurin assay kit (Thermofisher, UK) was utilized, which is specifically designed for detecting cell viability and cell death. The Resazurin dye is initially blue and non-fluorescent, but upon entering living cells, it undergoes a chemical reduction to resorufin, emitting red fluorescence. The reduction process is maintained by metabolically active cells, making the color change directly proportional to the number of living cells. The quantification of this color change was achieved using a plate reader that measured the fluorescence or absorbance of the dye.

For a period of six days, the cells with specific gene knockout and the control cells were allowed to grow separately in the 96-well plate. Each day, the PrestoBlue reagent was added to the wells, and the plates were then placed in a cell culture incubator for a duration of two hours to allow the dye to react with the cells. Subsequently, the absorbance was measured at 570 nm using a spectrophotometer (Labtech, UK), with the absorbance at 600 nm serving as the baseline wavelength.To establish a reliable baseline, two control types were employed: parental cells that were grown in wells, and growth medium without the presence of cells. By comparing the absorbance values between the control and knockout cells, the impact of FABP5 or AR gene knockout on cell growth and viability could be determined.It is worth noting that triplicate experiments help to reduce experimental variations and enhance the statistical significance of the results. Additionally, the PrestoBlue Cell Viability Reagent provided

a time-saving advantage, as it yielded accurate viability measurements just 10 minutes after the addition of the reagent, allowing for efficient data acquisition and analysis.

2.5.2 Motility assay

Upon reaching 100% confluency in both the parental cells and FABP5 or AR knockout cells, the motility of the cells was assessed using a cell motility assay. This assay utilized an Ibidi culture-Insert (Ibidi TM, Germany) to analyze the behavior of motile cells. This experiment was performed in triplicate at different times.The Ibidi culture-Insert consisted of two cell culture reservoirs separated by a wall. Cell suspensions were added to the reservoirs and allowed to attach and grow. Once the cells were firmly attached, the insert was carefully withdrawn, creating a defined space of 500 µm width. Following the removal of the insert, 100 µl of the cell suspension was added to each cell culture well.To assess the motility of the cells, the culture dishes were placed in a humidified culture incubator at 37 °C and 5% CO_2 for a minimum of 24 hours. During this incubation period, the cells exhibited motility and attempted to close the gaps created by the withdrawn insert, demonstrating their ability to move and migrate.To evaluate the motility activity, microscopy was performed, and images were captured at specified time intervals. The images were analyzed using software such as Image J to quantify the motility response. The diameter of the gradually narrowing gaps was measured to determine the extent of motility by the cells.It is important to note that sterile tweezers were used to delicately remove the insert from the culture dish to avoid disturbing the intact monolayer of cells that had formed. Image J was used to perform quantitative analysis on the pictures taken under a microscope. The cell motility assay provided valuable insights into how the knockout of the FABP5 or AR gene affected the motility of the cells, offering information about their ability to move and close the gap in comparison to the control parental cells.

2.5.3 Invasion assay

The capacity for invading surrounding tissue forms a malignant characteristic of cancer cells which may differentiate benign from malignant lesions. The invasion assay is a tried-and-true technique for determining the probable degree of cancer cell spread. The basic idea is that those cells move down the chemoattractant gradient to a lower compartment after passing through a porous membrane. A BD BioCoatTM Growth Factor Reduced (GFR) MatrigelTM Invasion Chamber with an 8μm pore size and a Matrigel basement membrane matrix (BD Biosciences, USA) was used for evaluating cell invasion (229). Growth factor, laminin, collagen type IV, heparin sulphate proteoglycan and entactin are the components that may be found in BD Matrigel Matrix, which is a solubilised preparation of tissue basement membrane. Parental cells and FABP5 or AR knockout cells that were actively growing and had a confluency of <80% were kept for 24h in serum-free RPMI 1640 medium before testing for invasion. After starving for twenty-four hours, the cells were collected, counted using a haemocytometer, and added to a serum-free medium to form a suspension of 50000 cells per ml within serum-free medium. Meanwhile, each chamber was removed from the -20°C freezer before warming them to ambient temperature. Following that, 0.5 ml medium at 37°C was administered into inserts, and they were left for two hours' rehydration inside a humidified tissue culture incubator in conditions of 37°C and 5% CO_2. Once rehydrated, removal of medium was performed very carefully to avoid disrupting the GFR MatrigelTM Matrix layer that was on the membrane. Lastly, 25,000 cells in 0.5 ml of medium were put into each upper compartment of the chambers, and 1 ml of regular medium containing 10% (v/v) FBS was poured into each well of the bottom compartments. The experiment was carried out within a humidified tissue culture chamber in conditions of 37°C with 5% CO_2 for 24 h. Each cell line was tested in triplicates. The cells that were still there on the filter's upper side after incubating for 24 h were carefully removed with a cotton swab, then

rinsed in PBS. This was followed by cell fixing and staining with crystal violet for ten minutes(**Figure18**). Following a number of washes in water, the chambers were allowed to dry at 37ºC and the number of the invading cells migrating to the lower filter area were counted using a microscope (EVOS, Thermo Scientific, UK) at 20 x magnification.
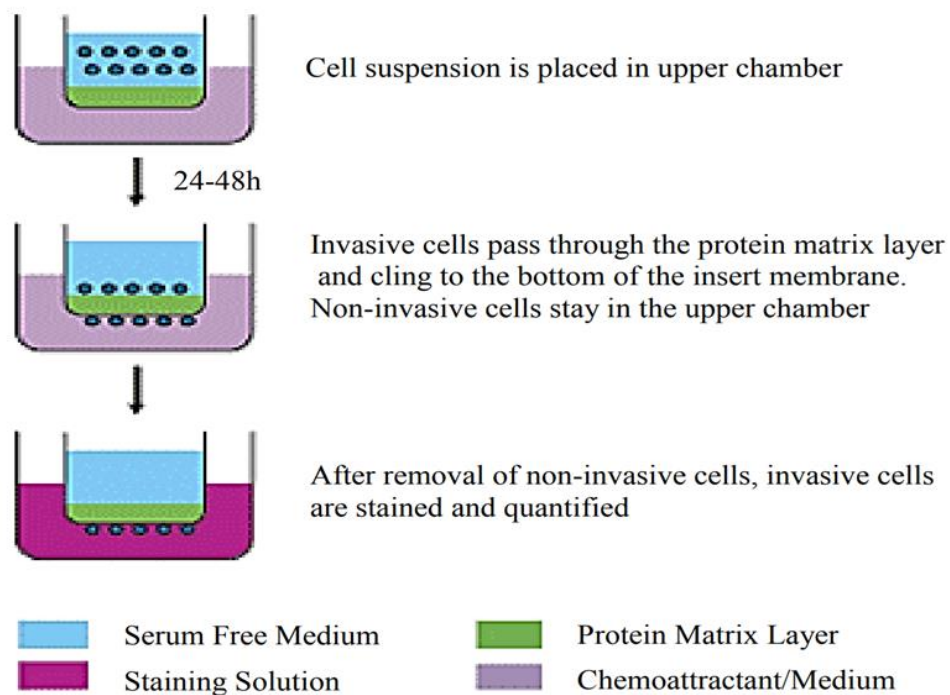
Figure 18.The workflow of the invasion experiment, which was carried out in chambers with a pore size of 8 µm and a Matrigel matrix coating.

2.5.4 Soft agar assay

Cell transformation and carcinogenesis are characterized by a number of hallmarks, one of which is anchorage-independent growth. The soft agar colony formation assay is a frequently used in vitro assay in monitoring anchorage-independent growth and measuring proliferative activity within a semisolid matrix. The technique is used to test

for malignant transformation in cells. The assay was designed to investigate the tumorigenic potential of cells in an environment that was independent of anchorage.

To carry out the test, six-well plates were initially covered with 2 ml of regular/selective culture medium containing 10% FCS as well as 2% (w/v) low melt agarose gel.After cooling at 4°C for 20 minutes, the mixture was placed in the refrigerator for solidification.

Routine growth was conducted with parental cells, and FABP5 or AR knockout cells until they reached 70–80% confluency, before detaching collecting, and adjusting them using routine medium to 5,000 cells per well. After that, 1 ml cell suspension from each cell line (containing 5000 cells/ml) and 1% low melt point agarose gel were combined. The resulting mixture was poured onto the top of wells in six-well plates that had previously been coated. For the purpose of consolidation, the complexes were chilled at 4°C for ten minutes. Each plate was then incubated at 37°C with 5% CO_2 for 28 days. During this period, cell cultures were maintained using standard culture medium applied at 200 ul/well weekly. Finally, the colony staining was performed using 0.5 ml 2% MTT (5mg/ml) (3-(4, 5-dimethylthiazl-2-yl)-2, 5-diphenylterazolium bromide) and incubating at 37°C with 5% CO_2 for 240 minutes. A Colony Counter (Oxford Optronix, UK) was used to count colonies that were bigger than 150um in diameter.

2.6 Statistical analysis

Prism 9 and ImageJ tools were used to conduct analysis on the data presented here. T-tests, comparing the means between two groups, were performed in this study to analyse any identified difference in the experimental group and controls for Western blotting, proliferation and invasion assays, and soft agar assay. The results are considered to have statistical significance at $p \leq 0.05$

Chapter 3 . Result-1 : Investigation of the expression status of FABP5-related proteins in PCa cell lines and establishment of *FABP5-* or *AR-* KO sublines

3.1 Introduction

Within the scope of this chapter, a comprehensive investigation was conducted to ascertain the expression status of FABP5 and its functionally related factors in prostate cells. The examination encompassed benign PNT2 cells, as well as prostate cancer cell lines including 22RV1, DU145, and PC3M. By scrutinizing these diverse cellular models, our objective was to acquire a thorough understanding of the intricate expression patterns and potential implications of FABP5 and its associated factors in prostate biology and the progression of cancer. our study also aimed to generate the FABP5 or AR knockout single clones using the RNP CRISPR-Cas9 system in both androgen-responsive and androgen-unresponsive cancer cell lines. These single clones provided us with valuable tools to further investigate the specific roles of FABP5 and AR in prostate cell behavior

3.2 Expression of FABP5 and its functionally related factors in prostate cell lines

3.2.1 Expression of FABP5

Western blot analysis was performed to detect the expression of FABP5 in benign and prostate epithelial cells(**Figure 19**). As shown in figure 19, A FABP5 expression was not detected in benign PNT2 cells. But a 15kDa FABP5 band was detected in moderately malignant cell line 22RV1 and strong band was detected in the highly malignant cell lines DU145, PC3M. Quantitative analysis with densitometric scanning showed that levels of FABP5 expressed in these cells are very different. When the level of FABP5 in 22RV1 was set at 1, relative levels in the malignant DU145 and PC3M cells were increased to 1.58 ± 0.075 and 2.9 ± 0.15, respectively. In contrast, no detectable level of FABP5 was found in the benign PNT2 cells (Figure 19, B)

A

	PNT2	22RV1	DU145	PC3M	
FABP5					15 KDa
β-Actin					42 KDa

B
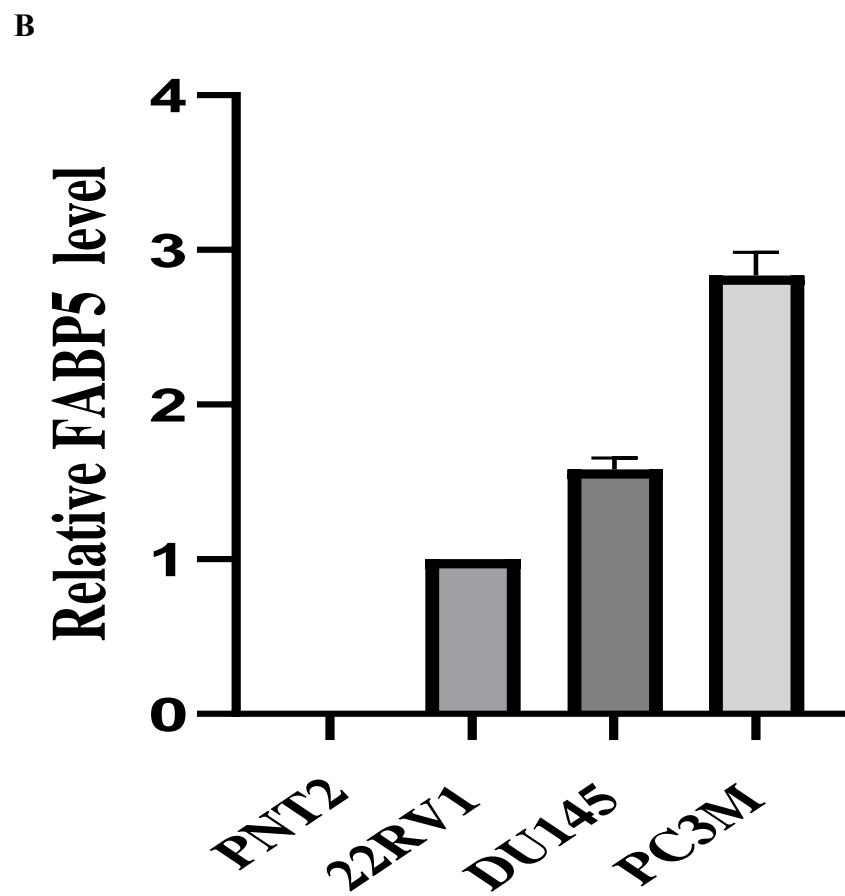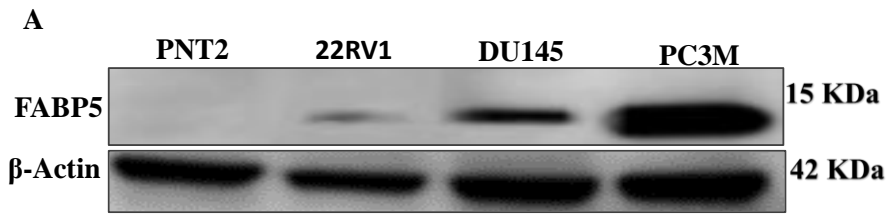
Figure 19. FABP5 expression in prostate epithelial cell lines. (A) FABP5 immunoblot analysis in benign and cancerous prostate cell lines. (B) Quantitative measurement of the peak area intensities of bands on the blot using densitometry scanning. Three separate independent experiments yielded the data (Mean ± SD). The image was used to measure the band intensities to determine the relative amounts of FABP5.

3.2.2 Expression of PPARγ1 & 2

Western blot analysis (**Figure 20**) showed that both PPARγ1 and PPARγ2 were expressed in PNT2 with strong bands. In 22RV1 cells, the PPARγ1 band was much stronger than that of PPARγ2. But in the DU145 cells the PPARγ1 band was very weaker than that of PPARγ2. In PC3M cells, PPARγ2 was weak, whereas PPARγ1 was moderately prevalent(Figure 20, A). When the level of PPARγ1or PPARγ2 in PNT2 was set to 1 respectively, the levels of PPARγ1 was 1.2 ± 0.026 in 22RV1 cells, 0.21 ±0.032 in DU145 cells, and 0.42 ± 0.02 in PC3M cells, respectively. PPARγ2 levels were 1.5 ± 0.1 in PNT-2 cells, 0.47 ± 0.04 in 22RV1 cells, 0.47 ±0.02 in DU145 cells, and 0.05 ± 0.08 in PC3M cells, respectively(Figure 20, B).

A

B
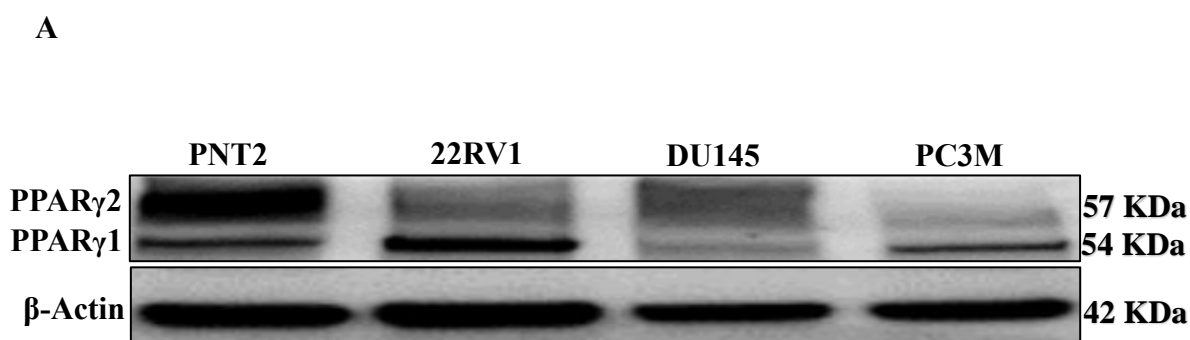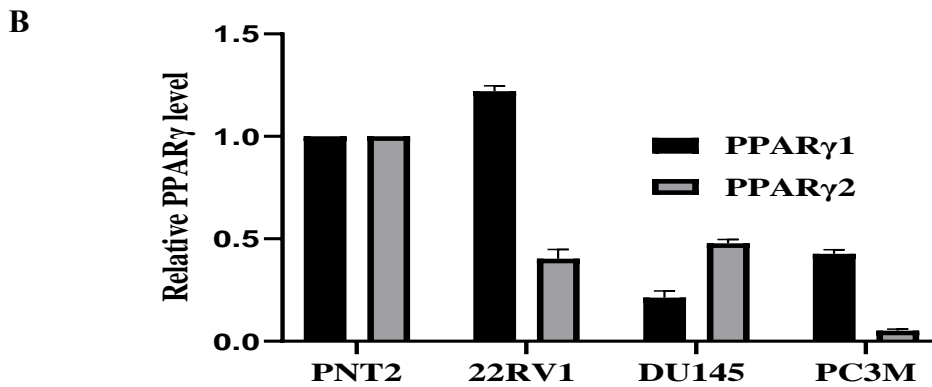
Figure 20. PPAR1 and PPAR2 expression in prostate cancer cell lines. (A). Western blot identification of PPAR1 and PPAR2 expression in several prostate cell lines. (B). Quantitative examination of band intensities using densitometry scanning of peak areas on the blot. Each result (Mean ± SD) was derived from three separate independent experiments. Image J was used to evaluate the band intensities photographs..

3.2.3 Expression of (Phosphorylated) p-PPARγ1 & 2 protein

The results of Western blot analysis of p-PPARγ1 and p-PPARγ2 expression were shown in **figure 21.** As shown in figure 21, A levels of p-PPARγ1 and p-PPARγ2 expression in the benign PNT2 cells were not detectable by Western blots. The p-PPARγ1 and p-

A
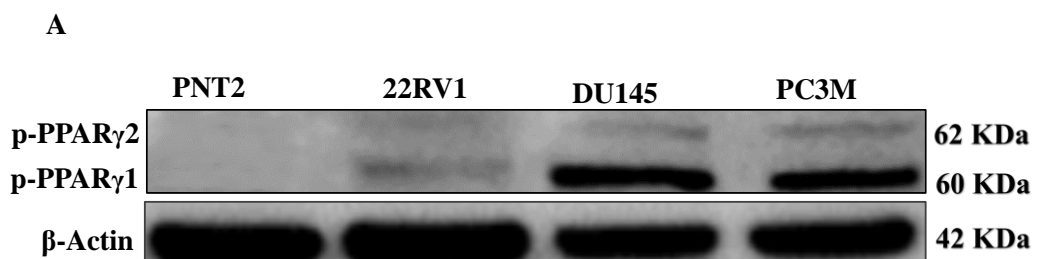
PPARγ2 bands in the moderately malignant 22RV1 cells were much weaker than those detected in the highly malignant DU145 and PC3M cells. Further quantitative analysis showed that the level of p-PPARγ1 was much higher than that of p-PPARγ2 in both DU145 and PC3M cells (figure 21, B). When the level of p-PPARγ1 in 22RV1 was set at 1, the relative levels of p-PPARγ1 were $2.3 \pm 0,06$ and 2.2 ± 0.08 in DU145 and PC3M, respectively. When the level of p-PPARγ2 was set at 1, relative levels of p-PPARγ2 in DU145 and PC3M were 1.02 ± 0.04 and 1.3 ± 0.03, respectively.

B
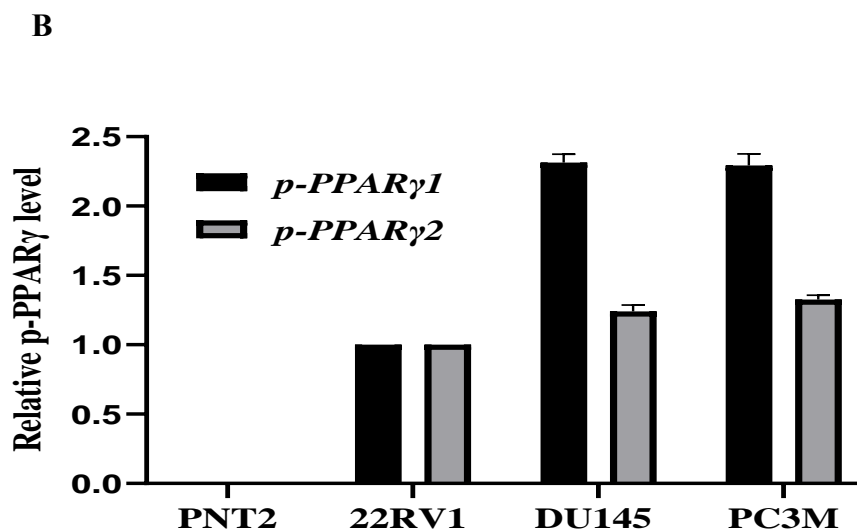
Figure 21. The expression of p-PPAR1 and p-PPAR2 in prostate cancer cell lines. (A) p-PPAR1 and p-PPAR2 Western blot analyses in benign and cancerous prostate cells. The B-Actin antibody was utilized to address any sample loading problems. (B) Relative levels of p-PPAR1 and p-PPAR2 expression in various prostate epithelial cells.

Densitometric scanning of the intensities of peak area of the bands on the blot yielded the results. The statistics reported here were the mean standard deviation (Mean ± SD) of three separate independent experiments. Image J program was used to evaluate the band intensity images.

3.2.4 Expression of AR and ARV7

Western blot analysis (**Figure 22**) showed that AR FL and ARV7 were expressed only in the androgen responsive 22RV1 cells. The expression of either AR FL or V7 were detected neither in the benign PNT2 cells, nor in the highly malignant cells DU145 and PC3M.
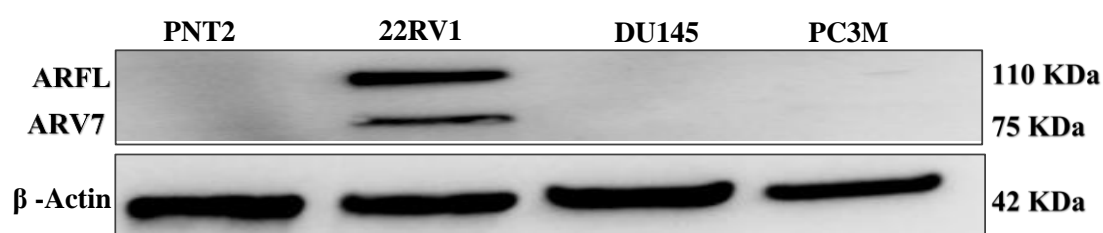
Figure 22. Western blot analysis of AR FL and ARV7 expression in benign and malignant prostate epithelial cells. An antibody against β-Actin was used to hybridize the blot to correct possible sample loading discrepancies.

3.2.5 Expression of VEGF

The results of Western bot analysis of VEGF expression in different prostate epithelial cells were shown in **figure 23**. Expression of VEGF was detected in all cell lines used in this study. The VEGF expression in PNT2 cells appeared to be lower than in any of the other cell lines. A strong VEGF band was detected in all three malignant cell lines(Figure 23, A). Relative levels of VEGF expression in all 4 cell lines were shown figure 23, B.

When the VEGF level is set at 1 in PNT2, its relative expression levels were 1.4 ± 0.05, 2.1 ± 0.11, and 1.9 ± 0.05 in 22RV1, DU145, and PC3M, respectively.

A

B
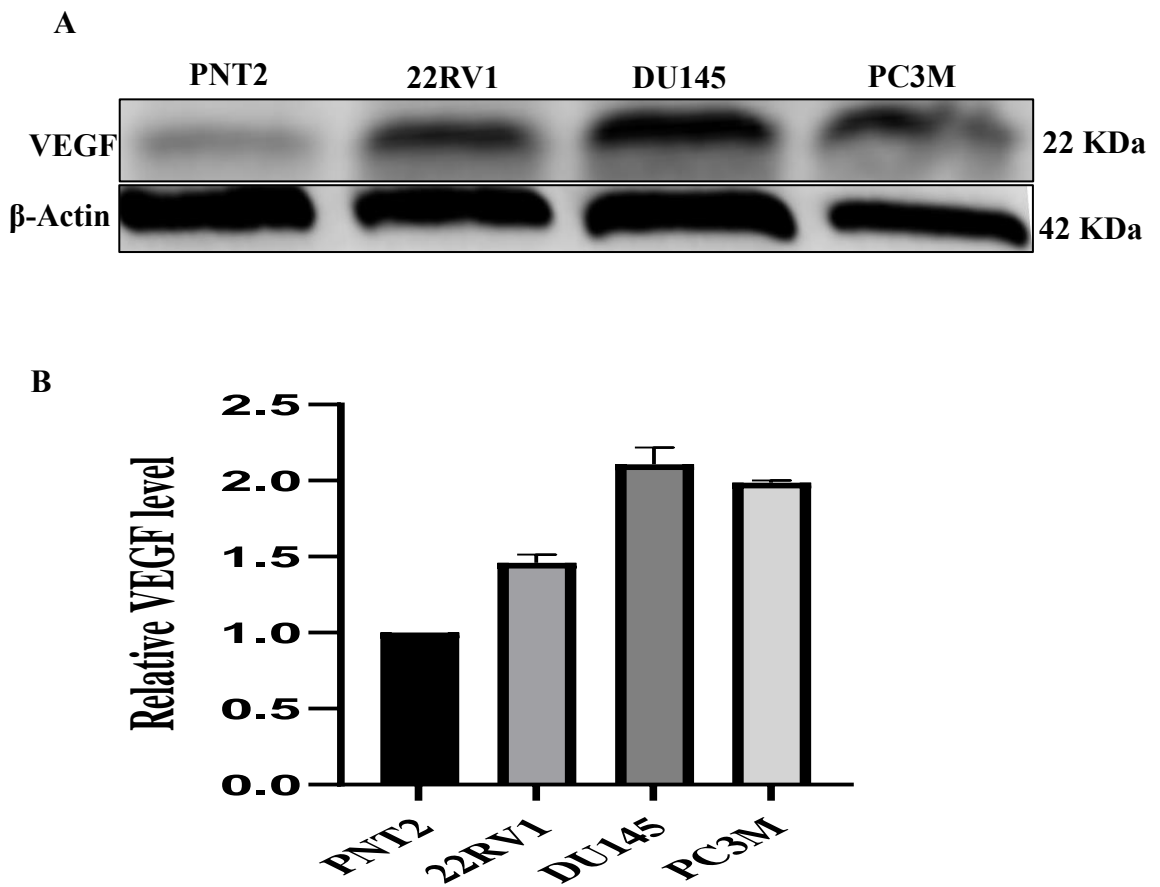
Figure 23. VEGF expression in normal and cancerous prostate epithelial cells. (A) VEGF Western blot investigation in various prostate epithelial cell lines. To hybridize the blot and address any sample loading problems, an anti-actin antibody was utilized. (B) Relative levels of VEGF expression in various prostate epithelial cells. Densitometric scanning of the intensities of peak area of the bands on the blot yielded the results. The statistics reported here were the mean standard deviation (Mean $\pm$ SD) of three different independent experiments. Image J program was used to evaluate the band intensity images.

Establishment of new cell lines derived from different prostate epithelial cell lines with either FABP5 or AR gene knocked out

The *FABP5* gene KO in 22RV1, DU145 and PC3M and the *AR* gene KO in 22RV1 cells were accomplished with the cutting-edge gene editing approach, CRISPR-Cas9. The gRNA sequences for FABP5 22RV1,DU145 and PC3M were 5'-AAGTATCAACTTCATCATAG -3, 5'- GATGAATACATGAAGGAGCT -3 and 5'-AAGTATCAACTTCATCATAG -3 respectively. The gRNA for AR 22RV1 was 5'-CAACGCCAAGGAGTTGTGTA-3', 5' GGTTACACCAAAGGGCTAGA -3' and 5' GCAGAAATGATTGCACTATT -3'. The gRNA sequences listed in table 1.3 section 2.3.2 were designed using Integrated DNA Technology's Alt-R® CRISPR-Cas9 guide RNA designing tools to target the FABP5 gene and the AR gene in different exons.

3.3 Generation of the *FABP5* KO sub-line from 22RV1 cells

3.3.1 Lipofection transfection efficiency of the Cas9 protein along with the crRNA:tracrRNA(sgRNA)-ATTO-550-RNP and FACS sorting of the fluorescently labelled cells.

Ribonucleoprotein (RNP), which consists of Cas9 nuclease associated with crRNA: tracrRNA duplex or sgRNA, was used to edit the genome of 22RV1 cells**.** The result of transfecting 22RV1 cells with the crRNA: tracrRNA or (sgRNA)-ATTO-550-RNP mixture were recorded in **figure 24** One hour after the Cas9 protein and the sgRNA-ATTO-550-RNP mixture was transfected, cell images taken under fluorescence microscope confirmed that the transfected cells (Figure 24, B) were successfully labelled with RFP (red), whereas the control (black and white) was not (Figure 24, A). After 24 hours the control cells and the transfected cells were subjected to FACS with the setup gating system to select the successfully transfected, or RFP- labeled cells. The control cells were shifted to the left side as shown in figure 24, C and the RFP- labelled

transfected cells shifted to the right side as shown in figure 25, D. As pointed by the black

arrowhead in Figure 25, D 97.2% of the cells were effectively transfected.
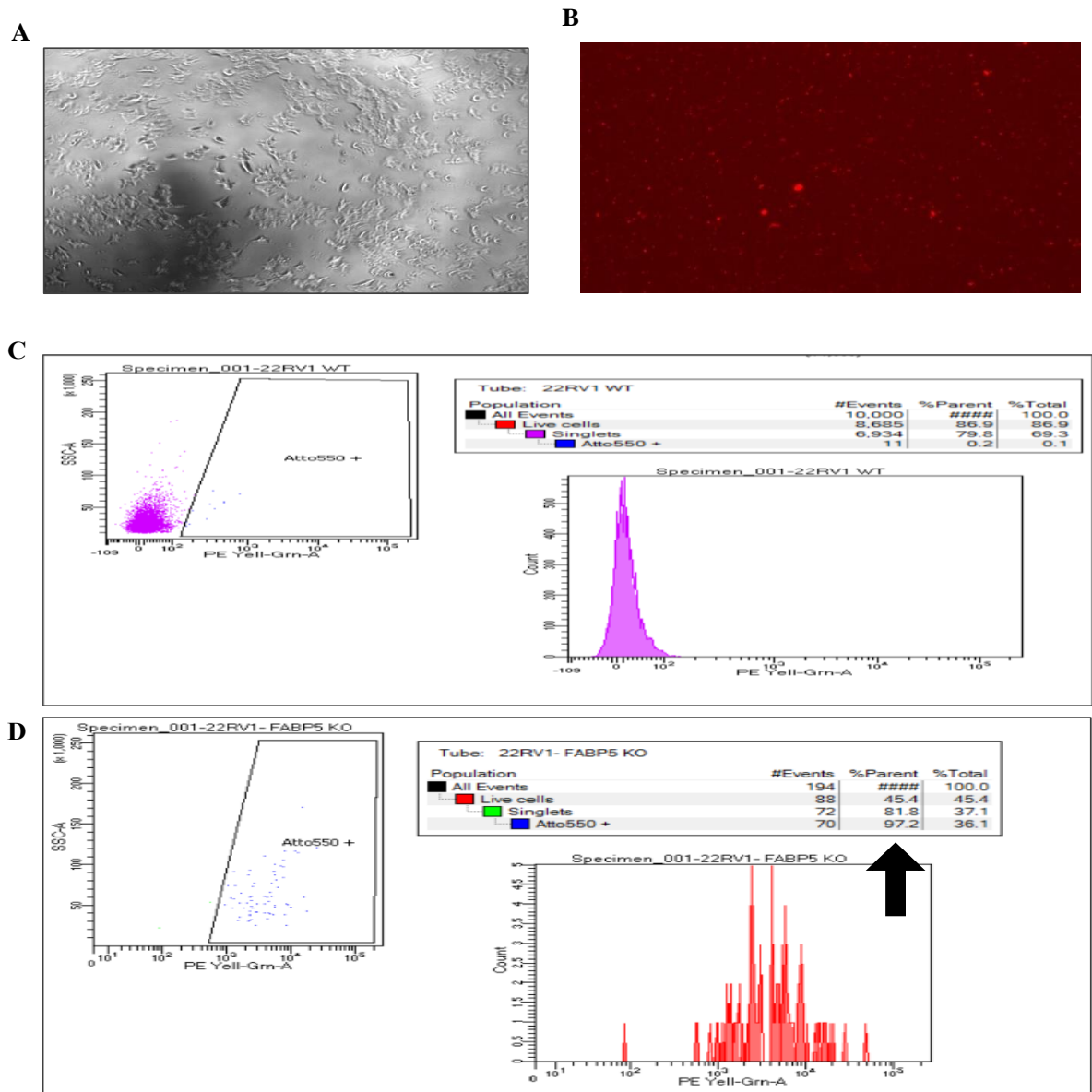
Figure 24. Transfection of 22RV1 with the sgRNA-ATTO-550-RNP mixture. **A)** Image

of control 22RV1 cells with no RFP labels under florescent microscope. **B)** Image of the

transfected 22RV1 cells labelled with RFP under florescent microscope. **C)** The control

22RV1 cells and the transfected, RFP-labelled cells were sorted by FACS and were

divided between the right and the left quadrant. **D)** 22RV1-FABP5-KO transfected or RFP-labelled cells sorted by FACS.

3.3.2 Confirmation of the successful *FABP5* KO in 22RV1 cells with Western blot

FABP5 expression was tested with Western blot in 22RV1 parental cells and the 5 KO colonies developed from 5 single transfect, respectively (**Figure 25**). As shown in figure 25, A the control 22RV1 (untreated parental cells) expressed the highest level of FABP5. No FABP5 was detected C5. For other 4 sub-lines, FABP5 was expressed at varies levels, although these levels were significantly lower than that expressed in the control cells. The relative levels of FABP5 in the control and in different sub-lines were obtained by further quantitative analysis of the intensities of the peak regions of the bands on the blot showed (Figure 25, B). When the FABP5 level in control cells was set at 1, the relative FABP5 levels of C1, C2, C3, C4, and C5 were 0.36 ±02, 0.52 ±07, 0.21 ±001, and 0.30 ±01, respectively. For C5, the expression of FABP5 was not detected. Thus C5 was identified as successful FABP5 KO cells which did not express FABP5 anymore.

A
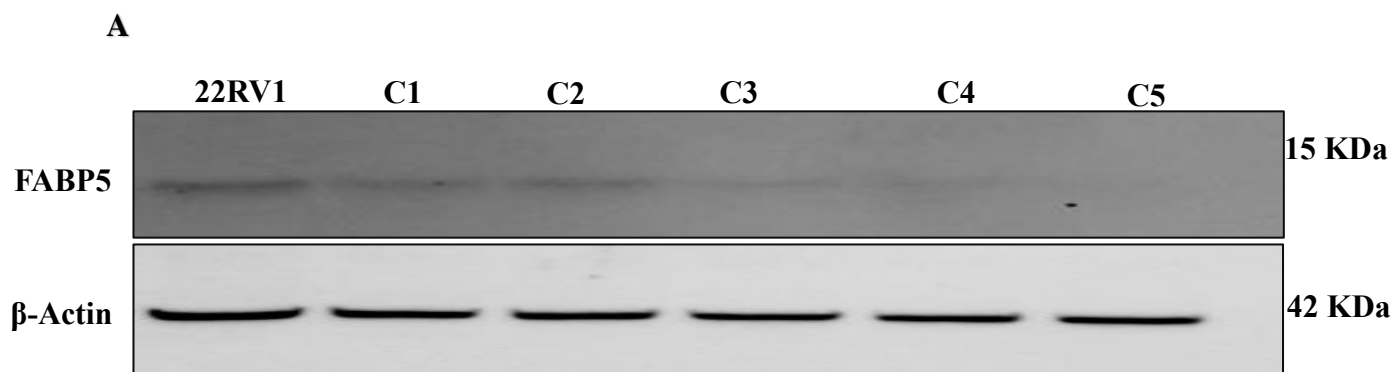
B
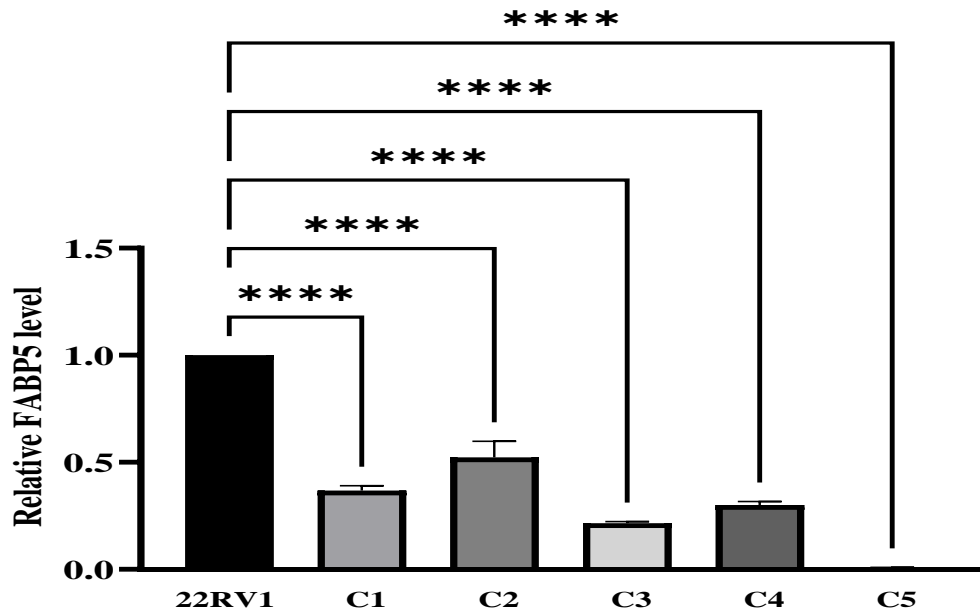
Figure 25. FABP5 expression levels were determined in parental 22RV1 cells and 5 KO transfect sub-lines. Individual colonies-developed sub-lines were labelled C1, C2, C3, C4, and C5, and each was created from a single transfect clone. **(A)**. FABP5 levels were measured using a Western blot in control 22RV1 cells and 5 sub-lines. To hybridize the blot and address any sample loading errors, an antibody against -Actin was utilized. **(B)**. FABP5 relative values were expressed in the control and five sub-lines. The outcome (mean ± SD) was derived from three separate independent experiments. Ns stands for not significant (p>0.05). When p0.05 was utilized, the result was considered significant, and the rising number of stars indicated the greater degree of significance.. *$p<0.05$, **$p<0.001$, ***$p<0.0002$ and ****$p<0.00001$.

3.3.3 The morphology of C5-derived KO cells.

After several passages of the 22RV1 C5 subline, Western blot analysis was performed to detect the expression of FABP5 once more to further confirm the KO effect, and light microscopy images were taken to check the morphological changes (**Figure 26**). As shown in figure 26, A, no FABP5 was detected in C5 cells, although it was expressed in the parental 22RV1 cells, further confirming that the *FABP5* gene was indeed knocked out in the C5 cells. The light microscopy images showed that C5 cell grew much slower than their parental cells, and the cell body was more elongated spindle form, a much less malignant morphological appearance (Figure 26, B).
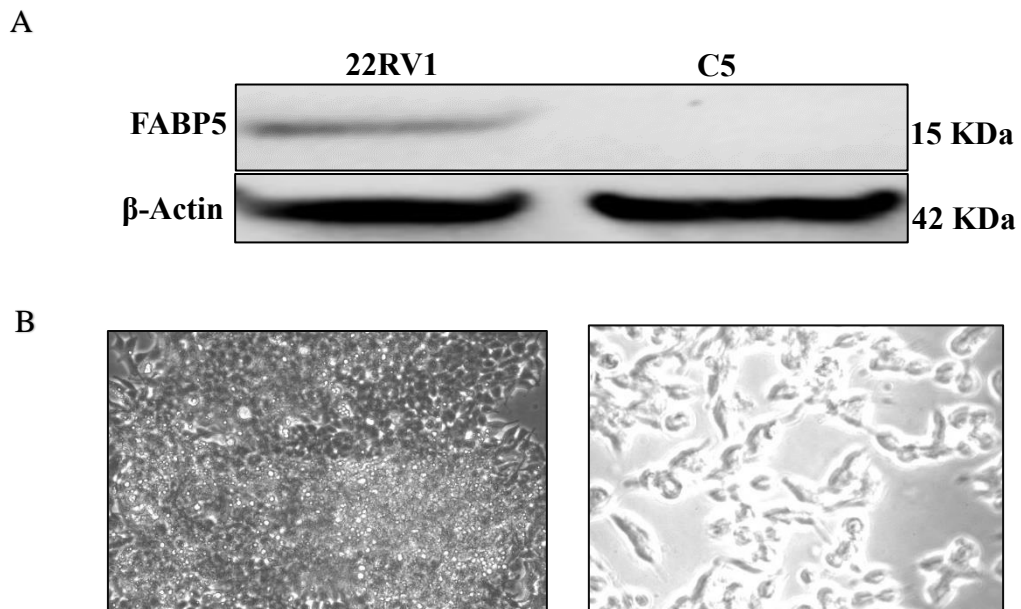
Figure 26. The expression of FABP5 in C5 cells was examined through Western blot analysis following multiple passages and their morphological changes. **(A)**. Western blot analysis of FABP5 expression in C5 cells. An antibody against β-Actin was used to hybridize the blot and to standardize the hybridization. **(B)** Microscopic images on the left showcases the typical morphology of the 22RV1 parental cells, while the image on the right displays the distinctive morphology of the C5 knockout cells. These images serve to illustrate the impact of the knockout on the cellular phenotype, highlighting the

morphological alterations resulting from the absence of the FABP5 gene. Magnification: 22RV1,20x C5, x20.

3.3.4 Nucleotide sequence analysis

Genomic DNA extracted from C5 cells was subjected to nucleotide sequence analysis to confirm the FABP5 gene was knocked out successfully. A segment of DNA in *FABP5* region was amplified by PCR with a positive primer 5-'GGCAAGAGGAGCTGGTTAG-3'and negative primer 5'GAGGGTCACGGTAGTTATTTCA-3'. The DNA fragment amplified by PCR was then subjected to Sanger sequencing. The result of the nucleotide sequence analysis was shown in **figure 27**. Sequence alignment analysis of the 22RV1 parental cells and the C5 cells (Figure 27, A) showed that the single mutation occurred in BP number 61 of targeted region of the *FABP5* gene: a "G" in the parental cells was mutated into a "C" in the C5 cells (pointed by the black arrow head). This was a frameshift mutation which led a complete inactivation of the *FABP5* gene. This mutation was also confirmed by the sequence analysis recording chart (Figure 27, B), pointed by the black arrow head).
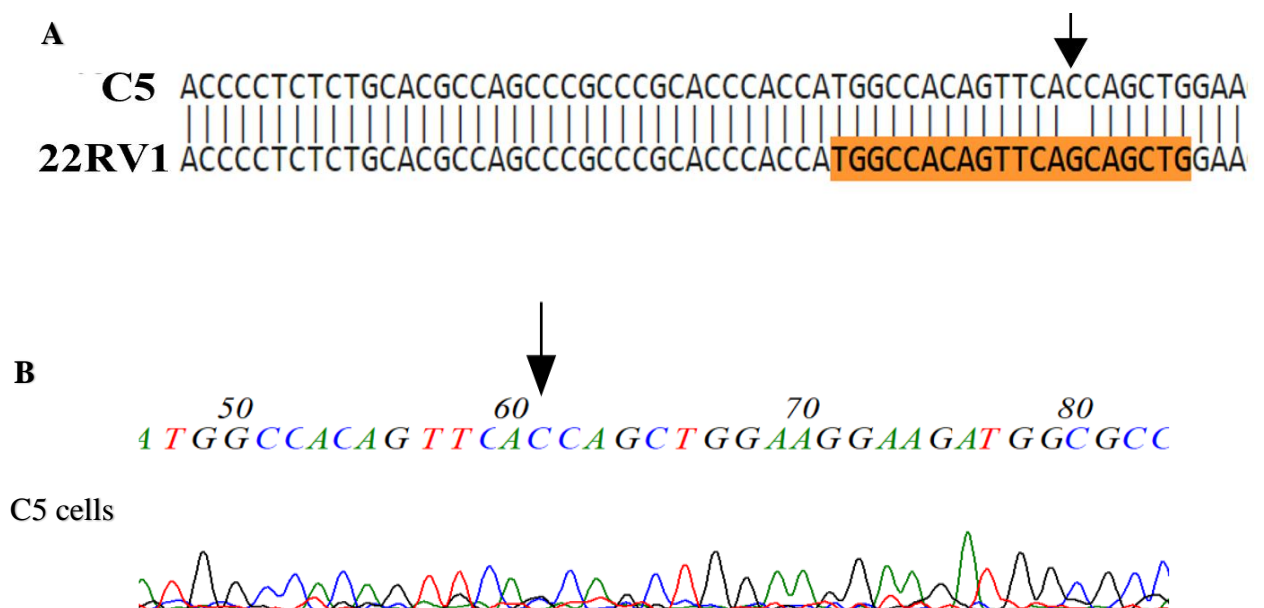
Figure 27. Nucleotide sequence analysis of the *FABP5* gene in the parental control and the C5 cells. **(A)**. Nucleotide sequence alignment on the targeted region of the *FABP5* gene of the 22RV1 cells and the C5 cells. The gRNA targeted region was highlighted with an orange color. **(B)**. Nucleotide sequence analysis recording chart. The black arrow head pointed to the mutated base.

3.4 Generation of *FABP5* KO sub-lines from DU145 cell lines

3.4.1 Lipofection transfection efficiency of the Cas9 protein along with the crRNA:tracrRNA(sgRNA)-ATTO-550-RNP and FACS sorting of the fluorescently labelled cells.

The result of transfecting DU145 cells with the crRNA: tracrRNA or (sgRNA)-ATTO-550-RNP mixture were recorded in **Figure 28** One hour after the Cas9 protein and the sgRNA-ATTO-550-RNP mixture was transfected, cell images taken under fluorescence microscope confirmed that the transfected cells (Figure 28, B) were successfully labelled with RFP (red), whereas the control (black and white) was not (Figure 28, A). After 24 hours the control cells and the transfected cells were subjected to FACS with the setup gating system to select the successfully transfected, or RFP- labeled cells. The control cells were shifted to the left side as shown in figure 28, C and the RFP- labelled transfected cells shifted to the right side as shown in figure 28, D. As pointed by the black arrowhead in Figure 29, D 98.3% of the cells were effectively transfected.
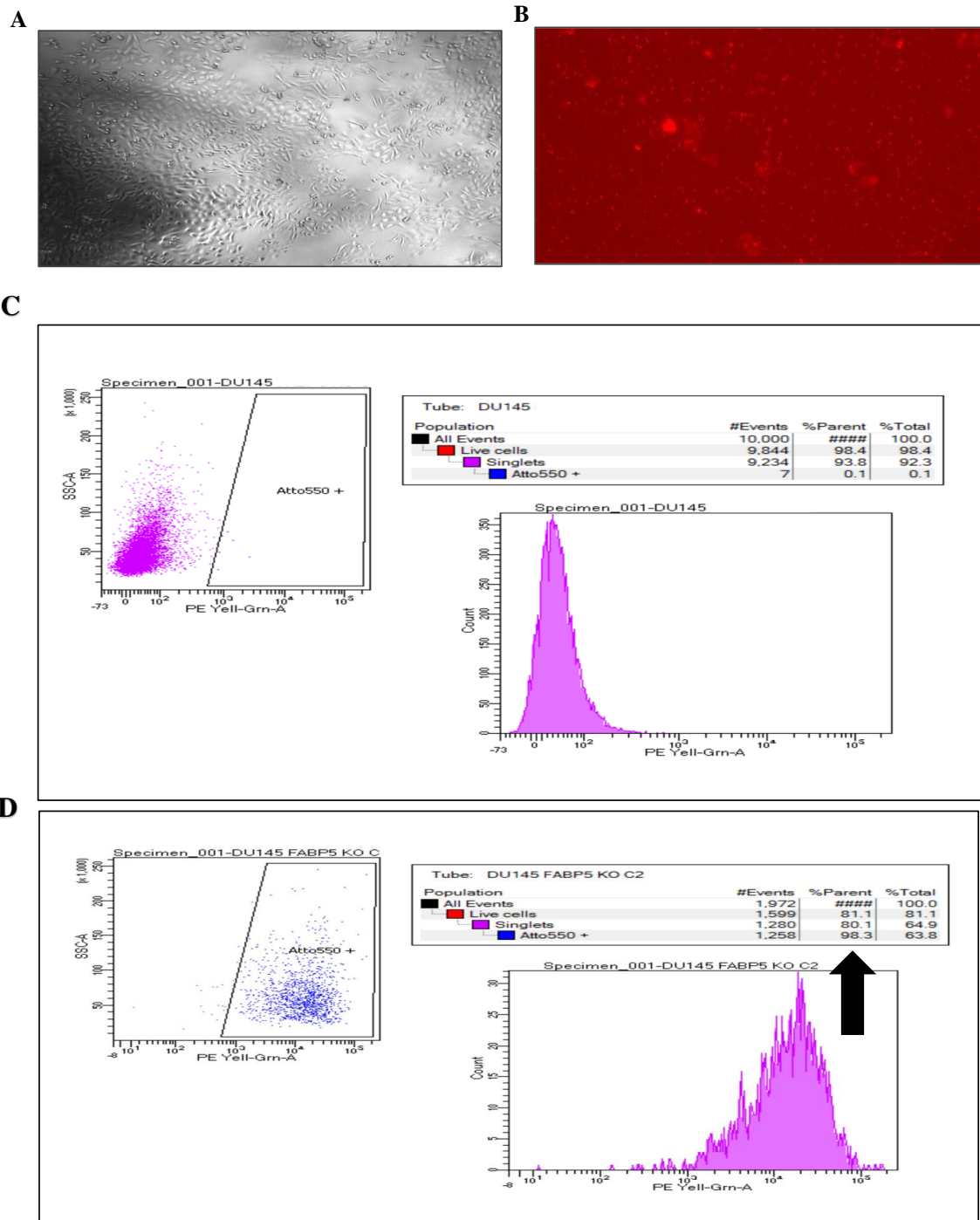
Figure 28. Transfection of DU145 with the sgRNA-ATTO-550-RNP mixture. **A)** Image of control DU145 cells with no RFP labels under florescent microscope. **B)** Image of the transfected DU145 cells labelled with RFP under florescent microscope. **C)** The control DU145 cells and the transfected, RFP-labelled cells were sorted by FACS and were

divided between the right and the left quadrant. **D)** DU145-FABP5-KO transfected or RFP-labelled cells sorted by FACS.

3.4.2 Confirmation of the successful *FABP5* KO in DU145 cells with Western blot

The results of the Western blot analysis on the expression of *FABP5* in DU145 parental control cells and two *FABP5*-KO sublines, C1 and C2, were shown in **figure 29**. The level of FABP5 expression was the highest in the parental control cells, as shown in Figure 29 ,A. The levels in both sublines C1 and C2 were much lower than that expressed in their parental control cells. The quantitative analysis of the relative levels of FABP5 expression was shown in figure 29 ,B. When FABP5 level in the control cells was set at 1, the relative levels of FABP5 in C1 and C2 were 0.1 ± 0.04 and 0.05 ±0.024; reducing 10 and 20 times, respectively, comparing to their parental control cells.

A
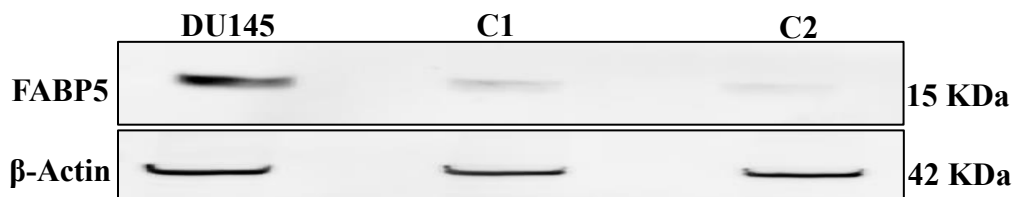
B
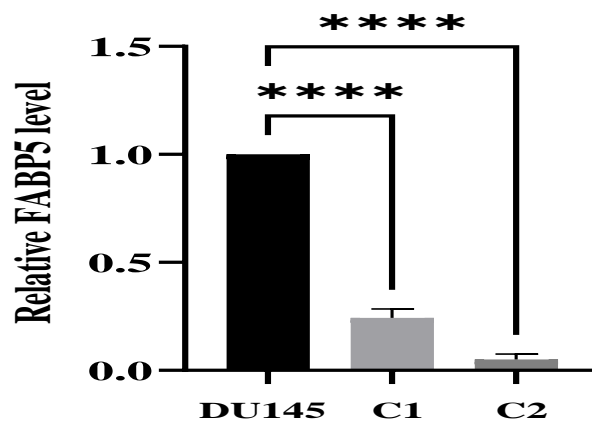
Figure 29. FABP5 expression levels in the parental DU145 cells and in sublines C1 and C2. **(A).** Western blot analysis of the expression of FABP5 in 3 different cell lines. An antibody against β-Actin was used to hybridize the blot to standardize the hybridization. **(B).** Quantitative analysis of the relative levels of FABP5 in the parental control cells and in C1 and C2 cells. The result (mean ± SD) was obtained from 3 separate densitometrical experiments of the intensities of peak areas of the bands on the blot. FABP5 levels between the control and the sublines were compared and the result was subjected to Student t-test. The difference is regarded as statistically significant when $p<0.05$ which was marked with a star. Then the number of stars was increased as the increasing degree of significance until 4 stars. $*P<0.05$, $**P<0.001$, $***P<0.0002$ and $****p<0.00001$.

3.4.3 The morphology of C2-derived KO cells

The above Western blot analysis indicated that most of C2 cells were successful KO transfectants. After several passages, a single cell clone selected from C2 was cultured continuedly to form a subline which was still named C2. A further Western blot analysis was performed to detect the FABP5 expression and the results were shown in **figure 30**. As shown in figure 30, A although a high level of FABP5 was expressed in the parental control cells, no FABP5 was detected in C2 cells, indicating the *FABP5* was completely knocked out. Microscopy images taken from the cultured cells (Figure 30, B) showed C2 cells grew much slower, and looked short with a spindle form. In contrast, the parental DU145 cells grew much faster, and look longer and exhibited a typical highly malignant morphology.

A
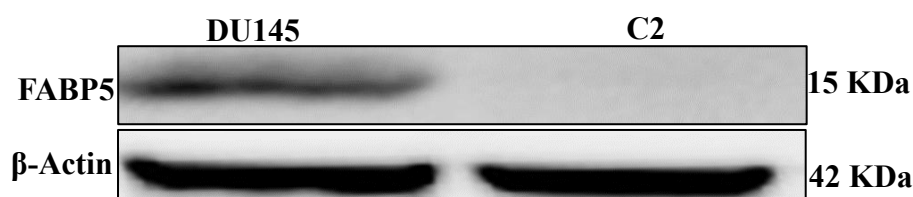
B
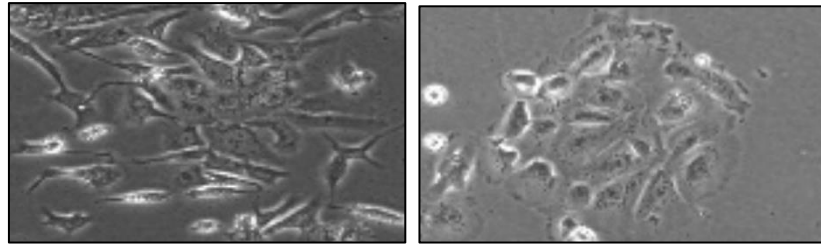
Figure 30. Morphological changes of C2 cells and their FABP5 expression. **A).** Western blot analysis of FABP5 expression in parental DU145 cells and in the C2 subline. An antibody against β-Actin was used to hybridize the blot and standardize the hybridization. **B).**Microscopic images of DU145 (left) and the C2 subline cells (right) .The image on the left showcases the typical morphology of the DU145 parental cells, while the image on the right displays the distinctive morphology of the C2 knockout cells. These images serve to illustrate the impact of the knockout on the cellular phenotype, highlighting the morphological alterations resulting from the absence of the FABP5 gene. Magnifications: DU145: x20; C2: x20.

3.4.4 Nucleotide sequence analysis of the targeted region in *FABP5* gene

The genomic DNA was prepared from both DU145 cells and the subline C2 cells. The targeted region of *FABP5* gene was amplified by PCR with positive primer 5-'GGCAAGAGGAGCTGGTTAG-3'and negative primer 5'GAGGGTCACGGTAGTTATTTCA-3'. Nucleotide sequence analysis was performed and the sequences of this region of genomes of DU145 and C2 cells were shown in **figure 31**. DNA sequence alignment analysis revealed that several base pairs from bp 117 to bp 130 of the FABP5 gene were deleted by KO, as shown in figure 31, A (the deleted segment was pointed by the arrow head). The sequencing analysis recording chart shown

in Figure 31, B further confirmed the loss of a 14bp DNA segment from the targeted region of the *FABP5* gene Pointed by the arrow head).

A

B
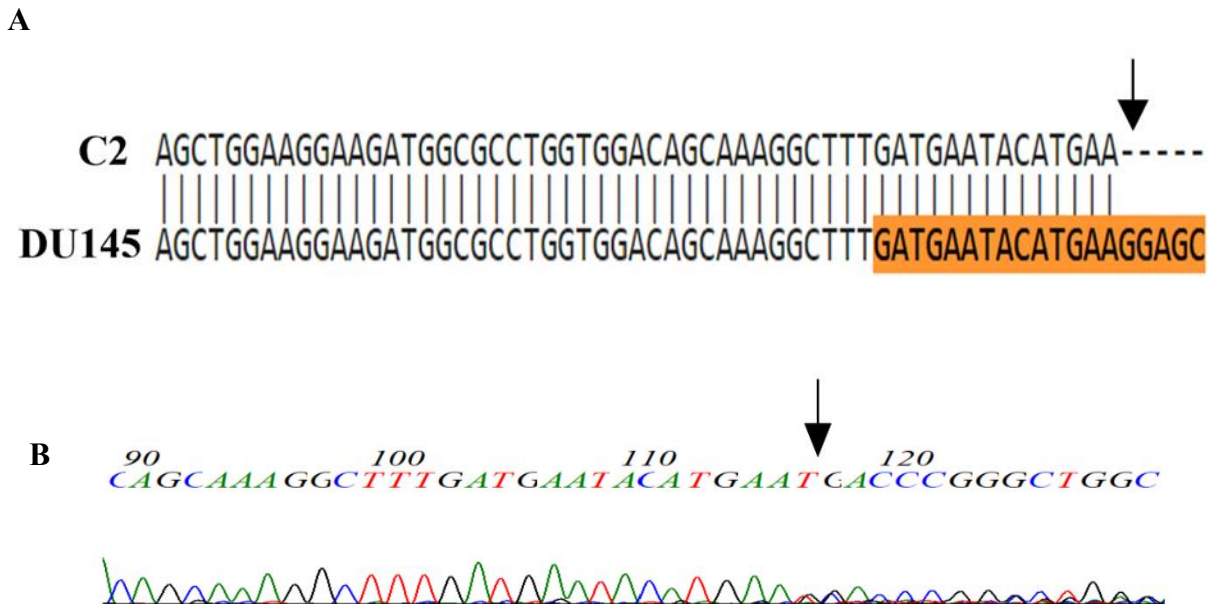
Figure 31. Nucleotide sequence analysis of the *FABP5* gene in the parental DU145 cells and in the C2 cells. **(A)**. Nucleotide sequence alignment on the targeted region of the *FABP5* gene of the DU145 cells and the C2 cells. The gRNA targeted region was highlighted with an orange color. **(B)**. Nucleotide sequence analysis recording chart. The black arrow head pointed to the location of the deleted 14bp DNA segment in the targeted region of the *FABP5* gene.

.

3.5 Generation of FABP5 knockout in PC3M cell lines

3.5.1 Lipofection transfection efficiency of the Cas9 protein along with the crRNA:tracrRNA(sgRNA)-ATTO-550-RNP and FACS sorting of the fluorescently labelled cells

The result of transfecting PC3M cells with the crRNA: tracrRNA or (sgRNA)-ATTO-550-RNP mixture were recorded in **Figure 32.**One hour after the Cas9 protein and the sgRNA-ATTO-550-RNP mixture was transfected, cell images taken under fluorescence microscope confirmed that the transfected cells (Figure 32, B) were successfully labelled with RFP (red), whereas the control (black and white) was not (Figure 32, A). After 24 hours the control cells and the transfected cells were subjected to FACS with the setup gating system to select the successfully transfected, or RFP- labeled cells. The control cells were shifted to the left side as shown in figure 32, C, and the RFP- labelled transfected cells shifted to the right side as shown in figure 32, D. As pointed by the black arrowhead in Figure 32, D, 100 % of the cells were effectively transfected.
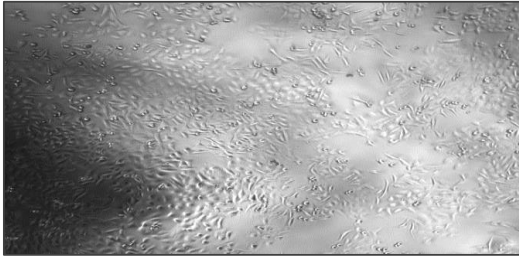
Figure 32. Transfection of PC3M with the sgRNA-ATTO-550-RNP mixture. **A)** Image of control PC3M cells with no RFP labels under florescent microscope. **B)** Image of the transfected PC3M cells labelled with RFP under florescent microscope. **C)** The control PC3M cells and the transfected, RFP-labelled cells were sorted by FACS and were divided between the right and the left quadrant. **D)** PC3M-FABP5-KO transfected or RFP-labelled cells sorted by FACS

3.5.2 Selection of the *FABP5*-KO clones from PC3M cells

Six colonies derived from the *FABP5*-KO transfectants were cultured to establish 6 separate sublines. These sublines were designated C1, C2, C3, C4, C5, and C6 respectively. All these 6 sublines and their parental PC3M cells were subjected to Western blot analysis to check the expression status of FABP5 expression. As shown in **figure 33**, the highest level of FABP5 expression was found in PC3M parental control cells. No FABP5 expression was detected in C6 cells. FABP5 was expressed in much lower levels than the control cells in other sublines (figure 33, A). The relative FABP5 levels in these cells were shown in figure 33, B. When the level of FABP5 expression in PC3M cells was set at 1, the relative FABP5 levels of C1, C2, C3,C4, and C5 were 0.06 ± 0.01 ,0.02 ± 0.08, 0.22 ± 0.09,0.05 ± 0.01 and 0.08 ± 0.04, respectively.   The FABP5 level in C6 cells was not detectable, indicating a complete success in knocking out the FABP5 gene.

A

B
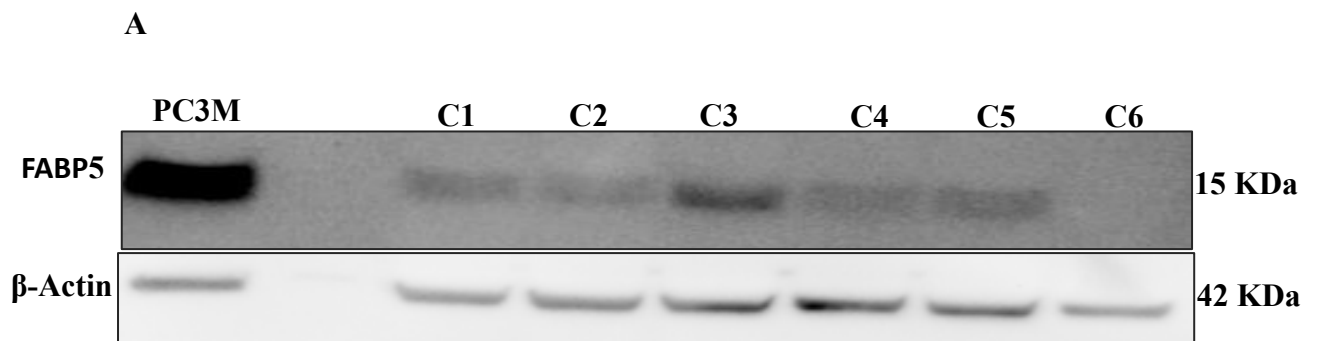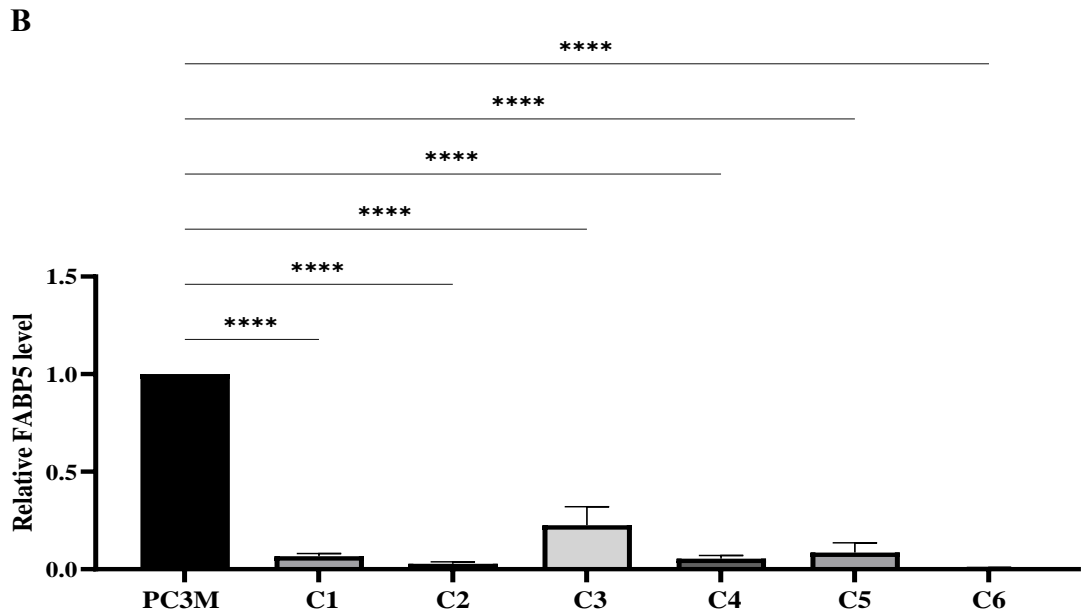
Figure 33. FABP5 levels in the parental control PC3M cells and in 6 sublines. **(A)**. Western blot analysis of the expression of FABP5 in the parental PC3M cells and 6 sublines. **(B)**. Relative levels of FABP5 in the control and 6 sublines measured by Quantitative analysis with a densitometrical scans of the peak regions of the bands on the blot. The result (mean ±S D) was obtained from 3 separate experiments. Student t-test was used to compare the means and the results were regarded as significant when p<0.05. the degree of significance was represented by the number of stars as following: *p 0.05, **p 0.001, ***p 0.0002, and ****p 0.0001.

3.5.3 Further detection of FABP5 in C6 and its morphological appearance

To further confirm the successful KO of *FABP5* gene in C6 cells, we performed a second western blot analysis of FABP5 gene after a few more passages of the C6 cells (**Figure 34**). As shown in figure 34, A, although FABP5 level in the parental PC3M cells was very high, no FABP5 was detected in C6 cells, further confirming that the FABP5 gene was completely inactivated. The light microscopy images taken from the cultured cells shown (Figure 34, B) the morphological appearance of the C6 cells (right) to be more shortened and spindle look when compared with their parental PC3M cells (left).

A

B
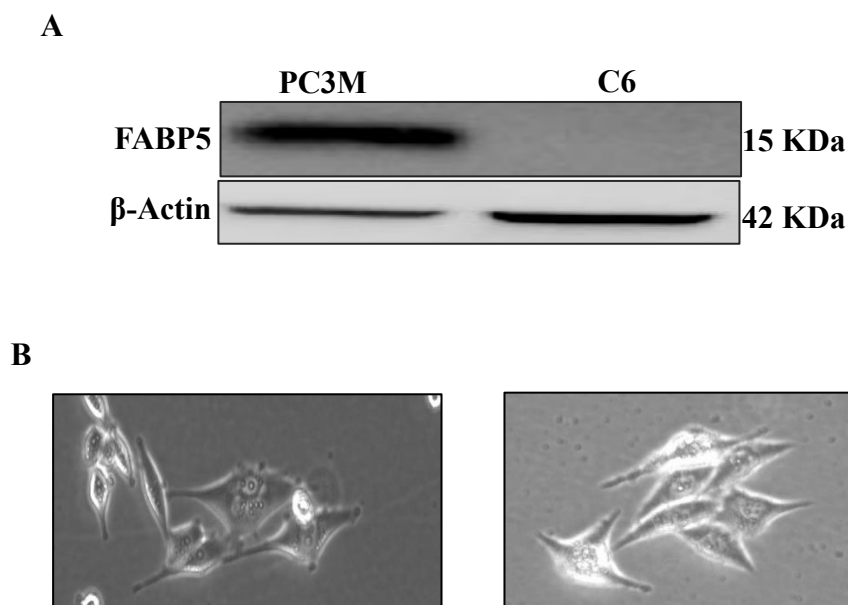
Figure 34. FABP5 expression in C6 cells after several passages and their morphological appearance. **(A)**. Western blot analysis of FABP5 (top panel) expression in the control PC3M cells and the subline C6 cells. An antibody against β-Actin was used to standardize the hybridization. **(B)** Microscopic images of PC3M (left) and the C6 subline cells (right).The image on the left showcases the typical morphology of the PC3M parental cells, while the image on the right displays the distinctive morphology of the C6 knockout cells. These images serve to illustrate the impact of the knockout on the cellular

phenotype, highlighting the morphological alterations resulting from the absence of the FABP5 gene. Magnifications: PC3M: x20; C6: x20.

3.5.4 Nucleotide sequence analysis

The genomic DNA was prepared from both PC3M cells and the subline C6 cells. The targeted region of *FABP5* gene was amplified by PCR with a positive primer 5-'GGCAAGAGGAGCTGGTTAG-3'and negative primer 5'GAGGGTCACGGTAGTTATTTCA-3'. Nucleotide sequence analysis was performed and the sequences of this region of genomes of PC3M and C6 cells were shown in **figure 35**. DNA sequence alignment analysis revealed that a single base "T" in the FABP5 gene was deleted by KO, as shown in figure 35, A (the deleted base was pointed by the arrow head). The sequencing analysis recording chart shown in figure 35, B further confirmed the deleted "T" was base 286 in the targeted region of the *FABP5* gene (Pointed by the arrow head). The frameshift single base deletion completely inactivated the FABP5 gene in PC3M cells.

Figure 35. Nucleotide sequence analysis of the *FABP5* gene in the parental PC3M cells and in the C6 cells. **(A)**. Nucleotide sequence alignment on the targeted region of the *FABP5* gene of the PC3M cells and the C6 cells. The gRNA targeted region was highlighted with an orange color. **(B)**. Nucleotide sequence analysis recording chart. The black arrow head pointed to the location of the deleted "T" base in the targeted region of the *FABP5* gene.

3.6 Generation of AR knockout in 22RV1 cell lines

3.6.1 Lipofection transfection efficiency of the Cas9 protein along with the crRNA:tracrRNA(sgRNA)-ATTO-550-RNP and FACS sorting of the fluorescently labelled cells.

The result of transfecting 22RV1 cells with the crRNA: tracrRNA or (sgRNA)-ATTO-550-RNP mixture were recorded in **figure 36.** One hour after the Cas9 protein and the sgRNA-ATTO-550-RNP mixture was transfected, cell images taken under fluorescence microscope confirmed that the transfected cells (Figure 36, B) were successfully labelled with RFP (red), whereas the control (black and white) was not (Figure 36, A). After 24 hours the control cells and the transfected cells were subjected to FACS with the setup gating system to select the successfully transfected, or RFP- labeled cells. The control cells were shifted to the left side as shown in figure 36, C, and the RFP- labelled transfected cells shifted to the right side as shown in figure 36, D. As pointed by the black arrowhead in Figure 36, D, 71.4 % of the cells were effectively transfected.
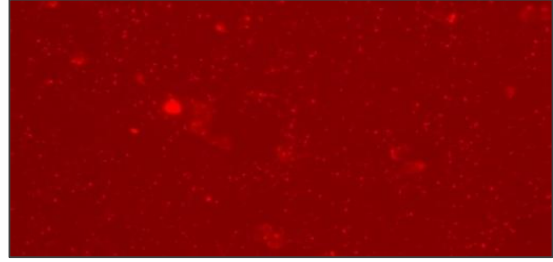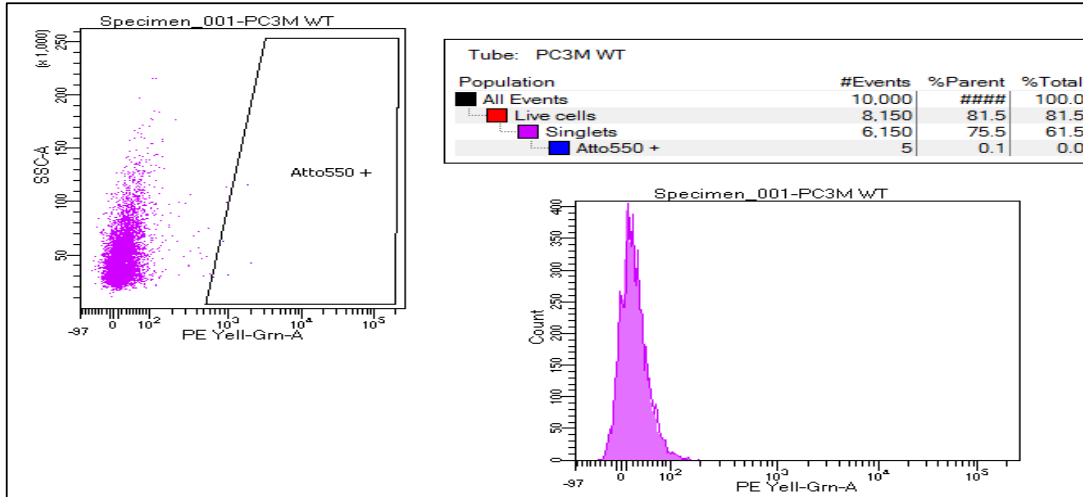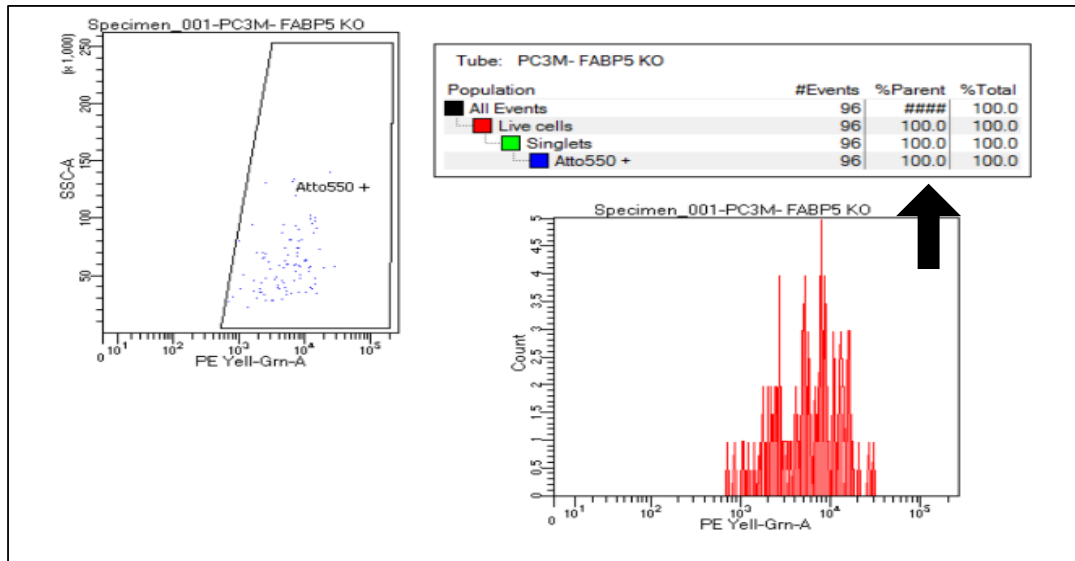
A
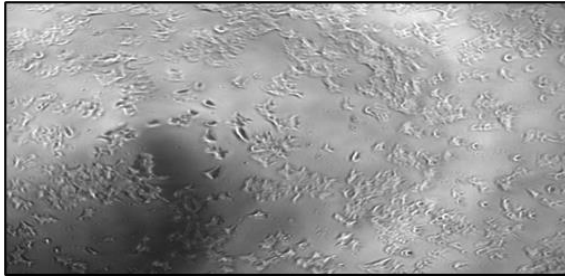
B
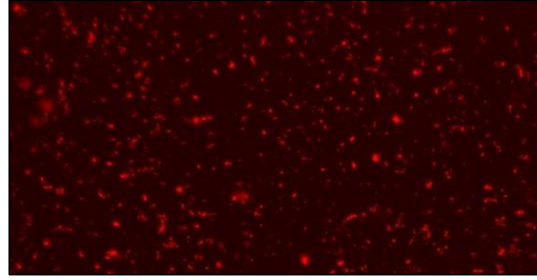
C
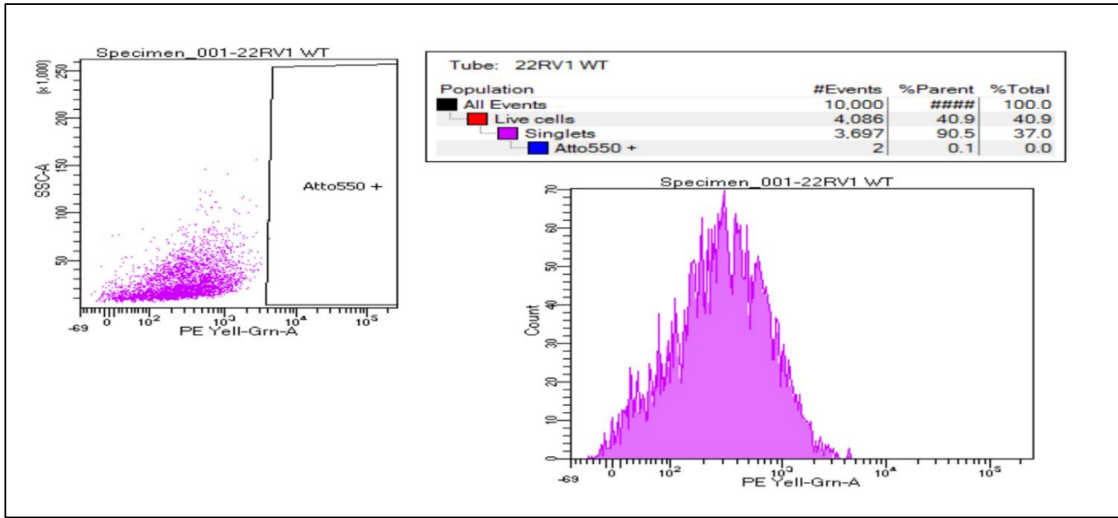
D
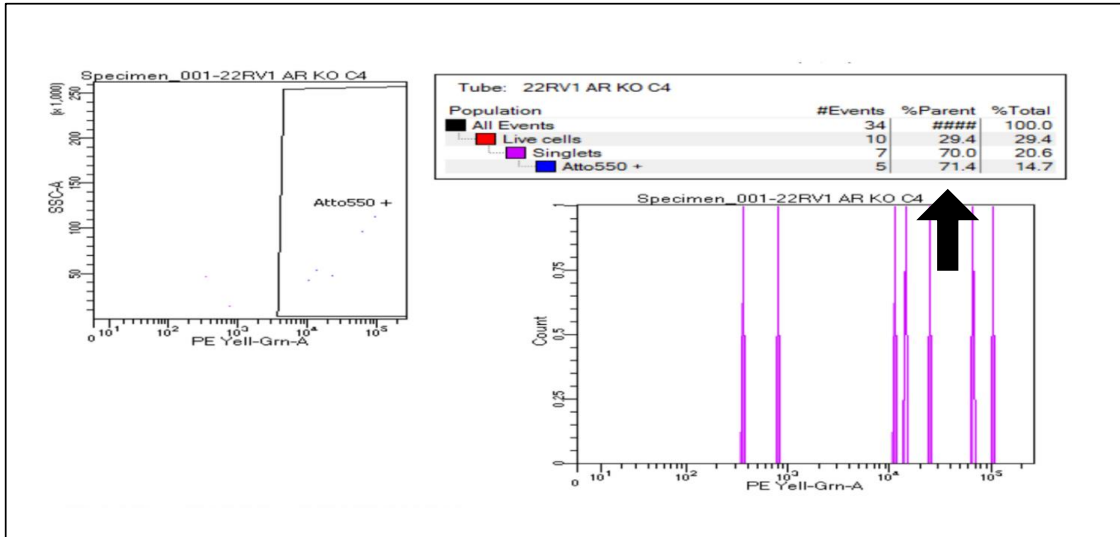
Figure 36. Transfection of 22RV1 with the sgRNA-ATTO-550-RNP mixture. **A)** Image of control 22RV1 cells with no RFP labels under florescent microscope. **B)** Image of the transfected 22RV1 cells labelled with RFP under florescent microscope. **C)** The control 22RV1 cells and the transfected, RFP-labelled cells were sorted by FACS and were divided between the right and the left quadrant. **D)** 22RV1-AR-KO transfected or RFP-labelled cells sorted by FACS..

3.6.2 Selection of successful *AR*-knocked out colonies derived from 22RV1 cells

In order to identify the colonies, in which the *AR* gene was successfully knocked out, the parental 22RV1 cells and their 8 derivative sub-lines, which was designated C1, C2, C3, C4, C5, C6, C7 and C8, respectively, were subjected to Western blot analysis to detect their AR expression (**Figure 37**). As shown in figure 37, A, the highest levels of AR (AR-FL, AR-V7) were seen in 22RV1 parental control cells and the C2 cells. The AR levels in all other sublines were lower than that of the control. Particularly in C1, C3 and C4 cells, levels of AR were greatly reduced. Relative levels of AR expressed in different cell lines were shown in figure 37, B. When the level of 22RV1 cells was set at 1, the relative levels of AR in C1, C2, C3, C4, C5, C6, C7, and C8 were 0.076 ± 0.04, 1 ± 0, 0.09 ± 0.04, 0.09 ± 0.01, 0.45 ± 0.05, 0.5 ± 0.05, 0.74 ± 0.56, and 0.69 ± 0.07, respectively.

A

	22RV1	C1	C2	C3	C4	C5	C6	C7	C8	
AR-FL										110 KDa
AR-V7										75 KDa
β-Actin										42 KDa
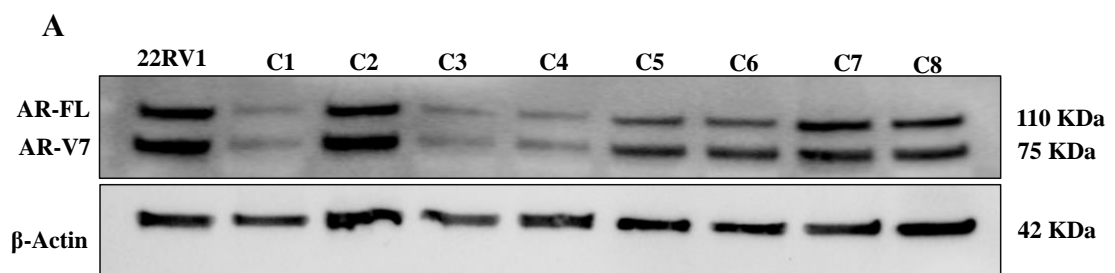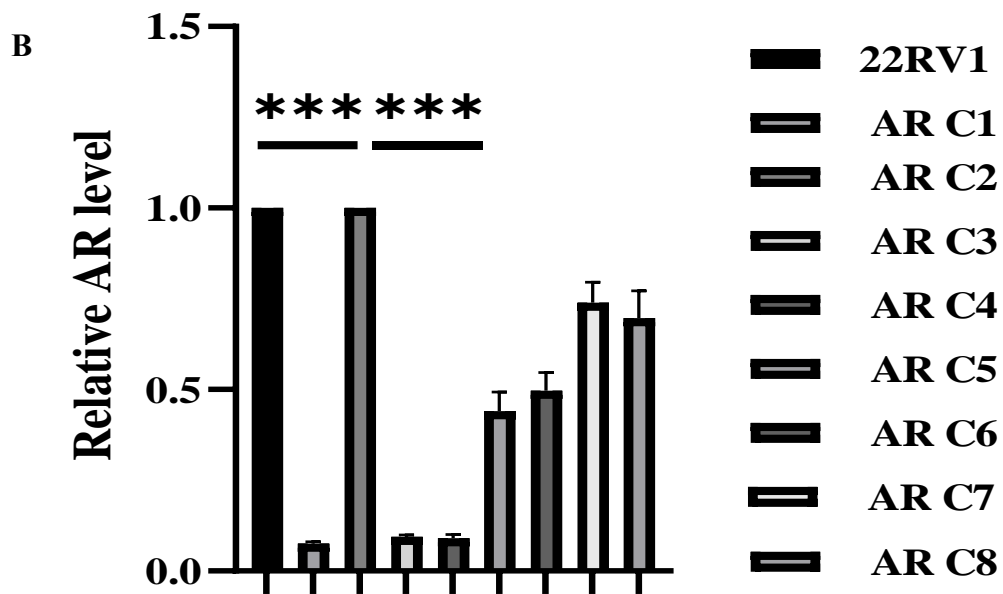
Figure 37. Levels of AR expression levels in the parental 22RV1 cells and 8 sub-lines. **(A)**. Western blot analysis of AR expression of AR in several cell lines. (AR-FL was detected at 110 KDa) (AR-V7 was detected at 75KDa). An antibody against β-Actin was used to standardize the hybridization. **(B)**. Relative levels of AR expressed in the parental 22RV1 cells and 8 sublines. The result (mean ± SD) was obtained by 3 separate densitometrical scanning experiments of the peak regions of the bands on the blot. Student t-test was used to compare the means between the control and each of the sublines. results. The result was regarded as statistically significant when p<0.05. The degree of significance was represented by the number of stars as following: $p<0.05$ *P 0.05, **p 0.001, ***p 0.0002, and ****p 0.0001 are all statistically significant.

3.6.3 Single clone confirmation

After several passages of the 22RV1 C1,C3 and C4 subline, a single colony was removed from each culture and a new subline was established from the new colonies which were still named C1, C3 and C4 respectively. The results of Western blot analysis of the AR levels expressed in the parental 22RV1 control cells and 3 new sublines were shown in **figure 38**. As shown in figure 38, A the AR gene was completely inactivated and no expression was detected. The results of further quantitative analysis of the relative levels of AR expression in the control and the sublines were shown in figure 38, B. When the level of expression in 22RV1 cells was set at 1, relative levels of AR in C1 and C3 were 0.07 ± 0.05, 0.04 ± 0.03, respectively. The level of AR in C4 was not detectable. Light microscopy images of the parental 22RV1 cells and the C4 cells were displayed in figure 38, C. The morphological appearance of C4 (right) was different from that of the parental 22RV1 cells (left), exhibiting a less malignant morphological appearance.

B

C
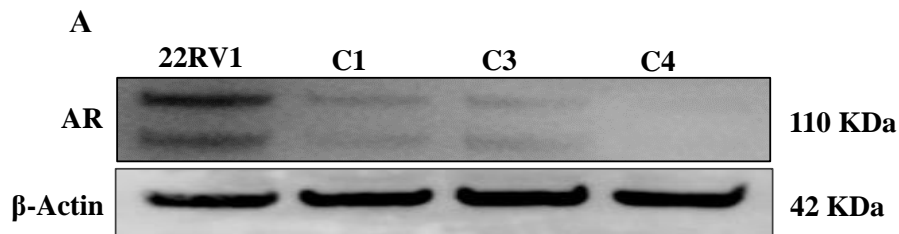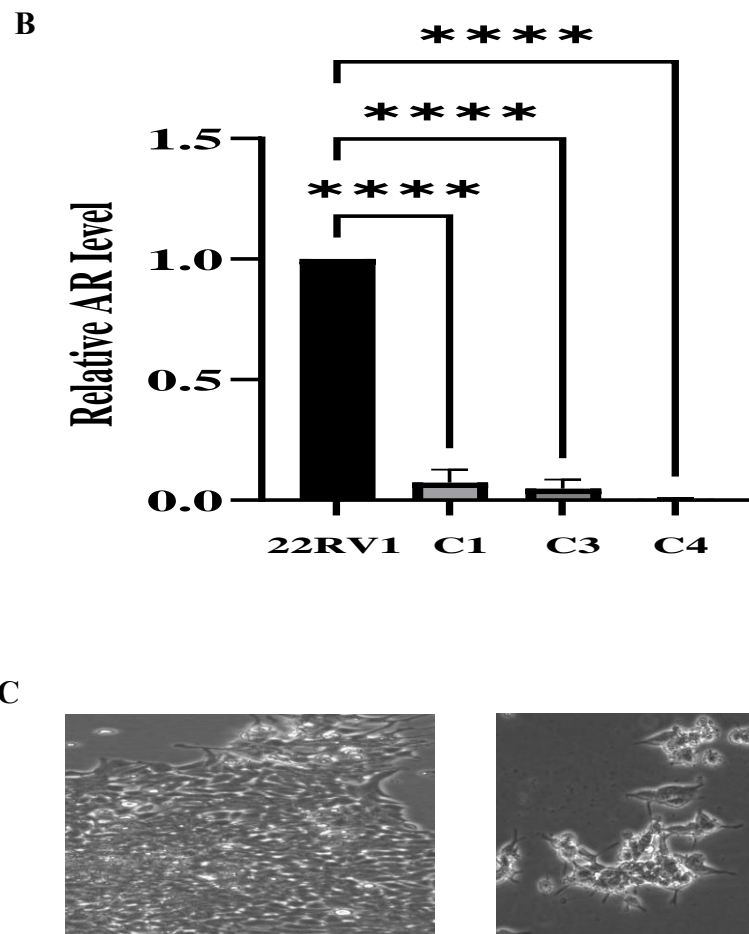
Figure 38. Further Western blot analysis of AR levels in different cells and their morphological appearance. (**A**). Western blot analysis of AR levels in the parental 22RV1 cells and in sublines C1,C3 and C4. An antibody against β-Actin was used to hybridize the blot to standardize the hybridization. (**B**). Relative levels of AR in parental 22RV1, C1, C3, and C4 Cells. (**C**). Microscopical images of the parental 22RV1 cells and the subline C4 cells. The levels of AR in the control and the sublines were compared and tested with Student *t*-test, the results were regarded as statistically significant when. The degree of significant was represented by the number of stars as following: $p < 0.05$. *p0.05, **p 0.001, ***p 0.0002, and ****p 0.0001.

3.6.4 Discussion

This study examined the expression of FABP5 and its related factors in prostate cells, including benign PNT2 cells and prostate cancer cell lines (22RV1, DU145, and PC3M). FABP5 showed increased expression with malignancy, being absent in PNT2 cells, moderate in 22RV1 cells, and high in DU145 and PC3M cells. PPARγ1 and PPARγ2 exhibited moderate expression in 22RV1 cells and slightly reduced levels in DU145 and PC3M cells, while p-PPARγ1 and p-PPARγ2 showed opposite patterns. AR and ARV7 expression was limited to 22RV1 cells, while VEGF expression was present in all cell lines, suggesting their roles in prostate cancer development and progression. Also In this study RNP technology successfully silenced FABP5 or AR expression by inducing various frameshift mutations in 22RV1, DU145, and PC3M cells. Western blot analysis confirmed the absence of FABP5 or AR in the mutant cells, demonstrating the effectiveness of RNP transfection for gene editing. The derived sublines with FABP5 or AR knockout were stable and served as valuable tools for subsequent investigations in the later stages of the study.

Table 4. The Expression Status of FABP5 and Related Factors in Prostate Cells

Cell Type	FABP5 Expression	PPARγ1 Expression	PPARγ2 Expression	p-PPARγ1 Expression	p-PPARγ2 Expression	AR Expression	ARV7 Expression	VEGF Expression
PNT2	Not detected	Strong	Strong	Not detected	Not detected	Not detected	Not detected	Lower
22RV1	Moderate	Moderate	Moderate	Moderate	Moderate	Present	Present	Higher
DU145	Very high	Slightly reduced	Slightly reduced	Very high	Very high	Not detected	Not detected	Higher
PC3M	Very high	Slightly reduced	Slightly reduced	Very high	Very high	Not detected	Not detected	Higher

Footnote: The table summarizes the expression levels of FABP5, its related factors (PPARγ1, PPARγ2, p-PPARγ1, p-PPARγ2), AR, ARV7, and VEGF in different cell types.

Chapter 4 , Result-2: Investigation of the effect of *FABP5*- or *AR*- KO on malignant characteristics of the PCa cells

4.1 Introduction

Understanding the factors that contribute to the malignant characteristics of prostate cancer cells is crucial for developing effective treatment strategies. In this chapter, we focused on investigating the impact of two specific factors, FABP5 or AR, by knocking them out in prostate cancer 22RV1,DU145 and PC3M cells. Our aim was to explore the influence of FABP5 or AR knockout on various malignant characteristics of prostate cancer cells. To achieve this, we conducted four bio-assays to compare the proliferation rate, invasiveness, anchorage-independent growth, and motility between the parental cells and the knockout sublines that were established from single cell colonies.

4.2 Effect of *FABP5* knockout on proliferation of 22RV1 cells

In order to establish the standard growth curves for 22RV1 cells and their FABP5 knockout derived, 22RV1-FABP5-KO cells, a linear regression analysis was performed on the relationship between the number of cells (X-axis) and the value of light absorbance at a wavelength of 570nm (Y-axis). The resulting plot is depicted in **figure 39**.
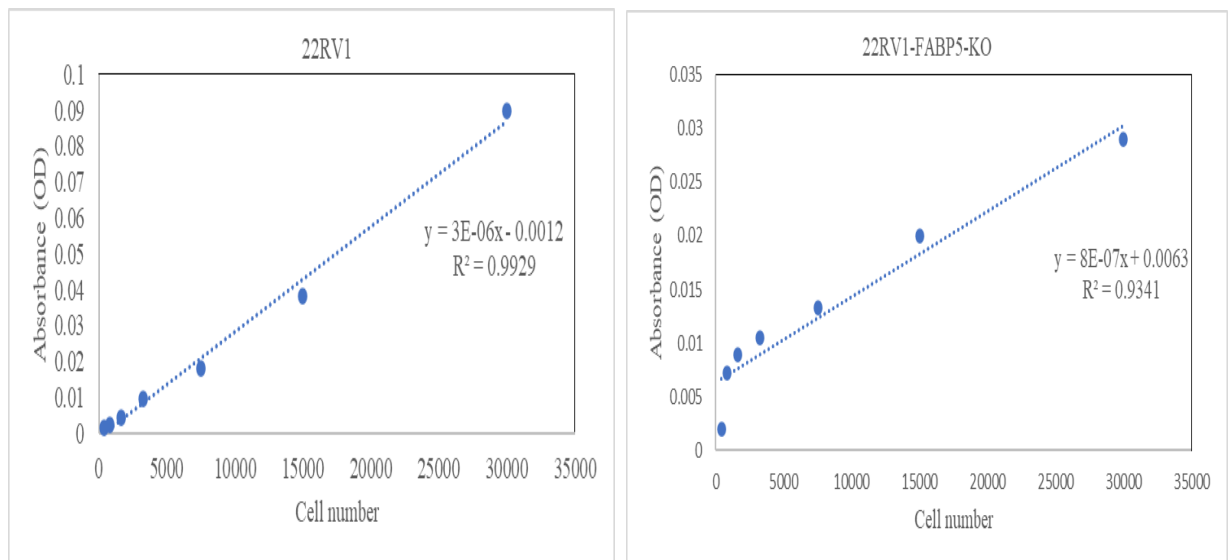
Figure 39 .Standard curves of the parental 22RV1 and 22RV1-FABP5-KO cells.

In **figure 40**, the growth rates of 22RV1 and 22RV1-FABP5-KO cells were compared. Although both cell lines were initially seeded with 5000 cells, variations between the two began to increase on day 2 and persisted until the end of the experiment on day 6. The average cell count for 22RV1-FABP5-KO cells was notably lower than that of the original 22RV1 cells (Student t-test, $P=0.0001$).

Figure 40. Proliferation rates of 22RV1 and 22RV1-FABP5-KO cells. 5000 cells from each cell line were cultured in triplicate in six 96 well plates, and one plate was removed each day to count cell numbers. The result (mean ± SD) was obtained from triplicate separate experiments. The means between the two groups was compared and tested by Student t-test.

The actual number of cells from both parental 22RV1 and 22RV1-FABP5-KO cells at different experimental time points (days) were shown in **table 5**. The significant difference in the number of cells appeared at day 2, at which, the number of cells of 22RV2-FABP5- KO cells was 5596± 163.09, about 18% lower than the control (Student test, $P=0.0191$). This difference was increased at day 3 and other time points until day 6.

Then the cell number from 22RV1-FABP5-KO was reduced to only 62% of the control. Thus, knocking out FABP5 gene from 22RV1 cells significantly suppressed their proliferation rate by 38%.

Table 4. Numbers 22RV1 and 22RV1-FABP5-Ko cells at different time points of the proliferation assay

Time	22RV1 Mean ± SD	22RV1-FABP5-Ko Mean ± SD	Significancy	P value
Day 1	5050±50	5037.33±152.844	Ns	>0.9999
Day 2	6822.33± 243.734	5596± 163.009	*	0.0191
Day 3	8952±146.079	6439± 151.562	***	0.0002
Day 4	10929±111.853	7344.67± 240.884	**	0.0015
Day 5	12698.7±325.707	8381± 104.79	**	0.0047
Day 6	14820 ±113.027	9196.67±165.198	****	<0.0001

Footnote: The result (mean ± SD) was obtained from three independent experiments. Student t-test was used to assess the difference of the means and p<0.05 was regarded as statistically significant. The degree of significance was expressed by the number of stars as following: *p<0.05, **p<0.001, ***p<0.0002, and ****p<0.0001, NS: not significant p>0.9999.

4.2.1 Effect of *FABP5* knockout on invasiveness of 22RV1 cells

The invasion assay was conducted to compare the invasiveness between 22RV1 cells, and their derivative 22RV1-FABP5-KO cells and the results were shown in **figure 41**. As illustrated in figure 41,A there were much more invaded cells from the parental 22RV1

than from 22RV1-FABP5-KO.The number of invading cells was 489 ± 10 from the

control 22RV1, that from 22RV1-FABP5-Ko cells was reduced to only 5 ± 2 (figure 41,

B). Thus, *FABP5* gene knockout in 22RV1 cells significantly (Student's t-test, $p < 0.0001$)

suppressed their invasiveness by nearly 99%.

A

22RV1   **22RV1-FABP5-KO**
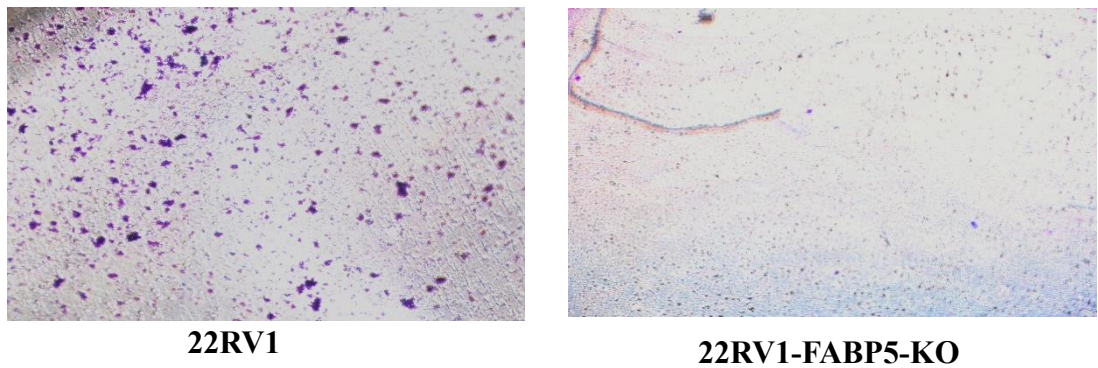
B

Figure 41.The effect of *FABP5* knockout on invasiveness of 22RV1 and 22RV1-FABP5-

KO cells. **A).** Microscopical images of the invaded cells from 22RV1 and 22RV1-

FABP5-KO Cells. (20X) **B).** Numbers of the invaded cells from control and testing cells.

The result (mean ± SD) was obtained from 3 sperate experiments . The student's t-test

was used to compare the means. P<0.05 was regarded as significant. The degree of significance was represented by the number of stars as following: ****p<0.0001.

4.2.2 Effect of *FABP5* knockout on anchorage-independent growth of 22RV1 cells

Soft agar assay was conducted to test the anchorage-independent growth of 22RV1 and 22RV1-FABP5-KO cells and the result were shown in **figure 42**. Whereas formation of a large number of colonies was seen by 22RV1 cells, only a very small number of colonies was form by 22RV1-FABP5-KO cells (Figure 42, A). The average number of colonies/per plate formed by parental 22RV1 cells and 22RV1-FABP5-KO cells was 60 ± 2. This number was substantially reduced to 4± 3 /per plate (Figure 42, B) by 93% (Student's t-test, *p*<0.0001). Thus, *FABP5* gene knockout in 22RV1 significantly suppressed the anchorage-independent growth of the cells.

A

22RV1   **22RV1-FABP5-KO**

B
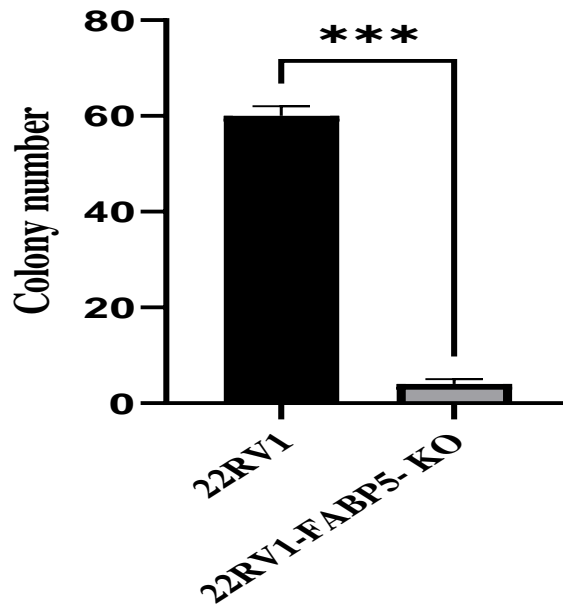
Figure 42. The effect of *FABP5* knockout on anchorage-independent growth of 22RV1 cells. **A)**. Cell colony formation in soft agar plates. **B)**. Numbers of cell colonies formed from 22RV1 and 22RV1-FABP5-KO cells, respectively. The result (means ± SD) was obtained from three separate experiments. Student's t-test was used to compare the means and $p < 0.05$ was regarded as significant. The degree of significance was represented by the number of stars as following: ***$p < 0.0002$.

4.2.3 Effect of *FABP5* gene knockout on motility of 22RV1 cells

Cell migration assay was conducted to test the motility of 22RV1 and 22RV1-FABP5-KO cells and the results were shown in **figure 43**. As shown by the images in figure 43, A no noticeable change at 24h after the incubation. However, remarkable differences were seen at 48h and 72h after incubation. Ninety-six percent of the wound gap was closed in control at 48h, whereas in the 22RV1-FABP5-KO cells, only 60% of the wound space was closed. This difference was even bigger when cells were incubated for 72 h, at which point the wound space gap in 22RV1 cells was closed by 98%, but only 67% of

122

the wound space gap in the 22RV1-FABP5-KO cells was closed. Thus *FABP5*-KO significantly reduced the wound healing ability (or motility) of the cells (Student t-test, *p*=0.0002) (Figure 43, B).

A			
22RV1			
22RV1-FABP5-KO			
0 H	**24 H**	**48 H**	**72 H**

B
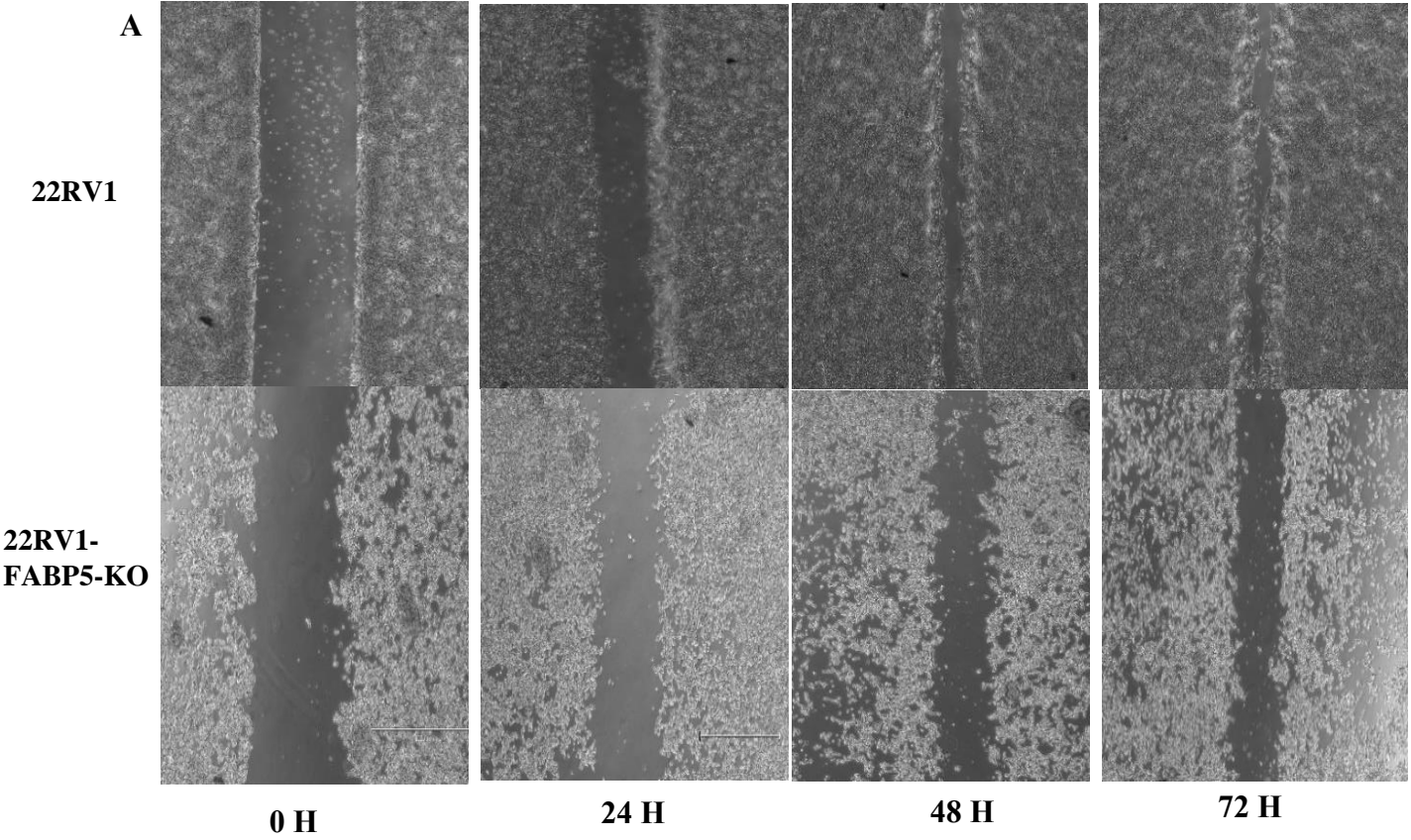
Figure 43. The effect of FABP5 knockout on migration rate of 22RV1 cells. **A)**. Images of wound healing space gaps of 22RV1 and 22RV1-FABP5-KO cells. **B).** The average sizes of wound healing space gaps at different experimental time points. The result (mean ± SD) was obtained from 3 sperate experiments . The degree of significance was represented by the number of stars as following: $p<0.05$. $*p0.05$, $**p\ 0.001$, $***p\ 0.0002$, and $****p\ 0.0001$.

4.3 Effect of *FABP5* knockout on proliferation of DU145 cells

In order to establish the standard growth curves for DU145 cells and their FABP5 knockout derived, DU145-FABP5-KO cells, a linear regression analysis was performed on the relationship between the number of cells (X-axis) and the value of light absorbance at a wavelength of 570nm (Y-axis). The resulting plot is depicted in **figure 44**.

Figure 44. Standard curves of the parental DU145 and DU145-FABP5-KO cells.

In **figure 45**, the growth rates of DU145 and DU145-FABP5-KO cells were compared. Although both cell lines were initially seeded with 5000 cells, variations between the two began to increase on day 2 and persisted until the end of the experiment on day 6. The average cell count for DU145-FABP5-KO cells was notably lower than that of the original DU145 cells (Student t-test, P=0.0001).
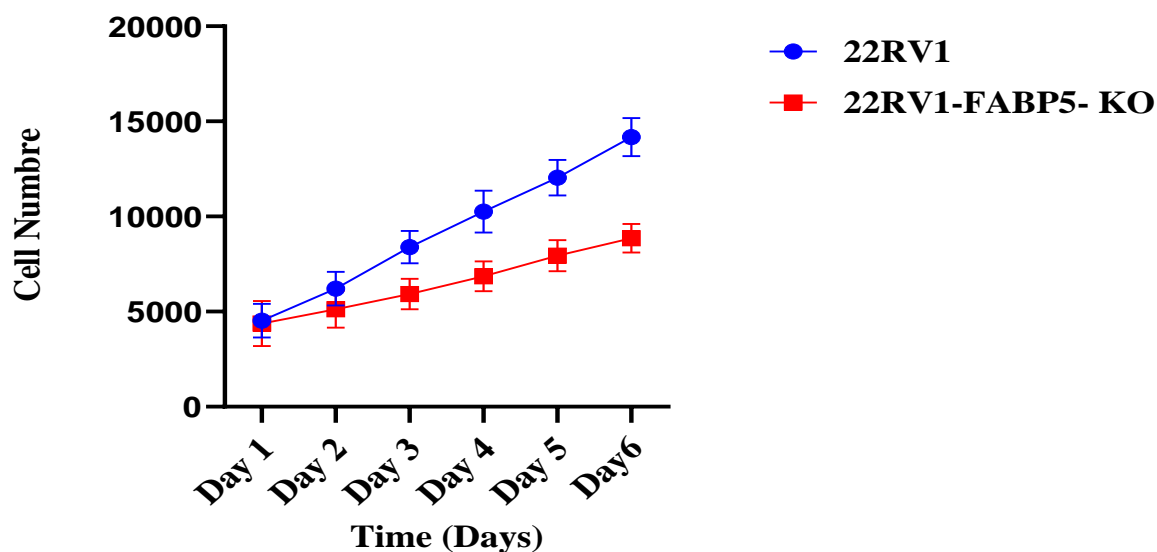
Figure 45. Proliferation rates of DU145 and DU145-FABP5-KO cells. 5000 cells from each cell line were cultured in triplicates in six 96 well plates, and one plate was removed each day to count cell numbers. The result (mean ± SD) was obtained from triplicate cultures. The means between the two groups was compared and tested by Student *t*-test.

The actual number of cells from both parental DU145 and DU145-FABP5-KO cells at different experimental time points (days) were shown in **table 6**. The significant difference in the number of cells appeared at day 2, at which, the number of cells of DU145-FABP5- KO cells was   6210.33 ± 101.58, about 38 % lower than that of the control (Student *t*-test, *P*=0.0184). This difference was increased at day 3 and other time points until day 6. Then the cell number from DU145-FABP5-KO was reduced to 61% of the control. Thus, knocking out *FABP5* gene from DU145 cells significantly suppressed their proliferation rate by 39%.

Table 5. Numbers of DU145 and DU145-FABP5-KO cells at different time points of the proliferation assay

| Time	DU145 Mean± SD	DU145-FABP5-KO Mean± SD	Significancy	*P* value
Day 1	5050±50	5037.33±152.84	NS	>0.9999
Day 2	9884.67±430.54	6210.33±101.58	*	0.0184
Day 3	15142.7±184.07	7332.67±419.66	***	0.0002
Day 4	18507 ±471.341	9455.67±417.23	***	0.0002
Day 5	21478.7±440.886	11570.7±320.22	****	<0.0001
Day6	24158.3±440.886	14754.7±312.97	****	<0.0001

Footnote: The result (mean ± SD) was obtained from three separate experiments. Student *t*-test was used to assess the difference of the means and *p<0.05* was regarded as statistically significant. The degree of significance was expressed by the number of stars as following: **p<0.05, **p<0.001, ***p<0.0002, and ****p<0.0001,* NS: not significant *p>0.9999*.

4.3.1 Effect of *FABP5* knockout on the invasiveness of DU145 cells

The invasion assay was conducted to compare the invasiveness between DU145 cells and their derivative DU145-FABP5-KO cells and the results were shown in **figure 46**. As illustrated in figure 46, A, there were much more invaded cells from the parental DU145 than those from DU145-FABP5-KO.   The number of invading cells was 510 ± 10 from the control DU145, that from DU145-FABP5-KO cells was reduced to only 181.33 ± 7.09 (Figure 46, B). Thus, *FABP5* gene knockout in DU145 cells significantly (Student's *t*-test, *p<0.0002*) suppressed their invasiveness by nearly 65%.
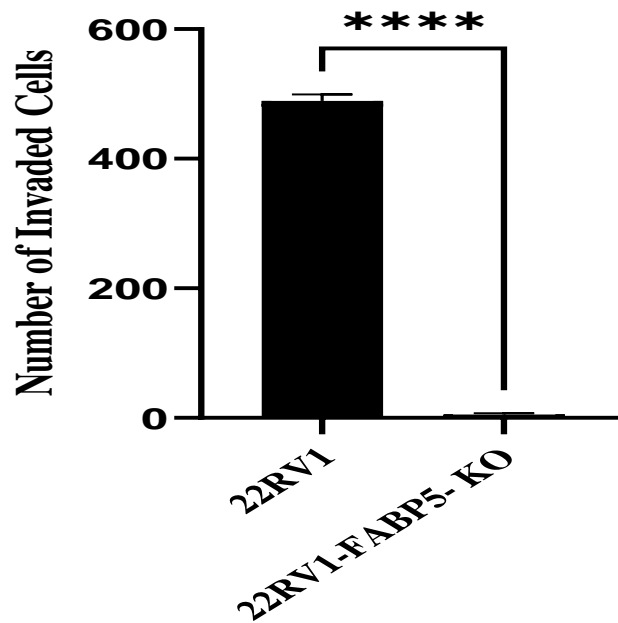
A
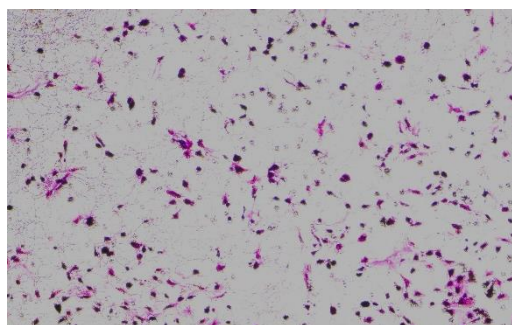
DU145   **DU145-FABP5-KO**

B
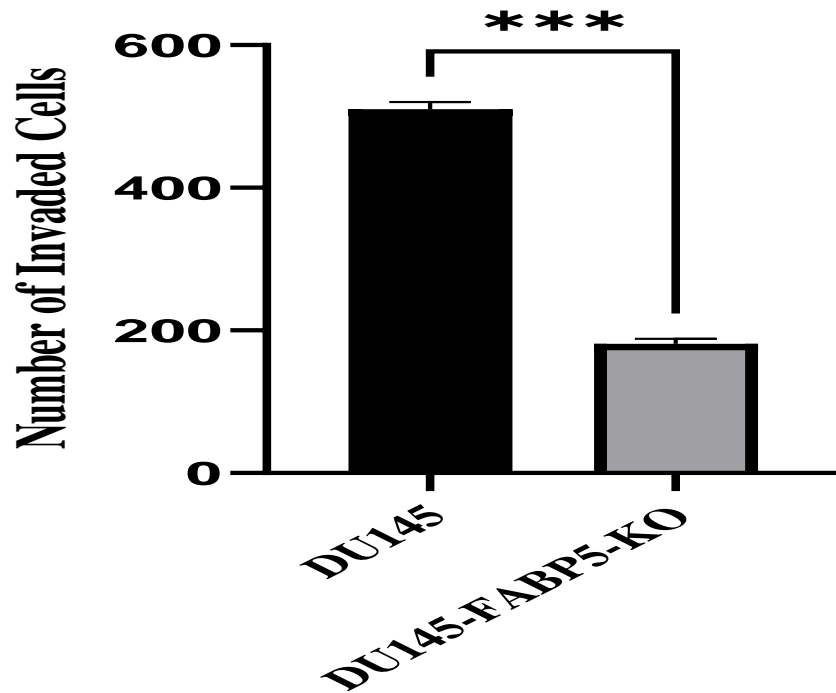
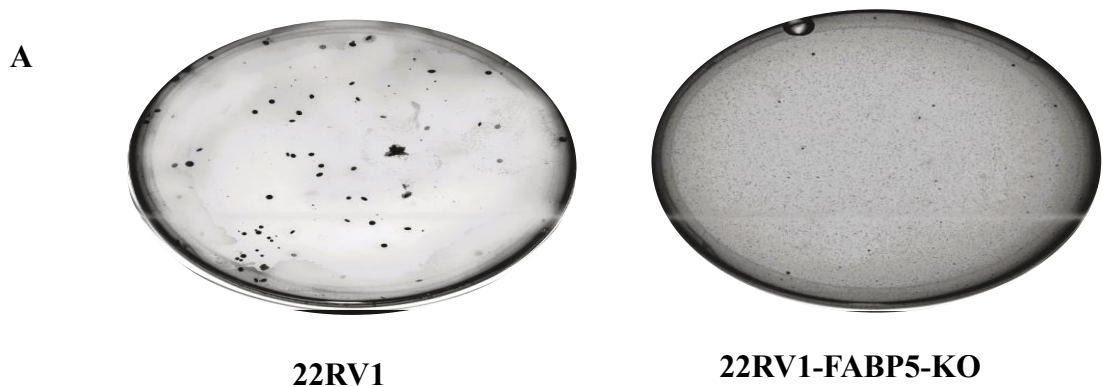**Figure 46**. The effect of *FABP5* knockout on invasiveness of DU145 cells. **A).** Microscopical images of the invaded cells from DU145 and DU145-FABP5-KO Cells. (20X) **B).** Numbers of the invaded cells from the control and the testing cells. The result (mean ± SD) was obtained from three separate experiments. The student's *t*-test was used to compare the means. *P*<0.05 was regarded as significant. The degree of significance was represented by the number of stars as following: ***p<0.0002.

4.3.2 Effect of *FABP5* knockout on anchorage-independent growth of DU145 cells

Soft agar assay was conducted to test the anchorage-independent growth of DU145 and DU145-FABP5-KO cells and the results were shown in **figure 47**. Whereas formation of a large number of colonies was seen by DU145 cells, only a very small number of colonies was formed by DU145-FABP5-Ko cells (Figure 47, A). The average number of colonies/per plate formed by the parental DU145 cells were 113.33 ± 7.6. This number formed by DU145-FABP5-KO cells was substantially reduced by 88% to 14 ± 3.6/per plate (Figure 47, B) (Student's *t*-test, $p<0.0001$). Thus *FABP5* gene knockout in DU145 significantly suppressed the anchorage-independent growth of the cells.

A

DU145   **DU145-FABP5-KO**

B

Figure 47. The effect of *FABP5* knockout on anchorage-independent growth of DU145 cells. **A)**. Cell colony formation in soft agar plates. **B)**. Numbers of cell colonies formed from DU145 and DU145-FABP5-KO cells, respectively. The result (means ± SD) was obtained from three separate experiments. The degree of significance was represented by the number of stars as following: ****$p < 0.0001$.

4.3.3 Effect of *FABP5* gene knockout on motility of DU145 cells

Cell migration assay was conducted to test the motility of DU145 and DU145-FABP5-KO cells and the results were shown in **figure 48**. As shown by the images in figure 48, A, no noticeable change 6h after the incubation. However, remarkable differences were seen at 12h.Ninety percent of the wound gap was closed in control at 12h, whereas for the DU145-FABP5-KO cells, only 76% of the wound space was closed. This difference was even bigger when cells were incubated for 24 h, at which point the wound space gap in DU145 cells was only 96%, but only 80% of wound space gap in the DU145-FABP5-KO cells was closed. Thus *FABP5*-KO significantly reduced the wound healing ability (or motility) of the cells (Student *t*-test, $p = 0.0002$)(Figure 48, B).
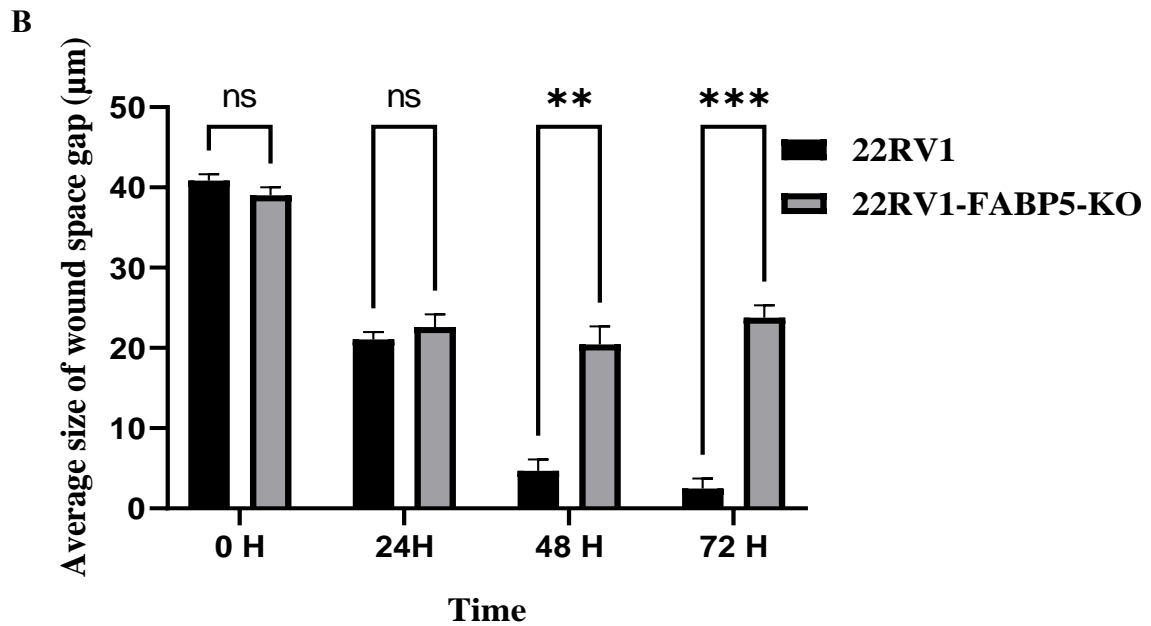
A

DU145

DU145-FABP5-KO

0 H   6 H   12 H   24 H

B

Figure 48. The effect of FABP5 knockout on migration rate of DU145 cells. **A)**. Images of wound healing space gaps of DU145 and DU145-FABP5-KO cells. **B).** The average sizes of wound healing space gaps at different experimental time points. The result (mean ± SD) was obtained from 3 sperate experiments . The degree of significance was represented by the number of stars as following: p<0.05. *p0.05, **p 0.001, ***p 0.0002, and ****p 0.0001.

4.4 Effect of *FABP5* knockout on proliferation of PC3M cells

In order to establish the standard growth curves for PC3M cells and their FABP5 knockout derived, PC3M-FABP5-KO cells, a linear regression analysis was performed on the relationship between the number of cells (X-axis) and the value of light absorbance at a wavelength of 570nm (Y-axis). The resulting plot is depicted in **figure 49**.
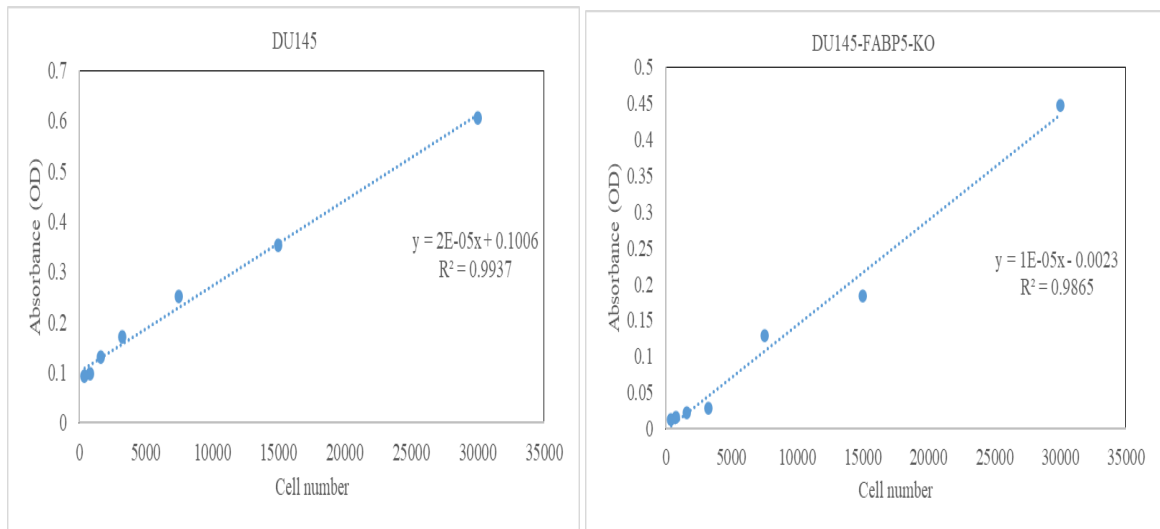

Figure 49. Standard curves of the parental PC3M and PC3M-FABP5-KO cells.

In **figure 50**, the growth rates of PC3M and PC3M-FABP5-KO cells were compared. Although both cell lines were initially seeded with 5000 cells, variations between the two began to increase on day 2 and persisted until the end of the experiment on day 6. The

average cell count for PC3M-FABP5-KO cells was notably lower than that of the original PC3M cells (Student t-test, P=0.0001).
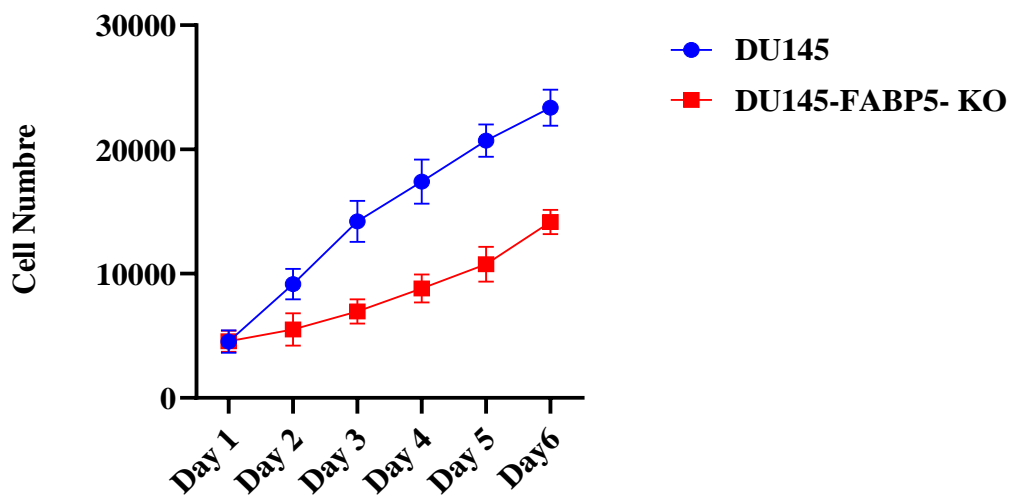

Figure 50. Proliferation rates of PC3M and PC3M-FABP5-KO cells. 5000 cells from each cell line were cultured in triplicate in six 96 well plates, and one plate was removed each day to count cell numbers. The result (mean ± SD) was obtained from triplicate cultures. The means between the two groups was compared and tested by Student t-test.

The actual number of cells from both parental PC3M and PC3M-FABP5-KO cells at different experimental time points (days) were shown in **table 6**. The significant difference in the number of cells appeared at day 3, at which, the number of cells of PC3M-FABP5- KO cells was 10220.33 ± 564.7, about 26 % lower than the control

(Student test, *P*=0.0001). This difference was increased at day 4 and other time points until day 6. Then the cell number from PC3M-FABP5-KO was reduced to 54% of the control. Thus, knocking out FABP5 gene from PC3M cells significantly suppressed their proliferation rate by 46%.

**Table 6.** Numbers PC3M and PC3M-FABP5-KO cells at different time points of the proliferation assay

Time	PC3M Mean± SD	PC3M-FABP5-KO Mean ± SD	Significance	*P* Value
Day1	5337.33±498.55	5306.66±513.93	Ns	>0.9999
Day2	7846.66±392.12	6214.33±492.96	Ns	>0.9999
Day3	13724±803.95	10220.33±564.7	****	<0.0001
Day4	18590±781.5184	14051±331.25	****	<0.0001
Day5	25307.33±1673.03	18229.33±790.10	****	<0.0001
Day6	39590±758.28	21598.67±709.18	****	<0.0001

Footnote: The result (mean ± SD) was obtained from three independent experiments. Student t-test was used to assess the difference of the means and $p<0.05$ was regarded as statistically significant. The degree of significance was expressed by the number of stars as following: *$p<0.05$, **$p<0.001$, ***$p<0.0002$, and ****$p<0.0001$,* NS: not significant *$p>0.9999$*

4.4.1 Effect of *FABP5* knockout on invasiveness of PC3M cells

The invasion assay was conducted to compare the invasiveness between PC3M cells and their derivative PC3M-FABP5-KO cells and the results were shown in **figure 51**. As illustrated in figure 51, A, there were much more invaded cells from the parental PC3M than from PC3M-FABP5-KO. The number of invading cells was 266.66 ± 20.81 from the control PC3M, that from PC3M-FABP5-KO cells was reduced to only 52.66 ± 5.50 (Figure 51, B). Thus *FABP5* gene knockout in PC3M cells significantly (Student's t-test, $p < 0.0001$) suppressed their invasiveness by nearly 81%.

A
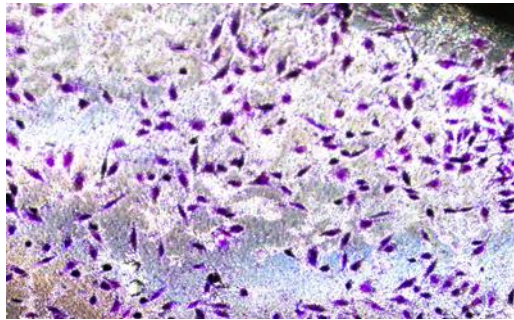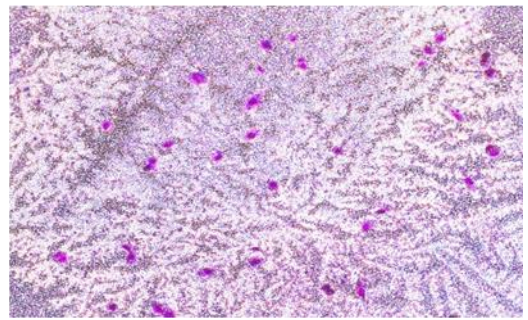
PC3M   **PC3M-FABP5-KO**

B
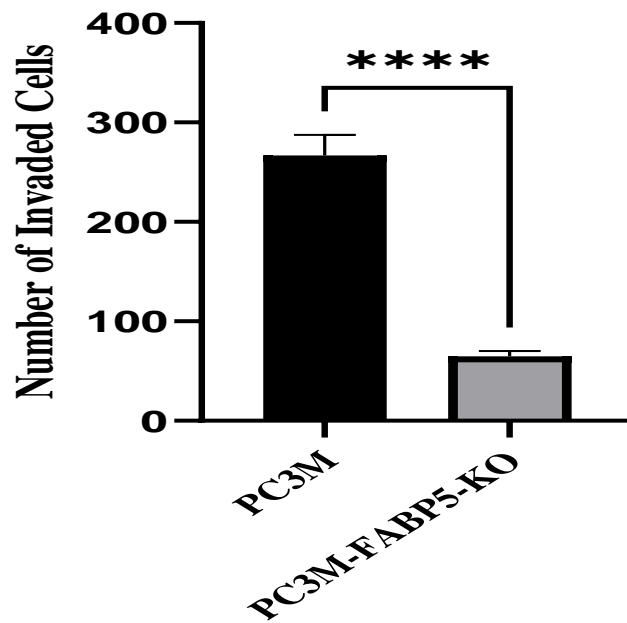
Figure 51. The effect of *FABP5* knockout on invasiveness of PC3M and PC3M-FABP5-KO cells. **A).** Microscopical images of the invaded cells from PC3M and PC3M-FABP5-KO Cells. (20X) **B).** Numbers of the invaded cells from control and testing cells. The result (mean ± SD) was obtained from 3 sperate experiments . The student's t-test was used to compare the means. P<0.05 was regarded as significant. The degree of significance was represented by the number of stars as following: ****p<0.0001.

4.4.2 Effect of *FABP5* knockout on anchorage-independent growth of PC3M cells

Soft agar assay was conducted to test the anchorage-independent growth of PC3M and PC3M-FABP5-KO cells and the result were shown in **figure 52**. Whereas formation of a large number of colonies was seen by PC3M cells, only a very small number of colonies was form by PC3M-FABP5-KO cells (Figure 52, A). The average number of colonies/per plate formed by parental PC3M cells and PC3M-FABP5-knockout cells was 61.33±3.21. This number was substantially reduced to 2.±2.6/per plate (Figure 52, B) by 96.73%

((Student's t-test, $p<0.0001$). Thus *FABP5* gene knockout in PC3M significantly suppressed the anchorage-independent growth of the cells.

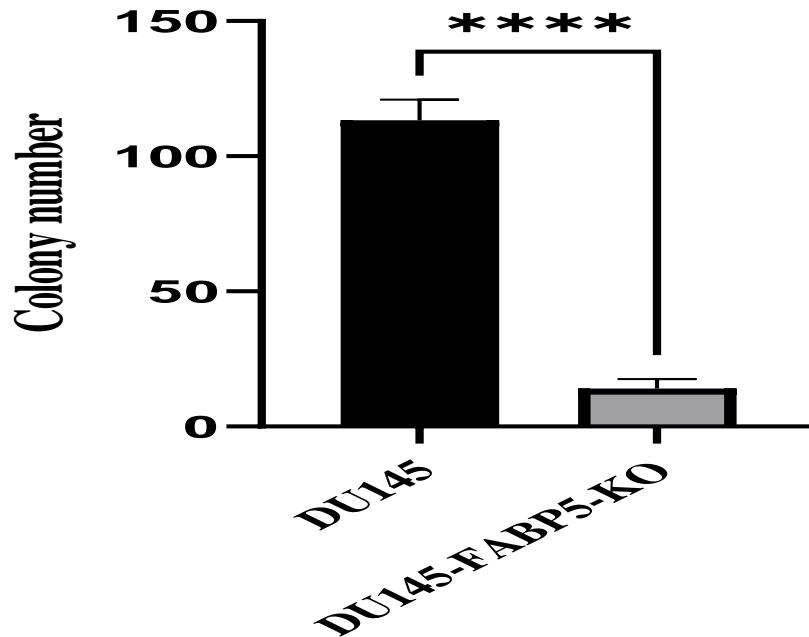

A

PC3M   PC3M-FABP5-KO

B
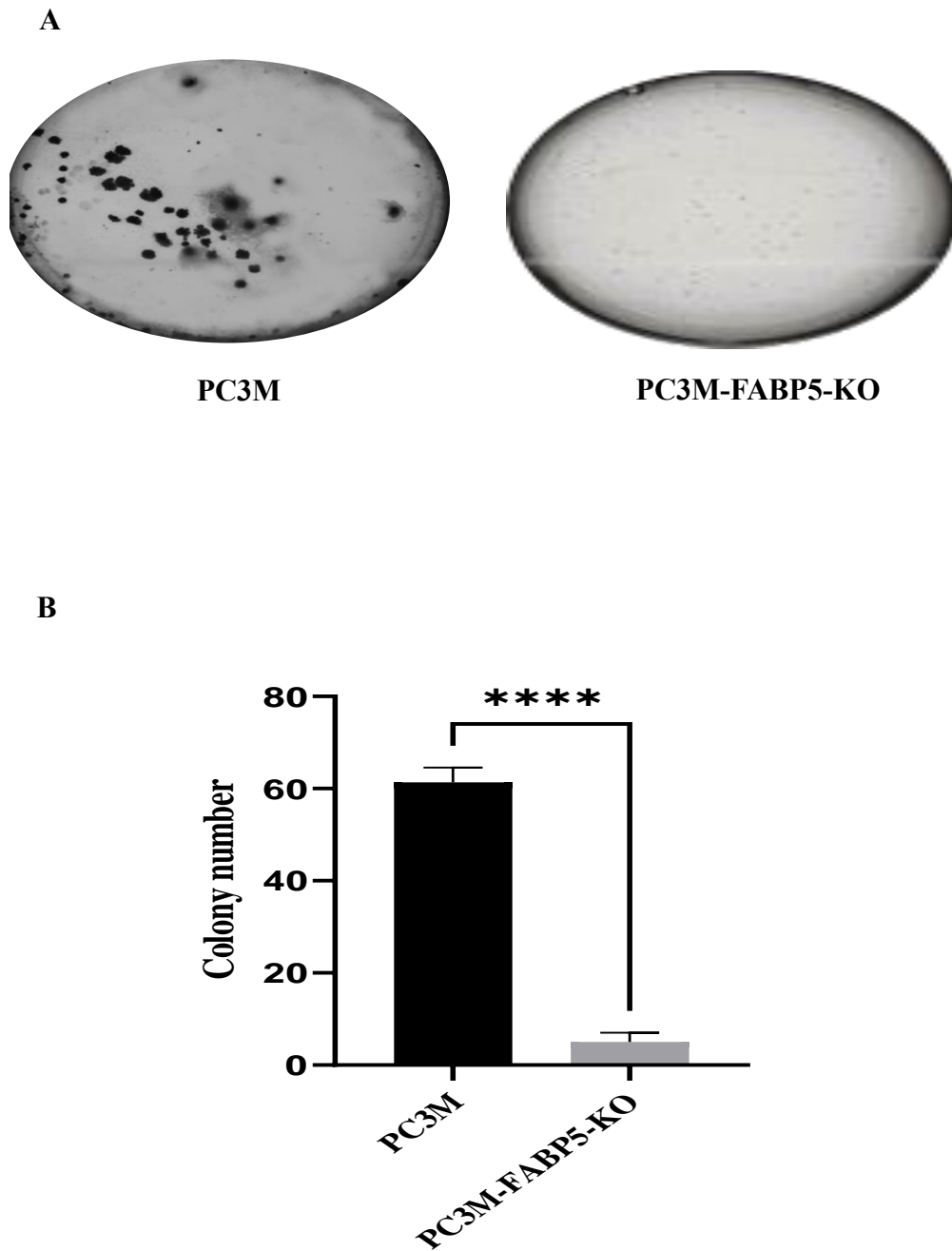
Figure 52. The effect of *FABP5* knockout on anchorage-independent growth of PC3M cells. **A)**. Cell colony formation in soft agar plates. **B)**. Numbers of cell colonies formed

from PC3M and PC3M-FABP5-KO cells, respectively. The result (means ± SD) was obtained from three separate experiments. Student's t-test was used to compare the means and p<0.05 was regarded as significant. The degree of significance was represented by the number of stars as following: ****p<0.0001.

4.4.3 Effect of *FABP5* gene knockout on motility of PC3M cells

Cell migration assay was conducted to test the motility of PC3M and PC3M-FABP5-KO cells and the results were shown in **figure 53**.As shown by the images in figure 53, A, no noticeable change at 6h after the incubation. However, remarkable differences were seen at 12h . Ninety percent of the wound gap was close in control, whereas for the PC3M-FABP5-KO cells, only 68% of the wound space was closed. This difference was even bigger when cells were incubated for 24 h, at which point the wound space gap in PC3M cells was closed by 98%, but only 80% of the wound space gap in the PC3M-FABP5-KO cells was closed. Thus *FABP5*-KO significantly reduced the wound healing ability (or motility) of the cells (Student t-test, *p*=0.0002)(Figure 53, B).
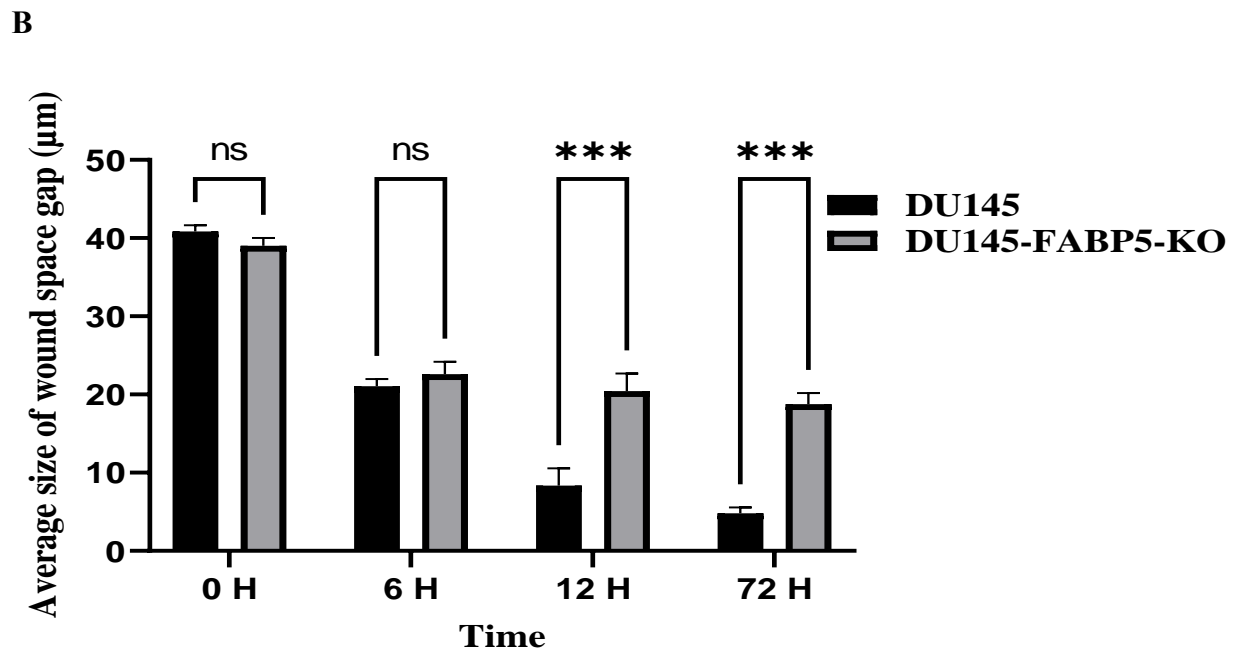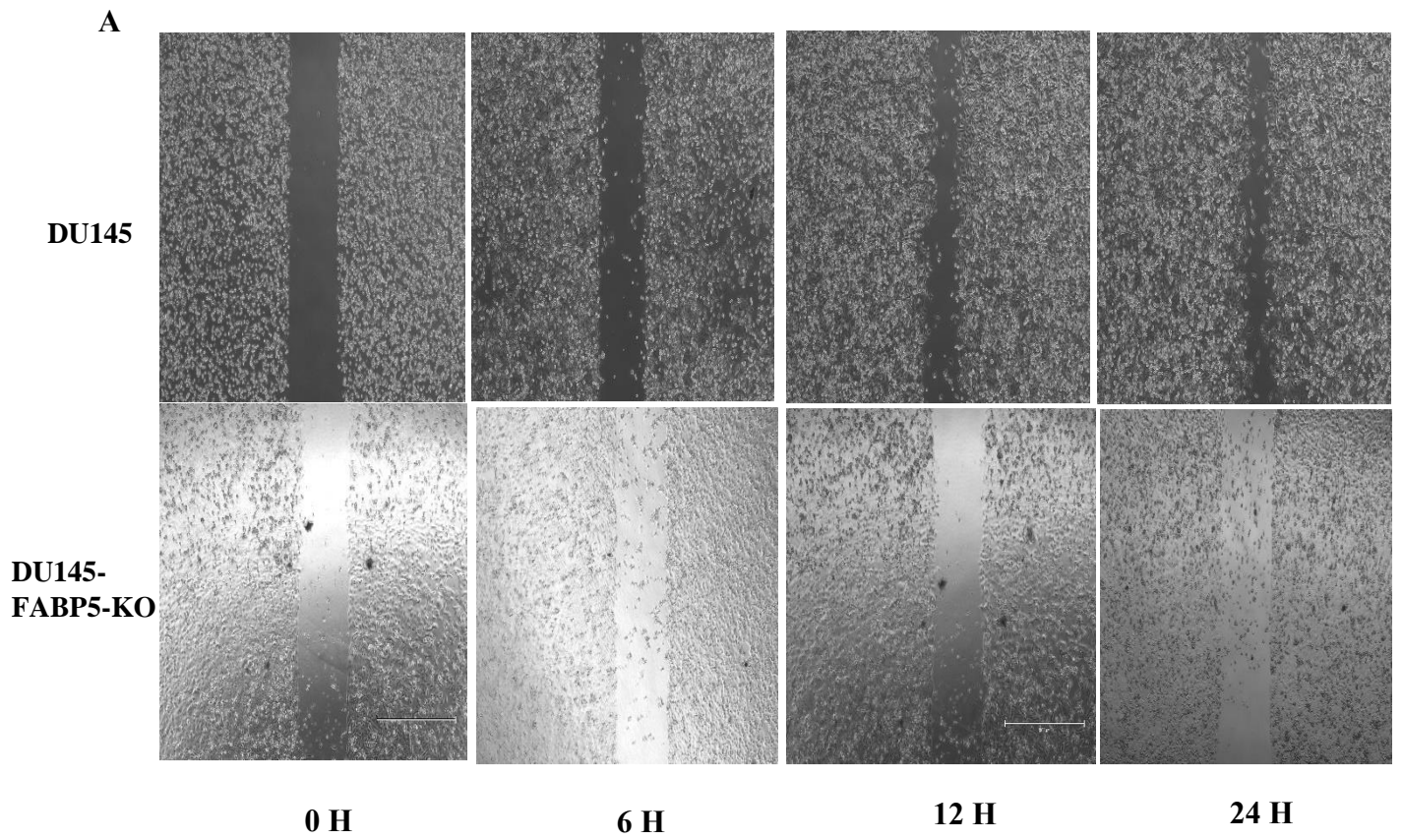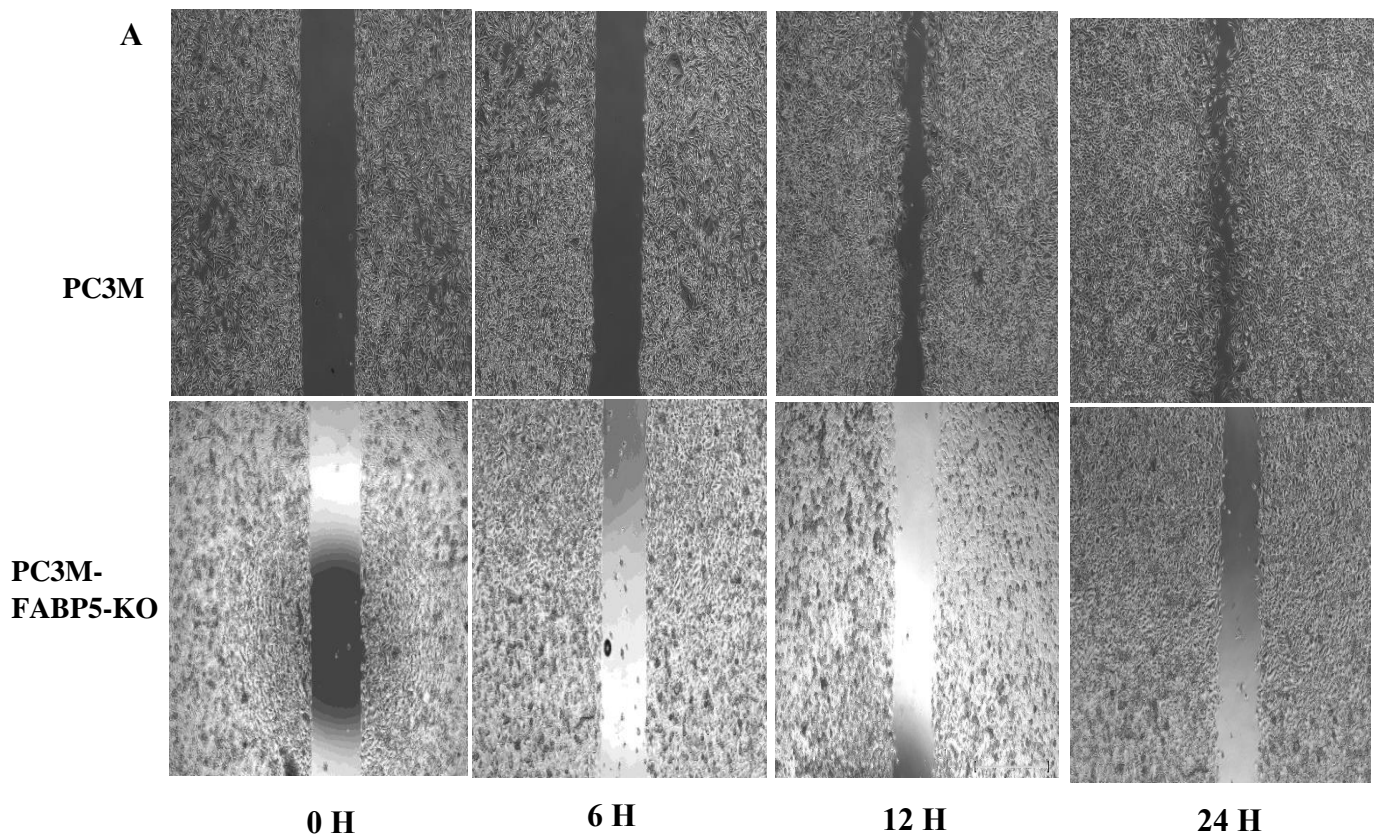
B

Figure 53.The effect of FABP5 knockout on migration rate of PC3M cells. **A)**. Images of wound healing space gaps of PC3M and PC3M-FABP5-KO cells. **B).** The average sizes of wound healing space gaps at different experimental time point. The result (mean ± SD) was obtained from 3 sperate experiments . The degree of significance was represented by the number of stars as following: p<0.05. *p0.05, **p 0.001, ***p 0.0002, and ****p 0.0001.

4.5 Effect of *AR* knockout on proliferation of 22RV1 cells

In order to establish the standard growth curves for 22RV1 cells and their FABP5 knockout derived, 22RV1-AR-KO cells, a linear regression analysis was performed on the relationship between the number of cells (X-axis) and the value of light absorbance at a wavelength of 570nm (Y-axis). The resulting plot is depicted in **Figure 54**.
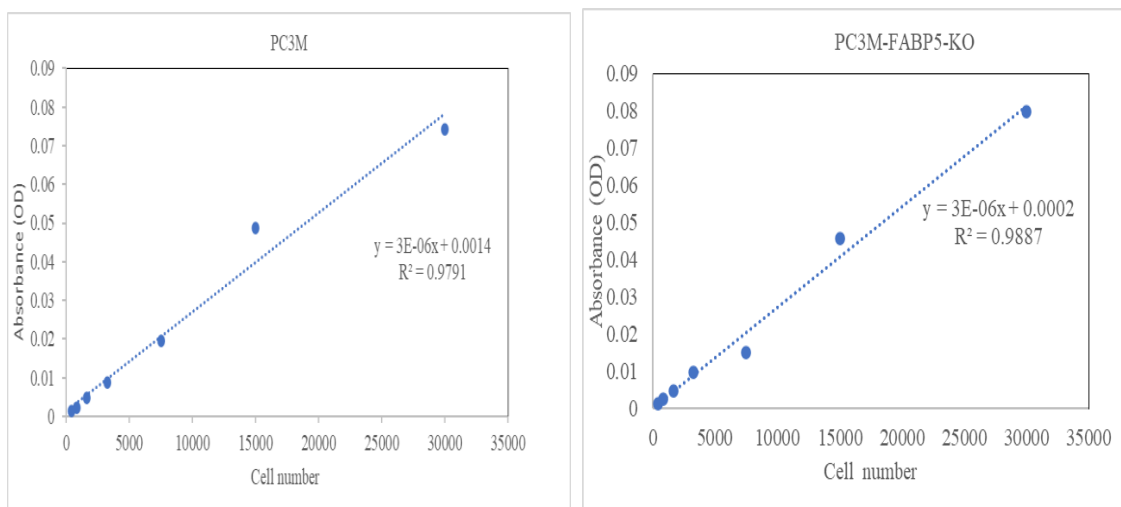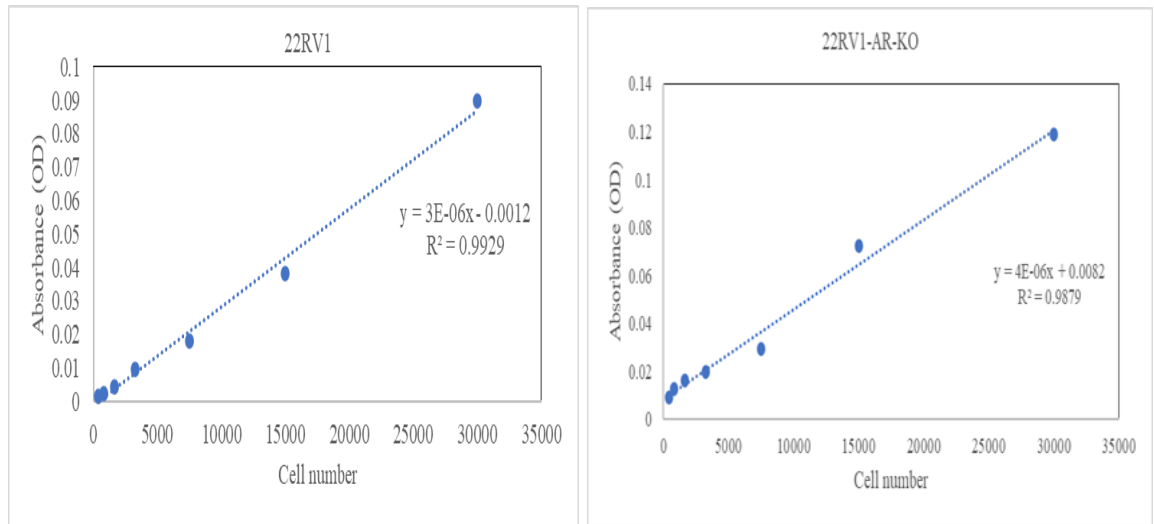

Figure 54. Standard curves of the parental 22RV1 and 22RV1-AR-KO cells.

In **figure 55**, the growth rates of 22RV1 and 22RV1-AR-KO cells were compared. Although both cell lines were initially seeded with 5000 cells, variations between the two began to increase on day 2 and persisted until the end of the experiment on day 6. The average cell count for 22RV1-AR-KO cells was notably lower than that of the original 22RV1 cells (Student t-test, P=0.0007).
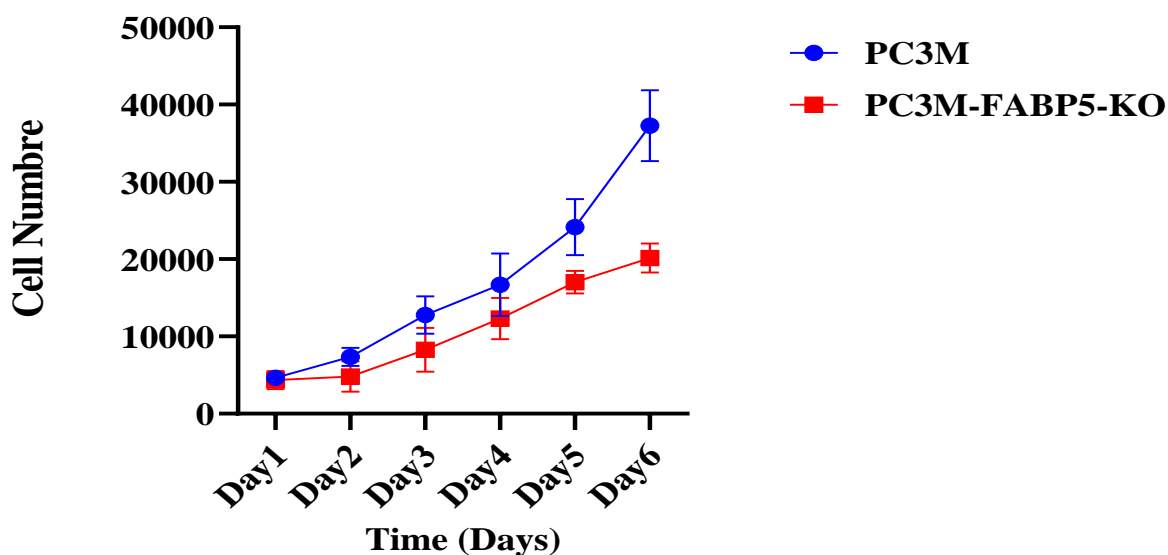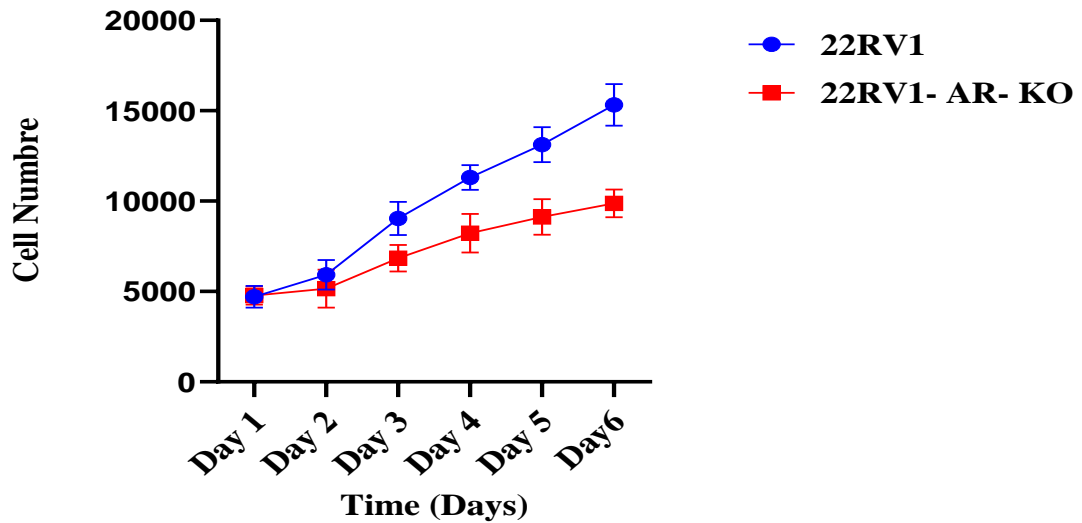
Figure 55. Proliferation rates of 22RV1 and 22RV1-AR-KO cells. 5000 cells from each cell line were cultured in triplicate in six 96 well plates, and one plate was removed each day to count cell numbers. The result (mean ± SD) was obtained from triplicate cultures. The means between the two groups was compared and tested by Student t-test.

The actual number of cells from both parental 22RV1 and 22RV1-AR-KO cells at different experimental time points (days) were shown in **table 7**. The significant difference in the number of cells appeared at day 3, at which, the number of cells of 22RV1-AR- KO cells was 7465.33± 341.21, about 24% lower than the control (Student test, *P*=0.0065). This difference was increased at day 4 and other time points until day 6. Then the cell number from 22RV1-AR-KO was reduced to 64% of the control. Thus, knocking out AR gene from 22RV1 cells significantly suppressed their proliferation rate by 36%.

Table 7. Numbers 22RV1 and 22RV1-AR-KO cells at different time points of the proliferation assay

Time	22RV1 Mean± SD	22RV1-AR-KO Mean± SD	Significancy	*P* value
Day 1	5050±50	5037.33±152.84	Ns	>0.9999
Day 2	6257.67±291.33	5578.67±386.36	Ns	>0.9999
Day 3	9707±283.88	7465.33±341.21	**	0.0065
Day 4	11791±160.477	8735.67±200.10	***	0.0003
Day 5	13785.7±207.51	9623±140.01	***	0.0002
Day6	15986.7±130.31	10293.67±118.03	***	0.0007

Footnote: The result (mean ± SD) was obtained from three independent experiments. Student t-test was used to assess the difference of the means and p<0.05 was regarded as statistically significant. The degree of significance was expressed by the number of stars as following*p<0.05, **p<0.001, ***p<0.0002, and ****p<0.0001, NS: not significant p>0.9999.

4.5.1 Effect of *AR* knockout on invasiveness of 22RV1 cells

The invasion assay was conducted to compare the invasiveness between 22RV1 cells and their derivative 22RV1-AR-KO cells and the results were shown in **figure 56**. As illustrated in figure 56, A, there were much more invaded cells from the parental 22RV1 than from 22RV1-AR-KO. The number of invading cells was 566 ± 25.16 from the control 22RV1, that from 22RV1-AR-KO cells was reduced to only 45 ± 10.26 (figure 56, B). Thus *AR* gene knockout in 22RV1 cells significantly (Student's t-test, $p < 0.0001$) suppressed their invasiveness by nearly 92%.

A
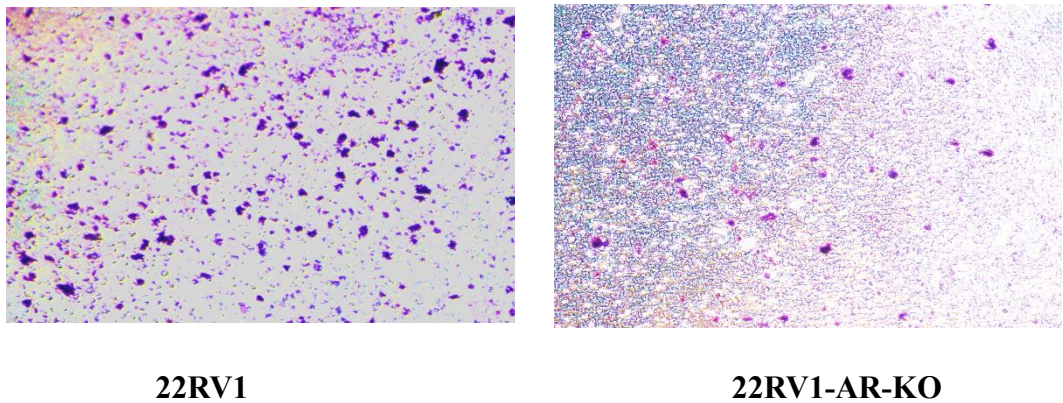
22RV1   22RV1-AR-KO

B
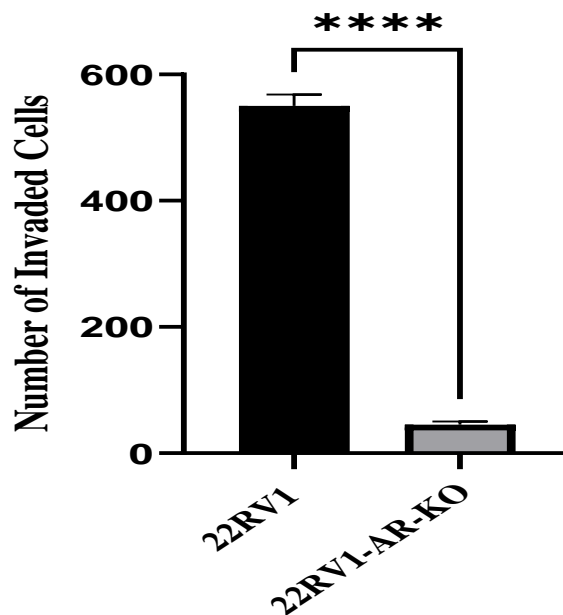
Figure 56.The effect of *AR* knockout on invasiveness of 22RV1 and 22RV1-AR-KO cells. **A).** Microscopical images of the invaded cells from 22RV1 and 22RV1-AR-KO Cells. (20X) **B).** Numbers of the invaded cells from control and testing cells. The result (mean ± SD) was obtained from 3 sperate experiments . The student's t-test was used to compare the means. P<0.05 was regarded as significant. The degree of significance was represented by the number of stars as following: ****p<0.0001.

4.5.2 Effect of *AR* knockout on anchorage-independent growth of 22RV1 cells

Soft agar assay was conducted to test the anchorage-independent growth of 22RV1 and 22RV1-AR-KO cells and the result were shown in **figure 57**. Whereas formation of a large number of colonies was seen by 22RV1 cells, only a very small number of colonies

was form by 22RV1-AR-KO cells (Figure 57, A). The average number of colonies/per plate formed by parental 22RV1 cells and 22RV1-AR-KO cells was 72 ± 3 This number was substantially reduced to 3 ± 2.5/per plate (Figure 57, B) by 97.2% (Student's t-test, *p*<0.0001). Thus, *AR* gene knockout in 22RV1 significantly suppressed the anchorage-independent growth of the cells.

A

B
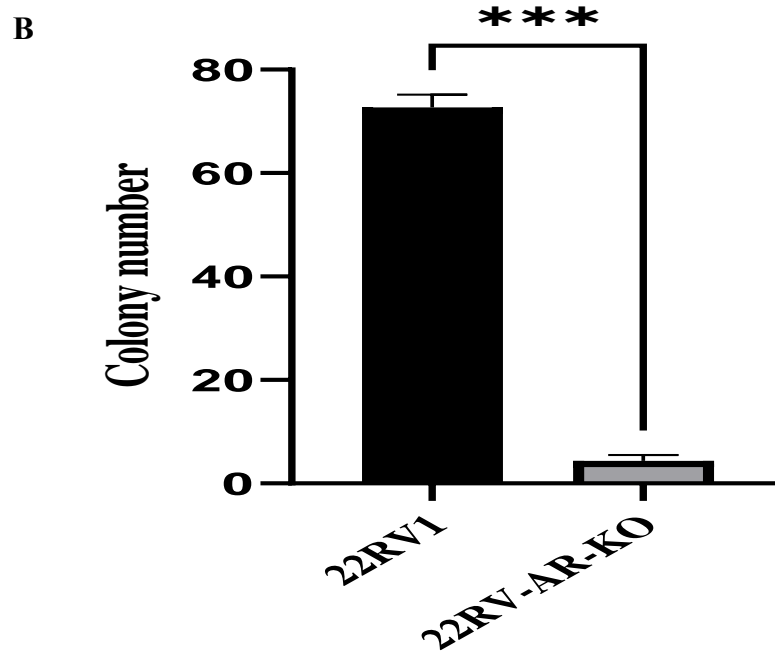
Figure 57. The effect of *AR* knockout on anchorage-independent growth of 22RV1 cells. **A)**. Cell colony formation in soft agar plates. **B)**. Numbers of cell colonies formed from 22RV1 and 22RV1-AR-KO cells, respectively. The result (means ± SD) was obtained from three separate experiments. Student's t-test was used to compare the means and $p<0.05$ was regarded as significant. The degree of significance was represented by the number of stars as following: ***$p<0.0002$.

4.5.3 Effect of *AR* gene knockout on motility of 22RV1 cells

Cell migration assay was conducted to test the motility of 22RV1 and 22RV1-AR-KO cells and the results were shown in **figure 58**. As shown by the images in figure 58, A, no noticeable change at 24h after the incubation. However, remarkable differences were seen at 24h,48h and 72h. Thirty percent of the wound gap was close in control, whereas for the 22RV1-AR-KO cells, only 18% of the wound space was closed. This difference was even bigger when cells were incubated for 42h and 72 h, at which point the wound space gap in 22RV1 cells was closed by 94% and 99% but this wound space gap were closed by 75% and 80% in the 22RV1-AR-KO cells. Thus *AR*-KO significantly reduced the wound healing ability (or motility) of the cells (Student t-test, *p*=0.0001)(Figure 58, B).
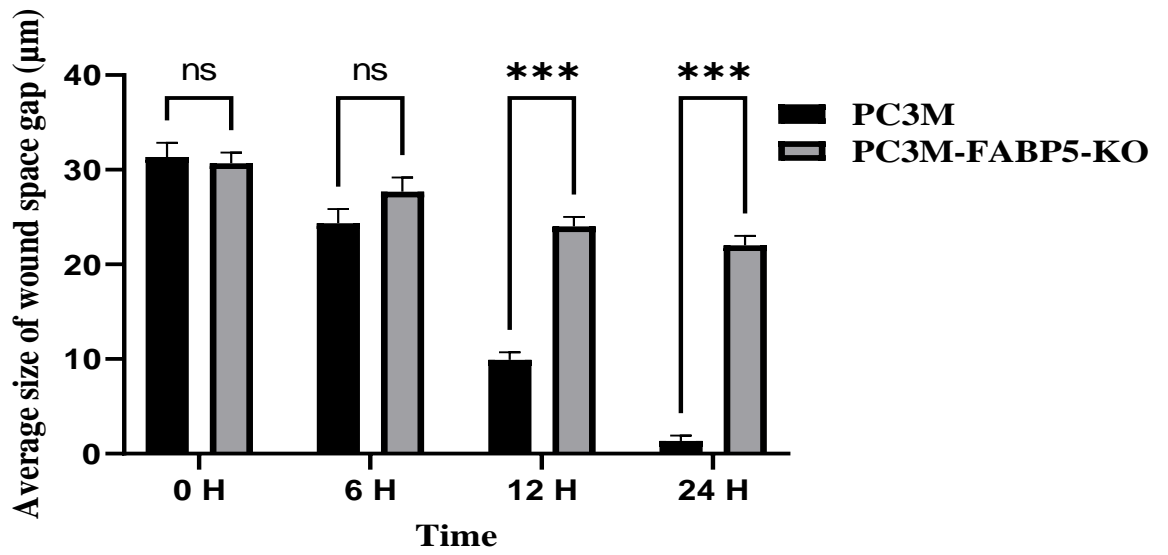
A

	0 H	24 H	48 H	72 H
22RV1				
22RV1-AR-KO				
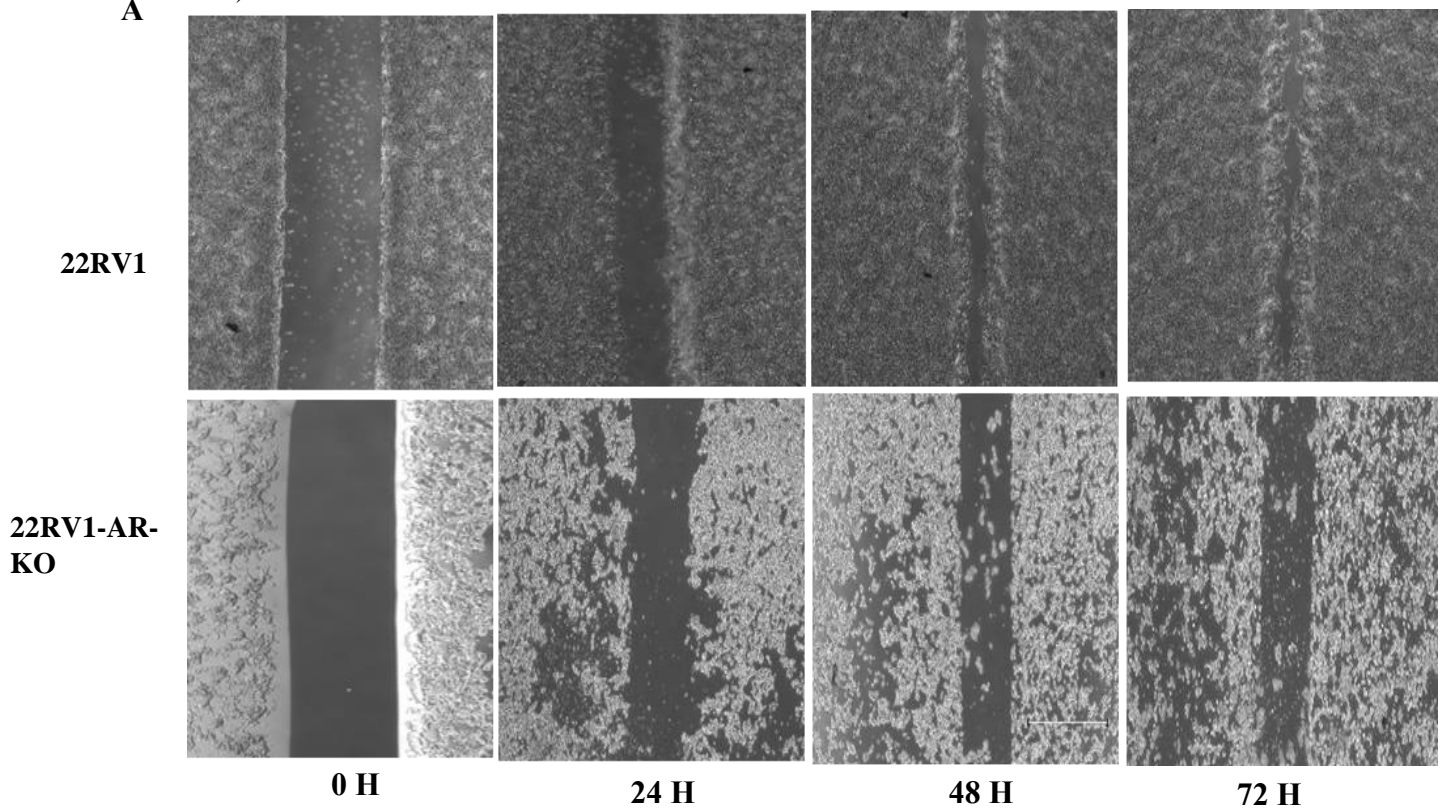
B
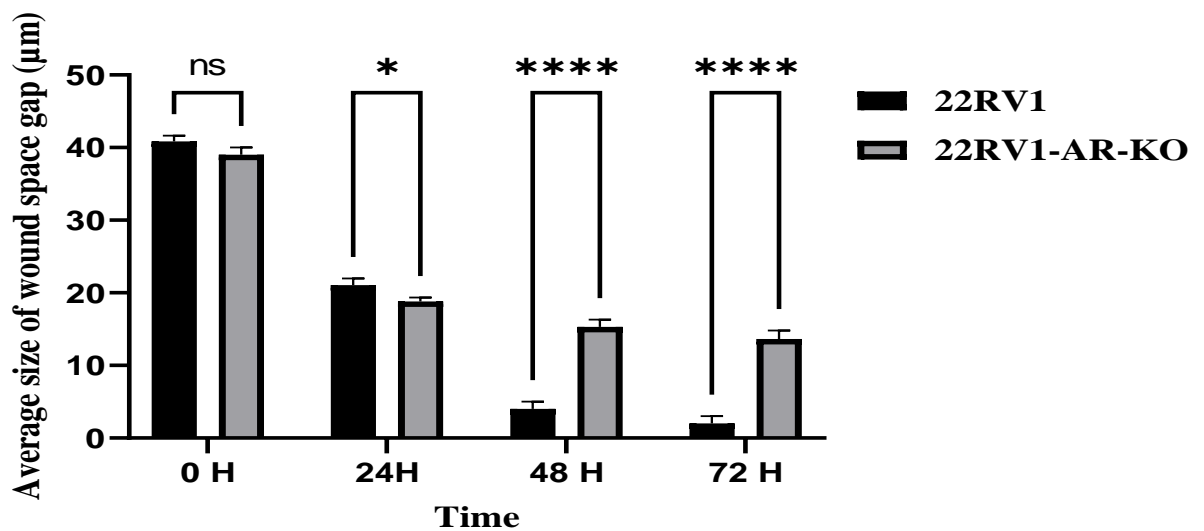
Figure 58.The effect of AR knockout on migration rate of 22RV1 cells. **A)**. Images of wound healing space gaps of 22RV1and 22RV1-AR-KO cells. **B).** The average sizes of wound healing space gaps at different experimental time points. The result (mean ± SD) was obtained from 3 sperate experiments . The degree of significance was represented by the number of stars as following: $p<0.05$. *p0.05, **p 0.001, ***p 0.0002, and ****p 0.0001.

4.5.4 Discussion

In this study, the impact of FABP5 and AR knockouts on prostate cancer cell behavior was investigated, focusing on proliferation, invasiveness, anchorage-independent growth, and cell motility. Experiments were conducted using the androgen-dependent cell line 22RV1 and androgen-independent cell lines DU145 and PC3M. The results showed that knocking out FABP5 led to significant suppression of cell proliferation, invasiveness, anchorage-independent growth and cell motility in all cell lines, while knocking out AR reduced these aspects specifically in AR-positive cells. FABP5 was found to be the primary promoter of cancer in negative prostate cancer cells, this study highlighted the

crucial roles of FABP5 and AR in regulating various aspects of prostate cancer cell behavior.

Chapter 5 , Result-3: investigation of the molecular mechanisms involved in the suppression effect of the *FABP5-* or *AR-* KO in PCa cells

5.1 Introduction

This chapter delves into the contribution of FABP5 and AR to the promotion of prostate cancer cell behavior. To investigate their roles, Western blot analyses conducted to measure changes in the expression of critical signal transduction pathway factors after FABP5 or AR knockouts. The study focused on specific genes and examined their expression in different cell lines. In the androgen-dependent cell line 22RV1, the genes ARFL, ARV7, PPARγ-1, PPARγ-2, p-PPARγ1, p-PPARγ2, and VEGF were analyzed following FABP5 or AR knockouts. Additionally, in the highly malignant and androgen receptor (AR)-negative castration-resistant prostate cancer (CRPC) cell lines DU145 and PC3M, the expressions of PPARγ-1, PPARγ-2, p-PPARγ1, p-PPARγ2, and VEGF were examined upon FABP5 knockout. Through these investigations, the chapter aims to provide insights into the intricate interplay between FABP5 and AR in regulating the expression of key genes associated with prostate cancer behavior.

The effect of *FABP5* KO on expression levels of PPARγ1, PPARγ2, p-PPARγ1, p-PPARγ2, VEGF, ARFL and ARV7

5.1.1 The effect of *FABP5* KO on expression of PPARγ1 and PPARγ2 in 22RV1 cells

To study the effect of *FABP5*- KO on expression of PPARγ in 22RV1, Western blot was used to detect the expression of both PPARγ1 and PPARγ2 in 22RV1 and its *FABP5*-KO derivative cells. The results were shown **figure 59**.Both PPARγ1 and PPARγ2 were expressed in the parental 22RV1 cells, whereas 22RV1-FABP5-KO cells exhibited a strong PPARγ1 band but PPARγ2 band was not detectable or barely visible, as shown in figure 59, A. When the levels of PPARγ1 and PPARγ2 in 22RV1 was set at 1, respectively; the relative levels of PPARγ1 and PPARγ2 in 22RV1-FABP5-KO were 1.75 ± 0.05 and 0.1 ± 0.03, respectively, as shown in figure 59, B. Comparing with those expressed in the parental control cells, level of PPARγ1 significantly increased by 75%

in 22RV1-FABP5-KO cells (Student's *t* test, $p < 0.0001$), but that of PPARγ2 significantly

decreased by 99% (Student's *t* test, $p < 0.0001$) .

A

B
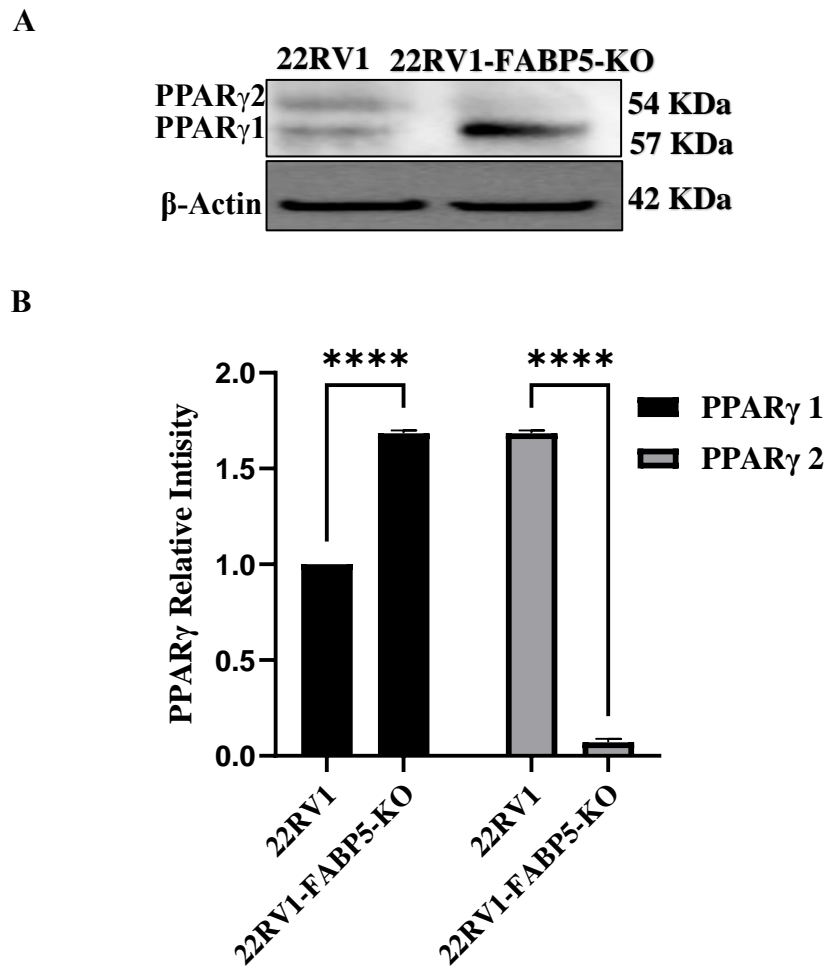
Figure 59. The effect of FABP5 knockout on PPARγ1 and PPARγ2 expression in 22RV1

lines. **A)** PPARγ1 and PPARγ2 Western blot analyses in 22RV1 prostate cancer cell lines.

B) Quantitative measurement of the peak area intensities of bands on the blot using

densitometry scanning. Three separate measurements yielded the data (Mean ± SD). The

band intensities were measured with the image J program to determine the relative

amounts of PPARγ1 and PPARγ2. The blot was hybridized with anti-actin to normalize

any loading inconsistencies. The 22RV1 and 22RV1-FABP5-KO cells were compared

using a two-tailed paired Student's t test. P<0.05 was considered significant. Four stars

(****) meant *P*<0.0001.

5.1.2 The effect of *FABP5* KO on expression of p-PPARγ1 and p-PPARγ2 in 22RV1 cells

The expression of p-PPARγ1 and p-PPARγ2 in 22RV1 and 22RV1-AR-KO cells was detected with Western blot analysis and the results were shown in **figure 60**. Both p-PPARγ1 and p-PPARγ2 were expressed in the parental 22RV1 cells at moderately abundant levels. But the expression of p-PPARγ2 was significantly reduced and that of p-PPARγ1 was noticeably decreased in 22RV1-FABP5-KO cells, as shown in figure 60, A. When p-PPARγ1and p-PPARγ2 levels in 22RV1 cells were respectively set at 1, their relative levels in 22RV1-FABP5-KO were significantly reduced to 0.36 ± 0.07 and 0.12 ± 0.03, respectively (Figure 60, B). While p-PPARγ1 level was decreased significantly by 64 % (Student's *t* test, $p < 0.0001$), p-PPARγ2 level was reduced significantly by 88 % in 22RV1- FABP5-KO cells (Student's *t* test, $p < 0.0001$) in comparison to the control 22RV1.

A
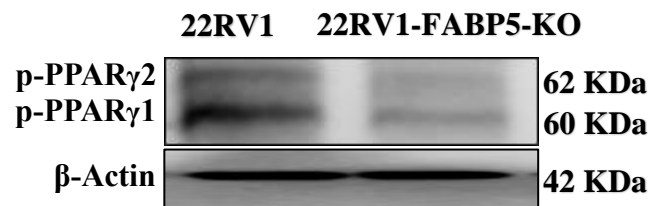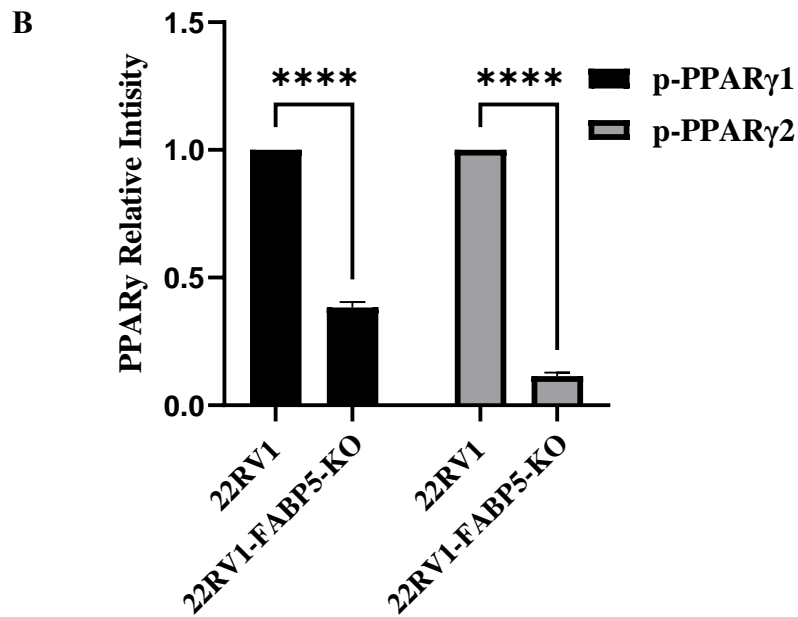
Figure 60. The effect of FABP5 knockout on p-PPARγ1 and p-PPARγ2 expression in 22RV1 cells. **A)** Western blot assessment of the expression of p-PPAR1 and p-PPAR2 in 22RV1 and 22RV1-FABP5-KO cells. **B)** p-PPARγ1 and p-PPARγ2 expression levels in 22Rv1 and its derivative cell line 22RV1-FABP5-KO cells. Three separate measurements yielded the data (Mean ± SD). The relative levels of p-PPARγ1 and p-PPARγ2 were calculated by measuring the intensity of the bands on the blot and analyzing the data with image J. To normalize any loading inconsistencies, anti-actin was employed to hybridize the blot. The 2-tailed paired Student's t test was used to compare 22RV1 cells to 22RV1-FABP5-KO cells. $P<0.05$ was considered significant. Four stars (****) meant P 0.0001.

5.1.3 The effect of *FABP5* KO on VEGF expression in 22RV1 cells

The expression status in 22RV1 cells and in 22RV1-FABP5-KO cells was detected and the results were shown in **figure 61**.A relatively strong VEGF band was detected in 22RV1 by Western blot and a much weaker VEGF band was detected in 22RV1-FABP5-KO cells, as shown in figure61, A. When the VEGF level in 22RV1 cells was set at 1, the relative level of VEGF in 22RV1- FABP5- KO cells was 0.1 ± 0.04 (Figure 61, B), significantly reduced by 90% (Student's t test, $p < 0.0001$).

A

22RV1   22RV1-FABP5-KO

VEGF   22 KDa

β-Actin   42 KDa

B

VEGF Relative Intensity

****
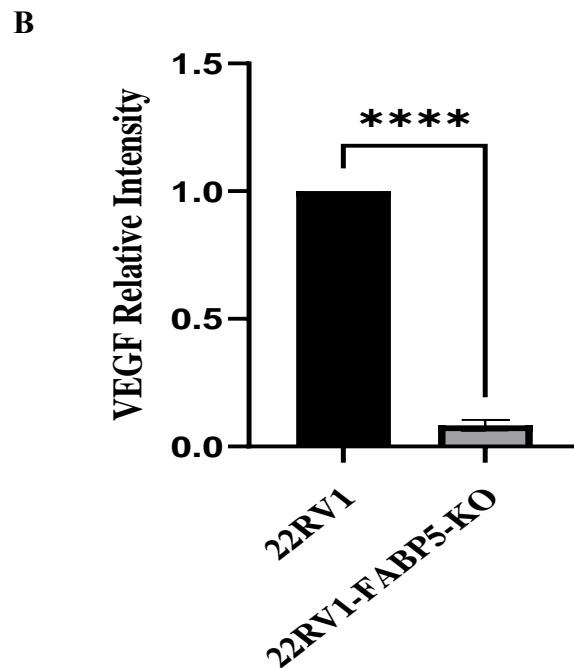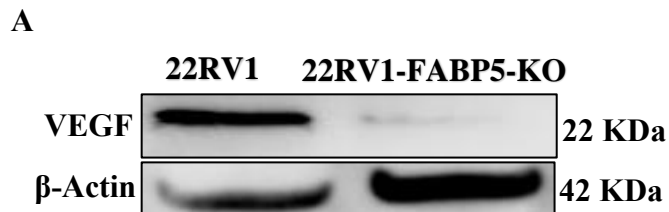
Figure 61. VEGF expression in 22RV1 and 22RV1-FABP5 cells after FABP5 knockout. **A)** VEGF expression assessment by Western blot in 22RV1 and 22RV1-FABP5-KO cells. **B)** VEGF expression levels in 22RV1 and 22RV1-FABP5-KO cells. Three separate measurements yielded the data (Mean ± SD). The relative amounts of VEGF were determined using densitometric measurements of the brightness of bands on the blot and image J software. To normalise any loading inconsistencies, anti-actin was utilised to hybridise the blot. The 2-tailed paired Student's t test was used to compare the 22RV1 and 22RV1-FABP5-KO cells. *P*<0.05 was considered significant.Four stars (****) meant *P* 0.0001.

5.1.4 The effect of *FABP5* KO on ARFL and ARV7 expression in 22RV1 cells

ARFL and ARV7 expression in 22RV1 cells before and after *FABP5* KO was detected by western blot and the results were shown in **figure 62.** ARFL and ARV7 were both expressed in 22RV1 cells (control), whereas only ARFL was expressed and no ARV7 band was detected in 22RV1-FABP5-KO cells, shown figure 62, A. When the level of ARFL and ARV7 in 22RV1 were respectively set at 1, the relative levels of ARFL and ARV7 in 22RV1- FABP5-KO were 1 and 0, respectively (Figure 62, B). Thus the level of ARFL in 22RV1-FABP5- KO cells wasn't changed when compared with that in 22RV1 cells; but the expression of ARV7 was totally abolished (by 100%) when compared with that in 22RV1 (Student's *t* test, $p < 0.0001$).

A
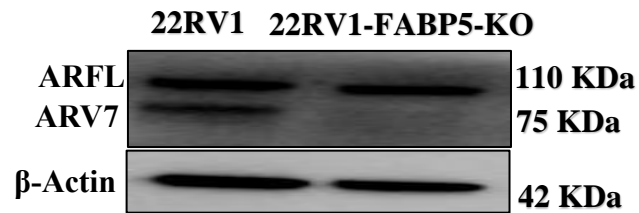
B
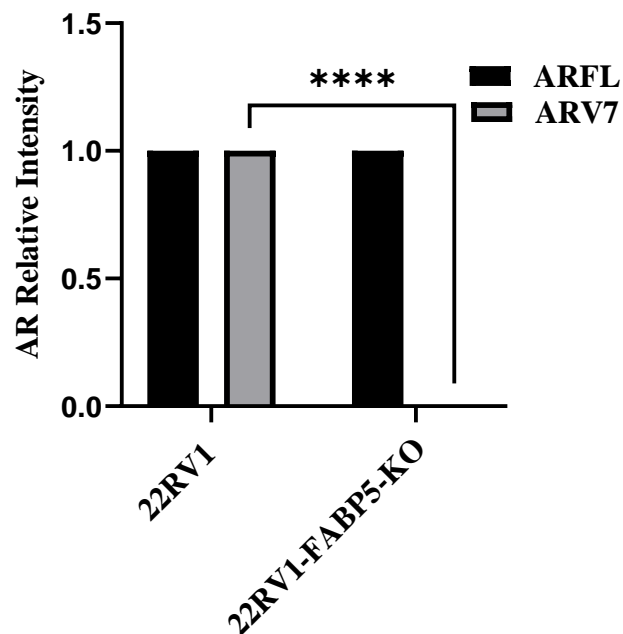
Figure 62. The effect of FABP5 knockout on ARFL and ARV7 expression in 22RV1 cells. **A)** Western blot examination of the expression of ARFL and ARV7 in 22RV1 and its FABP5-KO derivative cells. **B)** ARFL and ARV7 levels in 22RV1 and 22RV1-FABP5-KO cells. Three separate measurements yielded the data (Mean ± SD). ARFL and ARV7 relative levels were determined by densitometrical measuring the intensity of the bands on the blot and analyzing the data with image J software. To normalize any loading inconsistencies, anti-actin was utilized to hybridize the blot. The 2-tailed paired

Student's t test was used to compare the parental 22RV1 cells to the 22RV1-FABP5-KO cells. P<0.05 was considered significant.. Four stars (****) meant $P < 0.0001$.

Assessing the effect of AR KO on expression levels of PPARγ1, PPARγ2, p-PPARγ1, p-PPARγ2, VEGF and FABP5 in 22RV1 cells

5.1.5 The effect of *AR* KO on expression of PPARγ1 and PPARγ2 in 22RV1 cells

To study the effect of *AR*- KO on expression of PPARγ in 22RV1, Western blot was used to detect the expression of both PPARγ1 and PPARγ2 in 22RV1 and its AR-KO derivative cells, and the results were shown **Figure 63**. Both PPARγ1 and PPARγ2 were expressed in the parental 22RV1 cells, their expression was greatly reduced in 22RV1-AR-KO cells. While a weak PPARγ1 band was detected in 22RV1-AR-KO cells, the expression of PPARγ2 was not detectable (Figure 63, A). When levels of PPARγ1 and PPARγ2 in 22RV1 were respectively set to 1, levels of PPARγ1 and PPARγ2 in 22RV1-AR-KO were greatly reduced by 86% and 100% to 0.140 ± 0.05 and 0 respectively (Figure 63, B). Thus the Level of PPARγ1 was significantly suppressed in 22RV1-AR-KO cells (Student's *t* test, $p < 0.0001$), level of PPARγ2 totally suppressed by AR-KO in 22RV1-AR-KO cells (Student's t test, $p < 0.0001$) .

A
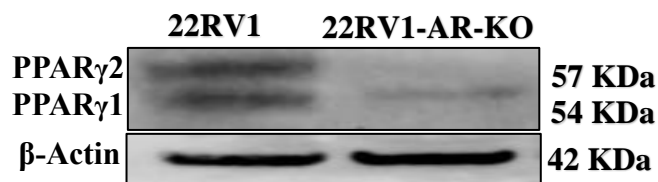
B
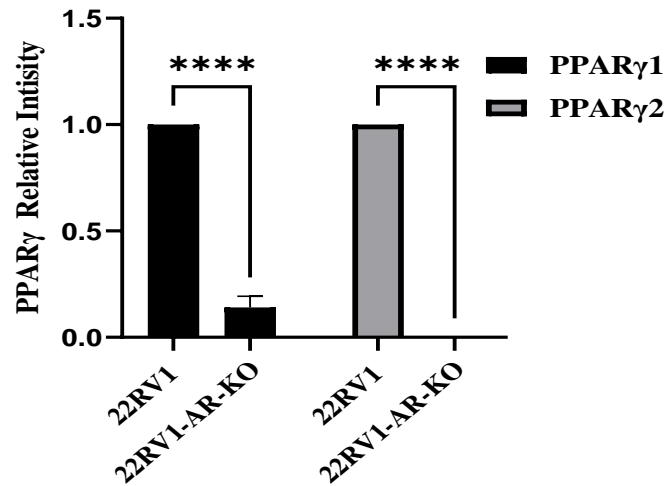
Figure 63. The effect of AR knockout on PPARγ1 and PPARγ2 expression in 22RV1

lines. **A)** PPARγ1 and PPARγ2 Western blot research in 22RV1 prostate cancer cell lines.

B) Quantitative measurement of the peak area intensities of bands on the blot using

densitometry scanning. Three separate measurements yielded the data (Mean ± SD). The

band intensities were measured with the image J program to determine the relative

amounts of PPARγ1 and PPARγ2. The blot was hybridised with anti-actin to normalise

any loading inconsistencies. The 22RV1 and 22RV1-AR-KO cells were compared using

a two-tailed paired Student's t test. P<0.05 was considered significant. Four stars (****)

meant *P*<0.0001.

5.1.6 The effect of *AR* KO on expression of p-PPARγ1 and p-PPARγ2 in 22RV1 cells

The expression of p-PPARγ1 and p-PPARγ2 in 22RV1 and 22RV1-AR-KO cells was detected with Western blot analysis and the results were shown in **figure 64**. Both p-PPARγ1 and p-PPARγ2 were expressed in the parental 22RV1 cells, their expressions were either greatly reduced (p-PPARγ2) or completely undetectable (p-PPARγ1) in 22RV1-AR-KO cells, as shown in figure 64, A. When levels of p-PPARγ1and p-PPARγ2 in 22RV1 were respectively set at 1, those in 22RV1-AR-KO were significantly reduced to 0 and 0.07 ± 0.015, respectively (Figure 64, B) in comparison to the levels expressed in 22RV1 cells (Student's *t* test, $p < 0.0001$).
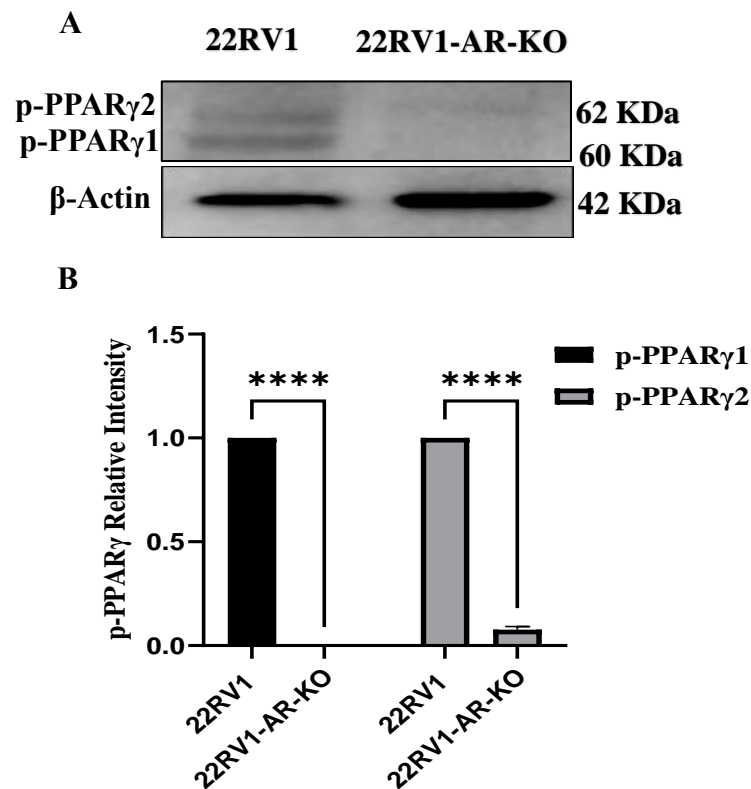
Figure 64. The effect of AR knockout on p-PPARγ1 and p-PPARγ2 expression in 22RV1 and its -KO- derivative cells. **A)** Western blot assessment of the expression of p-PPARγ1 and p-PPARγ2 in 22RV1 and 22RV1-AR-KO cells. **B)** Quantitative measurement of the

peak area intensities of bands on the blot using densitometry scanning. Three separate measurements yielded the data (Mean ± SD). The band intensities were measured with the image J program to determine the relative amounts of p-PPARγ1 and p-PPARγ2. To normalize any loading inconsistencies, anti-actin was employed to hybridize the blot. The 2-tailed paired Student's t test was used to compare 22RV1 cells to 22RV1-AR-KO cells. $P<0.05$was considered significant. Four stars (****) meant P 0.0001.

5.1.7 The effect of AR KO on VEGF expression in 22RV1 cells

Western blot was used to study the AR KO on VEGF expression and the results were shown in **figure 65.** A moderately strong VEGF band was detected in 22RV1 cells, but the VEGF expression was barely detectable in 22RV1-AR-KO cells (Figure 65, A). When the level of VEGF in 22RV1 was set at 1, the level in 22RV1-AR- KO (Figure 65, B) was high significantly reduced to 0.05 ± 0.010 in 22RV1-AR-KO cells (Student's t test, $p < 0.0001$)
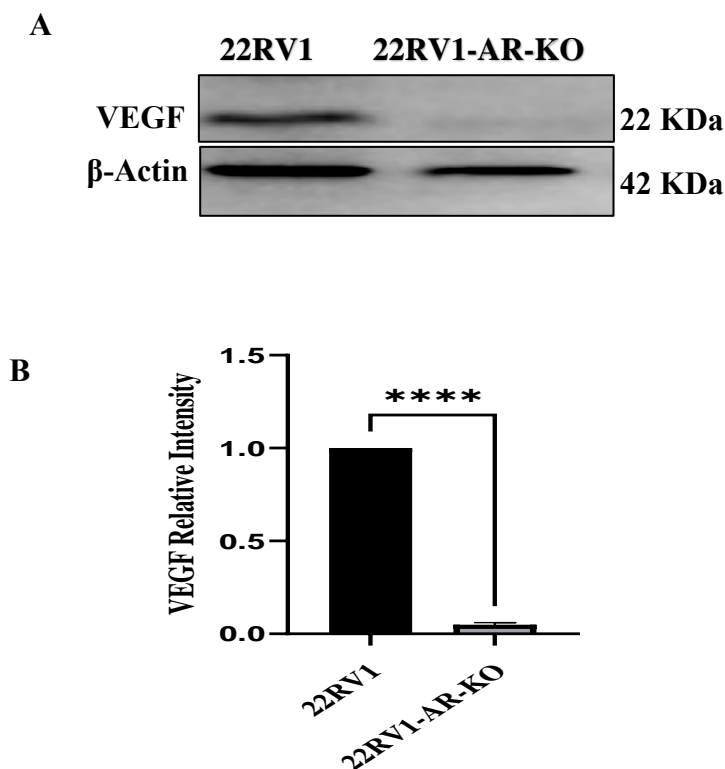
Figure 65. AR knockout affects VEGF expression in 22RV1 and 22RV1-AR-KO cells.

A) VEGF expression investigation by Western blot in 22RV1 and 22RV1-AR-KO cells.

B) Quantitative measurement of the peak area intensities of bands on the blot using

159

densitometry scanning. Three separate measurements yielded the data (Mean ± SD). The relative amounts of VEGF were determined by measuring band intensities with image J. To normalise any loading inconsistencies, anti-actin was utilized to hybridize the blot. A 2-tailed paired Student's t test was used to compare the 22RV1 and 22RV1-AR- KO cells. P<0.05was considered significant.Four stars (****) meant *P* 0.0001.

5.1.8 The effect of AR KO on FABP5 expression in 22RV1 cells

Western blot was used to study the *AR*-KO on FABP5 expression and the results were shown in **figure 66.** A moderate FABP5 expression was detected in 22RV1, but the level of FABP5 expressed in 22RV1-AR- KO cells was not detectable (Figure 66, A). When the level of FABP5 in 22RV1 was set at 1, the level in 22RV1-AR-KO significantly reduced to 0 (Student's *t* test, *p* < 0.0001).

Figure 66. AR-KO affects FABP5 expression in 22RV1 and 22RV1-AR-KO cells. A) FABP5 Western blot analysis in 22RV1 and 22RV1-AR-KO cells. B) Quantitative measurement of the peak area intensities of bands on the blot using densitometry scanning. Three separate measurements yielded the data (Mean ± SD). FABP5 relative levels were determined by measuring band intensities with image J software. To normalize any loading inconsistencies, anti-actin was utilized to hybridize the blot. A 2-tailed paired Student's t test was used to compare the 22RV1 and 22RV1-AR- KO cells. P<0.05was considered significant.. Four stars (****) meant *P* 0.0001

The effect of FABP5 KO on expression levels of PPARγ1, PPARγ2, p-PPARγ1, p-PPARγ2, VEGF, ARFL and ARV7 in DU145 cells

5.2 The effect of *FABP5* KO on PPARγ1 and PPARγ2 expression in DU145 cells

The expression of PPARγ1 and PPARγ2 in DU145 and DU145-FABP5-KO cells was detected with Western blot analysis and the results were shown in **figure 67.** Both PPARγ1 and PPARγ2 were expressed in the parental DU145 cells, their expressions were either greatly reduced (PPARγ1) or completely undetectable (PPARγ2) in DU145-FABP5-KO cells, as shown in figure 67, A. When levels of PPARγ1and PPARγ2 in DU145 were respectively set at 1, the levels of those in DU145-FABP5-KO were significantly reduced to 0 respectively (Figure 67, B) in comparison to the levels expressed in DU145 cells. (Student's *t* test, $p < 0.0001$).Thus, in DU145-FABP5-KO cells, the expression of PPARγ1 or PPARγ2 was totally abolished (by 100%).

A
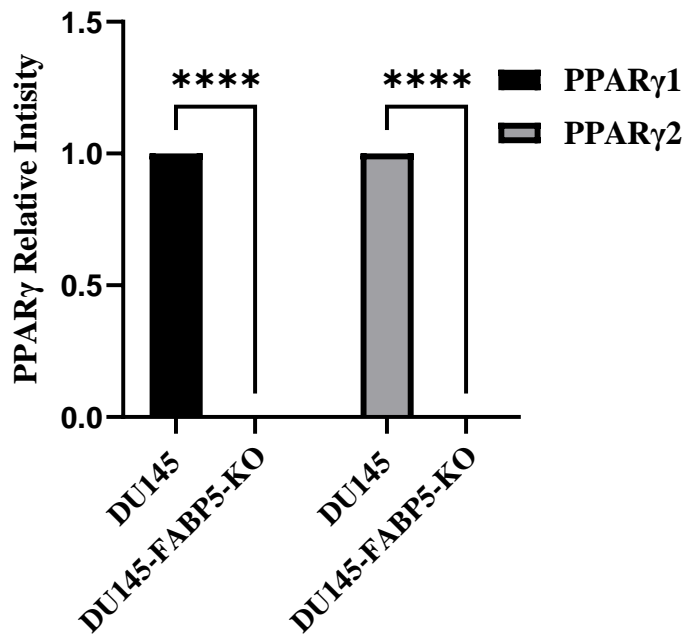
Figure 67. The effect of FABP5 knockout on PPARγ1 and PPARγ2 expression in DU145 and DU145-FABP5-KO cells. **A)** PPARγ1 and PPARγ2 Western blot analysis in DU145 and DU145-FABP5-KO cells. **B)** PPARγ1 and PPARγ2 relative levels determined by densitometric analysis of band intensities on the blot and evaluated with Image J software. Three separate measurements yielded the data (Mean ± SD). The blot was hybridized with anti-actin to normalize any loading inconsistencies. The 2-tail paired Student's t test was used to compare the DU145 and DU145-FABP5-KO cells. *P*<0.05 was considered significant. Four stars (****) meant *P*<0.0001.

5.2.1 The effect of *FABP5* KO on expression of p-PPARγ1 and p-PPARγ2 in DU145 cells

The expression of p-PPARγ1 and p-PPARγ2 in DU145 and DU145-FABP5-KO cells was detected with Western blot and the results were shown in **figure 68**. Both p-PPARγ1 and p-PPARγ2 were expressed in the parental DU145 cells. However, the level of p-PPARγ1 was much higher than that of p-PPARγ2. Comparing to the DU145 control cells, the expression of p-PPARγ1 was significantly reduced and the level of p-PPARγ2 was undetectable in DU145-FABP5-KO cells, as shown in figure 68A. When p-PPARγ1and p-PPARγ2 levels in DU145 cells were respectively set at 1, their relative levels in DU145-FABP5-KO were significantly reduced to 0.15 ± 0.02 and 0, respectively (Figure 68B). While p-PPARγ1 level was decreased significantly by 85 % (Student's *t* test, $p < 0.0001$), p-PPARγ2 level was completely inhibited by 100 % in DU145- FABP5-KO cells (Student's *t* test, $p < 0.0001$).

B

Figure 68. The effect of FABP5 knockout on p-PPARγ1 and p-PPARγ2 expression in DU145 and DU145-FABP5-KO cells. **A)** p-PPARγ1 and p-PPARγ2 Western blot analysis in DU145 and DU145-FABP5-KO cells. **B)** PPARγ1 and PPARγ2 relative levels determined by densitometric analysis of band intensities on the blot and evaluated with Image J software. Three separate measurements yielded the data (Mean ± SD). The blot was hybridized with anti-actin to normalize any loading inconsistencies. The 2-tail paired Student's t test was used to compare the DU145 and DU145-FABP5-KO cells. P<0.05 was considered significant. Four stars (****) meant *P*<0.0001.

5.2.2 The effect of *FABP5* KO on VEGF expression in DU145 cells

The expression status of VEGF in DU145 and DU145-FABP5-KO cells was detected and the results were shown in **figure 69.** A relatively strong VEGF band was detected in DU145 by Western blot and a barely detectable VEGF band was seen in DU145-FABP5-KO cells, as shown in figure 69, A. When the VEGF level in DU145 cells was set at 1, the relative level of VEGF in DU145- FABP5-KO cells was 0.1 ± 0.05 (Figure 69, B), significantly reduced by 90% (Student's *t* test, $p < 0.0001$).
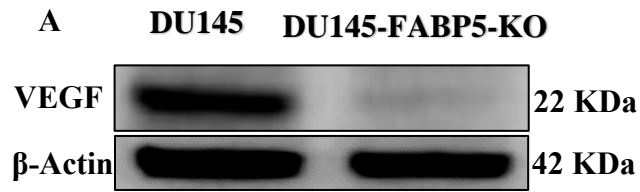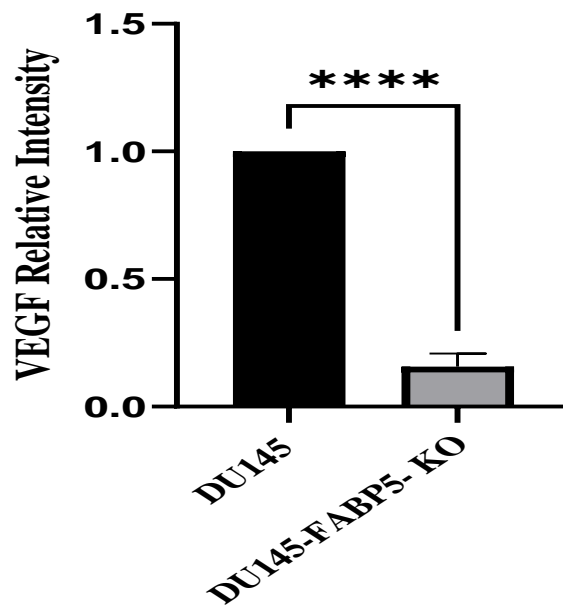
Figure 69. FABP5 knockout affects VEGF expression in DU145 and DU145-FABP5 knockout cells. **A)** VEGF expression study in DU145 and DU145-FABP5-KO cells using Western blot. **B)** VEGF expression levels in DU145 and DU145-FABP5-KO cells. Three separate measurements yielded the data (Mean ± SD). The relative amounts of VEGF were determined using densitometric measurements of the brightness of bands on the blot and image J software. To normalize any loading inconsistencies, anti-actin was utilized to hybridize the blot. The 2-tail paired Student's t test was used to compare the DU145 and DU145-FABP5-KO cells. P<0.05 was considered significant.. Four stars (****) meant *P* 0.0001.

5.2.3 The effect of *FABP5* KO on AR expression in DU145 cell

AR expression was detected neither in DU145, nor in DU145-FABP5-Ko cells, as shown in **figure 70**.

DU145   DU145-FABP5-KO

AR — 110 KDa

β-Actin — 42 KDa

Figure 70. The effect of *FABP5* KO on expression of AR in DU145 cells. Western blot detection of AR expression in DU145 and Du145-FABP5-KO cells.

The effect of FABP5 KO on expression levels of PPARγ 1&2, p-PPARγ1 & 2, VEGF, ARFL and ARV7 in PC3M cells

5.2.4 The effect of FABP5 KO on PPARγ1 and PPARγ2 expression in PC3M cells

The expression of PPARγ1 and PPARγ2 in PC3M and PC3M-FABP5-KO cells was detected with Western blot analysis and the results were shown in **figure 71.** A strong PPARγ1 band and a weak PPARγ2 band were detected in PC3M parental cells (control), whereas in PC3M-FABP5 knockout cells, a very weak PPARγ1 band and no PPARγ2 band were detected, as seen in figure 71, A. When the level of PPARγ1and PPARγ2 in PC3M were set at 1, relative levels of PPARγ1 and PPARγ2 in PC3M- FABP5-KO were 0.022 ± 0.003 and 0 respectively, as depicted in figure 71, B. Level of PPARγ1 significantly reduced by 97.8% (Student's t test, $p < 0.0001$), and the expression of PPARγ2 was totally abolished (by 100%) (Student's t test, $p < 0.0001$) in PC3M-FABP5-KO cells.

A

B
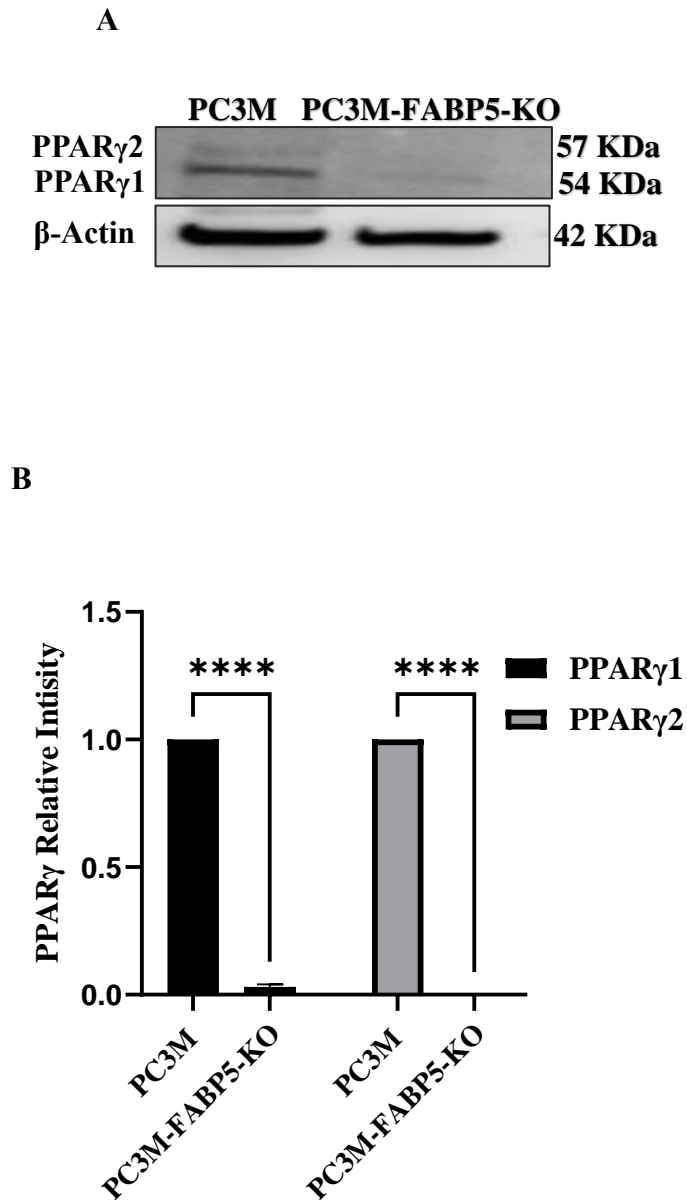
Figure 71. The effect of FABP5 knockout on PPARγ1 and PPARγ2 expression in PC3M and PC3M-FABP5-KO cells. **A)** PPARγ1 and PPARγ2 Western blot analysis in PC3M and PC3M-FABP5-KO cells. **B)** Relative levels of PPARγ1 and PPARγ2 in PC3M and PC3M-FABP5-KO cells determined by quantitative measurement of peak area intensities on the blot using densitometry scanning and Image J software program. Three separate measurements yielded the data (Mean ± SD). The blot was hybridized with anti-actin to normalize any loading inconsistencies. The 2-tail paired Student's t test was used to

compare the PC3M and PC3M-FABP5-KO cells. P<0.05was considered significant..
Four stars (****) meant *P*<0.0001.

5.2.5 The effect of PC3M FABP5 knockout on p-PPARγ1 and p-PPARγ2

The expression of p-PPARγ1 and p-PPARγ2 in PC3M and PC3M-FABP5-KO cells was detected with Western blot and the results were shown in **figure 72**. Both p-PPARγ1 and p-PPARγ2 were expressed in the parental PC3M cells. However, the level of p-PPARγ1 was much higher than that of p-PPARγ2 (Figure 72, A). Comparing to the PC3M control cells, the expression of p-PPARγ1 was reduced by 50% and the level of p-PPARγ2 was reduced by 43% in PC3M-FABP5-KO cells, as shown in figure 72, B. When the level of p- PPARγ1and p-PPARγ2 in PC3M were respectively set at 1, the relative levels of p-PPARγ1 and p-PPARγ2 in PC3M FABP5 KO were 0.45 ± 0.05 and 0.57 ± 0.04, respectively. Level of p-PPARγ1 and p-PPARγ2 significantly suppressed in PC3M-FABP5-KO cells (Student's t test, p < 0.001), comparing to the control.

A
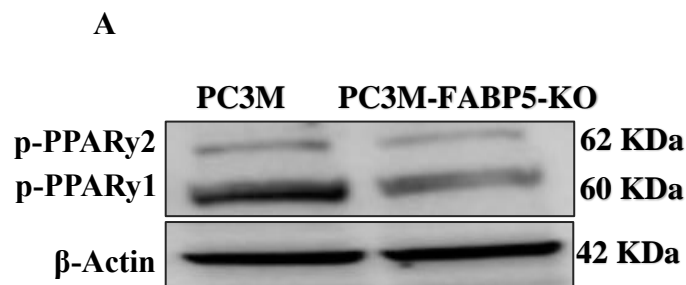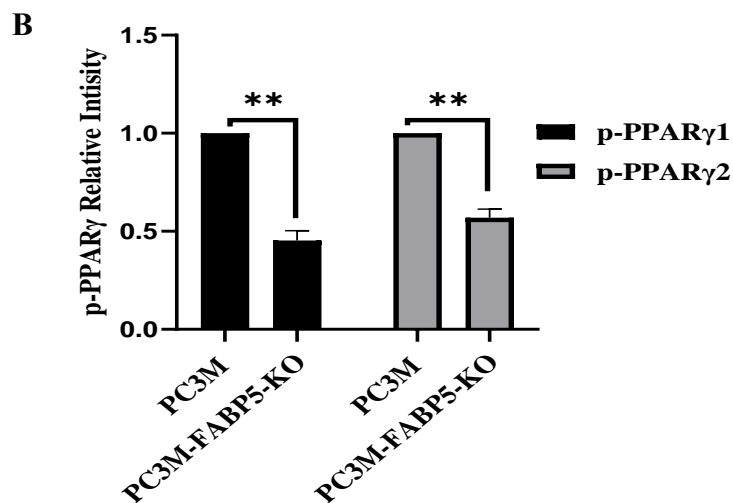
Figure 72. The effect of FABP5 knockout on p-PPARγ1 and p-PPARγ2 expression in PC3M and PC3M-FABP5-KO cells. **A)** p-PPARγ1 and p-PPARγ2 Western blot analysis in PC3M and PC3M-FABP5-KO cells. **B)** Relative p-PPARγ1 and p-PPARγ2 levels determined by densitometric measurement of band intensities and evaluated using Image J software. Three separate measurements yielded the data (Mean ± SD). The blot was hybridized with anti-actin to normalize any loading inconsistencies. The 2-tail paired Student's t test was used to compare the PC3M and PC3M-FABP5-KO cells. P<0.05was considered significant. Four stars (****) meant *P*<0.0001.

5.2.6 The effect of *FABP5* KO on VEGF expression in PC3M cells

The expression status of VEGF in PC3M and PC3M-FABP5-KO cells was detected and the results were shown in **figure 73.** A strong VEGF band was detected in PC3M by Western blot and a much smaller VEGF band was seen in PC3M-FABP5-KO cells, as shown in figure 73, A. When the VEGF level in PC3M cells was set at 1, the relative level of VEGF in PC3M-FABP5-KO cells was 0.42 ± 0.03 (Figure 73, B), significantly reduced by 58 % (Student's *t* test, *p* < 0,001).
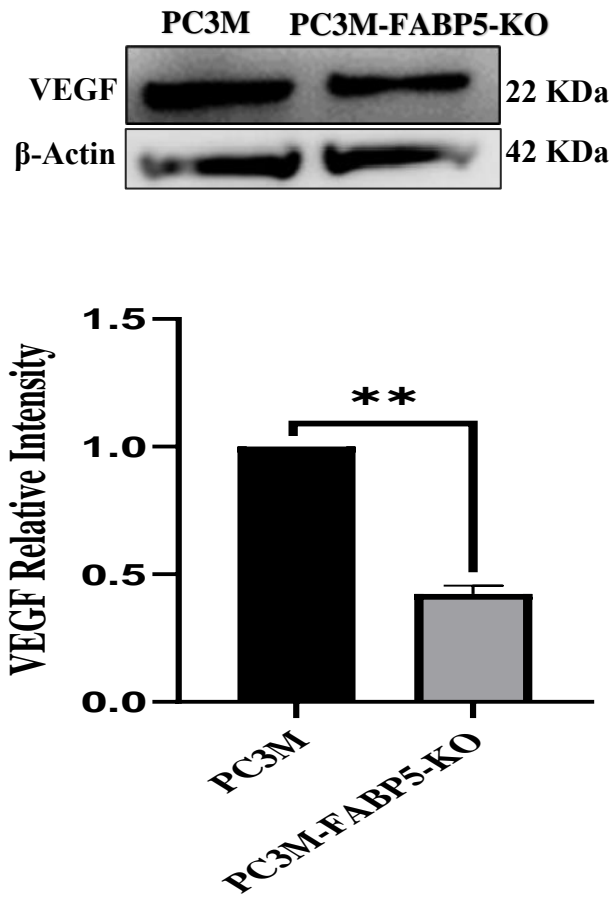
Figure 73. FABP5 knockout affects VEGF expression in PC3M and PC3M-FABP5 knockout cells. **A)** VEGF expression study in PC3M and PC3M-FABP5-KO cells using Western blot. **B)** VEGF expression levels in PC3M and PC3M-FABP5-KO cells. Three separate measurements yielded the data (Mean $\pm$ SD). The relative amounts of VEGF were determined using densitometric measurements of the brightness of bands on the blot and image J software. To normalize any loading inconsistencies, anti-actin was utilized to hybridize the blot. The 2-tail paired Student's t test was used to compare the PC3M and PC3M-FABP5-KO cells. P<0.05 was considered significant. Two star meant **P 0.001

5.2.7 The effect of *FABP5* KO on AR expression in PC3M cells

AR expression was detected neither in PC3M, nor in PC3M-FABP5-KO cells, as shown in **figure 74**.

PC3M   PC3M-FABP5-KO

AR   110 KDa

β-Actin   42 KDa

Figure 74. The effect of *FABP5* KO on expression of AR in PC3M cells. Western blot analysis of AR expression in PC3M and PC3M-FABP5-KO.

5.2.8 Discussion

In this chapter, the contribution of FABP5 and AR to the promotion of prostate cancer cell behavior was explored through Western blot analyses measuring changes in the expression of important signal transduction pathway factors upon FABP5 or AR knockouts. Specific proteins were investigated in different cell lines, including androgen-dependent 22RV1 cells and highly malignant and androgen receptor (AR)-negative castration-resistant prostate cancer (CRPC) cells DU145 and PC3M. The results showed that FABP5 expression depended on ARFL, while ARFL expression remained unaffected by the absence of FABP5. Additionally, FABP5 influenced the expression of ARV7, which plays a crucial role in ADT resistance. Significant reductions in malignant characteristics were observed in 22RV1-FABP5-KO cells, with altered expression of proteins involved in cell proliferation and survival. In 22RV1-AR-KO cells, AR knockout led to notable changes in regulating these processes. Furthermore, in highly malignant AR-negative CRPC cells, FABP5 played a major regulatory role, completely replacing AR in promoting malignant progression through the FABP5-PPARγ-VEGF axis.

Table 8. Summary of Protein Effects in Prostate Cancer Cell Lines after FABP5 or AR

knockout

Cell Line	Protein	Effect
22RV1-FABP5-KO Cells	ARFL	No change
	ARV7	Not detectable
	PPARγ-1	Increased by 75%
	PPARγ-2	Decreased by 68%
	p-PPARγ1	Decreased by 64%
	p-PPARγ2	Decreased by 88%
	VEGF	Reduced by 90%
22RV1-AR-KO Cells	FABP5	Not detectable
	PPARγ-1	Reduced by 86%
	PPARγ-2	Reduced by 100%
	p-PPARγ1	Decreased by 100%
	p-PPARγ2	Decreased by 93%
	VEGF	Reduced by 95%
DU145-FABP5-KO Cells	PPARγ-1	Completely inhibited
	PPARγ-2	Completely inhibited
	p-PPARγ1	Reduced by 85%

	p-PPARγ2	Reduced by 100%
	VEGF	Reduced by 90%
PC3M-FABP5-KO Cells	PPARγ-1	Reduced by 97.8%
	PPARγ-2	Reduced by 100%
	p-PPARγ1	Decreased by 50%
	p-PPARγ2	Decreased by 43%
	VEGF	Reduced by 58%

Footnote: The table summarizes the effect of FABP5 or AR knockout , its related factors (PPARγ1, PPARγ2, p-PPARγ1, p-PPARγ2), AR, ARV7, and VEGF in different cell types.

These results indicated that FABP5 and AR played distinct roles in regulating the expression of various proteins associated with prostate cancer behavior. Knocking out FABP5 or AR resulted in specific changes in proteins expression compared to the expression in parental cells. Notably, ARV7 and FABP5 were not detectable in knockout cells, indicating a loss of these proteins. Knockout cells also displayed altered expression levels of PPARγ-1, PPARγ-2, p-PPARγ1, p-PPARγ2, and VEGF, with some proteins completely inhibited or significantly reduced in their expression. This suggests the essential roles of FABP5 and AR in regulating these proteins' expression and influencing prostate cancer cell behavior, potentially providing valuable insights into the underlying mechanisms of prostate cancer development and progression, suggesting its crucial role in promoting malignant progression.

Chapter 6 -Result-4:Identification of the differentially expressed genes and the relevant pathways between the parental control cells and the *FABP5*- or *AR*- KO cells

6.1 Introduction

This chapter delves deeper into understanding the genes regulated by FABP5 and AR in prostate cancer cells. By comparing the expression profiles of FABP5- or AR-knockout (KO) cells with the control parental cells 22RV1 and DU145, and identify differentially expressed genes (DEGs) to elucidate the specific genes influenced by FABP5 and AR in prostate cancer cells. Additionally, the chapter aims to validate the expression of the six most pronounced DEGs which were commonly upregulated or downregulated in both 22RV1-FABP5-KO and 22RV1-AR-KO cell lines, as well as in the highly malignant and androgen receptor (AR)-negative castration-resistant prostate cancer (CRPC) cell line DU145-FABP5-KO, to gain insights into their potential roles in prostate cancer development and progression. Also, Gene ontology (GO) pathway analysis will be conducted to uncover the functional significance of the identified DEGs and their potential implications in the transition of prostate cancer cells from androgen-responsive (22RV1) to androgen-unresponsive states (DU145).

6.2 Identification of the FABP5-regulated genes by comparing the expression profiles between 22RV1 and 22RV1-FABP5-KO cells

Gene expression profile comparison was performed to identify the DEGs between the parental 22RV1 cells and its derivative 22RV1-FABP5-KO cells to assess the FABP5 regulated genes. DEGs were those genes whose expression levels between the two cell lines were significantly different by at least one fold (Student t-test, $p < 0.05$). Altogether, 250 upregulated and 250 downregulated genes were identified (Supplementary file). As shown in **figure 75**, a volcano plot (A) and two heat maps (B, C), reflected all 500 DEGs and the top 40 genes which exhibited the most pronounced differences between the two RNA sources. The volcano plot showed that 22RV1-FABP5-KO cells exhibited a large transcriptomic change compared to its parental 22RV1 cells. The heat map revealed that the expression levels of many genes in 22RV1-FABP5-KO were significantly different from those in 22RV1 (B). The top 20 up- and down- regulated genes ranked by their levels of differences (C) were listed in **table 9**. with details of gene ID and names.

A

22RV1 vs 22RV1-FABP5-KO

B

22RV1
22RV1-FABP5-KO

22RV1   22RV1-FABP5-KO

C

	KRT19
	STEAP1
	HSPB6
	LDLR
	SEMA4A
	MLPH
	STAT6
	GLYATL1
	TSPAN8
	HGF
	FBLIM1
	UGT2B15
	CDH17
	AKR1C3
	MUC13
	PRSS21
	ALB
	CX3CL1
	TMPRSS4
	NR1H4
	SFRP1
	DLL3
	ESRRB
	ADAM19
	IRX4
	COL4A1
	PPP4R4
	BARX2
	ANO1
	NEFL
	RPH3AL
	EPB41L3
	STOX2
	DOC2B
	LAMA1
	SOCS2
	CDH18
	CUX2
	COL6A2
	ASS1

22RV1   22RV1-FABP5-KO

Color Key

-4 -2 0 2 4
Value

Figure 75. Investigation of FABP5-regulated genes by comparing expression profiles between the *FABP5*-positive and *FABP5*-knockout 22RV1 cells. **A)** Volcano plot showing the differentially expressed genes between 22RV1 and 22RV1-FABP5-KO cells. Each scattered dot represents a gene with a significant change of at least one log2 fold (Student's t test, $p < 0.05$). Genes that are up-regulated are indicated by red dots, while down-regulated genes are indicated by blue dots. **B)** Heat map visualizing the top 500 DEGs between 22RV1 and 22RV1-FABP5-KO cells. Red indicates upregulation and green indicates downregulation. Levels of changes were reflected by color intensities as showed in the color key. **C)** Heat map visualizing the top 40 most pronounced DEGs between 22RV1 and 22RV1-FABP5-KO cells.

Table 9. The ID, name, fold and significance of the changes of the top 40 most pronounced DEGs tween 22RV1 and 22RV1-FABP5-KO cells

Gene ID	Gene Name	log2FoldChange	*p* value
ENSG00000171345	KRT19	-4.76503	1.95E-09
ENSG00000164647	STEAP1	-4.58614	9.77E-11
ENSG00000004776	HSPB6	-4.52465	8.59E-11
ENSG00000130164	LDLR	-4.05123	6.01E-12
ENSG00000196189	SEMA4A	-5.77535	3.73E-17
ENSG00000115648	MLPH	-6.85049	2.48E-36
ENSG00000166888	STAT6	-7.03778	4.68E-26
ENSG00000166840	GLYATL1	-9.07851	4.27E-09
ENSG00000127324	TSPAN8	-5.19101	1.83E-10

ENSG00000019991	HGF	-6.59939	1.83E-08
ENSG00000162458	FBLIM1	-5.75828	5.97E-08
ENSG00000196620	UGT2B15	-8.72938	2.40E-08
ENSG00000079112	CDH17	-7.72931	1.88E-06
ENSG00000196139	AKR1C3	-7.91328	6.99E-07
ENSG00000173702	MUC13	-7.62374	2.46E-06
ENSG00000007038	PRSS21	-7.43399	5.13E-06
ENSG00000163631	ALB	-4.91839	2.25E-06
ENSG00000006210	CX3CL1	-7.3886	6.02E-06
ENSG00000137648	TMPRSS4	-6.58036	0.00013
ENSG00000012504	NR1H4	-6.21572	0.000518
ENSG00000104332	SFRP1	7.918877	1.48E-06
ENSG00000090932	DLL3	7.051427	5.35E-10
ENSG00000119715	ESRRB	8.843079	1.52E-07
ENSG00000135074	ADAM19	8.656002	3.69E-07
ENSG00000113430	IRX4	9.309391	1.13E-08
ENSG00000187498	COL4A1	9.357618	8.34E-09
ENSG00000119698	PPP4R4	9.965597	4.78E-10
ENSG00000043039	BARX2	9.926337	4.91E-10

ENSG00000131620	ANO1	6.833901	1.86E-10
ENSG00000277586	NEFL	7.651159	1.82E-16
ENSG00000181031	RPH3AL	7.112501	9.85E-12
ENSG00000082397	EPB41L3	6.417703	2.01E-14
ENSG00000173320	STOX2	9.442916	6.22E-10
ENSG00000272636	DOC2B	9.415629	5.40E-10
ENSG00000101680	LAMA1	8.007561	6.76E-21
ENSG00000120833	SOCS2	7.073519	4.57E-22
ENSG00000079112	CDH17	-7.72931	1.88E-06
ENSG00000111249	CUX2	8.552648	2.88E-38
ENSG00000142173	COL6A2	6.638127	1.48E-31
ENSG00000130707	ASS1	8.848459	2.58E-78

6.2.1 The Impact of *FABP5* Knockout on Gene Ontology (GO) of Biological Processes Enriched in DEGs between 22RV1 and 22RV1-FABP5-KO cells

In this study, 250 upregulated genes and 250 downregulated genes were analyzed with the GO Biological Process- enrichment terms and the top 30 pathways were selected as shown in **figure 76** and **table 10**. Many of the pathways identified in this Enrichment bar chart could affect the biological processes potentially related *FABP5* gene. The DEGs were associated with processes such as cellular response to fatty acids, cellular response to prostaglandin D stimulus, progesterone metabolism and the response to corticosteroid**.** The majority of the DEGs were involved in the fatty acid responsive pathway. The results

of this analysis suggested that *FABP5* KO could block numerous pathways, including the steroid metabolic process and hormone responsive pathways, both of which are key processes involved in the transformation of the cancer cells from androgen-dependent to androgen-independent state.

Figure 76. Gene Ontology Biological Process Enrichment bar chart of the Top 30 Pathways connected to DEGs between 22RV1 and 22RV1-FABP5-KO cells. Folds of pathway enrichment were proportional to the length of the bar charts. Levels of pathway changes were indicated by –log10(FDR).

Table 10. The top 30 GO Enriched pathways connected with the DEGs between 22RV1 and 22RV1-FABP5-KO cells

Enrichment FDR	Fold Enrichment	Pathway
3.95E-10	20.85289	**Response to fatty acid**
4.10E-08	25.27623	**Cellular response to fatty acid**
4.05E-05	92.41622	**Response to jasmonic acid**
4.05E-05	92.41622	**Cellular response to jasmonic acid stimulus**
4.05E-05	92.41622	**Response to prostaglandin D**
4.05E-05	92.41622	**Cellular response to prostaglandin D stimulus**
1.68E-07	13.39365	**Odontogenesis of dentin-containing tooth**
2.64E-05	25.67117	**Ammonium ion metabolic proc.**
5.65E-07	14.03791	**Pancreas development**
2.18E-07	12.9707	**Pos. reg. of neuron differentiation**
0.000152	61.61081	**Convergent extension involved in axis elongation**
2.98E-05	16.80295	**Exocrine system development**
1.86E-06	12.05429	**Artery development**
2.13E-12	8.143958	**Urogenital system development**

3.75E-08	9.949572	**Eye morphogenesis**
5.17E-09	9.382357	**Reg. of neuron differentiation**
1.63E-11	8.293763	**Renal system development**
3.90E-07	10.34685	**Camera-type eye morphogenesis**
6.22E-09	9.241622	**Multicellular organismal signaling**
4.18E-07	10.26847	**Odontogenesis**
7.71E-11	8.13344	**Kidney development**
0.000167	27.38258	**Progesterone metabolic proc.**
0.000167	27.38258	**Paraxial mesoderm development**
0.000347	46.20811	**Paraxial mesoderm formation**
5.81E-05	14.78659	**Pos. reg. of epithelial to mesenchymal transition**
2.30E-05	13.06896	**Artery morphogenesis**
9.56E-10	8.065415	**Heart contraction**
9.16E-08	9.153606	**Response to corticosteroid**
7.58E-09	8.249146	**Reg. of heart contraction**
1.57E-09	7.782418	**Heart proc.**

6.3 Identification of the AR- regulated genes by comparing the expression profiles between 22RV1 and 22RV1-AR-KO cells

Gene expression profile comparison was performed to identify the DEGs between the parental 22RV1 cells and its derivative 22RV1-AR-KO cells to assess the AR regulated genes. DEGs were those genes whose expression levels between the two cell lines were significantly different by at least one fold (Student t-test, $p < 0.05$). Altogether, 250 upregulated and 250 downregulated genes were identified (Supplementary file). As shown in **figure 77**, a volcano plot (A) and two heat maps (B, C), reflected all 500 DEGs and the top 40 genes which exhibited the most pronounced differences between the two RNA sources. The volcano plot showed that 22RV1-AR-KO cells exhibited a large transcriptomic change compared to its parental 22RV1 cells. The heat map revealed that the expression levels of many genes in 22RV1-AR-KO were significantly different from those in 22RV1 (B). The top 20 up- and down- regulated genes ranked by their levels of differences (C) were listed in **table 11** with details of gene ID and names.

A

22RV1vs 22RV1-AR-KO

-log10-(*p*-value)

log2-Fold

B

22RV1
22RV1-AR-KO

22RV1   22RV1-AR-KO

C

MT-CO1
MT-ND2
LDLR
MT-ATP8
MT-ND3
FDFT1
SCD
HMGCS1
ATF5
MT-TL2
UGT2B15
GUCY1B2
VWA2
MUC1
AVEN
ALB
ASB9
NR1H4
CYP2C8
SPI1
RORB-AS1
B3GAT1
ONECUT1
PPARGC1A
ROR1
DLC1
ITPR1
RASAL1
BCAN
UCN2
ASS1
HLA-A
CYP4F8
GAS1
TMEM59L
RORB
GNAO1
PPP2R2C
CACNA1I
HMOX1

22RV1   22RV1-AR-KO
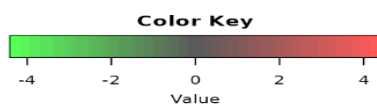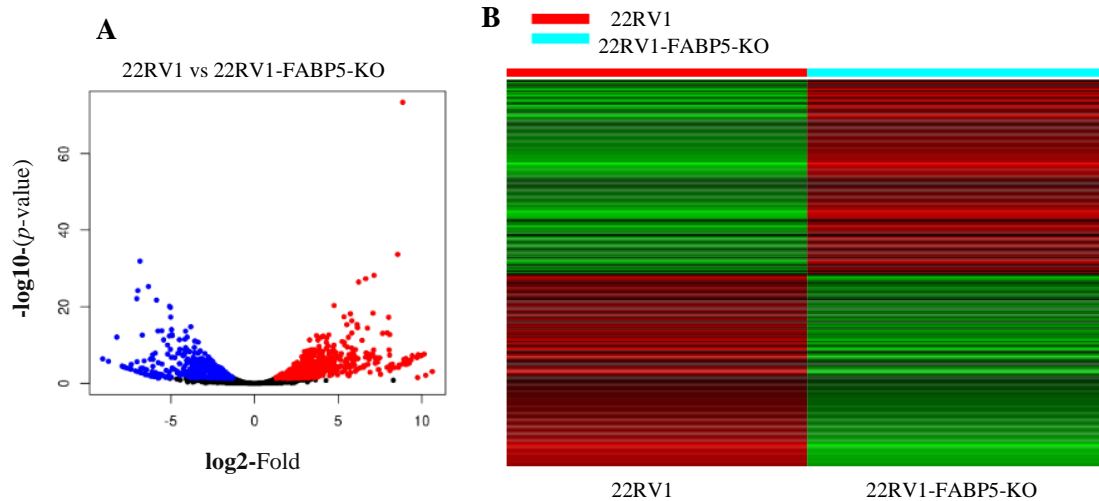
Color Key

-4   -2   0   2   4
Value

185

Figure 77. Investigation of AR-regulated genes by comparing expression profiles between the *AR*-positive and *AR*-knockout 22RV1 cells. **A)** Volcano plot showing the differentially expressed genes between 22RV1 and 22RV1-AR-KO cells. Each scattered dot represents a gene with a significant change of at least one log2 fold (*P*<0.05). Genes that are up-regulated are indicated by red dots, while down-regulated genes are indicated by blue dots. **B**) Heat map visualizing the top 500 DEGs between 22RV1 and 22RV1-AR-KO cells. Red indicates upregulation and green indicates downregulation. Levels of changes were reflected by color intensities as showed in the color key. **C**) Heat map visualizing the top 40 most pronounced DEGs between 22RV1 and 22RV1-AR-KO cells.

Table 11. The ID, name, fold and significance of the changes of the top 40 most pronounced DEGs between 22RV1 and 22RV1-AR-KO cells

Gene ID	Gene Name	log2FoldChange	*p* value
ENSG00000198804	MT-CO1	-2.83267	2.10E-06
ENSG00000198763	MT-ND2	-2.72373	1.07E-07
ENSG00000130164	LDLR	-4.52892	5.40E-14
ENSG00000228253	MT-ATP8	-2.54158	1.35E-07
ENSG00000198840	MT-ND3	-2.7471	4.75E-08

ENSG00000079459	FDFT1	-2.36796	2.18E-06
ENSG00000099194	SCD	-2.95305	5.43E-06
ENSG00000112972	HMGCS1	-3.05897	1.14E-07
ENSG00000169136	ATF5	-2.9933	2.13E-07
ENSG00000210191	MT-TL2	-2.82356	6.33E-06
ENSG00000196620	UGT2B15	-4.47231	2.16E-10
ENSG00000123201	GUCY1B2	-3.11183	1.93E-07
ENSG00000165816	VWA2	-3.47047	7.10E-05
ENSG00000185499	MUC1	-2.37316	0.000577
ENSG00000169857	AVEN	-3.17426	7.45E-06
ENSG00000163631	ALB	-3.66914	1.29E-05
ENSG00000102048	ASB9	-3.09574	0.0017

ENSG00000012504	NR1H4	-5.83903	0.000323
ENSG00000138115	CYP2C8	-5.71716	0.000638
ENSG00000066336	SPI1	-4.24645	0.001002
ENSG00000224825	RORB-AS1	4.911157	0.00167
ENSG00000109956	B3GAT1	7.906402	7.39E-06
ENSG00000169856	ONECUT1	4.772941	7.69E-05
ENSG00000109819	PPARGC1A	3.53184	0.00054
ENSG00000185483	ROR1	3.163251	1.35E-05
ENSG00000164741	DLC1	4.441879	5.59E-05
ENSG00000058335	ITPR1	4.817764	1.23E-10
ENSG00000111344	RASAL1	2.512553	0.000921
ENSG00000132692	BCAN	4.632247	4.54E-07

ENSG00000145040	UCN2	3.26252	5.12E-06
ENSG00000130707	ASS1	2.624126	0.000342
ENSG00000206503	HLA-A	4.722258	3.18E-09
ENSG00000186526	CYP4F8	4.63578	6.29E-10
ENSG00000180447	GAS1	10.8462	2.58E-12
ENSG00000105696	TMEM59L	4.920548	1.18E-13
ENSG00000198963	RORB	3.151807	1.03E-05
ENSG00000087258	GNAO1	3.95591	7.50E-10
ENSG00000074211	PPP2R2C	2.778014	9.65E-05
ENSG00000100292	HMOX1	7.007461	6.12E-05
ENSG00000100346	CACNA1I	4.142474	8.39E-10

6.3.1 The Impact of *AR* Knockout on Gene Ontology (GO) of Biological Processes Enriched-DEGs between 22RV1 and 22RV1-AR-KO cells

In this study, 250 upregulated genes and 250 downregulated genes caused by *AR*-knockout were analyzed with the GO Biological Process- enrichment terms and the top 30 pathways were selected as shown in **figure 78** and **table 12** . Many of the pathways identified in this Enrichment bar chart could affect the biological processes potentially related to the activity of AR. These DEGs were associated with processes, such as cholesterol biosynthesis, and sterol hormone synthesis and metabolism**.** These results suggested that *AR*- KO could block numerous pathways, particularly the cholesterol biosynthesis, and steroid hormone synthesis and metabolisms, both of which are likely to play key roles in the transition of the cancer cells from androgen-dependent to castration-resistant state.

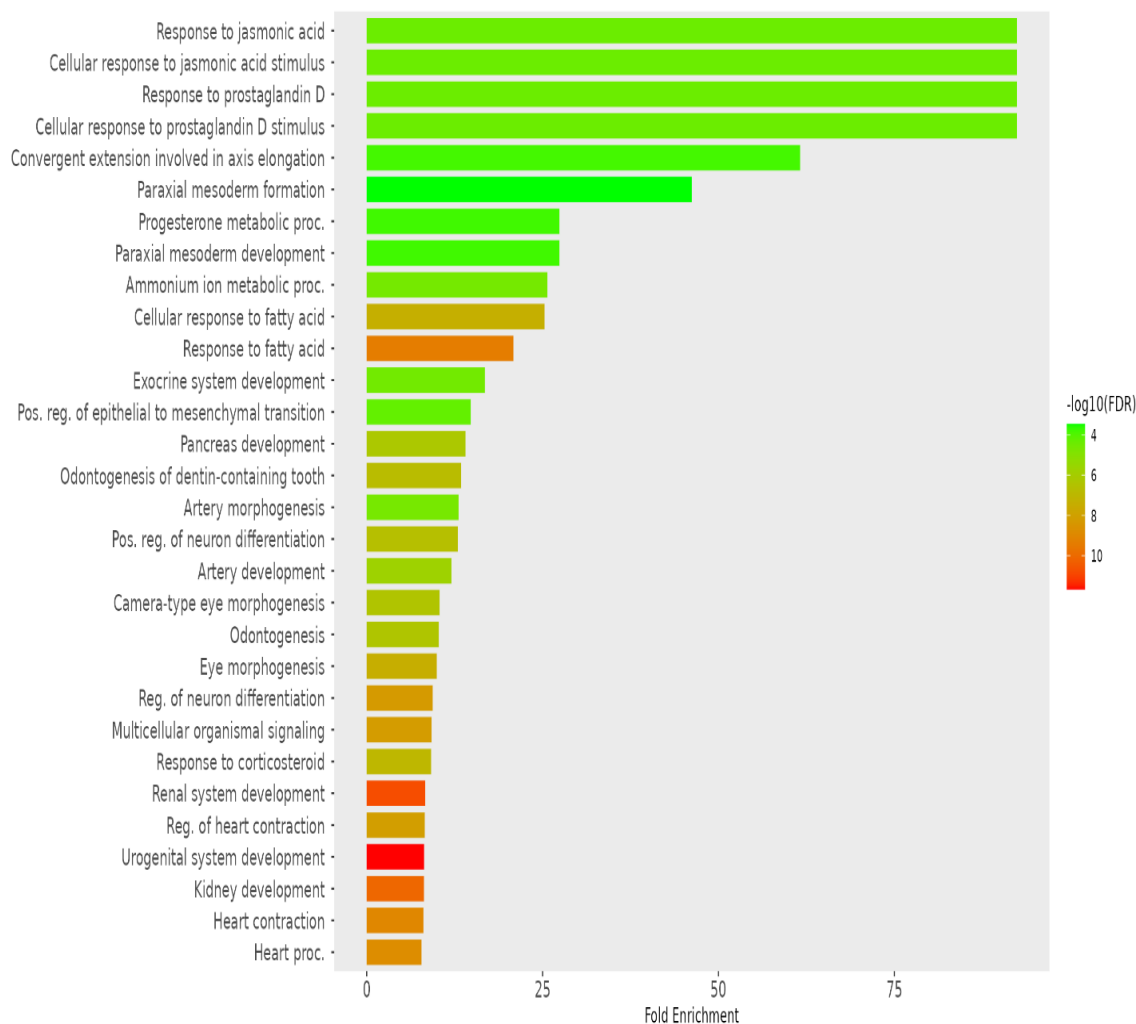**Figure 78**.Gene Ontology Biological Process Enrichment bar chart of the Top 30 Pathways connected to DEGs between 22RV1 and 22RV1-AR-KO cells. Folds of pathway enrichment were proportional to the length of the bar charts. Levels of pathway changes were indicated by –log10(FDR).

Table 12. The top 30 GO Enriched pathways connected with the DEGs between 22RV1 and 22RV1-AR-KO cells

Enrichment FDR	Fold Enrichment	Pathway
1.95E-05	7.070876	Cholesterol biosynthetic proc.
1.95E-05	7.070876	Secondary alcohol biosynthetic proc.
6.08E-05	6.320935	Sterol biosynthetic proc.
0.002098	23.83895	Energy coupled proton transmembrane transport, against electrochemical gradient
0.002098	23.83895	Electron transport coupled proton transport
0.000384	3.877912	Cholesterol metabolic proc.
0.000833	3.629328	Secondary alcohol metabolic proc.
0.004529	19.8658	Reg. of DNA topoisomerase (ATP-hydrolyzing) activity
0.002037	3.350149	Sterol metabolic proc.

0.002037	3.310966	Homophilic cell adhesion via plasma membrane adhesion molecules
0.000114	2.330347	Chromatin organization
0.006759	7.192788	Placenta blood vessel development
0.00386	2.74148	Organic hydroxy compound biosynthetic proc.
0.000193	1.910173	Chromosome organization
0.017932	13.24386	Reg. of isomerase activity
0.017932	13.24386	Pos. reg. of isomerase activity
0.000292	1.815268	Pos. reg. of transcription by RNA polymerase II
0.017702	5.182381	Pos. reg. of pri-miRNA transcription by RNA polymerase II
0.000632	1.799259	Reg. of cell cycle
0.003985	2.158457	Histone modification
0.028007	8.277415	Labyrinthine layer blood vessel development
0.016746	3.082623	Alcohol biosynthetic proc.

0.027098	5.489233	Reg. of stem cell proliferation
0.008525	2.802847	Steroid biosynthetic proc.
0.017213	3.06151	Placenta development
0.002037	1.631789	Neg. reg. of nucleobase-containing compound metabolic proc.
0.016942	2.943081	Histone acetylation
0.026789	3.373437	Aerobic electron transport chain
0.037973	5.959739	Isoprenoid biosynthetic proc.
0.002037	1.597599	Pos. reg. of transcription, DNA-templated

6.4 Identification of the FABP5-regulated genes by comparing the expression profiles between DU145 and DU145-FABP5-KO cells

Gene expression profile comparison was performed to identify the DEGs between the parental DU145 cells and its derivative DU145-FABP5-KO cells to assess the FABP5 regulated genes. DEGs were those genes whose expression levels between the two cell lines were significantly different by at least one fold (Student t-test, $p < 0.05$). Altogether, 300 upregulated and 200 downregulated genes were identified (Supplementary file). As shown in **figure 79**, a volcano plot (A) and two heat maps (B, C), reflected all 500 DEGs and the top 40 genes which exhibited the most pronounced differences between the two RNA sources. The volcano plot showed that DU145-FABP5-KO cells exhibited a large transcriptomic change compared to its parental DU145 cells. The heat map revealed that the expression levels of many genes in DU145-FABP5-KO were significantly different from those in DU145 (B). The top 20 up- and down- regulated genes ranked by their levels of differences (C) were listed in **table 13** with details of gene ID and names.
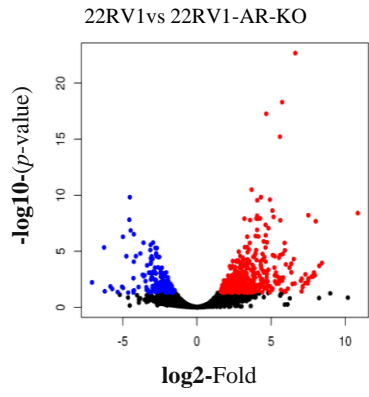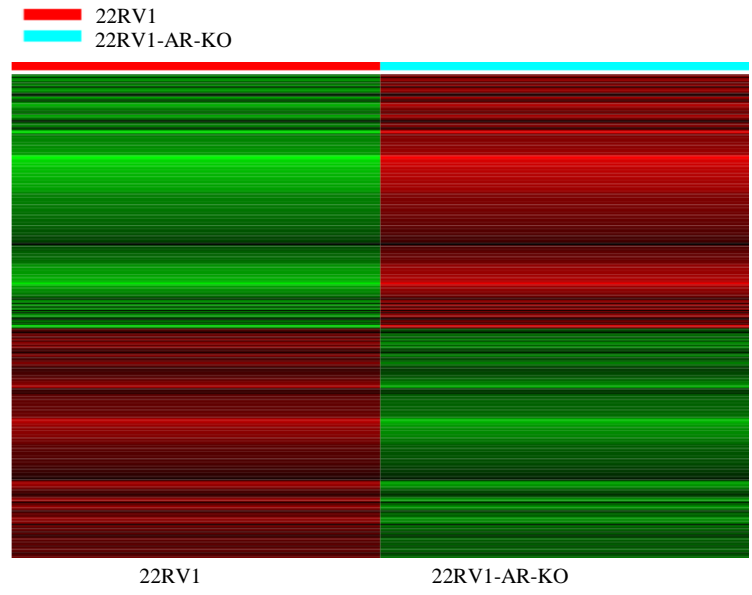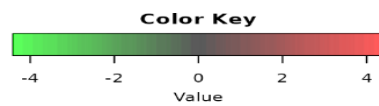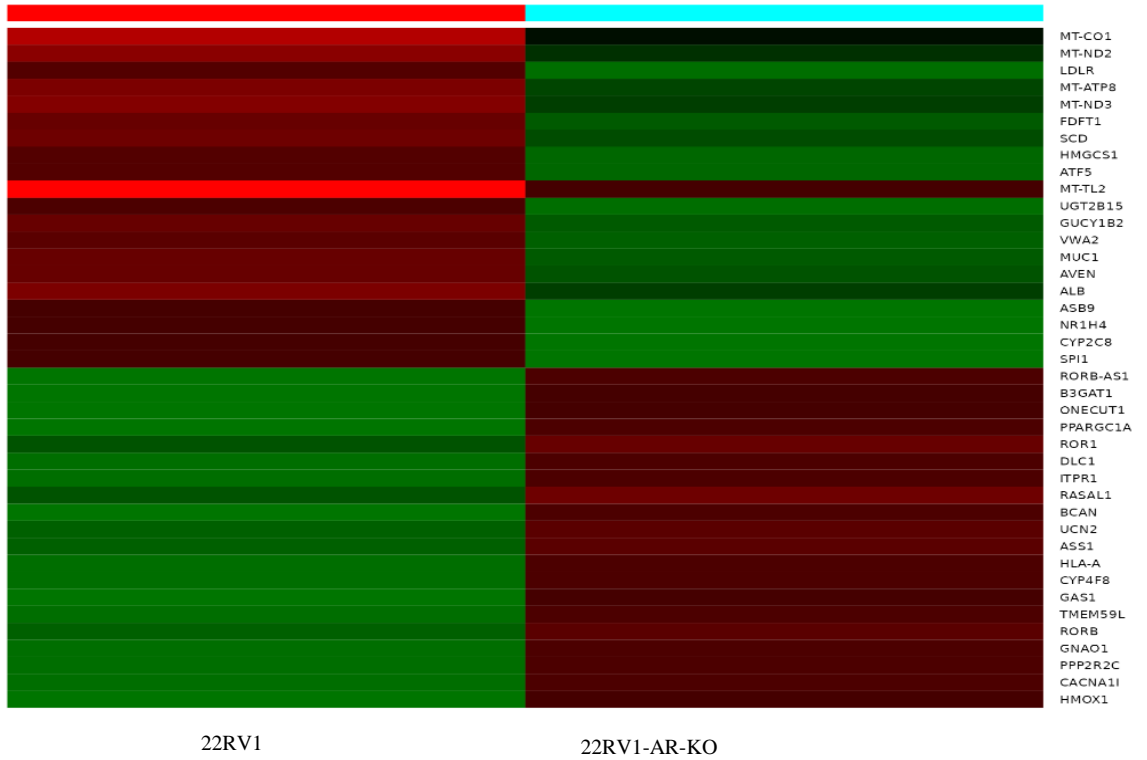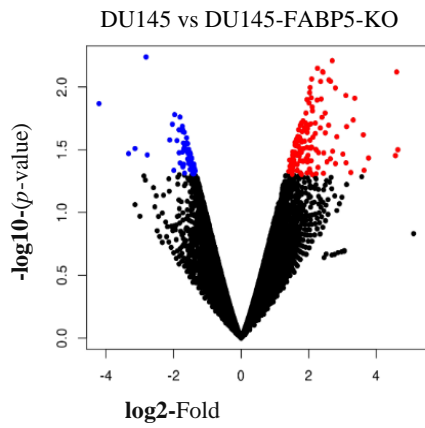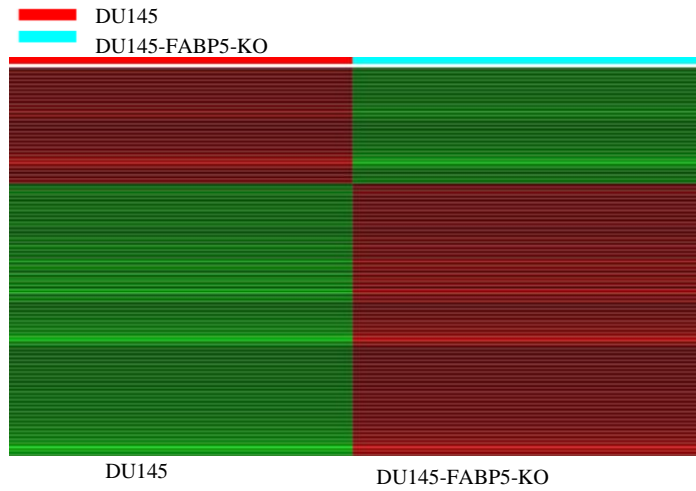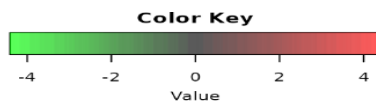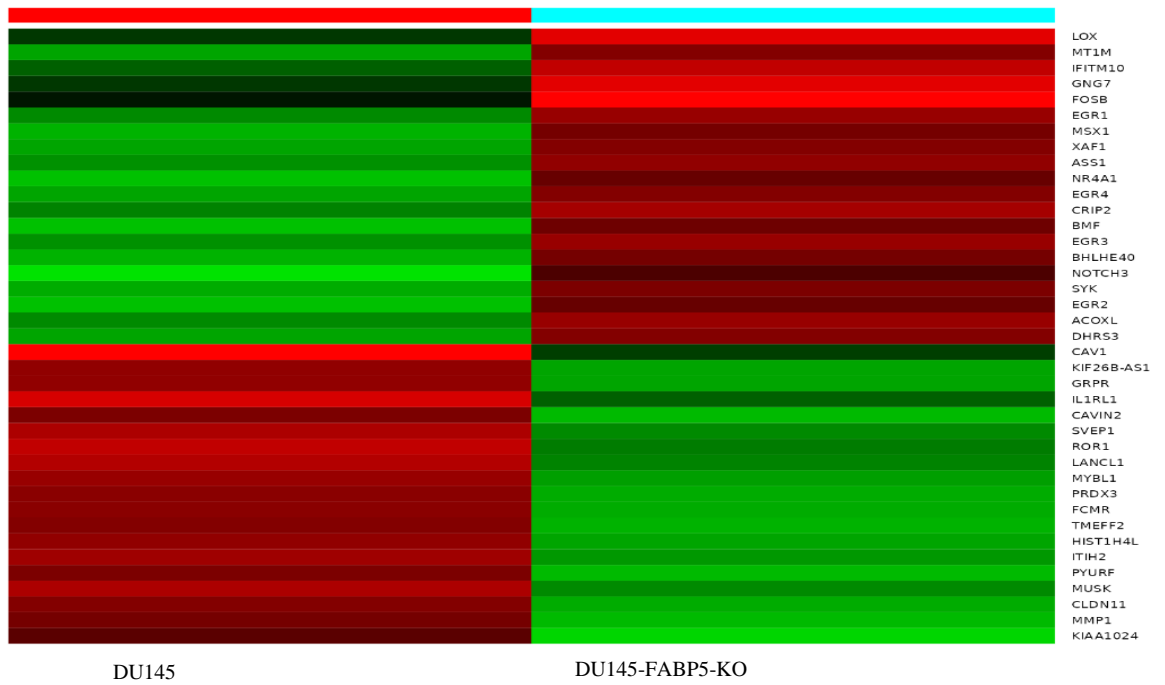
Figure 79. Investigation of FABP5-regulated genes by comparing expression profiles between the *FABP5*-positive and *FABP5*-knockout DU145 cells. **A)** Volcano plot showing the differentially expressed genes between DU145 and DU145-FABP5-KO cells. Each scattered dot represents a gene with a significant change of at least one log2 fold (*P*<0.05). Genes that are up-regulated are indicated by red dots, while down-regulated genes are indicated by blue dots. **B)** Heat map visualizing the top 500 DEGs between DU145 and DU145-FABP5-KO cells. Red indicates upregulation and green indicates downregulation. Levels of changes were reflected by color intensities as showed in the color key. **C)** Heat map visualizing the top 40 most pronounced DEGs between DU145 and DU145-FABP5-KO cells.

Table 13. The ID, name, fold and significance of the changes of the top 40 most pronounced DEGs between DU145 and DU145-FABP5-KO cells

Gene ID	Gene Name	log2FoldChange	*p* value
ENSG00000113083	LOX	2.568477	3.80E-43
ENSG00000205364	MT1M	1.836739	0.011298
ENSG00000244242	IFITM10	2.114165	0.015518
ENSG00000176533	GNG7	2.065239	0.019687
ENSG00000125740	FOSB	3.057334	0.020109

ENSG0000012073 8	EGR1	1.313533	0.05133
ENSG0000016313 2	MSX1	2.474824	0.001865
ENSG0000013253 0	XAF1	5.107902	0.147392
ENSG0000013070 7	ASS1	1.740535	1.72E-05
ENSG0000012335 8	NR4A1	2.089559	0.008646
ENSG0000013562 5	EGR4	1.764551	0.02066
ENSG0000018280 9	CRIP2	1.553935	0.051683
ENSG0000010408 1	BMF	2.235654	2.82E-05
ENSG0000017938 8	EGR3	4.607518	0.007603
ENSG0000013410 7	BHLHE40	2.504767	3.84E-48
ENSG0000007418 1	NOTCH3	2.462673	1.79E-37
ENSG0000016502 5	SYK	2.018064	1.72E-07

ENSG0000012287 7	EGR2	2.442622	0.065936
ENSG0000015309 3	ACOXL	2.698124	0.006185
ENSG0000016249 6	DHRS3	2.41196	1.56E-25
ENSG0000010597 4	CAV1	-2.73978	0.010563
ENSG0000023219 2	KIF26B-AS1	-1.78448	0.02797
ENSG0000012601 0	GRPR	-4.20944	0.013582
ENSG0000011560 2	IL1RL1	-2.33115	0.001441
ENSG0000016849 7	CAVIN2	-2.37219	1.29E-07
ENSG0000016512 4	SVEP1	-1.78449	0.041951
ENSG0000018548 3	ROR1	-1.56502	4.73E-05
ENSG0000011536 5	LANCL1	-1.56907	0.04581
ENSG0000018569 7	MYBL1	-1.8815	2.71E-05

ENSG0000016567 2	PRDX3	-1.51662	0.045619
ENSG0000016289 4	FCMR	-2.18935	7.20E-05
ENSG0000014433 9	TMEFF2	-1.78211	0.031605
ENSG0000027512 6	HIST1H4 L	-2.55737	0.090252
ENSG0000015165 5	ITIH2	-2.33497	0.017281
ENSG0000014533 7	PYURF	-2.11067	0.03719
ENSG0000003030 4	MUSK	-1.7563	0.026985
ENSG0000001329 7	CLDN11	-1.79274	0.000161
ENSG0000016933 0	KIAA1024	-3.04372	0.001224

6.4.1 The Impact of *FABP5* Knockout on GO of Biological Processes Enriched in DEGs between DU145 and DU145-FABP5-KO cells

In this study, 300 upregulated genes and 200 downregulated genes were analyzed with the GO Biological Process- enrichment terms and the top 30 pathways were selected as shown in **Figure 80** and **table 14**. Many of the pathways and biological processes related *FABP5* KO were identified through this Enrichment bar chart. The DEGs were associated with processes such as positive regulation of lipid transport and localization, positive regulation of fatty acid transport and cholesterol efflux, as well as the response to progesterone. The majority of the DEGs were involved in the lipid and fatty acid transport and metabolic pathway. These results suggested that *FABP5* KO could block such pathways, as those for fatty acid and lipid transport and for regulation of cholesterol hormone responsive, both of which involved in key processes during the transformation of the cancer cells from androgen-dependent to androgen-independent state.
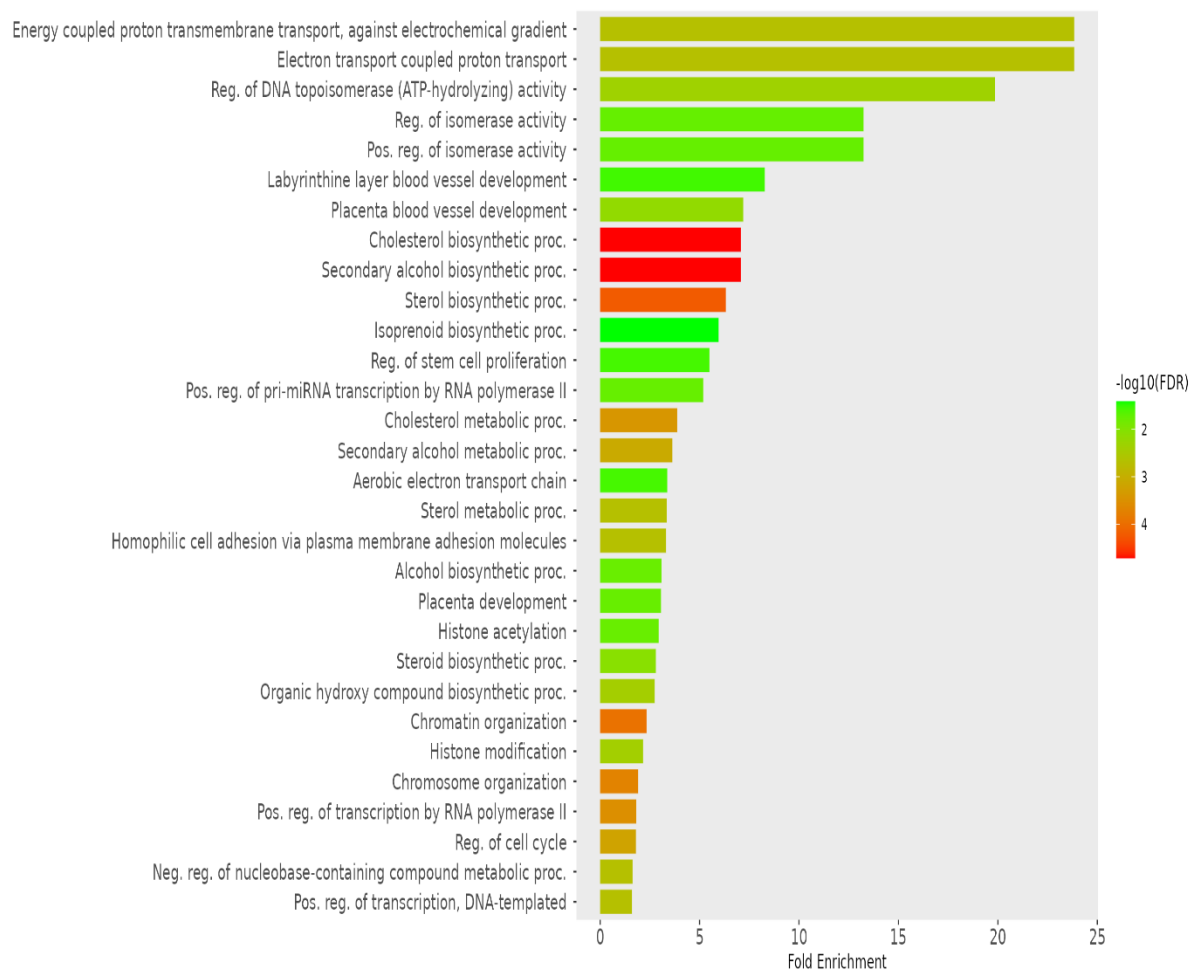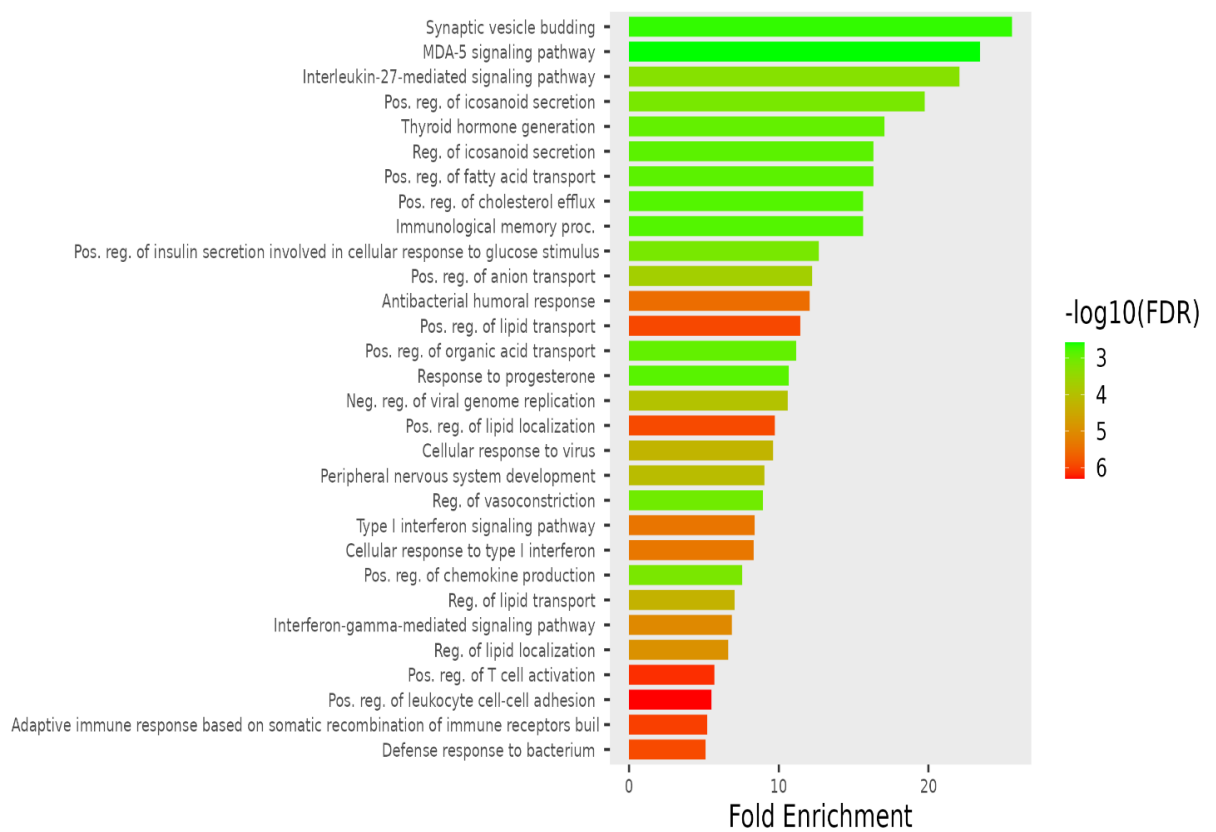
Figure 80. Gene Ontology Biological Process Enrichment bar chart of the Top 30 Pathways connected to DEGs between 22RV1 and 22RV1-AR-KO cells. Folds of pathway enrichment were proportional to the length of the bar charts. Levels of pathway changes were indicated by –log10(FDR).

Table 14. The top 30 GO Enriched pathways connected with the DEGs between DU145 and DU145-FABP5-KO cells

Enrichment FDR	Fold Enrichment	Pathway
1.15E-06	11.44033	Pos. reg. of lipid transport
3.12E-06	12.06138	Antibacterial humoral response
1.18E-06	9.735073	Pos. reg. of lipid localization
0.00053	22.07311	Interleukin-27-mediated signaling pathway
4.16E-06	8.389575	Type I interferon signaling pathway
4.42E-06	8.321917	Cellular response to type I interferon
0.000763	19.74962	Pos. reg. of icosanoid secretion
0.00021	12.23618	Pos. reg. of anion transport
5.46E-05	9.62161	Cellular response to virus
0.000109	10.59153	Neg. reg. of viral genome replication
8.22E-05	9.041995	Peripheral nervous system development
0.001184	17.05649	Thyroid hormone generation
0.000769	12.67712	Pos. reg. of insulin secretion involved in cellular response to glucose stimulus
0.001346	16.3149	Reg. of icosanoid secretion
0.001346	16.3149	Pos. reg. of fatty acid transport

8.44E-06	6.864198	Interferon-gamma-mediated signaling pathway
1.20E-05	6.621932	Reg. of lipid localization
0.001512	15.63512	Pos. reg. of cholesterol efflux
0.001512	15.63512	Immunological memory proc.
5.07E-05	7.053436	Reg. of lipid transport
7.18E-07	5.69565	Pos. reg. of T cell activation
0.002166	25.58474	Synaptic vesicle budding
5.06E-07	5.500302	Pos. reg. of leukocyte cell-cell adhesion
0.001199	11.16794	Pos. reg. of organic acid transport
0.002655	23.45267	MDA-5 signaling pathway
9.51E-07	5.211706	Adaptive immune response based on somatic recombination of immune receptors buil
0.000911	8.934352	Reg. of vasoconstriction
0.001412	10.66031	Response to progesterone
0.000735	7.547987	Pos. reg. of chemokine production
1.18E-06	5.116947	Defense response to bacterium

6.5 Identification the six most pronounced carcinogenesis-related DEGs between *FABP5-* or *AR*-KO cells and their parental cells

Further analysis identified the following 6 most pronounced DEGs: CRIP2, ERG3, FOSB, GRPR, CAV1, and NR1H4. The first 3 were upregulated and the later 3 were down-regulated when either *FABP5* or *AR* was knocked out in 22RV1 cells. Except NR1H4, the same up- or down- regulation for the rest 5 genes were seen between the FABP5-KO and the parental DU145 cells. Careful analyzing the pathway bar chart shown in (**Figure 76,78,80**), it was found that CRIP2 ,ERG3 and FOSB were involved in regulation of cellular response to type I interferon pathway, response to progesterone signaling pathway and peripheral nervous system development that played an important suppressive role in initiation and expansion of prostate cancer.All 3 down-regulated genes GRPR, CAV1, and NR1H4 played roles in fatty acid and lipid transport related pathways, including steroid and cholesterol metabolic processes(**Figure 76,78,80**). The heat maps reflecting the expression profiles of these top 6 DEGs were displayed in **figure 81**. The differential expression between 22RV1 and 22RV1-FABP5-KO or 22RV1-AR-KO cells was shown in A; the differential expression between DU145 and DU145-FABP5-KO cells was shown in B.
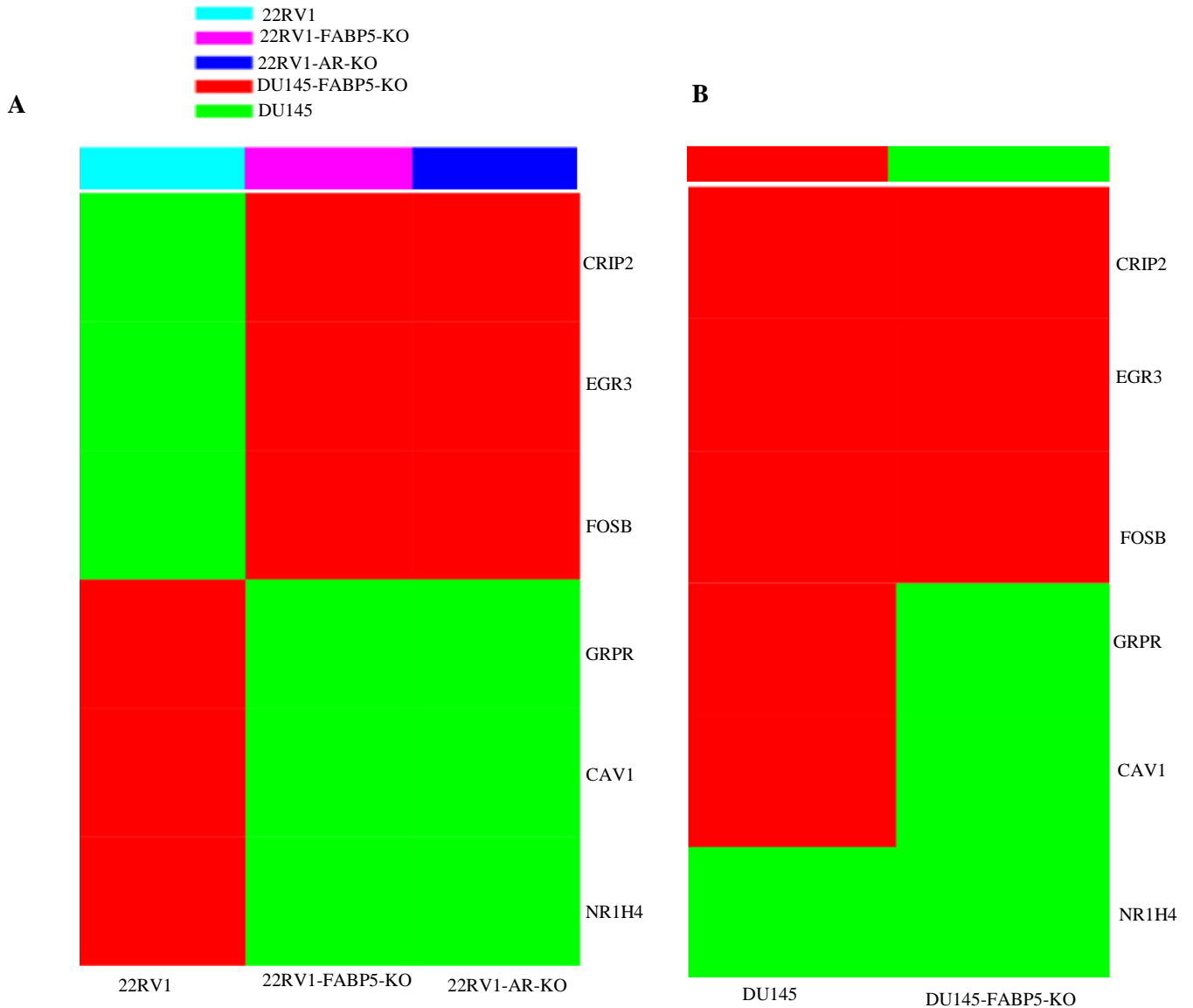
Figure 81. Expression changes of the six top DEGs produced by *FABP5-* or *AR-* knockout and dmrFABP5 treatment in CRPC cells. **A)** The heat map showing the effect of FABP5 or AR knockout on the expression of upregulated genes CRIP2, ERG3 and FOSB and the downregulated genes GRPR, CAV1 and NR1H4 in the androgen-responsive 22RV1 cells. The red represents upregulation and the green represents downregulation. **B)** The heat map showing the effect of FABP5 knockout or dmrFABP5 treatment on the expression status of upregulated genes CRIP2, ERG3 and FOSB, and the downregulated genes

GRPR, CAV1 and NR1H4 in the AR-negative DU145 cells. The red represents upregulation and the green represents downregulation or no-expression.

6.5.1 The effect of *FABP5* KO on expression of CRIP2, ERG3, FOSB, GRPR, CAV1 and NR1H4 in 22RV1 cells

The 3 upregulated and 3 downregulated DEGs (CRIP2,ERG3 and FOSB and GRPR,CAV1 and NR1H4) detected by comparing the RNA profiles between 22RV1 and 22RV1-FABP5-KO cells were verified with Western blot and the results were shown in **figure 82.** In the parental 22RV1 cells, *ERG3* and *FOSB* were expressed, but the expression of *CRIP2* was not detectable, whereas all these 3 genes were highly expressed in 22RV1-FABP5-KO cells (A). While CRIP was not expressed in the parental 22RV1 cells, a moderately high level of this protein was detected in 22RV1-FABP5-KO cells. When levels of ERG3 and FOSB in 22RV1 were set at 1 and 1, respectively, their relative levels in 22RV1-FABP5-KO were significantly increased to 2.87 ± 0.09 and 2.1 ± 0.09, respectively (C). Thus, comparing to the expressions in the parental cells, the levels of ERG and FOSB increased by 187% and 110%, respectively (Student's *t* test, $p < 0.0001$) in the cells with *FABP5* knocked out. Contrary to the 3 upregulated- gene products, expression of GRPR, CAV1 and NR1H4 were either greatly reduced or completely abrogated in 22RV1-FABP5-KO cells, as showed in B. While the expression of NR1H4 was not detectable, levels of GRPR, CAV1 were significantly reduced respectively to 0.04 ± 0.02, 0.20 ± 0.03 in 22RV1-FABP5-KO cells when those in 22RV1-parental cells were set at 1, respectively (C). Levels of GRPR and CAV1 decreased by 96% (Student's *t* test, $p < 0.0001$), 80% (Student's *t* test, $p < 0.0002$) respectively in comparison to those in the control.
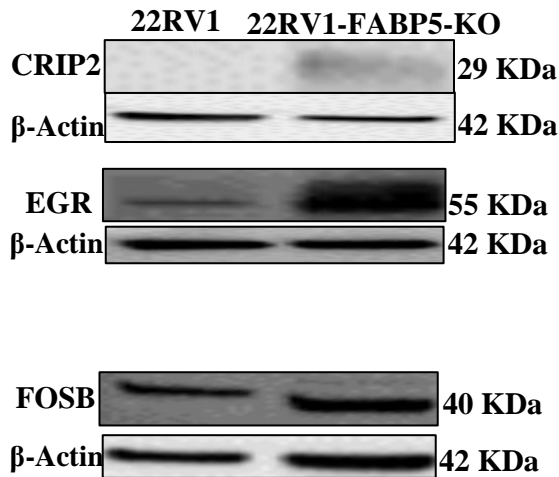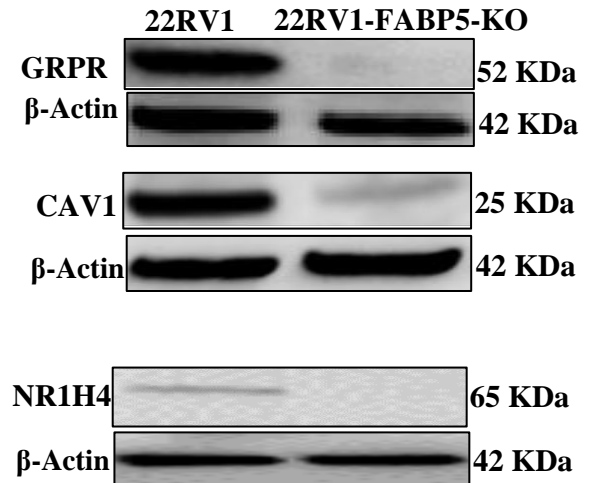
Figure 82. Verification of the six top DEGs by assessing the different expression at the protein levels with Western blot. **A)** Western blot analysis of the expression status of upregulated DEGs CRIP2, ERG3 and FOSB expressed in 22RV1 and 22RV1-FABP5-KO cells. **B)** Western blot analysis of the expression status of the downregulated DEGs GRPR, CAV1 and NR1H4 in 22RV1 and 22RV1-FABP5-KO cells. **C)** Quantitative assessments of expression levels of 6 DEGs in parental 22RV1 and 22RV1-FABP5-KO cells. Except NR1H4, which was not expressed in 22RV1-FABP5-KO cells, the levels for all 5 other DEGs in 22RV1 cells were set at 1, the levels in 22RV1-FABP5-KO cells were calculated by relating to those expressed in 22RV1 cells. The results (Mean ± SD)

were obtained from 3 separate measurements, the intensities of the bands on the blot were subjected to densitometry scanning and the data was analyzed with the image J software. Anti-β-actin was used to hybridize the blot to normalize possible loading discrepancies. The differences between the 22RV1 and 22RV1-FABP5-KO cells were assessed with Student t-test, the results were regarded as statistically significant when $p<0.05$. The degree of significance was represented by the number of stars as following: *$p<0.05$, **$p<0.001$, ***$p<0.0002$, and ****$p<0.0001$

6.5.2 The effect of *AR* KO on expression of CRIP2, ERG3, FOSB, GRPR, CAV1 and NR1H4 in 22RV1 cells

The 3 upregulated and 3 downregulated DEGs (CRIP2,ERG3 and FOSB and GRPR,CAV1 and NR1H4) detected by comparing the RNA profiles between 22RV1 and 22RV1-AR-KO cells were verified with Western blot and the results were shown in **figure 83** In the parental 22RV1 cells, *ERG3* and *FOSB* were expressed, but the expression of *CRIP2* was not detectable, whereas all these 3 genes were highly expressed in 22RV1-AR-KO cells (A). While CRIP was not expressed in the parental 22RV1 cells, a moderately high level of this protein was detected in 22RV1-AR-KO cells. When levels of ERG3 and FOSB in 22RV1 were set at 1 and 1, respectively, their relative levels in 22RV1-AR-KO were significantly increased to 2.5 ± 0.04 and $2. \pm 0.06$ respectively, (C). Thus, comparing to the expressions in the parental cells, the levels of ERG and FOSB increased by 150% and 100%, respectively (Student's t test, $p < 0.0001$) in the cells with *AR* knocked out. Contrary to the 3 upregulated- gene products, expression of GRPR, CAV1 and NR1H4 were either greatly reduced or completely abrogated in 22RV1-AR-KO cells, as showed in B. While the expression of NR1H4 was not detectable, levels of GRPR, CAV1 were significantly reduced respectively to 0.02 ± 0.02, 0.15 ± 0.05 in 22RV1-AR-KO cells when those in 22RV1-parental cells were set at 1, respectively (C).

Levels of GRPR and CAV1 decreased by 98% and 85% (Student's *t* test, $p < 0.0001$), respectively in comparison to those in the control.
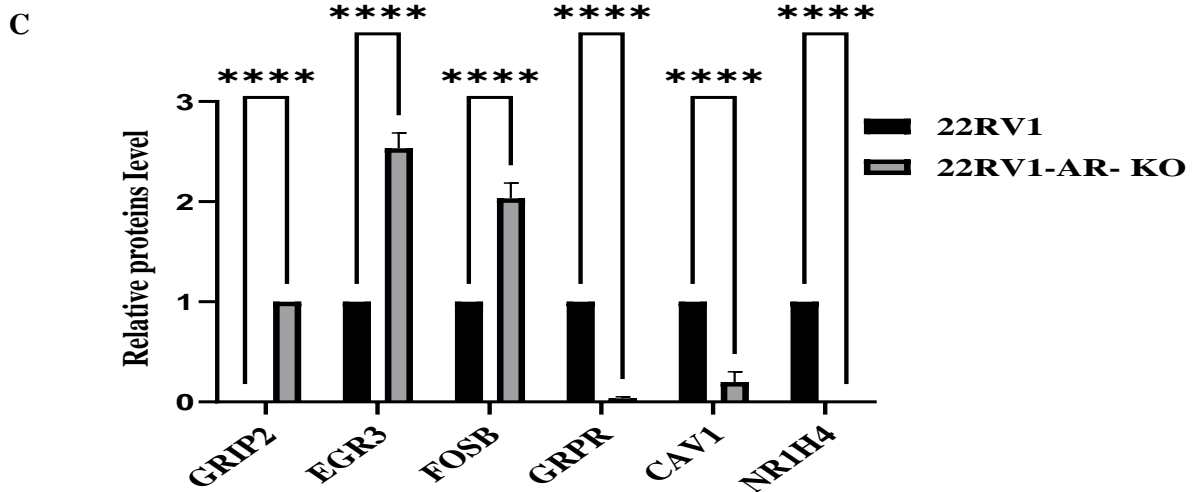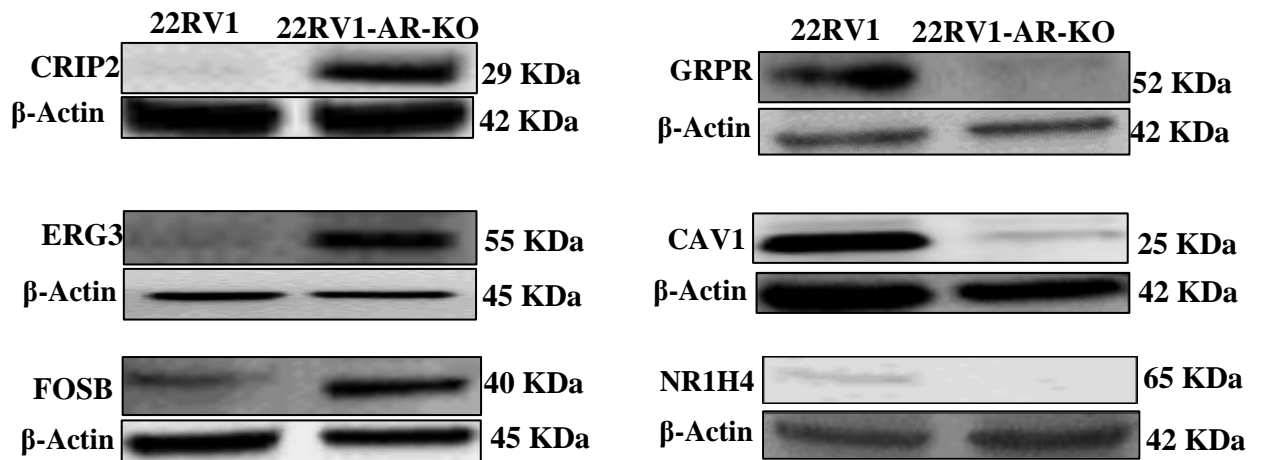
Figure 83. Verification of the six top DEGs by assessing the different expression at the protein levels with Western blot. **A)** Western blot analysis of the expression status of upregulated DEGs CRIP2, ERG3 and FOSB expressed in 22RV1 and 22RV1-AR-KO cells. **B)** Western blot analysis of the expression status of the downregulated DEGs GRPR, CAV1 and NR1H4 in 22RV1 and 22RV1-AR-KO cells. **C)** Quantitative assessments of expression levels of 6 DEGs in parental 22RV1 and 22RV1-AR-KO cells. Except NR1H4, which was not expressed in 22RV1-AR-KO cells, the levels for all 5 other DEGs in 22RV1 cells were set at 1, the levels in 22RV1-AR-KO cells were calculated by relating to those expressed in 22RV1 cells. The results (Mean ± SD) were

obtained from 3 separate measurements, the intensities of the bands on the blot were subjected to densitometry scanning and the data was analyzed with the image J software. Anti-β-actin was used to hybridize the blot to normalize possible loading discrepancies. The differences between the 22RV1 and 22RV1-AR-KO cells were assessed with Student t-test, the results were regarded as statistically significant when $p<0.05$. The degree of significance was represented by the number of stars as following: $*p<0.05$, $**p<0.001$, $***p<0.0002$, and $****p<0.0001$

6.5.3 The effect of *FABP5* KO on expression of CRIP2, ERG3, FOSB, GRPR,CAV1 and NR1H4 in DU145 cells

The 3 upregulated and 3 downregulated DEGs (CRIP2,ERG3 and FOSB and GRPR,CAV1 and NR1H4) detected by comparing the RNA profiles between DU145 and DU145-FABP5-KO cells were verified with Western blot and the results were shown in **figure 84** In the parental DU145 cells, CRIP, ERG3 and FOSB were expressed, whereas all these 3 genes were highly expressed in DU145-FABP5-KO cells (A). When CRIP2, ERG3 and FOSB level in DU145 set at 1 their relative levels in DU145-FABP5-KO were significantly increased to 2.7 ± 0.08, 2.16 ± 0.028 and 2.5 ± 0.03 respectively (C).Thus, comparing to the expressions in the parental cells, the levels of CRIP, ERG and FOSB increased by 170%,116% and 150% respectively (Student's t test, $p < 0.0001$) in the cells with FABP5 knocked out. The GRPR and CAV1 were expressed in the parental DU145 whereas NR1H4 only expressed in androgen dependent cell lines 22RV1 and not expressed in androgen independent CRPC DU145 cell lines(B). The DU145-FABP5-KO cells shows significantly reduced level of GRPR and CAV1 and not detectable level of NR1H4 (B). When GRPR and CAV1 in DU145 cells were set at 1, their relative levels in DU145-FABP5-KO were significantly reduced to 0.04 ± 0.03 and 0.15 ± 0.08 respectively (C).The level of GRPR and CAV1

decreased by 96% (Student's t test, $p < 0.0001$) and 85% (Student's t test, $p < 0.0002$) respectively in comparison to the control DU145.
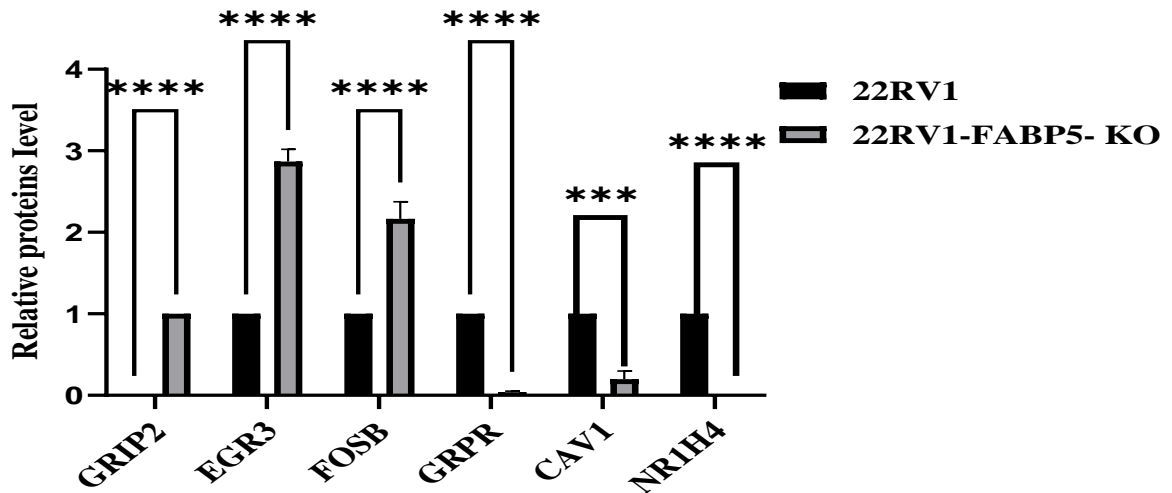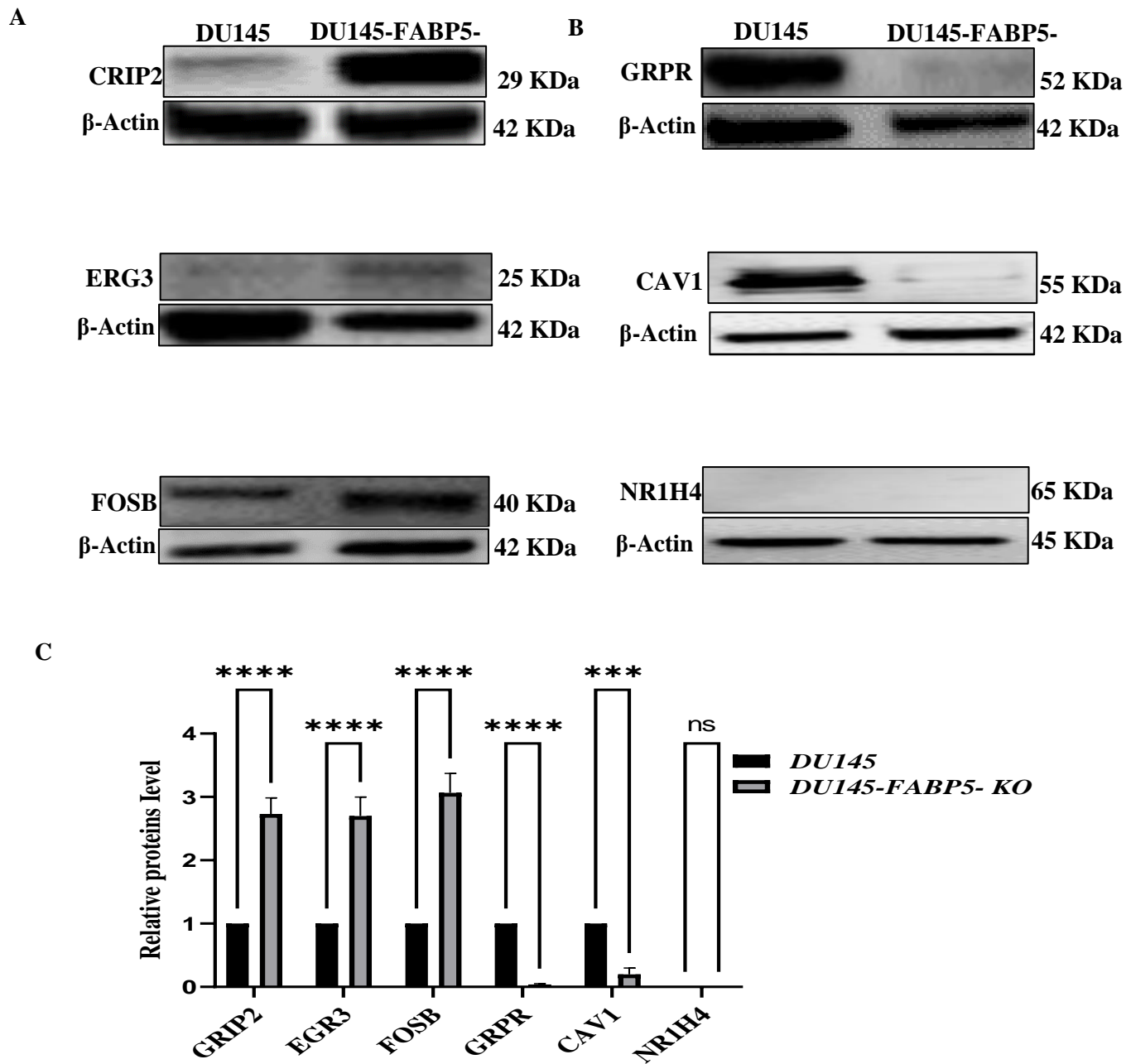

Figure 84. Verification of the six top DEGs by assessing the different expression at the protein levels with Western blot. **A)** Western blot analysis of the expression status of upregulated DEGs CRIP2, ERG3 and FOSB expressed in DU145 and DU145-FABP5-KO cells. **B)** Western blot analysis of the expression status of the downregulated DEGs

GRPR, CAV1 and NR1H4 in DU145 and DU145-FABP5-KO cells. **C)** Quantitative assessments of expression levels of 6 DEGs in parental DU145 and DU145-FABP5-KO cells. Except NR1H4, which was not expressed in DU145 or DU145-FABP5-KO cells, the levels for all 5 other DEGs in DU145 cells were set at 1, the levels in DU145-FABP5-KO cells were calculated by relating to those expressed in DU145 cells. The results (Mean ± SD) were obtained from 3 separate measurements, the intensities of the bands on the blot were subjected to densitometry scanning and the data was analyzed with the image J software. Anti-β-actin was used to hybridize the blot to normalize possible loading discrepancies. The differences between the DU145 and DU145-FABP5-KO cells were assessed with Student t-test, the results were regarded as statistically significant when

$p<0.05$. The degree of significance was represented by the number of stars as following: *$p<0.05$, **$p<0.001$, ***$p<0.0002$, and ****$p<0.0001$

Table 15. Summary of Differentially Expressed Genes (DEGs) and Biological Effects in FABP5 and AR Knockout Prostate Cancer Cells

DEGs Identified in FABP5- or AR-KO Cells	Expression Changes in FABP5-KO Cells	Expression Changes in AR-KO Cells	Expression Changes in DU145-FABP5-KO Cells	Biological Effects	Pathways
CRIP2	Upregulated by 170%	Upregulated by 116%	Upregulated	Suppression of prostate cancer initiation	Regulation of cellular response to type I

				and progression	interferon pathway
ERG3	Upregulated by 187%	Upregulated by 150%	Upregulated by 150%	Suppression of prostate cancer initiation and progression	Response to progesterone signaling pathway
FOSB	Upregulated by 110%	Upregulated by 100%	Upregulated by 100%	Suppression of prostate cancer initiation and progression	Peripheral nervous system development
GRPR	Downregulated by 96%	Downregulated by 98%	Downregulated by 96%	Suppression of prostate cancer initiation and progression	Fatty acid and lipid transport related pathways
CAV1	Downregulated by 80%	Downregulated by 85%	Downregulated by 85%	Suppression of prostate cancer initiation and progression	Steroid and cholesterol metabolic processes

NR1H4	Not expressed in KO cells	Not expressed in KO cells	Not expressed	Suppression of prostate cancer initiation and progression	Steroid and cholesterol metabolic processes

Footnote: The table summarizes the effect of FABP5 or AR knockout on the Differentially Expressed Genes (DEGs) and Biological Effects in Prostate Cancer Cells

6.5.4 Discussion

Exploring the interactions between FABP5, AR, and other genes in prostate cancer: insights from the gene expression profile analysis

In this study, we conducted a gene-expression profile analysis to investigate the molecular mechanisms underlying the functional roles of FABP5 and AR in prostate cancer. Using differential expression analysis, we identified several genes that exhibited highly significant changes in levels of expression following *FABP5-* and *AR-* knockout in 22RV1 and DU145 cells. Our results showed that Knocking out *FABP5* in 22RV1 cells led to the downregulation of *NR1H4* and *ARV7* might lead to the downregulation of *GRPR* and *CAV1* through their nuclear receptor p-PPARγ and the upregulated genes *CRIP, FOSB, ERG3* caused by *FABP5*-KO can reduce the expression level of VEGF (**Figure 85A**). Knocking out *AR* in 22RV1 cells led to the downregulation of FABP5, which may in turn led to the downregulation of NR1H4, CAV1, and GRPR through their nuclear receptors p-PPARγ, resulting in the upregulation of CRIP, FOSB and ERG3 and the downregulation of VEGF (**Figure 85B**). These findings demonstrated the cross talks and communications occurred between FABP5 and AR in the development and progression

of prostate cancer. When FABP5 was knocked out in androgen-independent cell line DU145, which, do not express androgen, led to the direct downregulation of CAV1 and GRPR through p-PPARγ, since NR1H4 was not expressed in this cell line. This resulted in the upregulation of CRIP, FOSB and ERG3 and the downregulation of VEGF (Figure 84C). These gene expression changes appeared to have a number of biological effects, including reducing proliferation, invasion, wound healing, and anchorage-independent growth in 22RV1 and DU145 cells (Chapter 4). Analysis of the RNA profile and gene ontology revealed that these changes in gene expression following the *FABP5* and *AR* KO were mediated through the response to fatty acids, cholesterol and sterol biosynthesis, and lipid and fatty acid transport which are all part of hormone responsive pathways. These findings revealed the functional role and the underlying mechanism of FABP5 in the transition of prostate cancer cells from androgen-dependent to androgen-independent state (CRPC). The complicated interactions of these important factors involved in the malignant progression of the cancer cells were illustrated schematically in **figure 85**.

A

22RV1-FABP5-KO → NR1H4 → ARV7 → CAV1 / p-PPARγ / GRPR → CRIP / FOSB / ERG3 → VEGF

B

22RV1-AR-KO → FABP5 → NR1H4 → CAV1 / p-PPARγ / GRPR → CRIP / FOSB / ERG3 → VEGF

C

DU145-FABP5-KO → GRPR → CAV1 → p-PPARγ → CRIP / FOSB / ERG3 → VEGF
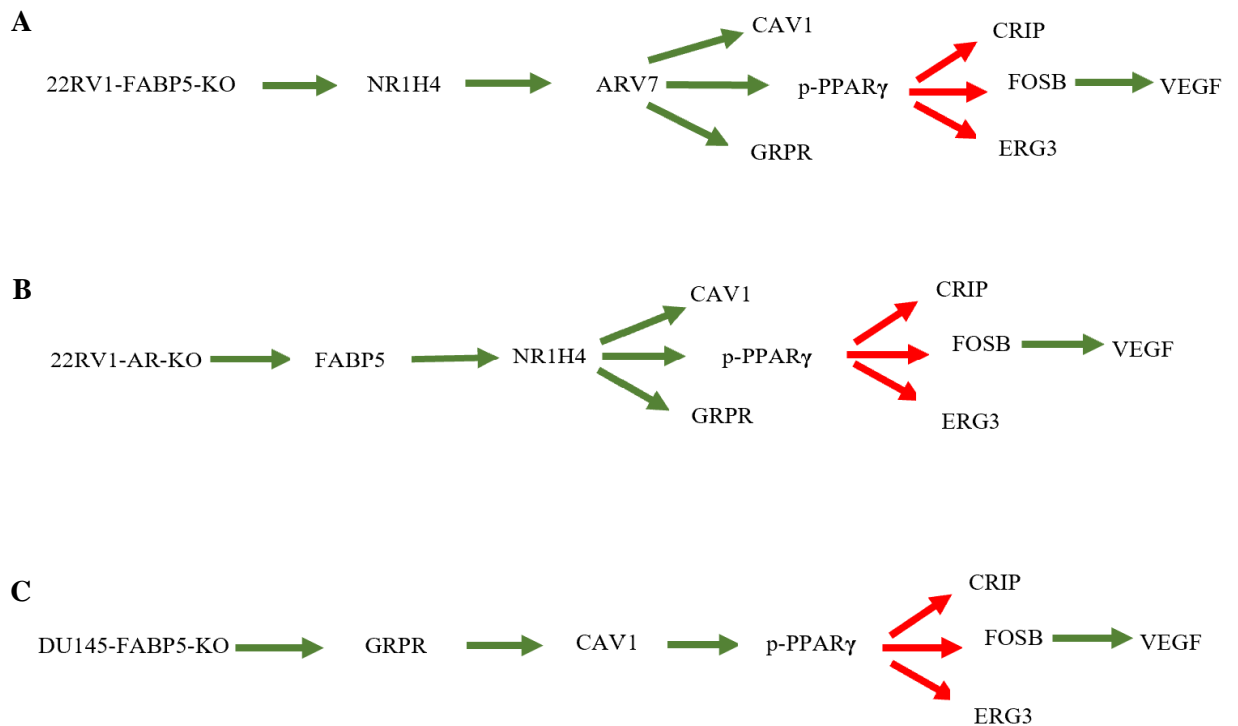
Figure 85. Interactions between *FABP5, AR,* and other genes in prostate cancer: insights from gene expression analysis

A) Potential molecular mechanism of *FABP5* KO in 22RV1 cells. The results showed that *FABP5* KO led to the downregulation of *NR1H4* and *ARV7*, which in turn resulted in the downregulation of *GRPR* and *CAV1* through their nuclear receptor p-PPARγ. This process then led to the upregulation of *CRIP, FOSB* and *ERG3* and the downregulation of VEGF, which finally led to a reduced proliferation, invasion, wound healing, and anchorage-independent growth in 22RV1 cells. These changes in gene expression were mediated through the steroid metabolic process, response to fatty acid, and androgen receptor signaling pathway. Red represents upregulation and green represents downregulation.

217

B) Potential Molecular Mechanism of *AR* KO in 22RV1 Prostate Cells. The results showed that AR KO led to the downregulation of *FABP5* and *NR1H4*, which in turn resulted in the downregulation of *GRPR* and *CAV1* through their nuclear receptor p-PPARγ. This process then leds to the upregulation of *CRIP ,FOSB* and *ERG3* and the downregulation of VEGF, which Finally led to a reduced proliferation, invasion, wound healing, and anchorage-independent growth in the 22RV1 cells. These changes in gene expression are mediated through the steroid metabolic process, response to fatty acid, and androgen receptor signaling pathway. Red represents upregulation and green represents downregulation.

C) Potential Molecular Mechanism of FABP5 KO in DU145 Prostate Cells. The FABP5 KO led to the downregulation of CAV1 and GRPR through their nuclear receptor p-PPARγ, This process then led to the upregulation of *CRIP ,FOSB* and *ERG3* and the downregulation of VEGF, which Finally led to a reduced proliferation, invasion, wound healing, and anchorage-independent growth in DU145.These effects are similar to those observed in the 22RV1 cell lines following FABP5 knockout, suggesting that FABP5 plays a similar role in the development and progression of prostate cancer in both cell lines. Red indicates upregulation and green indicates downregulation genes

Chapter 7 :General Discussion

7.1 An Overview and Technical Aspects

Prostate cancer is the most frequent male cancer and the second greatest cause of cancer-related death in men in developed countries (2). Since Higgins and colleagues found that prostate cancer growth and expansion are dependent on stimulations of male hormones given by peripheral blood circulation (55), androgen deprivation via physical and pharmacological castration or decreasing the biological activity of AR has been the major treatment for patients with prostate cancer for the past 50 years (230). Despite the initial efficacy, prostate cancer frequently returns in approximately two years with a more aggressive hormone independent phenotype, or CRPC. CRPC no longer responds to ADT because the growth and advancement of CRPC cells is no longer dependent on circulating hormones (231). The transformation of androgen-dependent cancer cells to androgen-independent CRPC cells is a major alteration, and the molecular mechanism underlying this transformation is not fully explored. (232). Previous study suggested that AR might not be directly responsible for the transitions of the cancer cells to castration-resistant status. Studies also suggested that FABP5 might gradually replace AR to promote the malignant progression in CRPC cells (233). But the molecular mechanism on how FABP5 played its tumor-promoting role was not fully understood. To develop new therapeutic strategies based on targeting *FABP5* gene, it is necessary to conduct further investigations on molecular mechanisms involved in FABP5-functional role in the malignant progression of prostate cancer. In this work, we investigated whether there was a cross-talk between FABP5 and AR via the FABP5-PPARy-VEGF (170,211) axis and the AR-PPARy-VEGF pathway. We also investigated those genes that were involved in this network. Fatty acids play important roles in the formation of the cellular structure of cancer. Fatty acids are signal molecules and can initiate cell signal transduction pathways to promote the tumorigenicity and metastatic ability of the cancer cells (234,235). FABP5 was implicated as a stimulator of cell proliferation and metastasis in prostate cancer(236).

In prostate cancer cells, it was demonstrated that FABP5 transported fatty acids from intracellular and extracellular sources into the cells and delivered them to their nuclear receptor PPARγ and to triggered a chain of molecular events that lead to facilitated malignant progression (170,211). Apart from the fatty acid- transportation function, the detailed molecular mechanisms underlying the promoting role of FABP5 and its possible relationship with AR in CRPC were not previously investigated. It is not clear whether therapeutic alteration of FABP5 gene expression can be employed as a strategy for CRPC treatment.

In the post genomic era, one of the most important issues in molecular biology is to find an efficient and reliable technique to manipulate genes for therapeutic purpose. The most straightforward way to determine whether FABP5 can be used as a therapeutic target is to find out whether abrogated or reduced *FABP5* expression can result in decreased tumorigenicity of cancer cells. There are two alternative approaches that can be used to disrupt with FABP5 expression: RNA interference (RNAi) (237) or the recently developed gene editing tool Clustered Regularly Interspaced Short Palindromic Repeats, or CRISPR/Cas9 (238). The inability to produce a complete suppression is a drawback for the RNAi approach, despite the fact that it was well established in our lab and frequently used previously. In most cases, once RNAi is used to examine the functional role of a gene, it is simple to notice a reduction in functional activity when the expression level of the gene is drastically reduced. With the exception of the often noticed off-target effect, RNAi technique can be the best option for these types of investigations since a full reduction of the gene's activity is not required. In some special cases for some genes, short interference RNA molecules may have the exact opposite effect to that of expected: Causing the target genes' expression levels to rise rather than fall. This is known as RNA activation, or RNAa (239). Another limitation of RNAi is that some suppressed genes were eventually reactivated in vivo(205). Comparing with the RNAi technique, the gene-

editing technique CRISPR-Cas9 can effectively delete a gene from the genome and generate a permanent and stable elimination of the targeted genes. Thus in this study, the CRISPR/Cas9 genome editing technology was chosen to completely knock out *FABP5* or *AR* from the prostate cancer cells. CRISPR/cas9 is a well-established technique that was used frequently in our laboratory's Its reliability, reproducibility, irreversibility, and verifiability were proved previously (240). Using CRISPR-Cas9 to knock out *FABP5* or *AR*, combined with RNA profile analysis to identify the DEGs between the parental and the KO cells will not only enable the therapeutic potential of these genes to be tested, but also provided valuable insights into the underlying molecular mechanisms of prostate cancer, particularly the malignant transition to CRPC.

7.1.1 The expression of FABP5 and its functionally- related factors in prostate cells

When the expression status of FABP5 and its functionally related factors in prostate cells were detected in the benign PNT2 cells and in prostate cancer cell lines 22RV1, DU145, and PC3M, it was found that while the level of FABP5 was not detected in PNT2, it was expressed at a moderate level in the moderately malignant 22RV1 cells and very high levels in the highly malignant DU145 and PC3M cells (Figure 19). This results suggested that the level of FABP5 was increased as the increasing malignancy of the cancer cells, indicating its increasingly important role in the malignant progression. Western blot analysis showed a moderate expression of PPARγ1 and PPARγ2 in the cancer cell lines 22RV1, and a slightly reduced expression the highly malignant DU145 and PC3M cells. But the their levels in benign PNT2 cells was even stronger than that in the 22RV1 cells. (Figure 20). When p-PPARγ1 and p-PPARγ2 (presumably the biologically active form) were detected, an opposite expression pattern was observed: while the levels of p-PPARγ1 and p-PPARγ2 expression were not detectable in benign PNT2 cells, moderate levels in 22RV1 cells and very high levels in DU145 and PC3M cells were measured

(Figure 21). These results suggested that it was the increase of biologically active form of p-PPARγ that was corrected to the elevated degree of malignancy of the cells, indicated a role of p-PPARγ on the malignant progression of the cancer cells. The observed decreasing levels of the PPARγ and the increasing p-PPARγ with the increasing malignancy of the cells suggested that the increased p-PPARγ in cancer cells was likely to be obtained by phosphorylating the wtPPARγ, rather than by synthesizing more proteins.

When the expression of AR and ARV7 were analyzed, they were expressed only in the androgen-responsive 22RV1 cells. Neither AR-FL nor V7 were detected in the benign PNT2 cells, nor in the highly malignant DU145 and PC3M cells (Figure 22). Additionally, we detected the presence of VEGF in all cell lines, with PNT2 cells exhibiting lower expression level compared to those expressed in the malignant cell lines (Figure 23). These results suggested that the increased levels of AR-FL or ARV7 were important in development and expansion of prostate cancer, they might not needed any more in the highly malignant, metastasized cancer cells. VEGF, like FABP5, may play an important promoting role in the malignant progression of the cancer cells.

7.1.2 Gene knockout using Crispr Cas9 technique

Plasmid transfection was a common method for delivering the CRISPR/Cas9 system into cells, but it has several limitations, including the possibility of the plasmid integration into the host genome, and the unintended off-target effects resulting from transcription and translation of the Cas9 protein inside the nucleus. These limitations made plasmid transfection less desirable for gene editing, and as a result, alternative approaches, such as RNP transfection, had been developed. As it minimizes off-target effects and avoids the transcription and translation of Cas9 within the nucleus, it reduces the likelihood of undesired off-target consequences(241,242).Thus, RNP transfection is a more precise and effective method for gene editing, making it an attractive choice for this study which was aimed to examine the knockout effects of *FABP5* or *AR* in androgen-responsive and androgen-unresponsive cancer cell lines. In this work, RNP was used to modify the genomes of 22RV1, DU145, and PC3M cells, resulting in a total silencing of *FABP5* or *AR*. Different sorts of mutations were detected after RNP transfection in the *FABP5* gene in various cell lines (Figure 27,31,35). These frameshift mutations rendered *FABP5* gene expression nonexistent in 22RV1, DU145, and PC3M cells. Western blot analysis demonstrated a complete absence of *FABP5* or *AR* expression in 22RV1, DU145 and PC3M mutant cells (Figure 26,30,34). These results proved RNP transfection method is an effective method for gene editing. The sublines derived from 22RV1, DU145, and PC3M cells with *FABP5* or *AR* KO are stable and valuable cell lines which provided a tools for the studies in the late stage of this work.

7.1.3 Proliferation assay

In this study, we used a proliferation assay to investigate the effect of knocking out the *FABP5* and *AR* on the proliferation of androgen-dependent cell line 22RV1 and androgen-independent cell lines DU145 and PC3M. Our results showed that knocking out the *FABP5* in 22RV1 cells resulted in a significant suppression of cell proliferation rate by 38% (Student *t*-test, $P<0.0001$) as compared to the control (Figure 40). Similarly, knocking out the FABP5 gene in the DU145 cells resulted in a significant suppression of proliferation rate by 39% (Student *t*-test, $P<0.0001$) (Figure 45). Knocking out *FABP5* in PC3M cells resulted in a significant suppression of cell proliferation by 46% (Student *t*-test, $P<0.0001$) (Figure 50). In addition, knocking out *AR* in the 22RV1 cells resulted in a significant suppression of cell proliferation by 36% (Student *t*-test, $P<0.0007$) (Figure 55). These findings suggested that both FABP5 and AR played almost equally important roles in regulating proliferation of the AR-positive 22RV1 cells. While both FABP5 and AR were expressed in 22RV1 cells, only FABP5 was present in the highly malignant AR-negative cancer cells DU145 and PC3M, indicating the promotion function on cell proliferation performed by both molecules in AR-positive cells, was performed by FABP5 alone in the AR-negative cancer cells. Both FABP5 and AR were suggested to be key factors in development and progression of prostate cancer cells (62,196). The present study suggested that part of the promoting effect of FABP5 or AR in prostate cancer were due to their promotion actions on cell proliferation.

7.1.4 Invasion assay

When the cell invasiveness were tested, it was revealed that the suppression of FABP5 expression in both the androgen-dependent cell line 22RV1 and the androgen-independent cell lines DU145 and PC3M resulted in a significant reduction of invasiveness. Specifically, knocking out *FABP5* in the 22RV1 cells resulted in a 99% reduction of invasiveness as compared to the control (Student's *t*-test, $P<0.0001$) (Figure 41). Similarly, knocking out the FABP5 gene in the DU145 and PC3M cells resulted respectively in a 65% and a 81% reduction of invasiveness (Student's *t*-test, $P<0.0002$, $P<0.0001$) (Figure 46,51). In addition, knocking out *AR* in the 22RV1 cells resulted in a 92% reduction of invasiveness (Student's *t*-test, $P<0.0001$) (Figure56).

These findings suggested that FABP5 and AR play a crucial role in regulating the invasiveness of prostate cancer cell lines. These results are consistent with previous studies that have shown that FABP5 is involved in cancer cell invasion and that AR played a key role in prostate cancer development and progression(50,233).

7.1.5 Anchorage-independent growth

When soft agar assay was performed to study the effect of knocking out *FABP5* and *AR* on cell anchorage-independent growth, it was found that knocking out *FABP5* in 22RV1, DU145 and PC3M cells resulted in significant suppressions by 93%, 88% and 96.73% respectively (Student's *t*-test, $P<0.0001$) (Figure 42,47,52). Knocking out *AR* in 22RV1 cells resulted in a 97.2% suppression of anchorage-independent growth as compared to the parental control cells (Student's *t*-test, $P<0.0001$) (Figure57).

These findings suggest that FABP5 and AR play a crucial role in regulating the anchorage-independent growth of prostate cancer cells. These results are consistent with previous studies that showed that FABP5 was involved in cancer cell invasion and that AR play a key role in prostate cancer development and progression(59,205).

7.1.6 Motility assay

When cell motility was tested, we found that knocking out *FABP5* produced a significant inhibition of cell motility in the androgen-dependent cell line 22RV1 and androgen-independent cell lines DU145 and PC3M. Our results showed that the effect of wound closure in the 22RV1-FABP5-KO cell line was reduced to 67% compared to 98% in the control, resulting in a significant reduction in wound closure by 1.4 fold (Student's *t*-test, $P<0.0002$) (Figure 43). Similarly, in DU145-FABP5-KO and PC3M-FABP5-KO cells, knocking out *FABP5* produced significant reductions in wound closure by 1.2 fold (Student's t-test, $P=0.0002$) (Figure 48) and 1.22 fold (Student's t-test, P=0.0002) (Figure 53) respectively. Knocking out *AR* in the 22RV1 cells resulted in a significant inhibition of cell motility by 1.23 fold (Student's *t*-test, $P<0.0001$) (Figure 58). These findings suggested that FABP5 and AR play important roles in regulating the motility of AR-positive prostate cancer cells, and this role was played by FABP5 alone in the AR-negative cancer cells. These results are consistent with previous findings that FABP5 was involved in promoting cancer cell invasion and that AR play a key role in carcinogenesis of prostate cancer(59,205).

7.2 Molecular mechanism involved in the tumor-promoting roles of FABP5 and AR

To study how FABP5 and AR played their promotion roles in prostate cancer cells, the changes in expression status of several important signal transduction pathway factors caused by FABP5 or AR knocking out were measured with western blot. In 22RV1-FABP5-KO cells, the ARFL level was not changed compared with the parental cells (Figure 62). In 22RV1-AR-KO cells, the level of FABP5 was not detectable (Figure 66). These results suggested that the expression of FABP5 depended on ARFL, whereas the expression of ARFL did not depend on the presence of FABP5. This result, combined with our previous observations suggested that the increased FABP5 level was a result of

the increased AR expression, and FABP5 gradually replaced AR until it was completely dominance in playing the promotion role for the malignant progression during the transition of the AR-positive cells to AR-negative CRPC cells(195). Our result also showed that ARV7 was expressed in 22RV1 cells, but not detectable in 22RV1-FABP5-KO cells(Figure 62), indicating that the expression of ARV7 depended on the presence of FABP5. Since ARV7 played a key role in ADT resistance(90),FABP5 may be involved in the development of ADT resistance of the prostate cancer cells. Further study is needed to investigate how FABP5 induced ARV7 expression.

Significant decrease in malignant characteristics of 22RV1-FABP5-KO cells was observed upon *FABP5* knocked out (Chapter 4), implying a crucial role played by FABP5 in the regulation of the malignant characteristics at the absence of AR. It was observed that reductions in expression levels of several genes, including PPARγ1, PPARγ, p-PPARγ1, p-PPARγ2 and VEGF which were involved in the regulation of cell proliferation and survival(Chapter 5). This result suggested that these genes may be regulated by FABP5 through ARV7, as ARV7 was completely disappeared when FABP5 was knocked out (Figure 62). Similarly, in 22RV1-AR-KO cells, *AR* knocked out resulted in a significant decrease in the malignant characteristics (chapter 4), highlighting the key role played by AR in the regulation of these processes in the absence of FABP5. It was observed that reductions in expression levels of several genes, including PPARγ1, PPARγ2, p-PPARγ1, p-PPARγ2 and VEGF, which were involved in cell proliferation and survival (Chapter 5), indicating that these genes may be regulated by FABP5 through AR, as FABP5 expression was abolished completely in 22RV1- AR- KO cells (Figure 66).

In 22RV1-FABP5-KO cells, the expression of PPARγ-1 was increased by75% and PPARγ-2 was decreased by68%. The expression of p-PPARγ1 and p-PPARγ2 was decreased by 64% and 88%, respectively. The result also showed that the of VEGF

expression was reduced by 90%(Figure 59,60,61). In 22RV1-AR-KO cells, the levels of PPARγ1 and PPARγ2 were reduced by 86% and 100%, respectively, while the levels of p-PPARγ1 and p-PPARγ2 decreased by 100% and 93%, respectively. The expression of VEGF was reduced by 95% (Figure 63,64,65) . These results suggested that either *FABP5*- or *AR*- knocking out can lead to significant changes to the FABP5-PPARγ-VEGF signal transduction axis in 22RV1 cells, and particularly that either AR or FABP5 can initiate this pathway when either one of them is absent.

In DU145-FABP5-KO cells, the expression of PPARγ1 and PPARγ2 was inhibited completely, the expression of p-PPARγ1 and p-PPARγ2 were reduced by 85% and 100% respectively. The expression of VEGF was reduced by 90%(Figure 67,68,69). In PC3M-FABP5-KO cells, the expression of PPARγ1 and PPARγ2 were reduced by 97.8% and 100%, respectively, while the expression of p-PPARγ1 and p-PPARγ2 was decreased by 50% and 43%, respectively. The expression of VEGF was reduced by 58%(Figure 71,72,73). These results indicated that in the highly malignant AR-negative CRPC cells(Figure 70,74), the major factors of the malignant signal transduction PPARγ and VEGF were fully regulated by FABP5 and FABP5 completely replaced the AR in promoting the malignant progression of the cancer cells through the FABP5-PPARγ-VEGF axis (Figure 67,68,69,71,72,73).

7.2.1 Identification of FABP5- or AR- regulated genes by RNA expression profile analysis

To further study the genes regulated by FABP5 or AR, the expression profiles of the FABP5- or AR- KO cells were compared with those of the control parental cells and the DEGs were identified. From the selected top 20 DEGs, six most pronounced DEGs were identified as CRIP2, ERG3, FOSB, GRPR, CAV1 and NR1H4, which were commonly upregulated or downregulated in both 22RV1-FABP5-KO and 22RV1-AR-KO cell lines, with the exception of NR1H4 which was only expressed in 22RV1 and not in DU145

(Figure 81). The expression of these six genes was verified through protein expression analysis. The study found that CRIP2 was only expressed in 22RV1-FABP5-KO and 22RV1-AR-KO, but not in the 22RV1 parental cells, and increased by 170% in DU145-FABP5-KO compared to its parental cell line. ERG3 and FOSB were upregulated by 187% and 110% in 22RV1-FABP5-KO and 150% and 100% in 22RV1-AR-KO, respectively, while they were upregulated by 116% and 150% in DU145-FABP5-KO(Figure 82,83,84). On the other hand, the downregulated genes GRPR, CAV1 and NR1H4 showed different patterns of expression. NR1H4 was only expressed in 22RV1 and not in the KO cell lines, while GRPR and CAV1 were expressed in all the cell lines, but were downregulated by 96% and 80% in 22RV1-FABP5-KO, 98% and 85% in 22RV1-AR-KO and 96% and 85% in DU145-FABP5-KO, respectively, compared to their parental cells (Figure 82,83,84). The gene ontology (GO) enriched pathway analysis of the three most upregulated DEGs (CRIP2, ERG3, and FOSB) revealed that they were involved in the regulation of cellular response to type I interferon pathway, response to progesterone signaling pathway and peripheral nervous system development, all of which play an important role in the suppression of prostate cancer initiation and progression (Figure 76,78,80)(243-247). On the other hand, the analysis of the three most downregulated DEGs (GRPR, CAV1 and NR1H4) revealed that they were involved in fatty acid and lipid transport related pathways and steroid and cholesterol metabolic processes (Figure 76,78,80)(248-253). This study highlights the key role of the top six DEGs in the transition of prostate cancer cells from androgen responsive to androgen unresponsive, and sheds light on the intricate relationship between FABP5, AR, PPARγ, p-PPARγ and VEGF in the regulation of prostate cancer development(Figure 85).

7.3 Roles of the top 6 DEGs in cancer

Previous work combined with this study showed that the top 6 DEGs, namely CRIP2, ERG3, FOSB, GRPR, CAV1, and NR1H4, respectively played critical roles in the development and progression of prostate and other cancer.

7.3.1 CRIP2

Cysteine-rich intestinal protein 2 (CRIP2) is a potential tumor suppressor gene located at the commonly deleted chromosomal region 14q32.3. Despite its association with development, previous research did not yet confirm its functional role in tumor formation. However, a recent study found that CRIP2 was significantly under-expressed in nasopharyngeal carcinoma cell lines and tumors. Re-expression of CRIP2 was able to suppress tumorigenesis and angiogenesis *in vivo* through its transcriptional repression capability. It was also demonstrated that CRIP2 interacted with NF-κB/p65 to inhibit its DNA-binding ability in the promoter regions of pro-angiogenesis cytokines, such as IL6, IL8, and VEGF. This provided evidence that CRIP2 functioned as a transcriptional repressor of NF-κB-mediated pro-angiogenic cytokine expression and inhibited tumor formation and angiogenesis[245,254]. These results highlighted the potential of CRIP2 as a therapeutic target for cancer treatment and aligned well with the current findings in this study, which showed that the depletion of FABP5 or AR in both androgen-responsive 22RV1 cells and androgen-unresponsive DU145 cells led to the upregulation of CRIP2[82,83,84] resulting in decreased cell proliferation, invasion, wound healing, and anchorage-independent growth (Chapter 5). Additionally, the Interleukin-27-mediated signaling pathway and the cellular response to type I interferon signaling pathway were enriched in FABP5 knockout cells, providing further evidence of CRIP2's potential role in inducing cell death and reducing VEGF expression(Figure 80,85).

7.3.2 ERG

ERG (a ETS related gene) codes a protein that plays a crucial role in the regulation of gene expression in cells. Its involvement was observed in various biological processes such as cell differentiation, development, and tumorigenesis. A study conducted on prostate cancer explored the interaction between ERG and the androgen receptor (AR). The study employed the use of Chromatin Immunoprecipitation followed by Massively Parallel Sequencing (ChIP-Seq) to comprehend the relationship between AR and ERG. The results revealed that ERG interferes with differentiation by directly binding to AR and its regulated genes. It works in conjunction with other proteins to control AR's ability to regulate gene expression. The study found that a reduction of ERG resulted in the induction of AR, and the reversal of ERG's capability to control gene expression (255). The current work further demonstrated that the depletion of FABP5 or AR in both androgen-responsive 22RV1 cells and androgen-unresponsive DU145 cells resulted in the upregulation of ERGs, leading to a decrease in ARV7 in 22RV1-FABP5-KO cells and a decrease in ARFL and ARV7 in 22RV1-AR-KO cells (Figure 62,66,82,83,84). The result in the current study combined with that of the previous work indicated a tumor-suppressing role of ERG and revealed a complicated relationship between FABP5, AR and ERG in process of the malignant progression of prostate cancer cells.

7.3.3 FOSB

FOSB, or FBJ Murine Osteosarcoma Viral Oncogene Homolog B, is a key player in regulation of cellular proliferation and differentiation. Multiple studies demonstrated FOSB's ability to inhibit cell growth and tumorigenesis. In one study, as a consequence of the inactivation of the p53 pathway, depletion of FOSB in triple-negative breast cancer cells resulted in increased cell proliferation and enhanced tumor growth. Conversely, upregulation of FOSB in colorectal cancer cells was found to suppress cell proliferation and induce cell cycle arrest(256,257) . In this work, we showed that the deletion of *FABP5*

or *AR* in both androgen-responsive and unresponsive cancer cells 22RV1 and DU145 led to the upregulation of FOSB (Figure 82,83,84), resulting in decreased cell proliferation, invasion, wound healing, and anchorage-independent growth. Furthermore, type I interferons played a crucial role in the regulation of the immune response and can activate apoptotic signaling pathways were enriched in *FABP5-* or *AR-* KO cells(Figure78,80), an evidence of FOSB's potential role in inducing cell death(258). These results obtained from this study, combined with those of the previous work, suggested that FOSB is tumor-suppressor which may be used as a therapeutic target for treatment of prostate cancer and some other cancers.

7.3.4 GRPR

GRPR expression was investigated in a previous study of 51 cases of human prostate cancer. The clinicopathological parameters were analyzed in correlation with GRPR expression and it was found to be present in carcinoma cells with a significantly positive relationship to the combined Gleason scores and the immunoreactivity of estrogen receptor βcx (ERβcx (259)). In another study, the development of CRPC was explored in relation to the role of Gastrin-Releasing Peptide (GRP) and its receptor (GRPR).The effect of ADT on GRP and GRPR expression was found to activate ARVs expression and contributed to the progression of CRPC. The selective GRPR antagonist RC-3095 was tested for its efficacy in blocking GRP/GRPR signaling, and it was found to inhibit NF-κB activity and the expression AR variants in CRPC and therapy-induced NEPC cells.In preclinical animal studies, the combination of the GRPR antagonist with anti-androgen treatment was demonstrated to inhibit CRPC and tNEPC tumor growth efficiently(260,261).

In this study, we found that following *FABP5-* or *AR-* KO in AR responsive cells 22RV1, GRPR expression decreased by 96% in 22RV1-FABP5-KO and 98% in 22RV1-AR KO, while it decreased by 96% in AR unresponsive DU145 cells(Figure 82,82,84). *FABP5-*

KO in 22RV1 resulted in a reduction of GRPR and a complete inhibition ARV7 expression(Figure 62). An enrichment analysis of *FABP5-* or *AR-* KO showed that fatty acid and lipid transport-related pathways and steroid and cholesterol metabolic processes, which involve GRPR, were all significantly enriched(Figure 76,78,80)(248,249). Our results combined with those of the previous studies suggested that GRPR may played a promotion roles in development and expansion of CRPC in an coordinated manner with FABP5 or AR. This provided theoretical basis for development of a GRPR-suppression therapy.

7.3.5 CAV1

CAV1 involved in various biological processes, including the formation of lipid rafts, and it was implicated in various diseases, including cancer. A study was conducted to understand the interactions between CAV1 and AR in prostate cancer and their roles in cell growth and development of the male reproductive tract. The results showed that the presence of androgen increased the activity of the AR and that CAV1 potentiated the AR even when androgen levels were low. High levels of CAV1 were found in prostate cancer, emphasizing the complexity of protein interactions in cancer development(262,263).The RNA expression profiles and protein expression analysis of *FABP5-* or *AR-* KO in 22RV1 and DU145 cells revealed that CAV1 expression was controlled by AR and FABP5 in androgen-responsive 22RV1 cells and only by FABP5 in androgen-unresponsive DU145 cells. The downregulation of AR or FABP5 also resulted in a decrease in CAV1 expression (Figure 82,83,84). An enrichment analysis of FABP5 or AR knockout showed that fatty acid and lipid transport-related pathways and steroid and cholesterol metabolic processes, which involves CAV1, were significantly enriched (Figure 76,78,80)(250,251). The results obtained from this current study, combined with those from previous investigations, suggested that CAV1 is tumor-promoter which coordinated with FABP5 or AR and played a facilitator role in malignant progression of CRPC cells.

7.3.6 NR1H4

NR1H4, also known as the farnesoid X receptor, plays a significant role in gene expression regulation in liver and other tissues.This protein was linked to the development of various types of cancer, including colon, breast, gastric, pancreatic, and ovarian tumors. The involvement of NR1H4 in promoting cancer cell growth and migration, as well as its regulation of metabolism, stem cell maintenance, and steroidogenesis, were well documented. A recent study indicated that NR1H4 may contribute to the progression of CRPC by promoting androgen synthesis in prostate cancer cells. Overexpression of NR1H4 was found to lead to androgen-independent growth or castration-resistant growth in prostate cancer cells . Another study explored the role of NR1H4 in colon cancer development and found that colon cancer cells with *NR1H4-* KO showed impaired cell proliferation, reduced colony formation, and increased apoptotic cell death compared to control cells. MYC was identified as a key mediator of the signaling pathway alterations induced by *NR1H4-* KO, with the study showing that NR1H4 silence reduced MYC protein levels and activation increased MYC levels(264,265). The result of this current study found that *FABP5-* or *AR-* KO completely inhibited the expression of NR1H4, which might lead to the initiation of the apoptotic pathway(Figure 82,83). NR1H4 was expressed in androgen responsive 22RV1 cells, but it was not expressed in androgen unresponsive DU145 cells (Figure84). The enrichment analysis of *FABP5-* or *AR-* KO showed that fatty acid and lipid transport-related pathways, as well as steroid and cholesterol metabolic processes, which involved NR1H4, were significantly enriched (Figure 76,78)(253). Our findings in this work, combined with those in in previous study NR1H4 is an important gene which may co-operated with AR in promoting malignant transition of prostate cancer cells into the castration-resistant state. Once FABP5 is increased to the level high enough to completely replaced AR, the

expression of both AR and NR1H4 was completely abrogated and their function in highly

malignant CRPC cells was played by FABP5 (Figure 82,83,84).

Chapter 8 :Final comments

8.1 Summary or Conclusion

This study investigated the impact of *FABP5-* and *AR-* KO on the malignant characteristics of androgen responsive cell line 22RV1 and androgen unresponsive cell lines DU145 and PC3M, and further investigated the molecular mechanisms involved in the reduced malignancy caused by the gene KO. Results showed that the knockouts of both genes in these cancer cells led to significant reductions in proliferation rate, invasive ability, motility rate, and the colony- formation ability in soft agar. The study found that FABP5 and AR interact with each other in the regulation of the FABP5 or AR -PPARγ - VEGF axis, with FABP5 controlling the ARV7 splice variant and AR regulating the expression of FABP5. When gene expression profiles between the parental cells and the *FABP5-* or *AR-* KO cells was compared, a large number of DEGs were identified. From 40 top DEGs, six most pronounced DEGs were found and they were CRIP2, ERG3, FOSB, GRPR, CAV1 and NR1H4. Gene ontology analysis of the DEGs revealed their involvements in various pathways including the pathway regulating cellular response to type I interferon, the pathway responding to progesterone signaling, and the pathway responding to peripheral nervous system development (for the upregulated DEGs), the pathways related to fatty acid and lipid transport, and the pathway related to steroid and cholesterol metabolic processes (for the downregulated DEGs). These pathways are all involved in promoting or suppressing of the malignant progression of the cancer cells. FABP5 or AR acted together with the identified 6 tumor-promoting or tumor-suppressing factors in a coordinated manner to modulate the transition of the cancer cells from AR-dependent state to castration-resistant state.

The results of this study provided a valuable insight into the biological functions and molecular mechanisms of FABP5 and AR in prostate cancer and it formed a theoretical basis for the development of new strategies for CRPC treatment.

8.2 Future work

Mechanisms of FABP5 regulation: The underlying mechanisms by which FABP5 regulates the expression of the 6 DEGs could be further explored. This could involve identifying the signaling pathways, transcription factors, and epigenetic modifications that are related to this regulation.

Functional studies: Functional studies can be performed to determine how the regulation of the 6 DEGs by FABP5 affects the cancer cell malignant characteristics. This could involve using *in vitro* and *in vivo* models to investigate the effects of FABP5 knockout on these processes, as well as the effects of overexpressing the 6 DEGs in FABP5 knockout cells.

Therapeutic implications: The potential therapeutic implications of FABP5 regulation of the 6 DEGs could be investigated further. This could involve testing the efficacy of targeting FABP5 or the 6 DEGs in cancer cell lines and animal models, as well as exploring the potential for combination therapies that target both FABP5 and the 6 DEGs using the bio-inhibitor dmrFFABP5.

Clinical studies: Clinical studies can be performed to validate the our findings and to determine the clinical relevance of FABP5 regulation of the 6 DEGs in patients with cancer. This could involve analyzing the expression of FABP5 and the 6 DEGs in patient tumor samples, as well as exploring the relationship between FABP5 and the 6 DEGs with clinical outcomes such as patient prognosis values and response to therapy.

Conducting large-scale human studies to validate the results obtained from *in vitro* and animal studies, and to determine the clinical relevance of the DEGs in human diseases.

These are just a starting point, and there can be many other avenues of exploration in future work related to the FABP5 and these DEGs in prostate cancer research and in the studies of other cancers.

References

1. Global Cancer Observatory,. Globocan <https://gco.iarc.fr/>. Accessed 2022.

2. Cancer research UK,. CRUK <https://www.cancerresearchuk.org/

>. Accessed 2022.

3. Rawla P. Epidemiology of prostate cancer. World journal of oncology **2019**;10:63

4. Center MM, Jemal A, Lortet-Tieulent J, Ward E, Ferlay J, Brawley O*, et al.* International variation in prostate cancer incidence and mortality rates. European urology **2012**;61:1079-92

5. Hsing AW, Chokkalingam AP. Prostate cancer epidemiology. Frontiers in Bioscience-Landmark **2006**;11:1388-413

6. Yeldir N, Yildiz E, Dündar G. Gleason score correlation between prostate needle biopsy and radical prostatectomy materials. trauma (such as transurethral resection, needle biopsy) **2019**;2:4

7. Zynger D, Parwani A. Prostate pathology. Demos Medical Publishing; 2014.

8. Gottlieb B, Beitel LK, Nadarajah A, Paliouras M, Trifiro M. The androgen receptor gene mutations database: 2012 update. Human mutation **2012**;33:887-94

9. Lloyd T, Hounsome L, Mehay A, Mee S, Verne J, Cooper A. Lifetime risk of being diagnosed with, or dying from, prostate cancer by major ethnic group in England 2008–2010. BMC medicine **2015**;13:1-10

10. Rebbeck TR. Prostate cancer genetics: variation by race, ethnicity, and geography. 2017. Elsevier. p 3-10.

11. Mäkinen T, Tammela TL, Stenman U-Hk, Määttänen L, Rannikko S, Aro J*, et al.* Family history and prostate cancer screening with prostate-specific antigen. Journal of clinical oncology **2002**;20:2658-63

12.   Weinrich SP, Network AAHPCS. Prostate cancer screening in high-risk men: African American Hereditary Prostate Cancer Study Network. Cancer **2006**;106:796-803

13.   Tan M, Li J, Xu HE, Melcher K, Yong E-l. Androgen receptor: structure, role in prostate cancer and drug discovery. Acta Pharmacologica Sinica **2015**;36:3-23

14.   Crawford ED. Epidemiology of prostate cancer. Urology **2003**;62:3-12

15.   Rose DP. Effects of dietary fatty acids on breast and prostate cancers: evidence from in vitro experiments and animal studies. The American journal of clinical nutrition **1997**;66:1513S-22S

16.   Russell PJ, Jackson P, Kingsley EA. Prostate cancer methods and protocols. Springer; 2003.

17.   Cook LS, GOLDOFT M, Schwartz SM, Weiss NS. Incidence of adenocarcinoma of the prostate in Asian immigrants to the United States and their descendants. The Journal of urology **1999**;161:152-5

18.   Harman SM, Metter EJ, Blackman MR, Landis PK, Carter HB. Serum levels of insulin-like growth factor I (IGF-I), IGF-II, IGF-binding protein-3, and prostate-specific antigen as predictors of clinical prostate cancer. The Journal of Clinical Endocrinology & Metabolism **2000**;85:4258-65

19.   Stattin Pr, Bylund A, Rinaldi S, Biessy C, Déchaud H, Stenman U-Hk*, et al.* Plasma insulin-like growth factor-I, insulin-like growth factor-binding proteins, and prostate cancer risk: a prospective study. Journal of the National Cancer Institute **2000**;92:1910-7

20.   Shimizu H, Ross R, Bernstein L, Yatani R, Henderson B, Mack T. Cancers of the prostate and breast among Japanese and white immigrants in Los Angeles County. British journal of cancer **1991**;63:963-6

21. Whittemore AS, Kolonel LN, Wu AH, John EM, Gallagher RP, Howe GR, *et al.* Prostate cancer in relation to diet, physical activity, and body size in blacks, whites, and Asians in the United States and Canada. JNCI: Journal of the National Cancer Institute **1995**;87:652-61

22. Chan JH, Lim S, Wong WF. Antisense oligonucleotides: from design to therapeutic application. Clinical and experimental pharmacology and physiology **2006**;33:533-40

23. Kasivisvanathan V, Challacombe B. The big prostate. Springer; 2018.

24. Lilja H, Ulmert D, Vickers AJ. Prostate-specific antigen and prostate cancer: prediction, detection and monitoring. Nature Reviews Cancer **2008**;8:268-78

25. Miller MC, Doyle GV, Terstappen LW. Significance of circulating tumor cells detected by the CellSearch system in patients with metastatic breast colorectal and prostate cancer. Journal of oncology **2010**;2010

26. Mcneal J, Kindrachuk R, Freiha F, Bostwick D, Redwine E, Stamey T. Patterns of progression in prostate cancer. The Lancet **1986**;327:60-3

27. Fine SW, Reuter VE. Anatomy of the prostate revisited: implications for prostate biopsy and zonal origins of prostate cancer. Histopathology **2012**;60:142-52

28. Abate-Shen C, Shen MM. Molecular genetics of prostate cancer. Genes & development **2000**;14:2410-34

29. McLatchie G, Borley N, Chikwe J. Oxford handbook of clinical surgery. OUP Oxford; 2013.

30. Emberton M, Fitzpatrick JM, Rees J. Risk stratification for benign prostatic hyperplasia (BPH) treatment. BJU international **2011**;107:876-80

31. Epstein JI, Allsbrook Jr WC, Amin MB, Egevad LL, Committee IG. The 2005 International Society of Urological Pathology (ISUP) consensus conference on

Gleason grading of prostatic carcinoma. The American journal of surgical pathology **2005**;29:1228-42

32.	Humphrey PA. Gleason grading and prognostic factors in carcinoma of the prostate. Modern pathology **2004**;17:292-306

33.	Marchiani S, Tamburrino L, Nesi G, Paglierani M, Gelmini S, Orlando C*, et al.* Androgen-responsive and-unresponsive prostate cancer cell lines respond differently to stimuli inducing neuroendocrine differentiation. International journal of andrology **2010**;33:784-93

34.	Sherwood ER, Berg LA, Mitchell NJ, McNeal JE, Kozlowski JM, Lee C. Differential cytokeratin expression in normal, hyperplastic and malignant epithelial cells from human prostate. The Journal of urology **1990**;143:167-71

35.	Sramkoski RM, Pretlow TG, Giaconia JM, Pretlow TP, Schwartz S, Sy M-S*, et al.* A new human prostate carcinoma cell line, 22Rv1. In Vitro Cellular & Developmental Biology-Animal **1999**;35:403-9

36.	Horoszewicz J. The LNCaP cell line-a new model for studies on human prostatic carcinoma. Prog Clin Biol Res **1980**;37:115-32

37.	Horoszewicz JS, Leong SS, Kawinski E, Karr JP, Rosenthal H, Chu TM*, et al.* LNCaP model of human prostatic carcinoma. Cancer research **1983**;43:1809-18

38.	Castanares MA, Copeland BT, Chowdhury WH, Liu MM, Rodriguez R, Pomper MG*, et al.* Characterization of a novel metastatic prostate cancer cell line of LNCaP origin. The Prostate **2016**;76:215-25

39.	Namekawa T, Ikeda K, Horie-Inoue K, Inoue S. Application of prostate cancer models for preclinical study: advantages and limitations of cell lines, patient-derived xenografts, and three-dimensional culture of patient-derived cells. Cells **2019**;8:74

40.   Naeem AA, Abdulsamad SA, Al-Bayati A, Zhang J, Malki MI, Ma H, *et al.* Prostate Cell Lines. Journal of Oncology and Medicine **2022**

41.   Kozlowski JM, Fidler IJ, Campbell D, Xu Z-l, Kaighn ME, Hart IR. Metastatic behavior of human tumor cell lines grown in the nude mouse. Cancer research **1984**;44:3522-9

42.   Stone KR, Mickey DD, Wunderli H, Mickey GH, Paulson DF. Isolation of a human prostate carcinoma cell line (DU 145). International journal of cancer **1978**;21:274-81

43.   Kaighn M, Narayan KS, Ohnuki Y, Lechner JF, Jones L. Establishment and characterization of a human prostatic carcinoma cell line (PC-3). Investigative urology **1979**;17:16-23

44.   Tai S, Sun Y, Squires JM, Zhang H, Oh WK, Liang CZ, *et al.* PC3 is a cell line characteristic of prostatic small cell carcinoma. The Prostate **2011**;71:1668-79

45.   Mickey DD, Stone KR, Wunderli H, Mickey GH, Vollmer RT, Paulson DF. Heterotransplantation of a human prostatic adenocarcinoma cell line in nude mice. Cancer research **1977**;37:4049-58

46.   Taplin ME, Ho S-M. The endocrinology of prostate cancer. The Journal of Clinical Endocrinology & Metabolism **2001**;86:3467-77

47.   Cunha GR, Donjacour AA, Cooke PS, Mee H, Bigsby RM, Higgins SJ, *et al.* The endocrinology and developmental biology of the prostate. Endocrine reviews **1987**;8:338-62

48.   Srinivas-Shankar U, Wu FC. Drug insight: testosterone preparations. Nature clinical practice Urology **2006**;3:653-65

49.   Dehm SM, Tindall DJ. Molecular regulation of androgen action in prostate cancer. Journal of cellular biochemistry **2006**;99:333-44

50. Heinlein CA, Chang C. Androgen receptor in prostate cancer. Endocrine reviews **2004**;25:276-308

51. Freedland SJ, Humphreys EB, Mangold LA, Eisenberger M, Dorey FJ, Walsh PC*, et al.* Death in patients with recurrent prostate cancer after radical prostatectomy: prostate-specific antigen doubling time subgroups and their associated contributions to all-cause mortality. Journal of Clinical Oncology **2007**;25:1765-71

52. Magnan S, Zarychanski R, Pilote L, Bernier L, Shemilt M, Vigneault E*, et al.* Intermittent vs continuous androgen deprivation therapy for prostate cancer: a systematic review and meta-analysis. JAMA oncology **2015**;1:1261-9

53. Miyamoto H, Messing EM, Chang C. Androgen deprivation therapy for prostate cancer: current status and future prospects. The Prostate **2004**;61:332-53

54. Attar RM, Takimoto CH, Gottardis MM. Castration-resistant prostate cancer: locking up the molecular escape routes. Clinical Cancer Research **2009**;15:3251-5

55. Huggins C, Stevens R, Hodges CV. Studies on prostatic cancer: II. The effects of castration on advanced carcinoma of the prostate gland. Archives of surgery **1941**;43:209-23

56. Dar JA, Eisermann K, Masoodi KZ, Ai J, Wang D, Severance T*, et al.* N-terminal domain of the androgen receptor contains a region that can promote cytoplasmic localization. The Journal of steroid biochemistry and molecular biology **2014**;139:16-24

57. Attard G, Cooper CS, de Bono JS. Steroid hormone receptors in prostate cancer: a hard habit to break? Cancer cell **2009**;16:458-62

58. Marques RB, Dits NF, Erkens-Schulze S, Van Weerden WM, Jenster G. Bypass mechanisms of the androgen receptor pathway in therapy-resistant prostate cancer cell models. PloS one **2010**;5:e13500

59. Harris WP, Mostaghel EA, Nelson PS, Montgomery B. Androgen deprivation therapy: progress in understanding mechanisms of resistance and optimizing androgen depletion. Nature clinical practice Urology **2009**;6:76-85

60. Scher HI, Sawyers CL. Biology of progressive, castration-resistant prostate cancer: directed therapies targeting the androgen-receptor signaling axis. Journal of Clinical Oncology **2005**;23:8253-61

61. Koivisto P, Kononen J, Palmberg C, Tammela T, Hyytinen E, Isola J, *et al.* Androgen receptor gene amplification: a possible molecular mechanism for androgen deprivation therapy failure in prostate cancer. Cancer research **1997**;57:314-9

62. Visakorpi T, Hyytinen E, Koivisto P, Tanner M, Keinänen R, Palmberg C*, et al.* In vivo amplification of the androgen receptor gene and progression of human prostate cancer. Nature genetics **1995**;9:401-6

63. Linja MJ, Savinainen KJ, Saramäki OR, Tammela TL, Vessella RL, Visakorpi T. Amplification and overexpression of androgen receptor gene in hormone-refractory prostate cancer. Cancer research **2001**;61:3550-5

64. Sharma A, Yeow W-S, Ertel A, Coleman I, Clegg N, Thangavel C*, et al.* The retinoblastoma tumor suppressor controls androgen signaling and human prostate cancer progression. The Journal of clinical investigation **2010**;120:4478-92

65. Quigley CA, De Bellis A, Marschke KB, El-Awady MK, Wilson EM, French FS. Androgen receptor defects: historical, clinical, and molecular perspectives. Endocrine reviews **1995**;16:271-321

66. Taplin M-E, Rajeshkumar B, Halabi S, Werner CP, Woda BA, Picus J, *et al.* Androgen receptor mutations in androgen-independent prostate cancer: Cancer and Leukemia Group B Study 9663. Journal of clinical oncology **2003**;21:2673-8

67. Taplin M-E, Bubley GJ, Ko Y-J, Small EJ, Upton M, Rajeshkumar B, *et al.* Selection for androgen receptor mutations in prostate cancers treated with androgen antagonist. Cancer research **1999**;59:2511-5

68. Bergerat JP, Céraline J. Pleiotropic functional properties of androgen receptor mutants in prostate cancer. Human mutation **2009**;30:145-57

69. Gaddipati JP, McLeod DG, Heidenberg HB, Sesterhenn IA, Finger MJ, Moul JW, *et al.* Frequent detection of codon 877 mutation in the androgen receptor gene in advanced prostate cancers. Cancer research **1994**;54:2861-4

70. Culig Z, Hobisch A, Cronauer MV, Cato A, Hittmair A, Radmayr C, *et al.* Mutant androgen receptor detected in an advanced-stage prostatic carcinoma is activated by adrenal androgens and progesterone. Molecular endocrinology **1993**;7:1541-50

71. Zhao X-Y, Malloy PJ, Krishnan AV, Swami S, Navone NM, Peehl DM, *et al.* Glucocorticoids can promote androgen-independent growth of prostate cancer cells through a mutated androgen receptor. Nature medicine **2000**;6:703-6

72. Chan SC, Dehm SM. Constitutive activity of the androgen receptor. Advances in pharmacology **2014**;70:327-66

73. Heemers HV, Tindall DJ. Androgen receptor (AR) coregulators: a diversity of functions converging on and regulating the AR transcriptional complex. Endocrine reviews **2007**;28:778-808

74. Xu J, Wu R-C, O'malley BW. Normal and cancer-related functions of the p160 steroid receptor co-activator (SRC) family. Nature Reviews Cancer **2009**;9:615-30

75. Wang Q, Zhou J-L, Wang H, Ju Q, Ding Z, Zhou X-L*, et al.* Inhibition effect of cypermethrin mediated by co-regulators SRC-1 and SMRT in interleukin-6-induced androgen receptor activation. Chemosphere **2016**;158:24-9

76. Chung AC, Zhou S, Liao L, Tien JC-Y, Greenberg NM, Xu J. Genetic ablation of the amplified-in-breast cancer 1 inhibits spontaneous prostate cancer progression in mice. Cancer research **2007**;67:5965-75

77. Debes JD, Schmidt LJ, Huang H, Tindall DJ. p300 mediates androgen-independent transactivation of the androgen receptor by interleukin 6. Cancer research **2002**;62:5632-6

78. Chandrasekar T, Yang JC, Gao AC, Evans CP. Mechanisms of resistance in castration-resistant prostate cancer (CRPC). Translational andrology and urology **2015**;4:365

79. Wang Q, Li W, Liu XS, Carroll JS, Jänne OA, Keeton EK*, et al.* A hierarchical network of transcription factors governs androgen receptor-dependent prostate cancer growth. Molecular cell **2007**;27:380-92

80. Augello MA, Hickey TE, Knudsen KE. FOXA1: master of steroid receptor function in cancer. The EMBO journal **2011**;30:3885-94

81. Böhm M, Locke W, Sutherland R, Kench J, Henshall S. A role for GATA-2 in transition to an aggressive phenotype in prostate cancer through modulation of key androgen-regulated genes. Oncogene **2009**;28:3847-56

82. Wang Q, Li W, Zhang Y, Yuan X, Xu K, Yu J*, et al.* Androgen receptor regulates a distinct transcription program in androgen-independent prostate cancer. Cell **2009**;138:245-56

83. Watson PA, Chen YF, Balbas MD, Wongvipat J, Socci ND, Viale A, *et al.* Constitutively active androgen receptor splice variants expressed in castration-resistant prostate cancer require full-length androgen receptor. Proceedings of the national academy of sciences **2010**;107:16759-65

84. Zhang X, Morrissey C, Sun S, Ketchandji M, Nelson PS, True LD, *et al.* Androgen receptor variants occur frequently in castration resistant prostate cancer metastases. PloS one **2011**;6:e27970

85. Hörnberg E, Ylitalo EB, Crnalic S, Antti H, Stattin P, Widmark A, *et al.* Expression of androgen receptor splice variants in prostate cancer bone metastases is associated with castration-resistance and short survival. PloS one **2011**;6:e19059

86. Li Y, Alsagabi M, Fan D, Bova GS, Tewfik AH, Dehm SM. Intragenic rearrangement and altered RNA splicing of the androgen receptor in a cell-based model of prostate cancer progression. Cancer research **2011**;71:2108-17

87. Welti J, Rodrigues DN, Sharp A, Sun S, Lorente D, Riisnaes R, *et al.* Analytical validation and clinical qualification of a new immunohistochemical assay for androgen receptor splice variant-7 protein expression in metastatic castration-resistant prostate cancer. European urology **2016**;70:599-608

88. Guo Z, Yang X, Sun F, Jiang R, Linn DE, Chen H, *et al.* A novel androgen receptor splice variant is up-regulated during prostate cancer progression and promotes androgen depletion–resistant growth. Cancer research **2009**;69:2305-13

89. Mostaghel EA, Marck BT, Plymate SR, Vessella RL, Balk S, Matsumoto AM, *et al.* Resistance to CYP17A1 inhibition with abiraterone in castration-resistant prostate cancer: induction of steroidogenesis and androgen receptor splice variants. Clinical cancer research **2011**;17:5913-25

90.   Maughan BL, Antonarakis ES. Clinical relevance of androgen receptor splice variants in castration-resistant prostate cancer. Current treatment options in oncology **2015**;16:1-14

91.   Van der Steen T, Tindall DJ, Huang H. Posttranslational modification of the androgen receptor in prostate cancer. International journal of molecular sciences **2013**;14:14833-59

92.   Culig Z, Hobisch A, Cronauer MV, Radmayr C, Trapman J, Hittmair A*, et al.* Androgen receptor activation in prostatic tumor cell lines by insulin-like growth factor-I, keratinocyte growth factor, and epidermal growth factor. Cancer research **1994**;54:5474-8

93.   Lamont KR, Tindall DJ. Minireview: Alternative activation pathways for the androgen receptor in prostate cancer. Molecular endocrinology **2011**;25:897-907

94.   Craft N, Shostak Y, Carey M, Sawyers CL. A mechanism for hormone-independent prostate cancer through modulation of androgen receptor signaling by the HER-2/neu tyrosine kinase. Nature medicine **1999**;5:280-5

95.   Nazareth LV, Weigel NL. Activation of the human androgen receptor through a protein kinase A signaling pathway. Journal of Biological Chemistry **1996**;271:19900-7

96.   Mahajan NP, Liu Y, Majumder S, Warren MR, Parker CE, Mohler JL*, et al.* Activated Cdc42-associated kinase Ack1 promotes prostate cancer progression via androgen receptor tyrosine phosphorylation. Proceedings of the National Academy of Sciences **2007**;104:8438-43

97.   Holzbeierlein J, Lal P, LaTulippe E, Smith A, Satagopan J, Zhang L*, et al.* Gene expression analysis of human prostate carcinoma during hormonal therapy identifies androgen-responsive genes and mechanisms of therapy resistance. The American journal of pathology **2004**;164:217-27

98.   Yuan X, Balk SP. Mechanisms mediating androgen receptor reactivation after castration. 2009. Elsevier. p 36-41.

99.   Cai C, He HH, Chen S, Coleman I, Wang H, Fang Z, *et al.* Androgen receptor gene expression in prostate cancer is directly suppressed by the androgen receptor through recruitment of lysine-specific demethylase 1. Cancer cell **2011**;20:457-71

100.   Whittington K, Connors B, King K, Assinder S, Hogarth K, Nicholson H. The effect of oxytocin on cell proliferation in the human prostate is modulated by gonadal steroids: implications for benign prostatic hyperplasia and carcinoma of the prostate. The Prostate **2007**;67:1132-42

101.   Schröder FH, Hugosson J, Roobol MJ, Tammela TL, Ciatto S, Nelen V, *et al.* Screening and prostate-cancer mortality in a randomized European study. New England journal of medicine **2009**;360:1320-8

102.   Moyer VA, Force* UPST. Screening for prostate cancer: US Preventive Services Task Force recommendation statement. Annals of internal medicine **2012**;157:120-34

103.   Schröder FH. Stratifying risk--the US Preventive Services Task Force and prostate-cancer screening. The New England journal of medicine **2011**;365:1953-5

104.   Institute NC. NCI Dictionary of Cancer Terms <https://www.cancer.gov/publications/dictionaries/cancer-terms/def/biomarker?redirect=true>. Accessed 2022.

105.   Velonas VM, Woo HH, Dos Remedios CG, Assinder SJ. Current status of biomarkers for prostate cancer. International journal of molecular sciences **2013**;14:11034-60

106. Gutman AB, Gutman EB. An "acid" phosphatase occurring in the serum of patients with metastasizing carcinoma of the prostate gland. The Journal of clinical investigation **1938**;17:473-8

107. Hernández J, Thompson IM. Prostate-specific antigen: a review of the validation of the most commonly used cancer biomarker. Cancer **2004**;101:894-904

108. Armbruster DA. Prostate-specific antigen: biochemistry, analytical methods, and clinical application. Clinical chemistry **1993**;39:181-95

109. Foster C, Bostwick D, Bonkhoff H, Damber J-E, Van der Kwast T, Montironi R, *et al.* Cellular and molecular pathology of prostate cancer precursors. Scandinavian Journal of Urology and Nephrology **2000**;34:19-43

110. Liu Y, Hegde P, Zhang F, Hampton G, Jia S. Prostate cancer–a biomarker perspective. Frontiers in endocrinology **2012**;3:72

111. Bodey B, Bodey Jr B, Kaiser H. Immunocytochemical detection of prostate specific antigen expression in human primary and metastatic melanomas. Anticancer research **1997**;17:2343-6

112. Hessels D, Schalken JA. Urinary biomarkers for prostate cancer: a review. Asian journal of andrology **2013**;15:333

113. Mistry K, Cable G. Meta-analysis of prostate-specific antigen and digital rectal examination as screening tests for prostate carcinoma. The Journal of the American Board of Family Practice **2003**;16:95-101

114. Lin M-W, Ho JW, Harrison LC, dos Remedios CG, Adelstein S. An antibody-based leukocyte-capture microarray for the diagnosis of systemic lupus erythematosus. PLoS One **2013**;8:e58199

115. Schröder FH, Van Der Cruijsen-Koeter I, De Koning HJ, Vis AN, Hoedemaeker RF, Kranse R. Prostate cancer detection at low prostate specific antigen. The Journal of urology **2000**;163:806-12

116. Andriole GL, Crawford ED, Grubb III RL, Buys SS, Chia D, Church TR, *et al.* Prostate cancer screening in the randomized Prostate, Lung, Colorectal, and Ovarian Cancer Screening Trial: mortality results after 13 years of follow-up. Journal of the National Cancer Institute **2012**;104:125-32

117. Roobol MJ, Zhu X, Schröder FH, van Leenders GJ, van Schaik RH, Bangma CH, *et al.* A calculator for prostate cancer risk 4 years after an initially negative screen: findings from ERSPC Rotterdam. European urology **2013**;63:627-33

118. Connolly D, Black A, Murray LJ, Napolitano G, Gavin A, Keane PF. Methods of calculating prostate-specific antigen velocity. European urology **2007**;52:1044-51

119. Capitanio U, Ahyai S, Graefen M, Jeldres C, Shariat SF, Erbersdobler A, *et al.* Assessment of biochemical recurrence rate in patients with pathologically confirmed insignificant prostate cancer. Urology **2008**;72:1208-11

120. Wu CC, Yates JR. The application of mass spectrometry to membrane proteomics. Nature biotechnology **2003**;21:262-7

121. Huang PY, Best OG, Belov L, Mulligan SP, Christopherson RI. Surface profiles for subclassification of chronic lymphocytic leukemia. Leukemia & lymphoma **2012**;53:1046-56

122. Fleshner NE, Lawrentschuk N. Risk of developing prostate cancer in the future: overview of prognostic biomarkers. Urology **2009**;73:S21-S7

123. Wan JC, Massie C, Garcia-Corbacho J, Mouliere F, Brenton JD, Caldas C, *et al.* Liquid biopsies come of age: towards implementation of circulating tumour DNA. Nature Reviews Cancer **2017**;17:223-38

124. Edwards SM, Evans DGR, Hope Q, Norman A, Barbachano Y, Bullock S, *et al.* Prostate cancer in BRCA2 germline mutation carriers is associated with poorer prognosis. British journal of cancer **2010**;103:918-24

125. Castro E, Goh C, Olmos D, Saunders E, Leongamornlert D, Tymrakiewicz M, *et al.* Germline BRCA mutations are associated with higher risk of nodal involvement, distant metastasis, and poor survival outcomes in prostate cancer. Journal of Clinical Oncology **2013**;31:1748

126. Salagierski M, Schalken JA. Molecular diagnosis of prostate cancer: PCA3 and TMPRSS2: ERG gene fusion. The Journal of urology **2012**;187:795-801

127. van Gils MP, Hessels D, van Hooij O, Jannink SA, Peelen WP, Hanssen SL, *et al.* The time-resolved fluorescence-based PCA3 test on urinary sediments after digital rectal examination; a Dutch multicenter validation of the diagnostic performance. Clinical Cancer Research **2007**;13:939-43

128. Hessels D, Smit FP, Verhaegh GW, Witjes JA, Cornel EB, Schalken JA. Detection of TMPRSS2-ERG fusion transcripts and prostate cancer antigen 3 in urinary sediments may improve diagnosis of prostate cancer. Clinical Cancer Research **2007**;13:5103-8

129. Saramäki OR, Harjula AE, Martikainen PM, Vessella RL, Tammela TL, Visakorpi T. TMPRSS2: ERG fusion identifies a subgroup of prostate cancers with a favorable prognosis. Clinical cancer research **2008**;14:3395-400

130. Zhao Z, Zeng G, Zhong W. Serum early prostate cancer antigen (EPCA) as a significant predictor of incidental prostate cancer in patients undergoing transurethral resection of the prostate for benign prostatic hyperplasia. The Prostate **2010**;70:1788-98

131. Zhao Z, Ma W, Zeng G, Qi D, Ou L, Liang Y. Preoperative serum levels of early prostate cancer antigen (EPCA) predict prostate cancer progression in patients undergoing radical prostatectomy. The Prostate **2012**;72:270-9

132. Guo Y, Xu F, Lu T, Duan Z, Zhang Z. Interleukin-6 signaling pathway in targeted therapy for cancer. Cancer treatment reviews **2012**;38:904-10

133. Qin J, Wu S-P, Creighton CJ, Dai F, Xie X, Cheng C-M, *et al.* COUP-TFII inhibits TGF-β-induced growth barrier to promote prostate tumorigenesis. Nature **2013**;493:236-40

134. Shariat SF, Shalev M, Menesses-Diaz A, Kim IY, Kattan MW, Wheeler TM, *et al.* Preoperative plasma levels of transforming growth factor beta1 (TGF-β1) strongly predict progression in patients undergoing radical prostatectomy. Journal of Clinical Oncology **2001**;19:2856-64

135. Ke Y, Jing C, Barraclough R, Smith P, Davies MP, Foster CS. Elevated expression of calcium-binding protein p9Ka is associated with increasing malignant characteristics of rat prostate carcinoma cells. International journal of cancer **1997**;71:832-7

136. Gupta S, Hussain T, MacLennan GT, Fu P, Patel J, Mukhtar H. Differential expression of S100A2 and S100A4 during progression of human prostate adenocarcinoma. Journal of Clinical Oncology **2003**;21:106-12

137. Madu CO, Lu Y. Novel diagnostic biomarkers for prostate cancer. Journal of Cancer **2010**;1:150

138. Beckett ML, Cazares LH, Vlahou A, Schellhammer PF, Wright Jr GL. Prostate-specific membrane antigen levels in sera from healthy men and patients with benign prostate hyperplasia or prostate cancer. Clinical cancer research **1999**;5:4034-40

139. Dreyer C, Krey G, Keller H, Givel F, Helftenbein G, Wahli W. Control of the peroxisomal β-oxidation pathway by a novel family of nuclear hormone receptors. Cell **1992**;68:879-87

140. Gurung S, Po Sin Chung K, Lee TKW. Emerging role of fatty acid binding proteins in cancer pathogenesis. **2019**

141. Anker P, Mulcahy H, Qi Chen X, Stroun M. Detection of circulating tumour DNA in the blood (plasma/serum) of cancer patients. Cancer and Metastasis Reviews **1999**;18:65-73

142. Schwarzenbach H, Alix-Panabières C, Müller I, Letang N, Vendrell J-P, Rebillard X, *et al.* Cell-free tumor DNA in blood plasma as a marker for circulating tumor cells in prostate cancer. Clinical Cancer Research **2009**;15:1032-8

143. Kote-Jarai Z, Leongamornlert D, Saunders E, Tymrakiewicz M, Castro E, Mahmud N, *et al.* BRCA2 is a moderate penetrance gene contributing to young-onset prostate cancer: implications for genetic testing in prostate cancer patients. British journal of cancer **2011**;105:1230-4

144. Leongamornlert D, Mahmud N, Tymrakiewicz M, Saunders E, Dadaev T, Castro E, *et al.* Germline BRCA1 mutations increase prostate cancer risk. British journal of cancer **2012**;106:1697-701

145. De Muga S, Hernandez S, Salido M, Lorenzo M, Agell L, Juanpere N, *et al.* CXCR4 mRNA overexpression in high grade prostate tumors: Lack of association with TMPRSS2-ERG rearrangement. Cancer Biomarkers **2013**;12:21-30

146. Paul W. IL-6: a multifunctional regulator of immunity and inflammation. Japanese journal of cancer research: Gann **1991**;82:1458-9

147. Zhang G-J, Adachi I. Serum interleukin-6 levels correlate to tumor progression and prognosis in metastatic breast carcinoma. Anticancer research **1999**;19:1427-32

148. Kattan MW, Shariat SF, Andrews B, Zhu K, Canto E, Matsumoto K, *et al.* The addition of interleukin-6 soluble receptor and transforming growth factor beta1 improves a preoperative nomogram for predicting biochemical progression in

patients with clinically localized prostate cancer. Journal of Clinical Oncology **2003**;21:3573-9

149. Donato R. Intracellular and extracellular roles of S100 proteins. Microscopy research and technique **2003**;60:540-51

150. Donato R. S100: a multigenic family of calcium-modulated proteins of the EF-hand type with intracellular and extracellular functional roles. The international journal of biochemistry & cell biology **2001**;33:637-68

151. Ilg EC, Schäfer BW, Heizmann CW. Expression pattern of S100 calcium-binding proteins in human tumors. International journal of cancer **1996**;68:325-32

152. Rehman I, Cross SS, Catto JW, Leiblich A, Mukherjee A, Azzouzi AR*, et al.* Promoter hyper-methylation of calcium binding proteins S100A6 and S100A2 in human prostate cancer. The Prostate **2005**;65:322-30

153. Zhang Y. Functional Characterization of three novel candidate biomarkers and therapeutic targets fro prostate cancer 2010.

154. Reiter RE, Gu Z, Watabe T, Thomas G, Szigeti K, Davis E*, et al.* Prostate stem cell antigen: a cell surface marker overexpressed in prostate cancer. Proceedings of the National Academy of Sciences **1998**;95:1735-40

155. Ramirez M, Nelson E, Evans CP. Beyond prostate-specific antigen: alternate serum markers. Prostate Cancer and Prostatic Diseases **2008**;11:216-29

156. Bonkhoff H, Remberger K. Differentiation pathways and histogenetic aspects of normal and abnormal prostatic growth: a stem cell model. The Prostate **1996**;28:98-106

157. Zimmerman A, Veerkamp J. New insights into the structure and function of fatty acid-binding proteins. Cellular and Molecular Life Sciences CMLS **2002**;59:1096-116

158. Furuhashi M, Hotamisligil GS. Fatty acid-binding proteins: role in metabolic diseases and potential as drug targets. Nature reviews Drug discovery **2008**;7:489-503

159. Haunerland NH, Spener F. Fatty acid-binding proteins–insights from genetic manipulations. Progress in lipid research **2004**;43:328-49

160. Veerkamp J, Van Moerkerk H. Fatty acid-binding protein and its relation to fatty acid oxidation. Cellular Fatty Acid-Binding Proteins II: Springer; 1993. p 101-6.

161. Chmurzyńska A. The multigene family of fatty acid-binding proteins (FABPs): function, structure and polymorphism. Journal of applied genetics **2006**;47:39-48

162. Sacchettini J, Gordon J, Banaszak L. The structure of crystalline Escherichia coli-derived rat intestinal fatty acid-binding protein at 2.5-A resolution. Journal of Biological Chemistry **1988**;263:5815-9

163. Xu Z, Bernlohr D, Banaszak LJ. The adipocyte lipid-binding protein at 1.6-A resolution. Crystal structures of the apoprotein and with bound saturated and unsaturated fatty acids. Journal of Biological Chemistry **1993**;268:7874-84

164. LaLonde JM, Levenson MA, Roe JJ, Bernlohr DA, Banaszak LJ. Adipocyte lipid-binding protein complexed with arachidonic acid. Titration calorimetry and X-ray crystallographic studies. Journal of Biological Chemistry **1994**;269:25339-47

165. Storch J, Thumser AE. The fatty acid transport function of fatty acid-binding proteins. Biochimica et Biophysica Acta (BBA)-Molecular and Cell Biology of Lipids **2000**;1486:28-44

166. Storch J, McDermott L. Structural and functional analysis of fatty acid-binding proteins. Journal of lipid research **2009**;50:S126-S31

167. Schachtrup C, Emmler T, Bleck B, Sandqvist A, Spener F. Functional analysis of peroxisome-proliferator-responsive element motifs in genes of fatty acid-binding proteins. Biochemical journal **2004**;382:239-45

168. Tan N-S, Shaw NS, Vinckenbosch N, Liu P, Yasmin R, Desvergne B, *et al.* Selective cooperation between fatty acid binding proteins and peroxisome proliferator-activated receptors in regulating transcription. Molecular and cellular biology **2002**;22:5114-27

169. Michalik L, Wahli W. PPARs mediate lipid signaling in inflammation and cancer. PPAR research **2008**;2008

170. Forootan FS, Forootan SS, Malki MI, Chen D, Li G, Lin K, *et al.* The expression of C-FABP and PPARγ and their prognostic significance in prostate cancer. International journal of oncology **2014**;44:265-75

171. Onstenk W, Sieuwerts AM, Mostert B, Lalmahomed Z, Bolt-de Vries JB, van Galen A, *et al.* Molecular characteristics of circulating tumor cells resemble the liver metastasis more closely than the primary tumor in metastatic colorectal cancer. Oncotarget **2016**;7:59058

172. Wood SM, Gill AJ, Brodsky AS, Lu S, Friedman K, Karashchuk G, *et al.* Fatty acid-binding protein 1 is preferentially lost in microsatellite instable colorectal carcinomas and is immune modulated via the interferon γ pathway. Modern Pathology **2017**;30:123-33

173. Ku C-Y, Liu Y-H, Lin H-Y, Lu S-C, Lin J-Y. Liver fatty acid-binding protein (L-FABP) promotes cellular angiogenesis and migration in hepatocellular carcinoma. Oncotarget **2016**;7:18229

174. Jiang Z, Shen H, Tang B, Yu Q, Ji X, Wang L. Quantitative proteomic analysis reveals that proteins required for fatty acid metabolism may serve as diagnostic markers for gastric cancer. Clinica Chimica Acta **2017**;464:148-54

175. Kato I, Land S, Majumdar AP, Barnholtz-Sloan J, Severson RK. Functional polymorphisms to modulate luminal lipid exposure and risk of colorectal cancer. Cancer epidemiology **2010**;34:291-7

176. Tang Z, Shen Q, Xie H, Zhou X, Li J, Feng J, *et al.* Elevated expression of FABP3 and FABP4 cooperatively correlates with poor prognosis in non-small cell lung cancer (NSCLC). Oncotarget **2016**;7:46253

177. Hashimoto T, Kusakabe T, Sugino T, Fukuda T, Watanabe K, Sato Y, *et al.* Expression of heart-type fatty acid-binding protein in human gastric carcinoma and its association with tumor aggressiveness, metastasis and poor prognosis. Pathobiology **2004**;71:267-73

178. Davidson B, Abeler VM, Hellesylt E, Holth A, Shih I-M, Skeie-Jensen T, *et al.* Gene expression signatures differentiate uterine endometrial stromal sarcoma from leiomyosarcoma. Gynecologic oncology **2013**;128:349-55

179. Cao H, Sekiya M, Ertunc ME, Burak MF, Mayers JR, White A, *et al.* Adipocyte lipid chaperone AP2 is a secreted adipokine regulating hepatic glucose production. Cell metabolism **2013**;17:768-78

180. Huynh H, Alpert L, Pollak M. Silencing of the mammary-derived growth inhibitor (MDGI) gene in breast neoplasms is associated with epigenetic changes. Cancer research **1996**;56:4865-70

181. Nevo J, Mattila E, Pellinen T, Yamamoto DL, Sara H, Iljin K, *et al.* Mammary-derived growth inhibitor alters traffic of EGFR and induces a novel form of cetuximab resistance. Clinical Cancer Research **2009**;15:6570-81

182. Okano T, Kondo T, Fujii K, Nishimura T, Takano T, Ohe Y, *et al.* Proteomic signature corresponding to the response to gefitinib (Iressa, ZD1839), an epidermal growth factor receptor tyrosine kinase inhibitor in lung adenocarcinoma. Clinical cancer research **2007**;13:799-805

183. Wu C-H, Sahoo D, Arvanitis C, Bradon N, Dill DL, Felsher DW. Combined analysis of murine and human microarrays and ChIP analysis reveals genes associated with the ability of MYC to maintain tumorigenesis. PLoS genetics **2008**;4:e1000090

184. Uehara H, Takahashi T, Oha M, Ogawa H, Izumi K. Exogenous fatty acid binding protein 4 promotes human prostate cancer cell progression. International journal of cancer **2014**;135:2558-68

185. Guaita-Esteruelas S, Guma J, Masana L, Borràs J. The peritumoural adipose tissue microenvironment and cancer. The roles of fatty acid binding protein 4 and fatty acid binding protein 5. Molecular and cellular endocrinology **2018**;462:107-18

186. Nie J, Zhang J, Wang L, Lu L, Yuan Q, An F, *et al.* Adipocytes promote cholangiocarcinoma metastasis through fatty acid binding protein 4. Journal of Experimental & Clinical Cancer Research **2017**;36:1-15

187. Cataltepe O, Arikan MC, Ghelfi E, Karaaslan C, Ozsurekci Y, Dresser K, *et al.* Fatty acid binding protein 4 is expressed in distinct endothelial and non-endothelial cell populations in glioblastoma. Neuropathology and applied neurobiology **2012**;38:400-10

188. Boiteux G, Lascombe I, Roche E, Plissonnier ML, Clairotte A, Bittard H, *et al.* A-FABP, a candidate progression marker of human transitional cell carcinoma of the bladder, is differentially regulated by PPAR in urothelial cancer cells. International journal of cancer **2009**;124:1820-8

189. Jin J, Zhang Z, Zhang S, Chen X, Chen Z, Hu P, *et al.* Fatty acid binding protein 4 promotes epithelial-mesenchymal transition in cervical squamous cell carcinoma through AKT/GSK3β/Snail signaling pathway. Molecular and cellular endocrinology **2018**;461:155-64

190. Zhao G, Wu M, Wang X, Du Z, Zhang G. Effect of FABP5 gene silencing on the proliferation, apoptosis and invasion of human gastric SGC-7901 cancer cells. Oncology Letters **2017**;14:4772-8

191. Levi L, Lobo G, Doud MK, Von Lintig J, Seachrist D, Tochtrop GP, *et al.* Genetic Ablation of the Fatty Acid–Binding Protein FABP5 Suppresses HER2-Induced Mammary TumorigenesisFABP5 Promotes Mammary Tumor Development. Cancer research **2013**;73:4770-80

192. Wang W, Chu H-j, Liang Y-c, Huang J-m, Shang C-l, Tan H, *et al.* FABP5 correlates with poor prognosis and promotes tumor cell growth and metastasis in cervical cancer. Tumor Biology **2016**;37:14873-83

193. Powell CA, Nasser MW, Zhao H, Wochna JC, Zhang X, Shapiro C, *et al.* Fatty acid binding protein 5 promotes metastatic potential of triple negative breast cancer cells through enhancing epidermal growth factor receptor stability. Oncotarget **2015**;6:6373

194. Myers JS, von Lersner AK, Sang Q-XA. Proteomic upregulation of fatty acid synthase and fatty acid binding protein 5 and identification of cancer-and race-specific pathway associations in human prostate cancer tissues. Journal of Cancer **2016**;7:1452

195. Kawaguchi K, Kinameri A, Suzuki S, Senga S, Ke Y, Fujii H. The cancer-promoting gene fatty acid-binding protein 5 (FABP5) is epigenetically regulated during human prostate carcinogenesis. Biochemical Journal **2016**;473:449-61

196. Al-Jameel W, Gou X, Jin X, Zhang J, Wei Q, Ai J, *et al.* Inactivated FABP5 suppresses malignant progression of prostate cancer cells by inhibiting the activation of nuclear fatty acid receptor PPARγ. Genes & cancer **2019**;10:80

197. Jeong C-Y, Hah Y-S, Cho BI, Lee SM, Joo Y-T, Jung E-J, *et al.* Fatty acid-binding protein 5 promotes cell proliferation and invasion in human intrahepatic cholangiocarcinoma. Oncology reports **2012**;28:1283-92

198. Fang LY, Wong TY, Chiang WF, Chen YL. Fatty-acid-binding protein 5 promotes cell proliferation and invasion in oral squamous cell carcinoma. Journal of oral pathology & medicine **2010**;39:342-8

199. McKillop IH, Girardi CA, Thompson KJ. Role of fatty acid binding proteins (FABPs) in cancer development and progression. Cellular Signalling **2019**;62:109336

200. Xie M, Wu X, Zhang J, He C, Wei S, Huang J, *et al.* The prognostic significance of Notch1 and fatty acid binding protein 7 (FABP7) expression in resected tracheobronchial adenoid cystic carcinoma: a multicenter retrospective study. Cancer Research and Treatment: Official Journal of Korean Cancer Association **2018**;50:1064-73

201. Slipicevic A, Jørgensen K, Skrede M, Rosnes AKR, Trøen G, Davidson B, *et al.* The fatty acid binding protein 7 (FABP7) is involved in proliferation and invasion of melanoma cells. BMC cancer **2008**;8:1-13

202. Al Fayi MS, Gou X, Forootan SS, Al-Jameel W, Bao Z, Rudland PR, *et al.* The increased expression of fatty acid-binding protein 9 in prostate cancer and its prognostic significance. Oncotarget **2016**;7:82783

203. Madsen P, Rasmussen HH, Leffers H, Honoré B, Celis JE. Molecular cloning and expression of a novel keratinocyte protein (psoriasis-associated fatty acid-binding protein [PA-FABP]) that is highly up-regulated in psoriatic skin and that shares similarity to fatty acid-binding proteins. Journal of Investigative Dermatology **1992**;99:299-305

204. Masouyé I, Saurat J-H, Siegenthaler G. Epidermal fatty-acid-binding protein in psoriasis, basal and squamous cell carcinomas: an immunohistological study. Dermatology **1996**;192:208-13

205. Morgan EA, Forootan SS, Adamson J, Foster CS, Fujii H, Igarashi M*, et al.* Expression of cutaneous fatty acid-binding protein (C-FABP) in prostate cancer: potential prognostic marker and target for tumourigenicity-suppression. International journal of oncology **2008**;32:767-75

206. Jing C, Beesley C, Foster CS, Chen H, Rudland PS, West DC*, et al.* Human cutaneous fatty acid-binding protein induces metastasis by up-regulating the expression of vascular endothelial growth factor gene in rat Rama 37 model cells. Cancer research **2001**;61:4357-64

207. Suojalehto H, Kinaret P, Kilpeläinen M, Toskala E, Ahonen N, Wolff H*, et al.* Level of fatty acid binding protein 5 (FABP5) is increased in sputum of allergic asthmatics and links to airway remodeling and inflammation. PLoS One **2015**;10:e0127003

208. Hu Z, Fan C, Livasy C, He X, Oh DS, Ewend MG*, et al.* A compact VEGF signature associated with distant metastases and poor outcomes. BMC medicine **2009**;7:1-14

209. Forootan SS, Bao ZZ, Forootan FS, Kamalian L, Zhang Y, Bee A*, et al.* Atelocollagen-delivered siRNA targeting the FABP5 gene as an experimental therapy for prostate cancer in mouse xenografts. International journal of oncology **2010**;36:69-76

210. Bao Z, Malki MI, Forootan SS, Adamson J, Forootan FS, Chen D*, et al.* A novel cutaneous Fatty Acid-binding protein-related signaling pathway leading to malignant progression in prostate cancer cells. Genes & cancer **2013**;4:297-314

211. Forootan FS, Forootan SS, Gou X, Yang J, Liu B, Chen D, *et al.* Fatty acid activated PPARγ promotes tumorigenicity of prostate cancer cells by up regulating VEGF via PPAR responsive elements of the promoter. Oncotarget **2016**;7:9322

212. Wiedenheft B, Sternberg SH, Doudna JA. RNA-guided genetic silencing systems in bacteria and archaea. Nature **2012**;482:331-8

213. Rath D, Amlinger L, Rath A, Lundgren M. The CRISPR-Cas immune system: biology, mechanisms and applications. Biochimie **2015**;117:119-28

214. Koonin EV, Wolf YI. Evolution of the CRISPR-Cas adaptive immunity systems in prokaryotes: models and observations on virus–host coevolution. Molecular BioSystems **2015**;11:20-7

215. Koonin EV, Makarova KS, Zhang F. Diversity, classification and evolution of CRISPR-Cas systems. Current opinion in microbiology **2017**;37:67-78

216. Makarova KS, Wolf YI, Alkhnbashi OS, Costa F, Shah SA, Saunders SJ, *et al.* An updated evolutionary classification of CRISPR–Cas systems. Nature Reviews Microbiology **2015**;13:722-36

217. Sternberg SH, LaFrance B, Kaplan M, Doudna JA. Conformational control of DNA target cleavage by CRISPR–Cas9. Nature **2015**;527:110-3

218. Deltcheva E, Chylinski K, Sharma CM, Gonzales K, Chao Y, Pirzada ZA, *et al.* CRISPR RNA maturation by trans-encoded small RNA and host factor RNase III. Nature **2011**;471:602-7

219. Pellagatti A, Dolatshad H, Yip BH, Valletta S, Boultwood J. Application of genome editing technologies to the study and treatment of hematological disease. Advances in biological regulation **2016**;60:122-34

220. Jinek M, Chylinski K, Fonfara I, Hauer M, Doudna JA, Charpentier E. A programmable dual-RNA–guided DNA endonuclease in adaptive bacterial immunity. science **2012**;337:816-21

221. Ran F, Hsu PD, Wright J, Agarwala V, Scott DA, Zhang F. Genome engineering using the CRISPR-Cas9 system. Nature protocols **2013**;8:2281-308

222. Wang H, Yang H, Shivalila CS, Dawlaty MM, Cheng AW, Zhang F, *et al.* One-step generation of mice carrying mutations in multiple genes by CRISPR/Cas-mediated genome engineering. cell **2013**;153:910-8

223. Xue W, Chen S, Yin H, Tammela T, Papagiannakopoulos T, Joshi NS, *et al.* CRISPR-mediated direct mutation of cancer genes in the mouse liver. Nature **2014**;514:380-4

224. Kannan R, Ventura A. The CRISPR revolution and its impact on cancer research. Swiss medical weekly **2015**;145:w14230

225. He F. Bradford protein assay. Bio-protocol **2011**:e45-e

226. Leszczyński P, Śmiech M, Salam Teeli A, Haque E, Viger R, Ogawa H, *et al.* Deletion of the Prdm3 Gene Causes a Neuronal Differentiation Deficiency in P19 Cells. International journal of molecular sciences **2020**;21:7192

227. GENEWIZ. RNA-Seq Analysis Report

 <file:///C:/Users/Abdul/OneDrive/Desktop/thesis%20correction/40-546310215_GENEWIZ_RNA-Seq_Analysis_Report.html>. Accessed 2022.

228. Ge SX, Son EW. Gaining insights from RNA-Seq data using iDEP. bioRxiv **2018**:148411

229. Albini A, Iwamoto Y, Kleinman H, Martin G, Aaronson S, Kozlowski J, *et al.* A rapid in vitro assay for quantitating the invasive potential of tumor cells. Cancer research **1987**;47:3239-45

230. Sharifi N, Gulley JL, Dahut WL. Androgen deprivation therapy for prostate cancer. Jama **2005**;294:238-44

231. Chen Y, Clegg NJ, Scher HI. Anti-androgens and androgen-depleting therapies in prostate cancer: new agents for an established target. The lancet oncology **2009**;10:981-91

232. Grasso CS, Wu Y-M, Robinson DR, Cao X, Dhanasekaran SM, Khan AP, *et al.* The mutational landscape of lethal castration-resistant prostate cancer. Nature **2012**;487:239-43

233. Naeem AA, Abdulsamad SA, Rudland PS, Malki MI, Ke Y. Fatty acid-binding protein 5 (FABP5)-related signal transduction pathway in castration-resistant prostate cancer cells: a potential therapeutic target. Precision Clinical Medicine **2019**;2:192-6

234. Currie E, Schulze A, Zechner R, Walther TC, Farese RV. Cellular fatty acid metabolism and cancer. Cell metabolism **2013**;18:153-61

235. Pascual G, Avgustinova A, Mejetta S, Martín M, Castellanos A, Attolini CS-O, *et al.* Targeting metastasis-initiating cells through the fatty acid receptor CD36. Nature **2017**;541:41-5

236. Adamson J, Morgan EA, Beesley C, Mei Y, Foster CS, Fujii H, *et al.* High-level expression of cutaneous fatty acid-binding protein in prostatic carcinomas and its effect on tumorigenicity. Oncogene **2003**;22:2739-49

237. Unniyampurath U, Pilankatta R, Krishnan MN. RNA interference in the age of CRISPR: will CRISPR interfere with RNAi? International journal of molecular sciences **2016**;17:291

238. Doudna JA, Charpentier E. The new frontier of genome engineering with CRISPR-Cas9. Science **2014**;346:1258096

239. Pushparaj PN, Aarthi JJ, Kumar SD, Manikandan J. RNAi and RNAa-the yin and yang of RNAome. Bioinformation **2008**;2:235

240. Al-Bayati A. Increased FABP12 expression in prostate cancer and its possible promoting role in tumorigenicity: University of Liverpool; 2021.

241. Tyumentseva MA, Tyumentsev AI, Akimkin VG. Protocol for assessment of the efficiency of CRISPR/Cas RNP delivery to different types of target cells. Plos one **2021**;16:e0259812

242. Xu X, Wan T, Xin H, Li D, Pan H, Wu J, *et al.* Delivery of CRISPR/Cas9 for therapeutic genome editing. The journal of gene medicine **2019**;21:e3107

243. Howe BM, Bruno SB, Higgs KA, Stigers RL, Cunningham JT. FosB expression in the central nervous system following isotonic volume expansion in unanesthetized rats. Experimental neurology **2004**;187:190-8

244. Mitchell JA, Shynlova O, Langille BL, Lye SJ. Mechanical stretch and progesterone differentially regulate activator protein-1 transcription factors in primary rat myometrial smooth muscle cells. American Journal of Physiology-Endocrinology and Metabolism **2004**;287:E439-E45

245. Lanningham-Foster L, Green CL, Langkamp-Henken B, Davis BA, Nguyen KT, Bender BS, *et al.* Overexpression of CRIP in transgenic mice alters cytokine patterns and the immune response. American Journal of Physiology-Endocrinology and Metabolism **2002**;282:E1197-E203

246. Papa M, Boscia F, Canitano A, Castaldo P, Sellitti S, Annunziato L, *et al.* Expression pattern of the ether-a-gogo-related (ERG) K+ channel-encoding genes ERG1, ERG2, and ERG3 in the adult rat central nervous system. Journal of Comparative Neurology **2003**;466:119-35

247. Shin S-H, Kim I, Lee JE, Lee M, Park J-W. Loss of EGR3 is an independent risk factor for metastatic progression in prostate cancer. Oncogene **2020**;39:5839-54

248. Mansi R, Fleischmann A, Mäcke HR, Reubi JC. Targeting GRPR in urological cancers—from basic research to clinical application. Nature reviews Urology **2013**;10:235-44

249. Christoforou P, Christopoulos PF, Koutsilieris M. The role of estrogen receptor β in prostate cancer. Molecular medicine **2014**;20:427-34

250. Meshulam T, Simard JR, Wharton J, Hamilton JA, Pilch PF. Role of caveolin-1 and cholesterol in transmembrane fatty acid movement. Biochemistry **2006**;45:2882-93

251. Trigatti BL, Anderson RG, Gerber GE. Identification of caveolin-1 as a fatty acid binding protein. Biochemical and biophysical research communications **1999**;255:34-9

252. Nath A, Chan C. Genetic alterations in fatty acid transport and metabolism genes are associated with metastatic progression and poor prognosis of human cancers. Scientific reports **2016**;6:18669

253. Edwards PA, Kast HR, Anisfeld AM. BAREing it all: the adoption of LXR and FXR and their roles in lipid homeostasis. Journal of lipid research **2002**;43:2-12

254. Cheung AKL, Ko JM, Lung HL, Chan KW, Stanbridge EJ, Zabarovsky E, *et al.* Cysteine-rich intestinal protein 2 (CRIP2) acts as a repressor of NF-κB–mediated proangiogenic cytokine transcription to suppress tumorigenesis and angiogenesis. Proceedings of the National Academy of Sciences **2011**;108:8390-5

255. Adamo P, Ladomery M. The oncogene ERG: a key factor in prostate cancer. Oncogene **2016**;35:403-14

256. Zhang R, Li X, Liu Z, Wang Y, Zhang H, Xu H. EZH2 inhibitors-mediated epigenetic reactivation of FOSB inhibits triple-negative breast cancer progress. Cancer Cell International **2020**;20:1-11

257.   Milde-Langosch K. The Fos family of transcription factors and their role in tumourigenesis. European journal of cancer **2005**;41:2449-61

258.   Platanias LC. Mechanisms of type-I-and type-II-interferon-mediated signalling. Nature Reviews Immunology **2005**;5:375-86

259.   Nagasaki S, Nakamura Y, Maekawa T, Akahira J, Miki Y, Suzuki T, *et al.* Immunohistochemical analysis of gastrin-releasing peptide receptor (GRPR) and possible regulation by estrogen receptor βcx in human prostate carcinoma. Neoplasma **2012**;59:224-32

260.   Case TC, Merkel A, Ramirez-Solano M, Liu Q, Sterling JA, Jin R. Blocking GRP/GRP-R signaling decreases expression of androgen receptor splice variants and inhibits tumor growth in castration-resistant prostate cancer. Translational Oncology **2021**;14:101213

261.   Dorsam RT, Gutkind JS. G-protein-coupled receptors and cancer. Nature reviews cancer **2007**;7:79-94

262.   Bennett N, Hooper JD, Lee CS, Gobe GC. Androgen receptor and caveolin-1 in prostate cancer. IUBMB life **2009**;61:961-70

263.   Goetz JG, Lajoie P, Wiseman SM, Nabi IR. Caveolin-1 in tumor progression: the good, the bad and the ugly. Cancer and metastasis reviews **2008**;27:715-35

264.   Lee YJ, Lee E-Y, Choi BH, Jang H, Myung J-K, You HJ. The role of nuclear receptor subfamily 1 group H member 4 (NR1H4) in colon cancer cell survival through the regulation of c-Myc stability. Molecules and cells **2020**;43:459-68

265.   Wu D, Cheung A, Wang Y, Yu S, Chan FL. The emerging roles of orphan nuclear receptors in prostate cancer. Biochimica et Biophysica Acta (BBA)-Reviews on Cancer **2016**;1866:23-36

Appendix. A

A 1. Cell culture re

DMSO	Sigma-Aldrich,
GermanyFoetal bovine serum	Gibco, Invitrogen, UK
L-Glutamine	Lonza, Belgium
Penicillin/Streptomycin	Lonza, Belgium
Phosphate buffered saline	Gibco, Invitrogen, UK
Phosphate buffered salibe (tablets)	Gibco, Invitrogen, UK
RPMI 1640	Gibco, Invitrogen, UK
Sodium pyruvate	Sigma, USA
TrypleE	Gibco, Invitrogen, UK

A 2. Routine cell culture medium

500ml of 1640 RPMI medium+ 50ml of Foetal bovine serum (10%)+ 5ml of Penicillin-Streptomycin (5000U/ml)+ 5ml L-Glutamine 20mM+ 5ml Sodium pyruvate 100mM

A 3. Freezing medium

Routine cell culture medium 95%(v/v)+ 5% of DMSO (v/v)

A 4. Reagents for molecular biology

Absolute ethanol	BDH, England, UK
Ampicillin	Invitrogen, CA, USA
BL21 E.coli bacteria	Invitrogen, CA, USA
Glycerol	Sigma, USA
Isopropylthiogalactoside (IPTG)	Sigma, USA
LB agar	Sigma, USA
LB broth	Sigma, USA
QIAGEN Ni-NTA Fast Start Kit	QIAGEN, UK
SDS	Sigma, UK
Magnesium chloride	Sigma, USA
Magnesium sulphate	Sigma, USA

A 5. Reagents for western blot

β-mercaptroethanol	Sigma, USA
Ammonium persulfate (APS)	Sigma, USA
Bradford reagent	Sigma, USA
Bromophenole blue	Sigma, USA
CelLytic-M	Sigam, USA
Coomassie blue	Bio-Rad GmbH, UK
ECL detection kit	GE Healthcare, UK
Glycine	Melford, UK
Methanol	Fisher scientific, UK

PVDF membrane	Millipore, USA
Quick Start Bradford Protein assay	Bio-Rad, UK
Tris Base salt	Melford, UK
Tween-20	Sigma, UK
dH$_2$O	

A 6. Reagents for CRISPR CAS9

ATTO550 sgRNA	Integrate DNA Technologies (USA).
CAS9	Thermofisher, UK

A 7. Reagents for cell viability detection

PrestoBlue HS	Thermofisher, UK

A 8. Reagents for invasion assay

Crystal violet	Sigma, USA

A 9. Reagent for soft agar assay

Low melting point agarose	Thermofisher, UK
MTT	Sigma, USA

B . Buffers

B 3. 100Mm of IPTG

238mg of IPTG

10ml of sterile distilled water

Sterilized filter

Routine cell culture

RPMI medium 1640 (500ml)

Foetal bovine serum 10%(v/v)

Pen/Strep (5000U/ML) 5ml

LGlutamine (20Mm) 5ml

Sodium pyruvate (100mM) 5ml

TrypleE 5ML

MTT (5mg/ml)

PBS (10ml)

Autoclaved

Western blot

3.1 1M Tris pH 6.8 = (12.1g of Tris base + 100ml of dH2HO). Ph adjusted with HCL

10% of SDS solution = (10g of Sodium Dodecyl Sulfate + 100ml of dH2O)

10% of APS solution = (100g of Ammonium persulfate + 1ml of dH2O)

Sample loading buffer = (2.5 ml of 1M of Tris-HCL, Ph 6.8 +4ml of Glycerol, 40%+ 0.8ml of Bromophenol blue, 0.5%+ 2ml of SDS, 10%+ 0.5ml of β-mercaptroethanol+ 4.7ml of dH2O)

Transfer buffer (pH 8.3) = (14.4g of Glycine, 192mM + 20% of Methanol, (v/v)+3.03g of Tris base, 25mM +up to 1 Lit of dH2O), HCL for pH adjustment

10x TBS buffer (pH 7.6)= (87.66g of Sodium chloride, 1500mM+ 60.58g of Tris base, 500mM+ up to 1Lit of dH2O) AUTOCLAVED

1x TBS-TWEEN 1%=(100ml of 10x TBS buffer+1ml of Tween20+ up to 1 Lit)

(Washing buffer) TBS-T milk 5% = (5g of Skimmed dried milk+ 100ml of 1x TBS-T buffer)

D. Equipment

Corning™ BioCoat™ Matrigel™ Invasion Chamber: With GFR Matrigel Matrix FisherScintific, UK

CO2 incubator

Borolabs, Basingstoke, UK

Cell culture filter cap flasks

Cell culture plates Cryogenic vial Nunc, Denmark

Carbon steel surgical blades

Swann-Morton, Sheffeild, UK

Falcon tubes

Becton, Dickinson, USA

Gel electrophoresis

Bio-Rad, UK

GelCount

OXFORD OPTRONIX, Oxford, UK

Haemocytometer slide

Weber Scientific International, NJ, USA

Hot plate

Thermofisher, UK

Haemocytometer

SLS LTD, Nottingham, UK

Immobilon, Transfer membrane

Milipore, UK

Microtubes

Starlab, Milton Keynes, UK

Multiskan MS plate reader

Labsystem, Finland

Needle

BD Microlance, Ireland

NanoDrop spectrophotometer

Labtech I nternational, Ringmer, UK

Pipetter tips

QIAGEN, UK

Syringes and filters

Fisherscintific, UK

Spectrophotometer

BioTec, UK

Pipettes for cell culture

Eppendorf, UK

Universal tube

Greiner Bio-One, UK

Water bath

Grant Instruments, UK

Whatman filter paper

Whatman, England, UK

Tips for pipettes

Eppendorf, UK

E. DNA authentications for PCa cell lines

![northgene™ A BIOFORTUNA brand]

Laboratory Report

Test Requested   **Cell Line Authentication**

Case Number   C-25831a
Date Sample Received   28/06/2022
Date Sample Tested   28/06/2022
Date Sample Reported   11/07/2022

Sample Name	Sample/Comparison Profile Source	Sample Number	DNA Number
PNT2 Secondary Pellet	University of Liverpool	S-1059517	D-1059517
PNT2	DSMZ/HPACC Database	N/A	N/A

Table of Allelic Data

STR Locus	Genotypes		Match vs. Mis-Match
	PNT2 Secondary Pellet (Test Sample)	PNT2 (Comparison Sample)	
D5	12 | 13	12 | 13	Match
D13	8 | 13	8 | 13	Match
D7	11 | 11	11 | 11	Match
D16	9 | 9	9 | 9	Match
vWA	17 | 17	17 | 17	Match
Amel	X | Y	X | Y	Match
TPOX	8 | 9	8 | 9	Match
CSF1PO	10 | 11 I 13	11 | 13	Mis-Match
THO1	6 | 9.3	6 | 9.3	Match

Matching Percentage: **97%**
Outcome: **Related**

The outcome percentage is calculated using a formulae which compares the number of alleles present against the number of alleles shared between the two DNA profiles. The outcome is designated one of the following statements based upon the outcome percentage:

Related (>80%)   The Cell Lines are considered to be related.
Inconclusive (56-79%)   Further profiling is required to determine whether the profiles are related.
No Match (55%>)   It is considered that the two cell lines are unrelated.
Misidentified   Cell Lines have been found to match a different donor within the database

Reported By: Mr. Benjamin Hickey (Laboratory Scientist)

Authorised By: Ms. Eleanor Ralston (Senior Scientist)

Date: 12/07/2022

Laboratory Report

Test Requested	Cell Line Authentication
Case Number	C-25831d
Date Sample Received	01/06/2022
Date Sample Tested	08/06/2022
Date Sample Reported	24/06/2022

Sample Name	Sample/Comparison Profile Source	Sample Number	DNA Number
DU145	University of Liverpool	S-1059099	D-1059099
DU-145	DSMZ Database	N/A	N/A

Table of Allelic Data

STR Locus	Genotypes		Match vs. Mis-Match
	DU145 (Test Sample)	DU-145 (Comparison Sample)	
D5	10 | 13	10 | 13	Match
D13	12 | 14	12 | 13 | 14	Mis-Match
D7	7 | 10 | 11	7 | 10 | 11	Match
D16	11 | 13	11 | 13	Match
vWA	17 | 18	17 | 18	Match
Amel	X | Y	X | Y	Match
TPOX	11 | 11	11 | 11	Match
CSF1PO	10 | 11	10 | 11	Match
THO1	7 | 7	7 | 7	Match

Matching Percentage: **97%**
Outcome: **Related**

The outcome percentage is calculated using a formulae which compares the number of alleles present against the number of alleles shared between the two DNA profiles. The outcome is designated one of the following statements based upon the outcome percentage:

Related (>80%)	The Cell Lines are considered to be related.
Inconclusive (56-79%)	Further profiling is required to determine whether the profiles are related.
No Match (55%>)	It is considered that the two cell lines are unrelated.
Misidentified	Cell Lines have been found to match a different donor within the database

Reported By: Mr. Callum Teeling (Laboratory Scientist)

Authorised By: Ms. Eleanor Ralston (Senior Scientist)

These test results should only be used in conjunction with a client's information. The results relate only to the items sampled, as received and

2

281

northgene™
A BIOFORTUNA brand

Laboratory Report

Test Requested   Cell Line Authentication

Case Number   C-25831d
Date Sample Received   28/06/2022
Date Sample Tested   28/06/2022
Date Sample Reported   11/07/2022

Sample Name	Sample/Comparison Profile Source	Sample Number	DNA Number
PC3M Secondary Pellet	University of Liverpool	S-1059518	D-1059518
PC-3M	DSMZ Database	N/A	N/A

Table of Allelic Data

STR Locus	Genotypes		Match vs. Mis-Match
	PC3M Secondary Pellet (Test Sample)	PC-3M (Comparison Sample)	
D5	13 | 13	13 | 13	Match
D13	11 | 11	11 | 11	Match
D7	8 | 11	8 | 11	Match
D16	11 | 11	11 | 11	Match
vWA	17 | 17	17 | 17	Match
Amel	X | X	X | X	Match
TPOX	8 | 9	8 | 9	Match
CSF1PO	11 | 11	11 | 11	Match
THO1	6 | 7	6 | 7	Match

Matching Percentage: **100%**
Outcome: **Related**

The outcome percentage is calculated using a formulae which compares the number of alleles present against the number of alleles shared between the two DNA profiles. The outcome is designated one of the following statements based upon the outcome percentage:

Related (>80%)   The Cell Lines are considered to be related.
Inconclusive (56-79%)   Further profiling is required to determine whether the profiles are related.
No Match (55%>)   It is considered that the two cell lines are unrelated.
Misidentified   Cell Lines have been found to match a different donor within the database

Reported By: Mr. Benjamin Hickey (Laboratory Scientist)

Authorised By: Ms. Eleanor Ralston (Senior Scientist)

Date: 12/07/2022

These test results should only be used in conjunction with a client's information. The results relate only to the items sampled, as received and tested at this time.

2
2

Published papers

OXFORD

SHORT COMMUNICATION

Fatty acid-binding protein 5 (FABP5)-related signal transduction pathway in castration-resistant prostate cancer cells: a potential therapeutic target

Abdulghani A. Naeem[1],[§], Saud A. Abdulsamad[1],[§], Philip S. Rudland[2], Mohammed I. Malki[3] and Youqiang Ke[1],*

[1]The Molecular Pathology Laboratory, Department of Molecular and Clinical Cancer Medicine; [2]Department of Biochemistry, Liverpool University, Liverpool L69 3GA, UK; and [3]College of Medicine, Qatar University, Doha 2713, Qatar

*Correspondence: Youqiang Ke, yqk@liverpool.ac.uk

Abstract

In this short communication, a novel fatty acid-binding protein 5 (FABP5)-related signal transduction pathway in prostate cancer is reviewed. In castration-resistant prostate cancer (CRPC) cells, the FABP5-related signal transduction pathway plays an important role during transformation of the cancer cells from androgen-dependent state to androgen-independent state. The detailed route of this signal transduction pathway can be described as follows: when FABP5 expression is increased as the increasing malignancy, excessive amounts of fatty acids from intra- and extra-cellular sources are transported into the nucleus of the cancer cells where they act as signalling molecules to stimulate their nuclear receptor peroxisome proliferator-activated receptor gamma (PPARγ). The phosphorylated or biologically activated PPARγ then modulates the expression of its downstream target regulatory genes to trigger a series of molecular events that eventually lead to enhanced tumour expansion and aggressiveness caused by an overgrowth of the cancer cells with a reduced apoptosis and an increased angiogenesis. Suppressing the FABP5-related pathway via RNA interference against FABP5 has produced a 63-fold reduction in the average size of the tumours developed from CRPC cells in nude mice, a seven-fold reduction of tumour incidence, and a 100% reduction of metastasis rate. Experimental treatments of CRPC with novel FABP5 inhibitors have successfully inhibited the malignant progression of CRPC cells both *in vitro* and in nude mouse. These studies suggest that FABP5-related signal transduction pathway is a novel target for therapeutic intervention of CRPC cells.

Key words: FABP5; CRPC; fatty acids; PPARγ; tumorigenicity; metastasis

Epidemiology of Prostate Cancer in Saudi Arabia

Abdulghani A. Naeem[1], Saud A. Abdulsamad[1], Xi Jin[2], Gang He[3], Jiachen Zhang[1], Qiang Wei[2*] and Youqiang Ke[1,2*]

ABSTRACT

Problem identification: Prostate Cancer and its prevalence worldwide have increased over the past several years as the knowledge and methods for early detection of cancer have been improving. Prostate Cancer is also considered to be the second most common cancer in Middle Eastern countries, and is ranked as the sixth leading cause of mortality among men. This study aims to identify the role of genetics and environmental factors in the development and progression of Prostate Cancer among Middle Eastern countries, with focus on the prevalence and mortality of Prostate Cancer in Saudi Arabia. The study also aims to examine proposed risk factors for the development of Prostate Cancer among Middle Eastern men.

Literature search: Extensive literature search was made to find articles and studies regarding to the prevalence of Prostate Cancer in Saudi Arabia, and the potential reasons for its increased prevalence over the years. Studies about the established and proposed risk factors contributing to the development of Prostate Cancer was also included in the literature search.

Conclusion: Results of literature reviewed and studied in this paper showed that genetics and individual anatomy of Arab men are of importance in the development of Prostate Cancer. For environmental causes, it was identified that the changing lifestyle of Arab men, and becoming more open to Western influence also contributed to the prevalence of Prostate Cancer. It was also found out that with the improving status of the medical practices in Saudi Arabia, it is expected that more cases are to be detected, as more access will be rendered available to the citizens for the immediate detection of Prostate Cancer..

Keywords: Prostate Cancer; Saudi Arabia; Epidemiology; Risk factors and prevention.

1. INTRODUCTION

Prostate Cancer is considered to be one of the most common types of cancer in men and the second most common cancer in the Middle Eastern region (Table 1) and has been ranked 6th on the most significant number of deaths associated with the disease [1]. It has become an emerging disease among developed and developing countries and is mostly associated with men over 55 years (Fig. 3) of age [2-3] Men affected by prostate cancer are on the rise and are expected to continuously rise [1]. Even though prostate cancer is far more common among African-American men [1] its incidence is considerably higher in the North American region and most European countries [4]. There has been continuous spike of reported cases of prostate cancer in the United States and Canadian region (Table 2), while the reports of prostate cancer as lower in the Asian region, specifically the Arabic region [5]. Though incidence rate of prostate cancer in Saudi Arabia does not match those with other American and European countries, Saudi nationals are still at risk and number of Saudi nationals affected each year is on the rise, a trend that has been observed from 2001 to 2008 (Fig. 1), as well as studies done in 2012 and 2018. It is expected that the number of affected in Middle Eastern countries in 2012 (29, 377) will increase to 38, 562 in 2020 [5,43]. This increase in affected persons will result in increased mortality associated with the disease from 15, 422 deaths in 2012 to 19, 681

[1]Department of Molecular & Clinical Cancer Medicine, Liverpool University, Liverpool, L69 3GA, United Kingdom.
[2]Institute of Urology, West China Hospital, Sichuan University, No.37 Guo Xue Xiang, Chengdu, Sichuan, 610041, China.
[3]Sichuan Antibiotics Industrial Institute, Chengdu University, Chengdu 610081, China.
*Corresponding author: E-mail: yqk@liverpool.ac.uk, wq933@hotmail.com;

Prostate Cell Lines

Abdulghani A Naeem[1], Saud A Abdulsamad[1], Asmaa Al Bayati[1], Jiacheng Zhang[1], Mohammed I Malki[2], Hongwen Ma[3], and Youqiang Ke[1]*

[1]Department of Molecular & Clinical Cancer Medicine, Liverpool University, Liverpool, United Kingdom

[2]College of Medicine, QU Health, Qatar university, Doha, Qatar

[3]Department of Urology, Institute of Urology, West China Hospital, Sichuan University, China

***Corresponding author:** Youqiang Ke, Professor, Department of Molecular & Clinical Cancer Medicine, Liverpool University, L69 3GA, United Kingdom

Abstract

When it comes to studying biological processes, cell lines are typically utilized in lieu of original cell samples. Like in the studies for other cancer types, researchers in prostate cancer can be constrained in their ability to discover new treatments because of a lack of cell lines to investigate pre-clinical status. There are various forms of prostate cancer cell lines that are reviewed in this work. A cautionary note is in need since cell lines may not always correctly mimic the original cells. Cancerous cells are immortal and using cell lines produced from cancer cells as a model to better understand cancer and to develop novel therapies are common in research. Apart from the prostate cancer cells, we also reviewed two cell lines PNT2 and RWPE-1 which were established from non-neoplastic male prostatic epithelial cells.

Introduction

Cancers are known for their ability to prolong life indefinitely [1,2]. However, it remains a mystery how mortal somatic cells become the source of immortal malignancies. Cancerous cells are immortal, despite the fact that healthy somatic cells may develop into organs as well as creatures that include much more cells than lethal tumors [3-11]. By exceeding the Hayflick threshold, which is approximately 50 cycles in vitro, immortality is established operationally. Telomerase stimulation is now the most widely accepted explanation of immortality [4-6]. Cancers are supposed to gain immortality via the stimulation of telomerase, which is a gene that is normally shut off throughout development in somatic cells. To put it another way, cells that have maintained their telomeres by the acts of telomerase process are considered to be immortalized. All individual tumors seem to be governed by the process of cell immortalization.

It is these cells that serve as a starting point for tumor development and are known as the cancer cells of origin. Unlike cancer stem cells, which constitute the cellular subfractions capable of regenerating tumors, these cells are classified in a different way. It's been a major focus of cancer research to identify the cells that give rise to the disease. Since there is so much interest in testing the concept that tumors are caused by various cell types, this has resulted in a lot of research being done in this area. This knowledge will aid in the early detection and precise prognosis of cancer, as well as in the development of new preventative treatments for people at high risk. Based on the histological appearance of malignancies, it was formerly considered that they had a cellular origin. We now know, based on our existing understanding, that tumor specimens may be deceiving when random as well as static observations are made. A direct genetic method should be used to test any hypotheses. Tumors may have gene expression patterns that are more like those of their own cells' ancestors than those of other cell types within the same tissue, which is a similar but much more elegant concept. The basal-like breast cancer may originate from luminal epithelial progenitors in the mammary gland luminal epithelium. Gene expression patterns may be used to classify brain tumors with similar histological characteristics into separate groups that represent the cellular genesis of the tumors. Molecular profiles don't always line up with tumor pathology, according to these findings. It is still necessary to do more direct genetic research in order to verify the findings drawn from these sorts of studies. Cell lines having diverse lineage features from human or mouse tissues may be established, transformed, and then analyzed

534

RESEARCH ARTICLE

Cell Biology International WILEY

Molecular mechanisms on how FABP5 inhibitors promote apoptosis-induction sensitivity of prostate cancer cells

Jiacheng Zhang[1] | Gang He[2] | Xi Jin[3] | Bandar T. Alenezi[1] | Abdulghani A. Naeem[1] | Saud A. Abdulsamad[1] | Youqiang Ke[1,2,3]

[1]Department of Molecular and Clinical Cancer Medicine, Liverpool University, Liverpool, UK

[2]Sichuan Industrial Institute of Antibiotics, Chengdu University, Chengdu, Sichuan, China

[3]Institute of Urology, West China Hospital, Sichuan University, Chengdu, Sichuan, China

Correspondence

Youqiang Ke and Jiacheng Zhang, Department of Molecular and Clinical Cancer Medicine, Liverpool University, the Cancer Research Centre Bldg, 200 London Rd, Liverpool L3 9TA, UK.
Email: yqk@liverpool.ac.uk and aster65@163.com

Abstract

Previous work showed that FABP5 inhibitors suppressed the malignant progression of prostate cancer cells, and this suppression might be achieved partially by promoting apoptosis. But the mechanisms involved were not known. Here, we investigated the effect of inhibitors on apoptosis and studied the relevant mechanisms. WtrFABP5 significantly reduced apoptotic cells in 22Rv1 and PC3 by 18% and 42%, respectively. In contrast, the chemical inhibitor SB-FI-26 produced significant increases in percentages of apoptotic cells in 22Rv1 and PC3 by 18.8% (±4.1) and 4.6% (±1.1), respectively. The bio- inhibitor dmrFABP5 also did so by 23.1% (±2.4) and 15.8% (±3.0), respectively, in these cell lines. Both FABP5 inhibitors significantly reduced the levels of the phosphorylated nuclear fatty acid receptor PPARγ, indicating that these inhibitors promoted apoptosis-induction sensitivity of the cancer cells by suppressing the biological activity of PPARγ. Thus, the phosphorylated PPARγ levels were reduced by FABP5 inhibitors, the levels of the phosphorylated AKT and activated nuclear factor kapper B (NFκB) were coordinately altered by additions of the inhibitors. These changes eventually led to the increased levels of cleaved caspase-9 and cleaved caspase-3; and thus, increase in the percentage of cells undergoing apoptosis. In untreated prostate cancer cells, increased FABP5 suppressed the apoptosis by increasing the biological activity of PPARγ, which, in turn, led to a reduced apoptosis by interfering with the AKT or NFκB signaling pathway. Our results suggested that the FABP5 inhibitors enhanced the apoptosis-induction of prostate cancer cells by reversing the biological effect of FABP5 and its related pathway.

KEYWORDS

AB-FI-26, apoptosis, dmrFABP5, FABP5, PPARγ, prostate cancer

287